

Advanced Photochemical Avenues to Monodisperse Sequence-Defined Macromolecules

Zur Erlangung des akademischen Grades eines
DOKTORS DER NATURWISSENSCHAFTEN

(Dr. rer. nat.)

von der KIT-Fakultät für Chemie und Biowissenschaften
des Karlsruher Instituts für Technologie (KIT)

genehmigte

DISSERTATION

von

M.Sc. Waldemar Konrad

aus

Smirnowo, Kasachstan

1. Referent: Prof. Dr. Christopher Barner-Kowollik

2. Referent: Prof. Dr. Hans-Achim Wagenknecht

Tag der mündlichen Prüfung: 24. Juli 2019

meiner Mutter und meiner Großmutter gewidmet

Die vorliegende Arbeit wurde im Zeitraum von Januar 2016 bis Juni 2019 am Institut für Technische Chemie und Polymerchemie am Karlsruher Institut für Technologie (KIT) – Universitätsbereich unter der Betreuung von Prof. Dr. Christopher Barner-Kowollik angefertigt.

Ich erkläre hiermit, dass ich die vorliegende Arbeit im Rahmen der Betreuung durch Prof. Dr. Christopher Barner-Kowollik selbstständig verfasst und keine anderen als die angegebenen Quellen und Hilfsmittel verwendet habe. Wörtlich oder inhaltlich übernommene Stellen sind als solche kenntlich gemacht und die Satzung des Karlsruher Instituts für Technologie (KIT) zur Sicherung guter wissenschaftlicher Praxis wurde beachtet. Des Weiteren erkläre ich, dass ich mich derzeit in keinem laufenden Promotionsverfahren befinde und auch keine vorausgegangenen Promotionsversuche unternommen habe.

Karlsruhe, den 11.06.2019

Waldemar Konrad

Publications

Publications Arising from this Thesis

- [3] *Protection Group Free Synthesis of Sequence-Defined Macromolecules via Precision λ -Orthogonal Photochemistry.* W. Konrad, C. Fengler, S. Putwa, C. Barner-Kowollik, *Angew. Chem. Int. Ed.* **2019**, 58, 7133-7137.
- [2] *A Combined Photochemical and Multicomponent Reaction Approach to Precision Oligomers.* W. Konrad, F. R. Bloesser, K. S. Wetzel, A. C. Boukis, M. A. R. Meier, C. Barner-Kowollik, *Chem. Eur. J.* **2018**, 24, 3413-3419.
- [1] *Coding and decoding libraries of sequence-defined functional copolymers synthesized via photoligation.* N. Zydziak, W. Konrad, F. Feist, S. Afonin, S. Weidner, C. Barner-Kowollik, *Nat. Commun.* **2016**, 7, 13672.

Other Publications

- [1] *Access to Multiblock Copolymers via Supramolecular Host–Guest Chemistry and Photochemical Ligation.* A. F. Hirschbiel, W. Konrad, D. Schulze-Sünninghausen, S. Wiedmann, B. Luy, B. V. K. J. Schmidt, C. Barner-Kowollik, *ACS Macro Lett.* **2015**, 4, 1062-1066.

Conference Contributions

- [3] *Protection Group Free Synthesis of Sequence-Defined Macromolecules via Precision λ -Orthogonal Photochemistry.* Poster at the Biennial Meeting of the GDCh-Division of Macromolecular Chemistry (MAKRO), September 24th-27th, 2018, Karlsruhe, Germany.
- [2] *Protection Group Free Synthesis of Sequence-Defined Macromolecules via Precision λ -Orthogonal Photochemistry.* Poster at the International Symposium on Photochemistry (PhotoIUPAC), July 8th-13th, 2018, Dublin, Ireland.
- [1] *Synthesis of Sequence-Defined Linear Macromolecules via Precision Photochemistry.* Poster at the European Polymer Federation (EPF) Conference, July 02nd– 07th, 2017, Lyon, France.

Abstract

In the present thesis novel avenues towards monodisperse sequence-defined macromolecules are developed. Here, highly efficient photoinduced ‘click’ reactions, such as Diels–Alder (DA) cycloaddition or nitrile imine carboxylic acid ligation (NICAL), were employed as ligation platforms for the synthesis of sequence-defined macromolecules. In addition, sequence-defined macromolecules are prepared by the combination of photochemistry and Passerini three-component reactions (P-3CRs). Moreover, photochemistry is investigated as a powerful tool for wavelength-orthogonal synthesis of monodisperse macromolecules without the need for protection group chemistry.

Modular strategies in which a symmetric linear molecule is ligated with previously synthesized building blocks are investigated for increasing the molecular weight in sequence-defined macromolecules significantly in one chain extension step. Furthermore, the synthesis of macromolecules by bidirectional growth is explored by employing symmetrical core units. Symmetrical core molecules also contribute to a significant increase of molecular weight per chain extension step due to the fact that two building units are added simultaneously per reaction step. Thus, a reduction of reactions steps is expected in order to build up a high molecular weight. An examination of how high molecular weights can be achieved by a combination of symmetrical cores and modular strategies is also explored. Moreover, the significantly higher increase of molecular weight per chain extension step is studied as a parameter in the purification of the macromolecules since it is expected that the chromatographic separation of the respective generations is therefore improved.

Three approaches towards sequence-defined macromolecules are demonstrated in the current thesis. The P-3CR is a one-pot reaction in which three components form a product. Consequently, structurally more complex reaction products can be prepared in just one synthetic step. Photochemistry, on the other hand, provides temporal and spatial control over reactions. Hence, both the photoinduced DA cycloaddition with *o*-methylbenzaldehydes (*o*-MBAs) and the Passerini reaction are combined in the first approach for the formation of precision oligomers, consisting of alternating P-3CR and photoblocks, exploiting the advantages of both ligation methods. Here, a modular approach is employed in combination

with bidirectional chain growth for the consecutive chain extension. In the first step, Passerini linkers are prepared as building blocks for the chain extension, providing maleimides as anchor points for subsequent light induced ligation. The photobuilding blocks are based on a UV-active benzaldehyde moiety, a photocaged diene, and furan protected maleimides. Starting from sebacic acid as the symmetric core molecule, the desired symmetric side chain functionalized, sequence-defined macromolecules with molecular weights of up to $3532.16 \text{ g mol}^{-1}$ are obtained by switching between photochemistry and Passerini reactions. The monodisperse, sequence-defined macromolecules synthesized by the convergent approach feature absolute chain-end fidelity and functional monomers are placed at exact positions along the chain.

Sequence-defined macromolecules exhibiting furan protected maleimides at their chain ends have to be thermally deprotected prior to further chain extension. Therefore, a combination of pyrene-functionalized tetrazoles responding to visible light between 410 – 420 nm (performing NICAL ligation) and *o*-MBAs being activated in the UV region at 365 nm (performing DA cycloaddition) are exploited for a wavelength-orthogonal platform in the second approach. Here, a custom made photoflow reactor is designed to provide scalability of the photochemical reactions. The synthesis of sequence-defined macromolecules is presented based on a two-monomer system by chain extension of a symmetrical core unit. Starting from a bifunctional carboxylic acid as a core unit, symmetrical sequence-defined macromolecules are prepared with a molecular weight up to $6257.10 \text{ g mol}^{-1}$.

In a third approach, a library of functional sequence-defined macromolecules varying in chain length and monomer sequence order is obtained based on the photoinduced DA reaction between UV-active *o*-MBAs and furan caged maleimides. Building blocks of α,ω -functionalized macromolecules consisting of up to five monomer units are prepared in the first step for modular chain extension, ready to be combined on demand. Starting from a bis-maleimide core unit, symmetrical sequence-defined decamers are obtained by the successive addition of the respective building units by UV-light.

In-depth characterization of the sequence-defined macromolecules confirming the monodisperse nature is conducted *via* size exclusion chromatography (SEC), nuclear magnetic resonance spectroscopy (NMR) and high resolution Orbitrap electrospray ionization – mass spectrometry (ESI-MS).

Zusammenfassung

In der vorliegenden Arbeit werden neue Wege zu monodispersen, sequenzdefinierten Makromolekülen entwickelt. Dazu wurden hocheffiziente photoinduzierte "Klick"-Reaktionen wie etwa die Diels-Alder (DA) Cycloaddition oder die Nitril-Imin-Carbonsäure-Ligation (NICAL) als Ligationsplattformen eingesetzt. Darüber hinaus wird die Bildung sequenzdefinierter Makromoleküle durch die Kombination von Photochemie und Passerini-Reaktionen demonstriert. Zusätzlich wird die Photochemie als geeignetes Werkzeug für die wellenlängenorthogonale Synthese monodisperser Makromoleküle unter Vermeidung von Schutzgruppenchemie untersucht.

Modulare Strategien, bei denen ein symmetrisches lineares Molekül mit zuvor synthetisierten Bausteinen ligiert wird, werden untersucht, um das Molekulargewicht in sequenzdefinierten Makromolekülen pro Kettenverlängerungsschritt erheblich zu erhöhen. Darüber hinaus wird die Synthese von Makromolekülen durch zweiseitiges Wachstum symmetrischer Kerneinheiten untersucht, da symmetrische Kernmoleküle ebenso zu einer signifikanten Erhöhung des Molekulargewichts pro Kettenverlängerungsschritt beitragen, weil zwei Bausteine gleichzeitig in einem Reaktionsschritt angebunden werden. Demzufolge wird der Aufbau eines hohen Molekulargewichts in weniger Reaktionsschritten realisiert. In der Folge wird untersucht, wie hohe Molekulargewichte durch eine Kombination von symmetrischen Kernen und modularen Strategien erreicht werden können. Des Weiteren wird der signifikant höhere Anstieg des Molekulargewichts pro Kettenverlängerungsschritt als Beitrag zur Aufreinigung der Makromoleküle untersucht, da damit zu rechnen ist, dass die chromatographische Auftrennung der jeweiligen Generationen vereinfacht wird.

In der vorliegenden Arbeit werden drei Ansätze für sequenzdefinierte Makromoleküle aufgezeigt. Die Passerini-Reaktion ist eine Eintopfreaktion, bei der drei Komponenten ein Produkt bilden, das direkt alle gewünschten Funktionen enthält. Folglich können strukturell komplexere Reaktionsprodukte in nur einem Syntheseschritt hergestellt werden. Die Photochemie bietet andererseits zeitliche und räumliche Kontrolle über Reaktionen. Im ersten Projekt werden daher beide, d.h. photoinduzierte DA-Cycloaddition mit *o*-Methylbenzaldehyd-

den (*o*-MBAs) und die Passerini-Reaktion, zur Bildung von Präzisionsoligomeren kombiniert, welche abwechselnd aus P-3CR und Photoblocken bestehen, wobei die Vorteile beider Ligationsmethoden ausgenutzt werden. Es wird ein modularer Ansatz in Kombination mit einem bidirektionalen Kettenwachstum für die aufeinanderfolgende Kettenverlängerung verfolgt. In einem ersten Schritt werden Passerini-Linker als Bausteine für die Kettenverlängerung hergestellt, welche Maleimide als Ankerpunkte für die anschließende lichtinduzierte Ligation liefern. Die Photoblocke werden auf der Basis einer UV-aktiven Benzaldehydeinheit, ein photoaktivierbares Dien, und einem furangeschützten Maleimid konzipiert. Ausgehend von Sebacinsäure als symmetrisches Kernmolekül werden durch Umschalten zwischen Photochemie und Passerini-Reaktionen die gewünschten symmetrischen, seitenkettenfunktionalisierten, sequenzdefinierten Makromoleküle mit Molekulargewichten von bis zu $3532.16 \text{ g mol}^{-1}$ erhalten. Die monodispersen, sequenzdefinierten Makromoleküle zeichnen sich durch absolute Endgruppentreue und der exakten Positionierung funktioneller Monomere entlang der Kette aus.

Sequenzdefinierte Makromoleküle mit furangeschützten Maleimiden an ihren Kettenenden müssen vor der weiteren Kettenverlängerung thermisch geschützt werden. Das Vermeiden überflüssiger Modifikationen, die mit den Makromolekülen selbst durchgeführt werden, ist vorteilhaft, um die Gesamteffizienz zu erhöhen. Im zweiten Ansatz wird daher eine Kombination von pyrenfunktionalisierten Tetrazolen, die auf sichtbares Licht zwischen 410 und 420 nm (NICAL Reaktion) reagieren, und auf im UV-Bereich bei 365 nm aktivierbare *o*-MBAs (DA-Cycloaddition), für einen wellenlängenunabhängigen Ansatz genutzt. Dazu wird im Hinblick auf die Skalierbarkeit der photochemischen Reaktionen ein Photodurchflussreaktor entwickelt. Die Synthese von sequenzdefinierten Makromolekülen basiert auf einem Zwei-Monomer-System durch Kettenverlängerung einer symmetrischen Kerneinheit. Ausgehend von einer bifunktionellen Carbonsäure als Kerneinheit werden symmetrische, sequenzdefinierte Makromoleküle mit einem Molekulargewicht von bis zu $6257.10 \text{ g mol}^{-1}$ hergestellt.

In einem dritten Ansatz wird basierend auf der photoinduzierten DA-Reaktion zwischen UV-aktiven *o*-MBAs und einem furangeschützten Maleimid eine Reihe funktioneller sequenzdefinierter Makromoleküle mit unterschiedlicher Kettenlänge und Monomersequenzreihenfolgen erhalten. Im ersten Schritt werden nach Bedarf kombinierbare Bausteine – α, ω -funktionalisierte Makromoleküle – bestehend aus bis zu fünf Monomereinheiten für die modulare

Kettenverlängerung hergestellt. Ausgehend von einer Bismaleimidkerneinheit werden durch sukzessive Addition der jeweiligen Baueinheiten durch UV-Licht symmetrische sequenzdefinierte Dekamere erhalten.

Die eingehende Charakterisierung der sequenzdefinierten Makromoleküle auf ihre monodisperse Natur wird über Größenausschlusschromatographie (SEC), Kernspinresonanz (NMR) Spektroskopie und hochauflösende Orbitrap Elektrospray-Ionisation – Massenspektrometrie (ESI-MS) sowie Matrix–Assistierte Laser–Desorption–Ionisierung - Flugzeitmassenspektrometrie (MALDI-ToF) durchgeführt.

Table of Contents

Publications	I
Abstract	III
Zusammenfassung	V
Table of Contents	IX
1. Introduction	1
2. Theoretical Background	5
2.1. Efficient Synthetic Tools for Sequence-Definition.....	5
2.1.1. The Diels–Alder Cycloaddition.....	7
2.1.2. Photochemistry.....	10
2.1.3. Photoinduced Release of Thioaldehydes from Phenacyl Sulfides.....	18
2.1.4. Photoinduced Enolization of <i>o</i> -Alkylbenzaldehydes.....	20
2.1.5. Photoinduced Release of Nitrile Imines from Tetrazoles.....	23
2.2. Multicomponent Reactions.....	28
2.2.1. Passerini Three-Component Reaction.....	33
2.3. Sequence-Definition in Polymer Chemistry.....	37
2.3.1. Biopolymers: The Foundation for Synthetic Monodisperse Macromolecules.....	38
2.3.2. Artificial Sequence-Defined Macromolecules for Encoding.....	43
2.3.3. Thiolactone-Based Synthesis on Solid Support.....	47
2.3.4. Iterative Exponential Growth by Copper-Catalyzed Azide-Alkyne Cycloaddition.....	50
2.3.5. Sequence-Defined Oligomers <i>via</i> Radical Single Unit Monomer Insertion.....	52
2.3.6. Sequence-Defined Macromolecules by Multicomponent Reactions.....	55
2.3.7. Methylbenzaldehydes and Phenacyl Sulfides in the Synthesis of Sequence- Defined Macromolecules.....	59
3. Results and Discussion	63
3.1. A Combined Photochemical and Multicomponent Approach.....	64
3.1.1. Synthesis of the Passerini Linkers.....	65
3.1.2. Synthesis of the Photobuilding Blocks.....	72
3.1.3. Combining Photochemistry and Passerini Reactions for Sequence-Defined Macromolecules.....	77
3.2. Protection-free Sequence-Defined Macromolecules <i>via</i> λ -Orthogonal Photochemistry.....	84
3.2.1. Synthesis of the Building Units.....	85
3.2.2. Preparation of the Sequence-Defined Macromolecules by NICAL Ligation and DA Cycloaddition.....	96
3.3. Multifunctional Sequence-Defined Macromolecules <i>via</i> Photoligation.....	108
3.3.1. Synthesis of a Photomonomer Library.....	109
3.3.2. α,ω -Functionalized Macromolecules as Building Blocks.....	111
3.3.3. Synthesis of α,ω -Functionalized Macromolecules.....	115
3.3.4. Modular Synthesis of Symmetric Sequence-Defined Macromolecules....	117

4. Conclusion and Outlook.....	125
5. Experimental Section	131
5.1. Instrumental Data and Methods	131
5.1.1. Nuclear Magnetic Resonance (NMR) Spectroscopy	131
5.1.2. Electrospray Ionization Mass Spectrometry (ESI-MS)	131
5.1.3. Size Exclusion Chromatography – Electrospray Ionization Mass Spectrometry (SEC-ESI-MS)	132
5.1.4. Matrix Assisted Laser Desorption Ionization – Time of Flight Mass-Spectrometry (MALDI-ToF-MS)	132
5.1.5. Matrix Assisted Laser Desorption Ionization – Time of Flight – Time of Flight (MALDI-ToF-ToF).....	133
5.1.6. Size Exclusion Chromatography (SEC)	133
5.1.7. Spectrophotometry to Determine Source Emission Spectra.....	133
5.1.8. Custom Built Photoreactor Employed for Batch Reactions	133
5.1.9. Custom Built Photoreactor for Irradiation under Flow Conditions.....	135
5.1.10. Vapourtec E2 Flow Reactor	136
5.1.11. Flash Column Chromatography.....	136
5.1.12. UV-VIS Spectroscopy (UV-VIS).....	137
5.1.13. Fluorescence Spectroscopy.....	137
5.2. Materials.....	138
5.3. Synthesis Procedures and Analytical Data.....	139
5.3.1. Synthesis of Passerini Linker	139
5.3.2. Synthesis of Photosensitive Compounds.....	148
5.3.3. Synthesis of Building Blocks and Core Units	164
5.3.4. Photoreactions	193
5.3.4.1. Photoreactions of the Test Systems	193
5.3.5. Synthesis of Sequence-Defined Macromolecules	194
5.3.5.1. Combination Approach for the Synthesis of Sequence-Defined Macromolecules Based on P-3CR and <i>o</i> -MBAs	194
5.3.5.2. Protection Group Free Synthesis of Sequence-Defined Macromolecules Based on Tetrazoles and <i>o</i> -MBAs	203
5.3.5.3. Synthesis of Sequence-Defined Macromolecules Based on <i>o</i> -MBAs and Maleimides	212
List of Abbreviations.....	228
List of Figures and Schemes	231
Acknowledgments.....	238
Bibliography	240

1

Introduction

Sequence-defined macromolecules represent a unique class of polymers mimicking nature's monodisperse precision macromolecules. Essential for the execution of complex biological functions, such as information storage or enzymatic activity being vital to life, nature's macromolecules, i.e. DNA or proteins, feature absolute sequence-definition in their structure. The monomer sequence order plays an important role for the formation of the characteristic higher order structures, such as the DNA double helix by Watson-Crick base-pairing. Moreover, the monomer sequence order is responsible for the chemical information storage by coding of monomer units.^[1] For decades, scientists have been pursuing nature's precision trying to decipher its secrets. Almost 100 years after Staudinger's macromolecular hypothesis, scientists started to develop platforms to mimic nature's precision. First avenues to precision polymers in synthetic chemistry were accomplished by reversible-deactivation radical polymerization (RDRP) techniques, enabling highly organized multiblock copolymers.^[2-8] Although control over molecular weight, functionality, and polymer topology was established, nature's precision remained unachieved as only sequence-controlled polymers with dispersities above 1.0 were achieved. However, sequence-defined macromolecules additionally feature monodispersity ($\mathcal{D} = 1.00$) with a perfectly defined primary structure. Hence, sequence-defined polymerizations are the key to modern macromolecular chemistry being viewed for a long time as the "holy grail" of polymer science.^[9]

The field of sequence-defined polymerization emerged with Merrifield's work on solid-phase peptide synthesis in 1963, who was awarded with a Nobel prize in 1984.^[10-11] Ever since, natural and non-natural peptides,^[12-13] peptoids,^[14] glycopeptides,^[15] oligonucleo-

1. Introduction

tides,^[16] and conjugated oligomers^[17] exhibiting monodispersity became synthetically accessible. Moreover, artificial sequence-defined macromolecules based on non-naturally occurring motifs have been targeted by many research groups. Different strategies to produce sequence-defined oligomers were presented, including single unit monomer insertions (SUMIs) based on radical processes,^[18-22] liquid phase reactions under batch or flow conditions,^[23-24] exponential growth strategies^[23-25] as well as solid templates based approaches.^[26-28] Two strategies can be identified from the previous approaches, i.e. iterative addition of small single units or insertion of larger building blocks. Modular synthetic concepts with sequence-defined building blocks significantly contribute to the overall reaction efficiency by an accelerated increase of the molecular weight per chain extension step.^[29] Hence, potential applications can be identified in the fields of bioconjugation, photoresists, network formation for NMR orientation media or information storage.^[30-32] Recently, the formation of perfectly monodisperse sequence-defined macromolecules containing chemical information by coding monomer units for data storage materials, molecular bar coding or biological applications in synthetic enzyme design have drawn increased attention.^[29, 33-53] Mimicking nature in coding and decoding of information into synthetic molecules has become a key challenge in macromolecular chemistry.

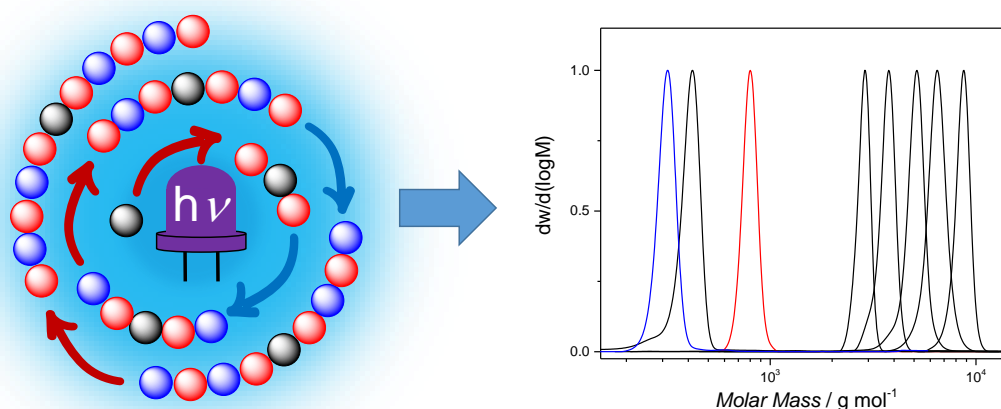


Figure 1. Graphical abstract for the photochemical synthesis of sequence-defined macromolecules.

The synthesis of sequence-defined macromolecules in multi-step approaches requires highly efficient coupling methods to ensure maximum conversion as overall yield decreases with each reaction step. Therefore, only a limited amount of reactions is viable for the synthesis

of sequence-defined macromolecules featuring simple, scalable, and orthogonal strategies. In the current thesis, monodisperse sequence-defined macromolecules are investigated employing advanced photochemical protocols initiating highly efficient coupling reactions. Moreover, the accurate placement of functional side chain groups at predetermined positions along the chain is explored. Photochemistry has the inherent advantage of simple reaction protocols as well as temporal and spatial control over reaction conditions. Photochemical protocols combined with highly efficient ‘click’ reactions provide truly a powerful platform for the synthesis of sequence-defined macromolecules. In the following sections, an overview about efficient synthetic tools and the state of the art is given by selected examples of monodisperse macromolecules.

2

Theoretical Background

The current introductory chapter addresses the theoretical background of specific aspects of the thesis, providing a concise overview of the synthetic methods employed in the current thesis as well as selected examples of sequence-definition. A short summary of highly efficient coupling methods for the synthesis of monodisperse macromolecules is described, focusing on light induced Diels–Alder (DA) cycloadditions and nitrile imine carboxylic acid ligation reactions. Thus, fundamental background of photophysics and photochemistry is discussed (Section 2.1). Subsequently, multicomponent reactions are reviewed as an advantageous approach for the introduction of additional chemical functional moieties into sequence-defined macromolecules in one reaction step. In addition, reaction mechanisms underpinning the employed synthetic methods are discussed (Section 2.2). The final section of the theoretical background addresses the state of the art of sequence-definition and selected examples of monodisperse macromolecules are presented (Section 2.3). Efficiency of the conjugation methods, degree of polymerization, advantages, and disadvantages as well as fields of applications are discussed in the final sections.

2.1. Efficient Synthetic Tools for Sequence-Definition

Given nature's precision in generating monodisperse macromolecules, sequence-defined polymers represent a unique class of macromolecules. However, only a limited amount of reactions is suitable for the synthesis of sequence-defined macromolecules. The synthesis of

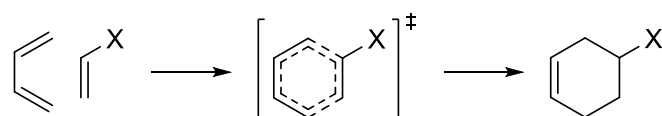
2. Theoretical Background

sequence-defined macromolecules in multi-step approaches requires highly efficient coupling methods to ensure maximum conversion as overall yield decreases with each reaction step. In addition, a high level of orthogonality of the employed reactions is desirable to prevent the formation of undesired side products on the one hand – on the other hand – orthogonality of chain extension steps allows the incorporation of numerous functional groups into the polymer backbone. Consequently, ‘click’ reactions are suitable to ensure the monodisperse nature of macromolecules with different monomer units placed at exact positions along the chain in synthetic polymer chemistry. In 2001 Sharpless and co-workers introduced the concept of ‘click’ chemistry and defined a precise set of parameters including modularity, simple reaction conditions or very high yield, to name a few, and a wide scope of further prerequisites to classify such highly efficient reactions.^[54] For instance, nucleophilic addition to alkenes or alkynes and opening of strained rings, such as aziridines or epoxides, are representative for the category of ‘click’ reactions. Cycloaddition reactions, such as the 1,3-dipolar cycloaddition and the [4+2] Diels–Alder (DA) reaction, are also classified as ‘click’ reactions. Hence, ‘click’ reactions are widely used for the synthesis of monodisperse macromolecules. Multicomponent reactions (MCRs),^[55] nucleophilic ring opening of thio-lactones,^[27] single unit radical monomer insertion (SUMI),^[19] copper-catalyzed azide-alkyne cycloaddition (CuAAC)^[24] or phosphoramidite chemistry^[56] have been applied for sequence-defined macromolecules among other highly efficient coupling reactions. However, photochemically driven cycloadditions entail mild reaction conditions and therefore enable spatial or temporal control over the reaction in contrast to thermally induced ‘click’ reactions.^[57-59] Thus, several examples of photoinduced ‘click’ reactions, such as the DA cycloaddition, have been reported and employed for the synthesis of sequence-defined macromolecules.^[21-22, 60-62] Photochemical approaches potentially extend the synthetic toolbox of techniques that can be used for preparing monodisperse multifunctional sequence-defined macromolecules. The present work exploits light induced processes to synthesize sequence-defined macromolecules. Photochemical strategies and the underpinning photophysics are discussed in the following section including photoinduced pericyclic cycloadditions as well as nucleophilic reaction types, significantly contributing towards a high level of control over the sequence-defined macromolecular formation processes.

2.1.1. The Diels–Alder Cycloaddition

Some Diels-Alder (DA) reactions represent one class of the so-called ‘click’ reactions as defined by Barry Sharpless fulfilling the strict criteria, such as being modular, selective, wide in scope, and high in yield.^[54] Cycloadditions can readily be executed at ambient temperatures and the resulting products can be obtained in high purity and in a regioselective manner. In principle, DA reactions are thermally allowed according to the Woodward-Hoffmann (W-H) rules but they can also be conducted under irradiation of light in some cases.^[63] Already in 1906 Albrecht reported the addition of cyclopentadiene to 1,4-benzoquinone, however, suggesting a reductive addition of cyclopentadiene to a methylene group of 1,4-benzoquinone rather than a cycloaddition.^[64] Later, in 1928, Diels and Alder identified the cyclohexene derivative arising from the [4+2] cycloaddition of cyclopentadiene to benzoquinone and proposed a reaction mechanism.^[65-66] Diels and Alder were subsequently awarded with the Nobel prize for their work on elucidating the mechanism of [4+2] cycloadditions.^[66-75] The extensively studied DA reaction enables facile trapping of reactive ene and diene species featuring ‘click’ criteria and thus manifold applications within organic chemistry have been developed.^[76] Among other ‘click’ reactions, DA cycloadditions, such as the photoinduced conjugation of thioaldehydes or *o*-methylbenzaldehydes (*o*-MBAs), show ‘click’ characteristics to enable efficient coupling of building units in a sequence-defined manner.^[59, 77-81]

DA cycloadditions are widely used synthetically to prepare six-membered rings. In **Scheme 1**, a general concerted DA reaction mechanism is depicted.^[82-83] Pericyclic reactions, such as the cycloaddition of an alkene (a dienophile) and a diene, proceed *via* a six-membered transition state, breaking and forming bonds simultaneously, thus resulting in a cyclohexene derivative. Consequently, in a DA reaction, no intermediates are generated in-between the reactants and the cycloadduct. The π -orbital symmetry state is a prerequisite for the development of stabilizing interactions in the transition state. The W-H rules allow the prediction



Scheme 1. DA reaction of a diene and a dienophile occurs *via* a six-membered transition state in order to form a cyclohexene derivative. Reproduced with permission of Springer.^[82-83]

2. Theoretical Background

of reaction behavior, addition products as well as reaction barrier heights based on the preservation of orbital symmetry. Accordingly, symmetry of the involved π -orbitals must be retained over the course of the reaction. A cycloaddition occurs in a suprafacial way when the same orbital lobe of a p -orbital or p -orbitals lobes on the same side of a conjugated π -system are involved in a new bond formation. Antarafacial behavior describes the opposite case, i.e. when both orbital lobes of a p -orbital or p -orbital lobes on both sides of a conjugated π -system contribute to a new bond formation (**Figure 2**). Thermal stimulation leads to DA additions occurring in a suprafacial configuration of the involved π -molecular orbitals (MOs), whereas stimulation by light leads to an antarafacial configuration of the pericyclic reaction. It is interesting to note that antarafacial cycloaddition conducted under thermal conditions is only possible for large systems and as a consequence antarafacial configuration of MOs is not occurring for [4+2] cycloadditions.^[84-85] In addition to the π -orbital symmetry, the energy gap between the frontier orbitals of the two reactants is a fundamental prerequisite for the formation of DA cycloadducts. In order to understand and predict the reactivity as well as the regioselectivity of pericyclic reactions, the frontier molecular orbital (FMO) theory has proven to be an efficient method.^[86] The regioselectivity in pericyclic reactions is related to the highest overlap between the orbital lobes of the FMOs. Therefore, equally polarized FMOs with the largest orbital coefficients form the strongest bonding interactions. Both reactants, diene and dienophile, approach each other in approximately coplanar orientation, which permits stabilizing interactions between the reactants' FMOs. For steric reasons, only the *cis*-conformation of the diene is able to advance into the transition state, while the *trans*-configured diene does not participate in a concerted pericyclic reaction.^[63] According to the FMO theory, the DA reaction is classified as a [4 π s+2 π s] cycloaddition. As depicted in **Figure 3**, three types of electron demand can be identified. A DA cycloaddition with normal electron demand occurs when the smallest energy gap is formed by the strongest bonding

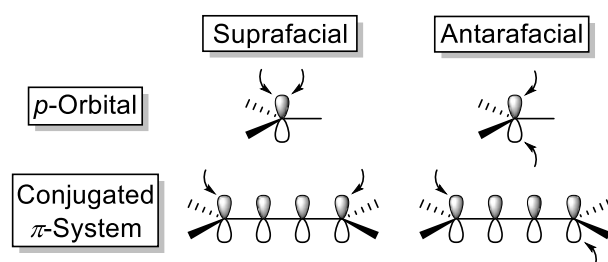


Figure 2. Exemplary illustration for a suprafacial and an antarafacial reaction progression for p -orbitals and p -orbitals in conjugated π -systems.^[84-85]

interaction between the highest occupied molecular orbital (HOMO) of the diene and the lowest unoccupied molecular orbital (LUMO) of the dienophile, since orbitals that are closest in energy interact most strongly with each other. An inverse DA reaction takes place when the smallest energy gap is formed by the LUMO of the diene and the HOMO of the dienophile.^[87] In general, the energy levels of the MOs can be influenced by introducing electron withdrawing or donating groups. Generally, electron withdrawing groups (EWG) lower the energy of the LUMO and electron donating groups (EDG) raise the energy of the HOMO.^[82-83, 85] A common example for normal electron demand, which was reported by Diels and Alder themselves, is the cycloaddition of cyclopentadiene and maleic anhydride.^[66] Cyclopentadiene is a relatively electron rich diene and maleic anhydride possesses two electron withdrawing carbonyl groups, thus the two reactants are reactive towards the formation of DA cycloadducts. An inverse electron demand DA cycloaddition proceeds when an electron poor diene and a dienophile equipped with an EDG react, for example, the addition of acrolein and ethyl vinyl ether. Furthermore, the DA cycloaddition can not only form carbon-carbon bonds, but also carbon-heteroatom bonds (Hetero-DA).

Moreover, DA reactions are reversible, the cycloreversion of the DA adduct to the starting components is referred to as retro-Diels–Alder (rDA) reaction. One of the best investigated rDA reactions is the thermal decomposition of a dimeric cyclopentadiene moiety to a monomeric cyclopentadiene in the presence of an iron containing catalyst.^[88] Furthermore, furan and maleimides form DA cycloadducts, which can be reopened under thermal treatment

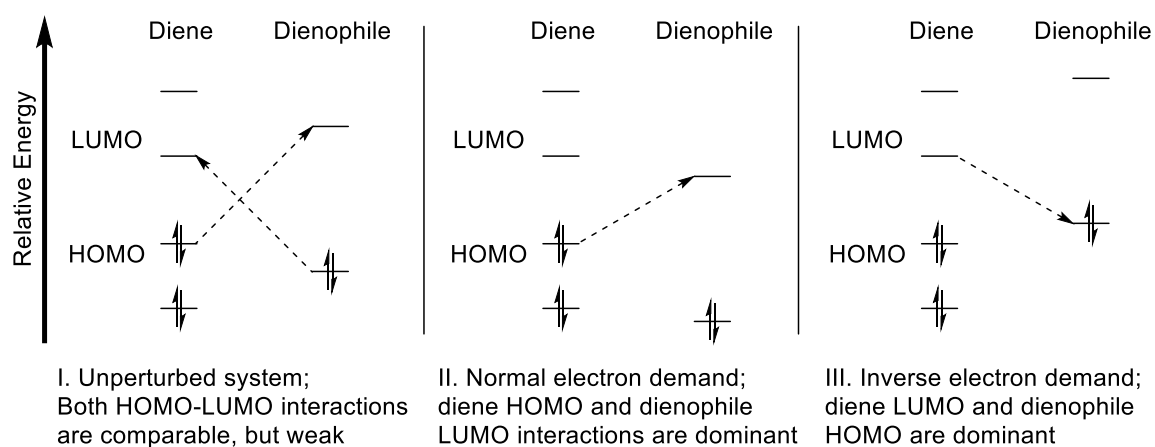
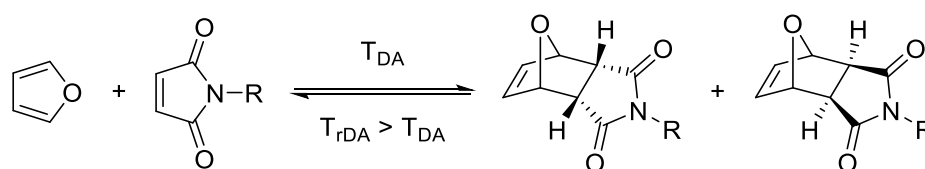


Figure 3. General mechanism of the concerted [4+2] cycloaddition and FMO interactions in DA reactions for unperturbed, normal, and inverse electron demand systems. Reproduced with permission from Springer.^[82-83]

2. Theoretical Background

($T_{rDA} > 70\text{ }^{\circ}\text{C}$) to release the starting components as depicted in **Scheme 2**.^[89] Maleimides represent a class of highly reactive dienophiles owing to their ring strain as well as the EWGs lowering the energy of the LUMO. Therefore, maleimides are widely used in macromolecular chemistry for polymer-polymer ligation to synthesize block copolymers, for instance, or for DA driven polymer immobilization reactions on surfaces with spatial resolution.^[80, 90-92] Since the DA cycloreversion of the furan-maleimide DA cycloadduct can already be observed at temperatures starting from $70\text{ }^{\circ}\text{C}$, mild conditions can be employed for the rDA reaction in macromolecular chemistry to reduce thermal induced polymer degradation. In the current thesis, DA trapping of maleimides employing furans was used as a protection group strategy to cage the reactive dienophile and thus enable macromolecular ligation on demand by preventing the maleimide from undergoing undesired oligomerization.



Scheme 2. Diastereomers (endo/exo adducts) obtained from the DA reaction between furan and maleimide. Thermal treatment leads to a rDA reaction and release of the starting materials.

DA and rDA reactions between furan and maleimides were used as protection/deprotection steps to enable sequence-defined polymerization on demand.^[60] Furthermore, light induced DA trapping of *o*-quinodimethanes generated from *o*-MBAs using maleimides and fumarates as dienophiles was investigated offering efficient coupling methods in order to obtain larger monodisperse macromolecules. Therefore, specific aspects of photochemistry and photoinduced DA reactions are discussed in more detail in the following sections.

2.1.2. Photochemistry

Light plays a key role in fundamental natural processes, for example in photosynthesis. For decades, researchers were investigating photoinduced biological processes but the first synthetic photochemical transformation was observed by Trommsdorff when he exposed san-tonin to UV-light observing a color change in 1834.^[93] Ever since light driven reactions drew scientific attention and first synthetic approaches have been reported by Ciamician and Silber in the early 1900s.^[94-98] In parallel, Planck developed the groundbreaking theory that

light has a quantum nature in 1901 leading into a fundamental investigation of photophysics.^[99-100] He investigated the spectral energy of electromagnetic radiation in a black body and postulated that the energy is quantized, which can be described by $E = nh\nu$, where n is the integer quantum number, h is the Planck constant, and ν is the oscillator frequency. Later, in 1905, based on the work of Planck, Einstein explored the photoelectric effect and proposed the quantum equivalence law to quantify photophysical processes.^[101] Ever since the first photochemical transformations and fundamental discoveries in photophysics have been reported, photochemistry finds application in a variety of chemical reactions. For instance, photoinduced reactions have been implemented in the field of organic chemistry leading to the synthesis of a variety of natural compounds. Light induced reactions have also been used for coupling macromolecules to form block copolymers, intra- or intermolecular cross-linking or surface functionalization in polymer science.^[80, 90, 102] In contrast to thermally controlled reactions, the main advantage of photochemistry is the spatial and temporal control over the reaction, since the reaction proceeds as long as irradiation in the desired area is continued. The advantages of light suggest that photochemistry is a possible powerful avenue towards monodisperse macromolecules.

Fundamentally, primary photochemical or -physical reactions are driven by excitation of electrons to higher energy levels leading to fluorescence or phosphorescence after absorption of energy. In general, two fundamental laws must be satisfied for photochemical transformations: (i) the Grotthus-Draper law – also referred to as the principle of photochemical

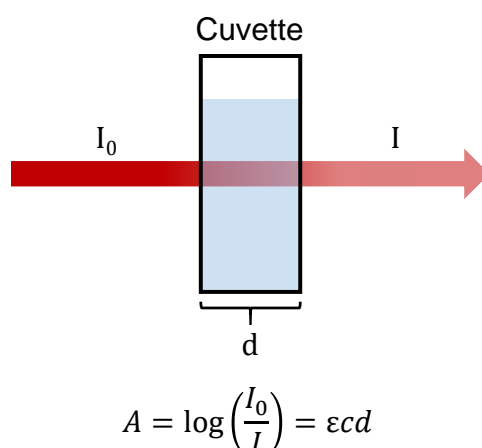


Figure 4. Illustration of Beer-Lambert's law for the determination of the Absorbance A of a light absorbing moiety, where I_0 is the incident intensity of the light source, I the transmitted intensity, ϵ the wavelength depending extinction coefficient, c the concentration of the absorbing molecule, and d the length of the absorption path.^[106]

activation – which states that photochemical processes are only initiated when a system absorbs light being the basis for fluorescence and phosphorescence;^[103] (ii) the Stark-Einstein law – the so-called photoequivalence law – which states that with each absorbed photon, a primary chemical or physical reaction is triggered.^[104] Furthermore, the absorption efficiency of a particular species can be determined by its quantum yield Φ , being defined as the ratio of light quanta involved in a resulting chemical or physical event, such as absorption, fluorescence or transformation reactions.^[105] Within the scope of photochemical transformations, the Beer-Lambert's law (**Figure 4**) is also important as it describes light absorption. For a given solution concentration c and path length d of the cell, the exponential attenuation of initial monochromatic light intensity I_0 passing through the solution results in the decreased transmitted intensity I . The molar extinction coefficient ϵ represents the absorbance strength of a solution or molecules in a solution at a given wavelength.^[106]

In 1935, Jablonski developed a method to graphically display photochemical processes induced by the irradiation of light as depicted in **Figure 5**.^[107] Changes in the chemical structure after light absorption are photochemical processes and are thus not described in the Jablonski diagram. The photophysical processes illustrated are based on the electronic states of an excited molecule and associated relative energy levels including absorption and emission of light (fluorescence and phosphorescence) as well as non-radiative transformations of

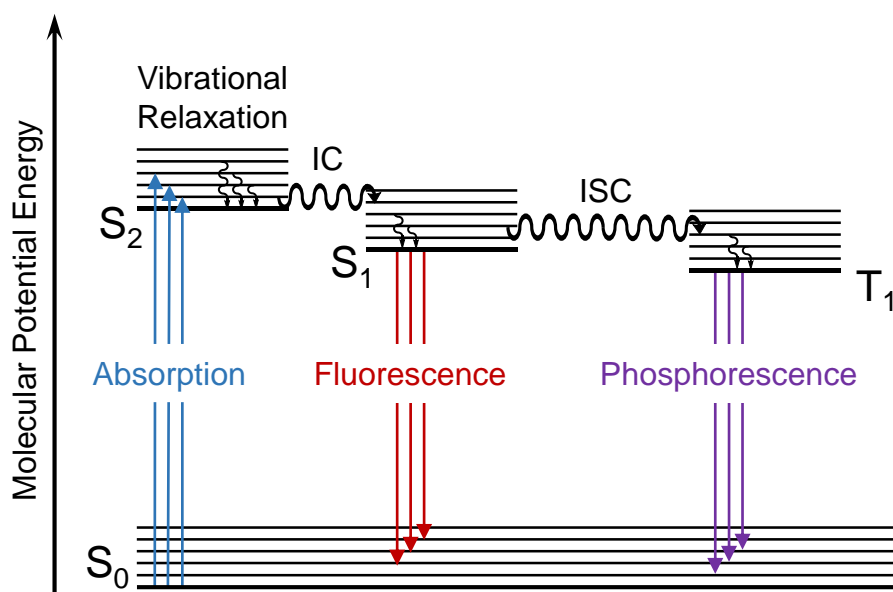


Figure 5. Schematic Jablonski diagram showing radiative and non-radiative photochemical transitions. The electronic energy levels are portrayed in a simplified way to illustrate internal conversion (IC) and intersystem crossing (ISC) as well as the principle of fluorescence and phosphorescence.^[107]

the respective excited states into each other considering inherent spin orientations like singlet and triplet states without bond cleavage. The transition probability between electronic states is described by the Franck–Condon principle as illustrated in **Figure 6**.^[108] According to quantum mechanics, the electronic state of a molecule can only accept certain quantized values, where a state is described by a wave function and an associated energy value. When the vibrational wave functions of two different states overlap significantly, the probability of an electronic transition is at its maximum. After irradiation of light, a molecule is excited and promoted from its electronic ground state (singlet state S_0) to an excited singlet state S_n by absorption of light. After excitation a range of radiative and non-radiative transitions can be performed based on the excited state. The molecule can relax to the lowest vibrational state of an excited singlet state S_n of the same multiplicity by vibrational relaxation. Spin allowed radiationless transfer into lower excited singlet states S_{n-1} or to the ground state S_0 can occur by internal conversion (IC) followed by vibrational relaxation. If the transfer from

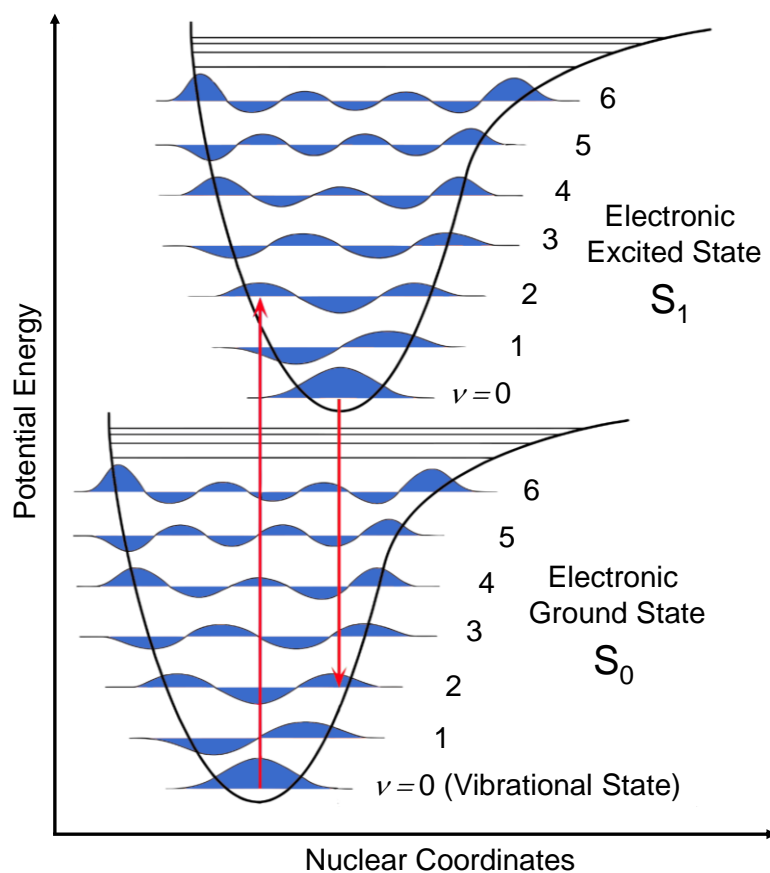


Figure 6. The Franck-Condon principle with vertical depicted electronic transitions between electronic states with the highest overlap of the vibrational wave function.^[108]

2. Theoretical Background

the excited singlet state S_1 into the singlet ground state S_0 is executed *via* emission of electromagnetic radiation, the process is referred to as fluorescence, with lifetimes in the magnitude of nanoseconds. Due to the Stokes shift, the emitted radiation displays a lower energy than the absorbed light and therefore a longer wavelength. The Stokes shift can be described by two effects. After absorption or emission, the electrons are rarely in the respective vibronic ground state of the electronically excited state or of the electronic ground state, leading to a non-radiative relaxation into the respective vibronic ground state. However, the stronger effect in most cases is the solvent relaxation. A spin-forbidden radiationless transfer of an electron from an electronically excited energy level (e.g. excited singlet state S_1) to another electronically excited energy level (e.g. excited triplet state T_1), which is executed under spin inversion by spin-orbit coupling is referred to as inter system crossing (ISC). Efficient ISC occurs when the energy gap ΔE_{ST} [kJ mol⁻¹] between the two excited states is sufficiently small. The energy gap ΔE_{ST} is larger for carbonyl compounds (n to π^* excitation, small orbital overlap) and is smaller for aromatic compounds (π to π^* excitation, significant orbital overlap). After vibrational relaxation into the lowest vibrational state of the excited triplet state T_1 , the molecule can return to its ground state S_0 under emission of radiation, being referred to as phosphorescence. The lifetime of phosphorescence can be above milliseconds up to hours, since the quantum mechanical forbidden transition between a singlet and a triplet state proceeds at lower rates.^[106] Other than the above described radiative and non-radiative transitions, excitation can also lead to a photochemical reaction, such as dissociation, isomerization, addition/insertion as well as abstraction/fragmentation.^[109-110]

In general, several electron transitions can be observed relative to the molecular electronic configuration. In an irradiated molecule, the energetically lowest electronic transition occurs by excitation from the HOMO into the LUMO exhibiting the smallest energy gap. An overview of the absorption regions is visualized in **Figure 7**. The electronic absorption wavelength range of irradiated organic molecules crucially relies upon the origin of electrons, mainly originating from $2s$ and $2p$ atom orbitals and are subject of electronic transitions. Depending on the interaction of associated atom orbitals that are responsible for bond formation, several types of MOs are developed. As a result, bonding σ and π , non-bonding n , and anti-bonding σ^* and π^* MOs are formed. Non-bonding n orbitals, originating from heteroatoms, such as oxygen, nitrogen, or halogens, are occupied by lone pair electrons, which

are not involved in direct bond formation.^[106, 111]

σ to σ^* transitions from the energetically highest bonding electron pair (σ) to the energetically lowest antibonding electron pair (σ^*) occur primarily in saturated hydrocarbons at wavelengths below 190 nm.

π to π^* transitions occur from occupied bonding π MOs to unoccupied antibonding π^* MOs – for instance in aromatic systems – when π electrons are involved in a bond formation. The energy gap between π to π^* transitions can be influenced by the size of the molecules conjugated π system.

n to π^* transitions from the localized n MOs of free electrons that are occupying the HOMO to delocalized antibonding π MOs exhibit a low UV-Vis intensity resulting from a poor orbital overlapping due to the spatial separation of n and π^* orbitals. Thus, transitions between localized n orbitals and delocalized π^* orbitals are forbidden.

Charge-Transfer (CT) transitions occur for strongly polarized molecules with delocalized non-bonding MOs, for example in electron-donor-acceptor complexes including organic or transition metal complexes. Upon irradiation, excited electrons are delocalized over the entire system resulting in the absorbance band being shifted towards higher wavelengths (red-shift).

A molecule's absorption behavior can be observed by UV-Vis spectroscopy, wherein the electronic transitions can be visualized as their absorption bands. As illustrated in **Figure 7**,

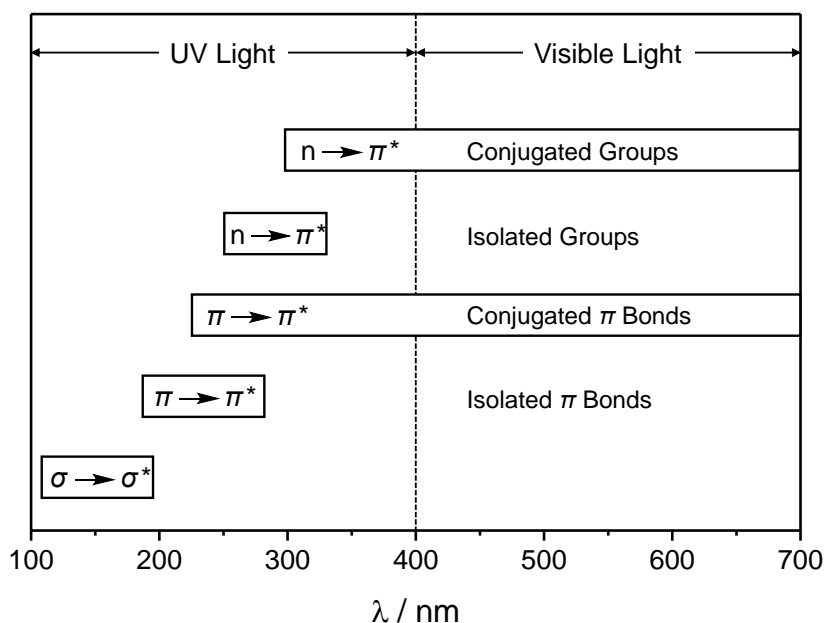
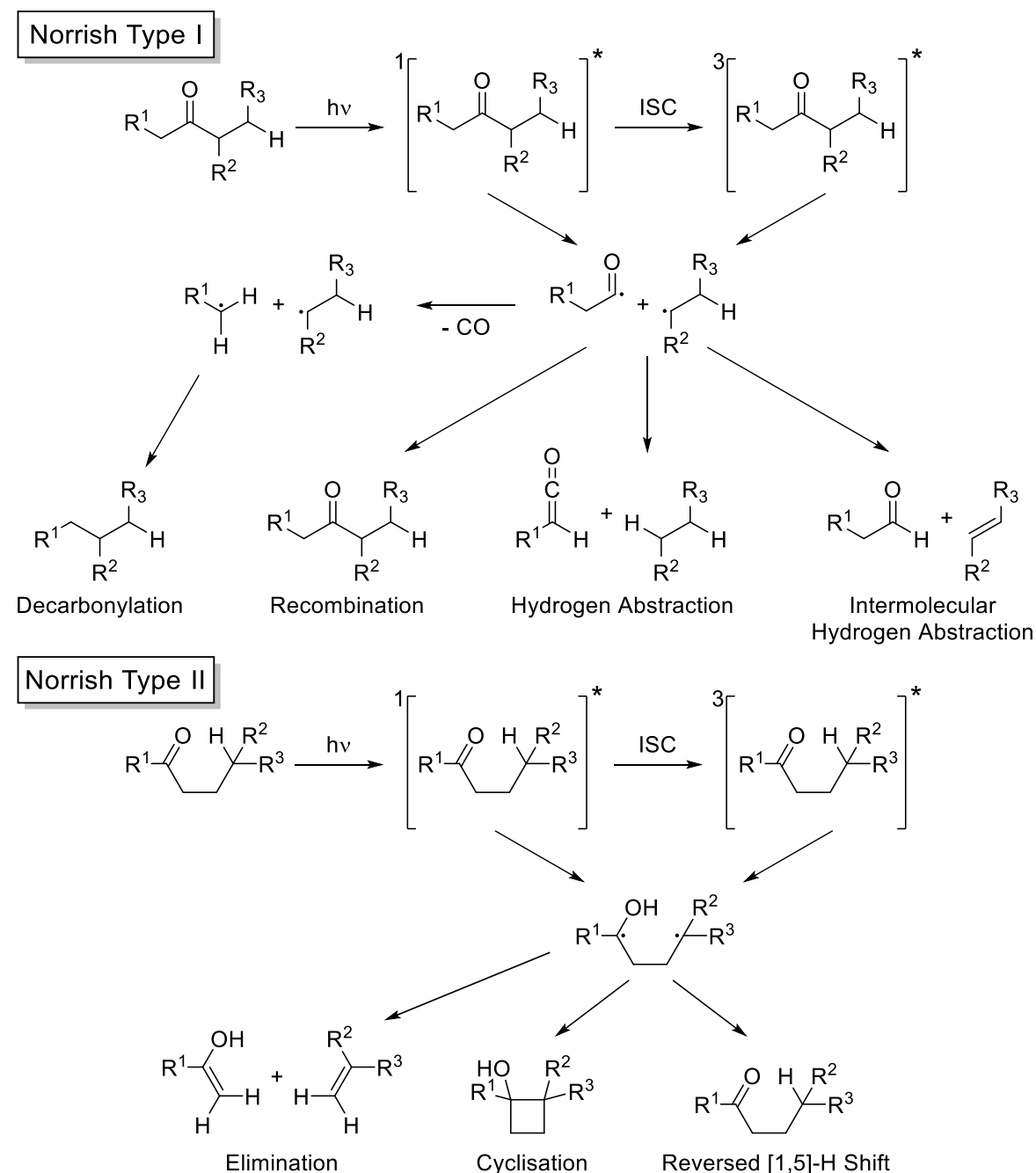


Figure 7. Visualization of the absorption wavelengths in relation of the main electronic transitions in organic molecules occurring upon irradiation of light.^[111]

2. Theoretical Background

only π to π^* as well as n to π^* transitions of conjugated aromatic systems can occur above 400 nm in the visible light region. Therefore, using conjugated systems as substituents influences the absorption spectrum by shifting a molecule's absorption towards higher wavelengths (bathochromic effect), enabling photochemical transformations under mild conditions. The bathochromic effect can further be induced by electron accepting groups with an



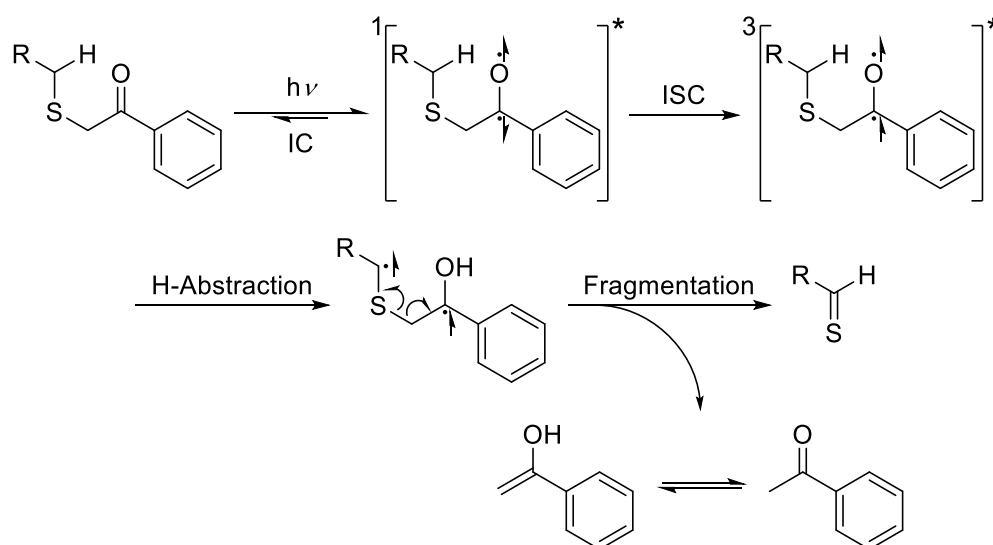
inductive effect, lowering the energy levels of HOMO, LUMO, and *n*-orbitals, as well as electron donating groups, lifting the energy levels of HOMO and LUMO.

Norrish and coworkers studied photochemical reactions in solution systematically for the first time to identify mechanisms behind photochemical processes.^[112-114] Decomposition of carbonyl compounds, such as aldehydes and ketones, was investigated and two mechanistic types of photodecomposition were identified – the Norrish type I and Norrish type II reactions as illustrated in **Scheme 3**. A carbonyl compound is excited by the absorption of photons generating singlet state radicals and triplet state radicals after ISC. The Norrish type I reaction results in alkyl and acyl radicals by carbon-carbon bond opening *via* α -cleavage from the excited carbonyl molecule. Due to the fact that the Norrish reaction leads to highly reactive radical intermediates, multiple reaction pathways are possible displaying a low selectivity. As a consequence, the formed radicals undergo recombination to form the starting material, decarbonylation and subsequent recombination as well as intra- and intermolecular hydrogen abstraction. The Norrish type II reaction results in a biradical intermediate *via* an intramolecular [1,5]-H shift of excited carbonyl functionalities either from a singlet or a triplet state. Subsequently, the biradical species is able to undergo a reversed [1,5]-H shift leading to the starting component, cyclization and elimination reactions.^[110, 115-118]

Various photochemical systems, for instance acyl sulfide ligation,^[60, 81, 119] anthracene dimerization,^[120-121] styrylpyrene cyclization,^[122-123] azirine ligation,^[124] *o*-MBA DA cycloaddition,^[59, 125] tetrazole reaction,^[90, 102] photoinitiated thiol-ene reactions^[126] or alkyne-azide cycloaddition,^[127] have been applied in polymer science for the synthesis of different polymer architectures or surface functionalization. Photoinduced release of thioaldehydes from phenacyl sulfides and subsequent DA trapping with dienes has already been employed for the synthesis of sequence-defined macromolecules (refer to Section 2.1.3 for further details).^[60] The *o*-MBA (refer to Section 2.1.4 for further details) and tetrazole ligation (refer to Section 2.1.5 for further details) for the formation of monodisperse oligomers are subjects of the current thesis. Therefore, photochemistry of thioaldehydes, *o*-MBAs, and tetrazoles are introduced in detail in the following sections.

2.1.3. Photoinduced Release of Thioaldehydes from Phenacyl Sulfides

Thioaldehydes have been used for the synthesis of natural products, such as opiate analgesics, and in the biosynthesis of aromatic amino acids in organic chemistry.^[128] Particularly, photogenerated thioaldehydes have been employed for the formation of sequence-defined macromolecules using an advanced photochemical protocol combining thioaldehydes and *o*-MBAs.^[60] In general, thiocarbonyl functionalities can be obtained by conversion of the corresponding oxygen carbonyl analogues with phosphorous pentasulfide or Lawesson reagent as well as elimination reactions.^[128-130] Vedejs *et al.* developed a light triggered, mild, and more straightforward approach towards thioaldehydes. A phenacyl sulfide (FAS) containing system has been used, which decomposes under irradiation of UV-light ($\lambda = 310 - 400$ nm) to acetophenone and a thioaldehyde moiety.^[131]



Scheme 4. Mechanism for the light induced formation of thioaldehydes generated from FAS groups.^[58]

Upon UV irradiation, a Norrish type II reaction pathway is followed. Consequently, after excitation, the FAS molecule is transferred from its ground state S_0 to its excited singlet state followed by an ISC to the excited triplet state T_1 . Afterwards, a hydrogen is abstracted in γ -position and subsequent fragmentation to acetophenone and a thioaldehyde species occurs as depicted in **Scheme 4**.^[58] Since Norrish type I decomposition occurs as an undesired side reaction, secondary reactions of photogenerated thioaldehydes lead to a complex product

mixture. By altering the substituents in the α -position to the ketone and using different solvents, undesired Norrish type I reactions leading to various side products can be suppressed. The *in situ* photogenerated thioaldehyde can be used for trapping reactions employing nucleophiles or dienes.

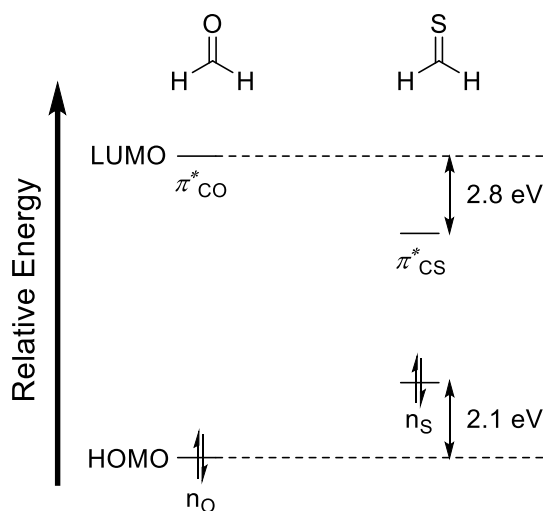


Figure 8. Comparison of FMOs of formaldehyde and thioformaldehyde as calculated by Vedejs *et al.*^[132]

Additionally, Vedejs *et al.* have reported that the reaction rates of thioaldehydes are higher owing to the electron withdrawing nature of the sulfur atom, leading to a higher conversion of in-situ trapped HDA products compared to the respective oxygen containing analogues. Consequently, side reactions, such as condensation reactions of thioaldehydes, are avoided because the HDA product is already preferably formed at ambient temperatures even with less activated dienes. MO calculations for the FMOs of formaldehyde and thioformaldehyde demonstrated that the HOMO and LUMO energy levels, being responsible for the reactivity, exhibit a smaller energy difference. In the molecular simulation, the HOMO and LUMO energy levels are approximately 2.1 eV higher and 2.8 eV lower in thioformaldehyde compared to formaldehyde, respectively (**Figure 8**).^[132] As a result, the energy gap between the HOMO-LUMO levels of dienes and thioaldehydes is smaller than the HOMO-LUMO gap of the respective oxygen containing analogues. As a consequence, thiocarbonyl compounds are more activated towards normal and inverse electron demand HDA reactions explaining a higher reactivity of the thioaldehyde group. The reaction is thus preferentially shifted towards the HDA product with accelerated reaction rates. However, the regioselectivity is reduced compared to that of HDA reactions of the respective oxygen containing analogues.

Due to the difference in electronegativity between oxygen and sulphur, the C=S carbon exhibits a lower polarization than the C=O carbon of the respective oxygen containing analogues. As a consequence, the MO coefficients of the C=S bond are equal providing reduced electrophilicity and thus exhibiting a lower reactivity towards nucleophiles and HDA reactions occur without regioselectivity resulting in a mixture of regioisomers. In general, the reactivity of thiocarbonyl compounds in nucleophilic reactions or HDA cycloadditions can be adjusted *via* the attachment of electron donating substituents decreasing the difference in polarity.^[132-133]

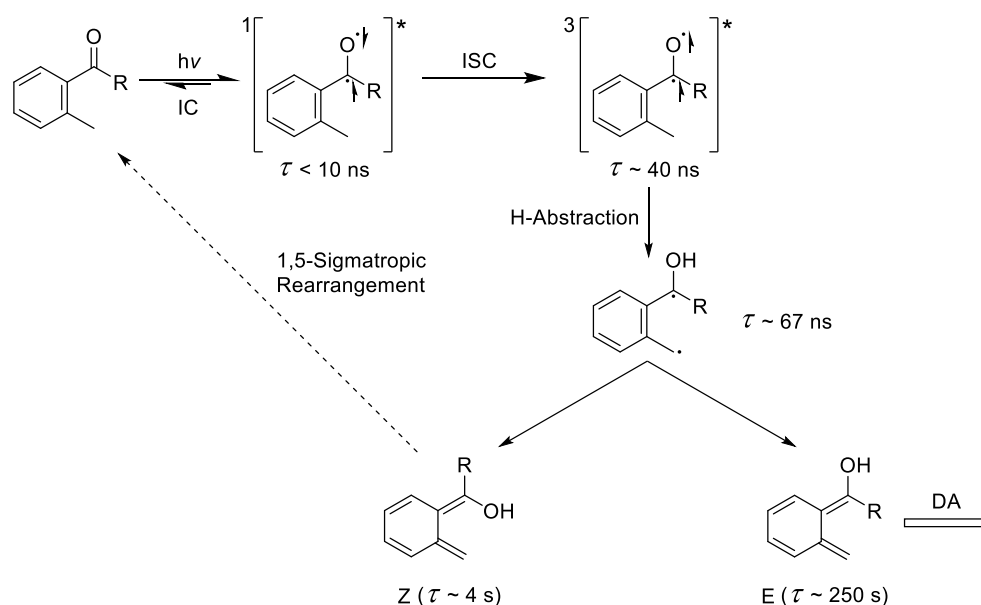
Substrates containing photogenerated thioaldehydes can be trapped *in situ* by nucleophiles, such as amines, oximes, or thiols, as well as *via* HDA cycloadditions benefiting from its reactivity and reaction compatibility. Different dienes, for instance cyclic dienes, e.g. cyclopentadiene or cyclohexadiene, as well as aliphatic dienes, e.g. 2,3-dimethyl butadiene (DMBD), sorbic acid, or sorbic alcohol, can be employed for the *in situ* trapping of photogenerated thioaldehydes *via* HDA cycloaddition. Barner-Kowollik and coworkers reported that thioaldehydes can be employed for spatially resolved surface patterning or achieve complex polymer architectures upon irradiation with UV-light ($\lambda_{\text{max}} = 355 \text{ nm}$).^[78, 81, 119, 134] The trapping reactions represent a highly efficient tool for the *in situ* formation of highly defined molecules to obtain monodisperse macromolecules. Zydziak *et al.* employed two bifunctional photosensitive building units carrying FAS groups and *o*-methylbenzaldehydes to demonstrate the generation of sequence-defined macromolecules *via* a photochemical protocol for the first time (for further details refer to Section 2.3.7).^[60] Based on the investigations of Zydziak *et al.*, photoinduced approaches for the formation of monodisperse macromolecules are investigated in the present thesis. Thus, the reactivity of *o*-alkylbenzaldehydes as well as tetrazoles upon irradiation of light are discussed in the following sections.

2.1.4. Photoinduced Enolization of *o*-Alkylbenzaldehydes

In the present thesis the photoinduced formation of dienes (i.e. *ortho*-quinodimethanes) generated from *o*-alkylbenzaldehydes was exploited for light induced DA cycloadditions to synthesize sequence-defined macromolecules. Yang and Rivas reported the photochemical enolization of benzophenones with alkyl group substituents in *ortho* position under UV influence for the first time.^[57] Mechanistic details of the *o*-quinodimethane formation from

2,4-dimethylbenzophenone – which is also referred to as photoenolization – was revealed by Porter and Tchir *via* flash photolysis conducted in cyclohexane.^[135] Later, Sammes investigated chemical trapping of dienol intermediates generated from 2-methyl- and 2-benzylbenzophenone by DA cycloaddition.^[136] An illustration of the photochemical mechanistic rearrangement of *o*-alkylbenzaldehydes and the lifetimes of the associated intermediates are depicted in **Scheme 5**.

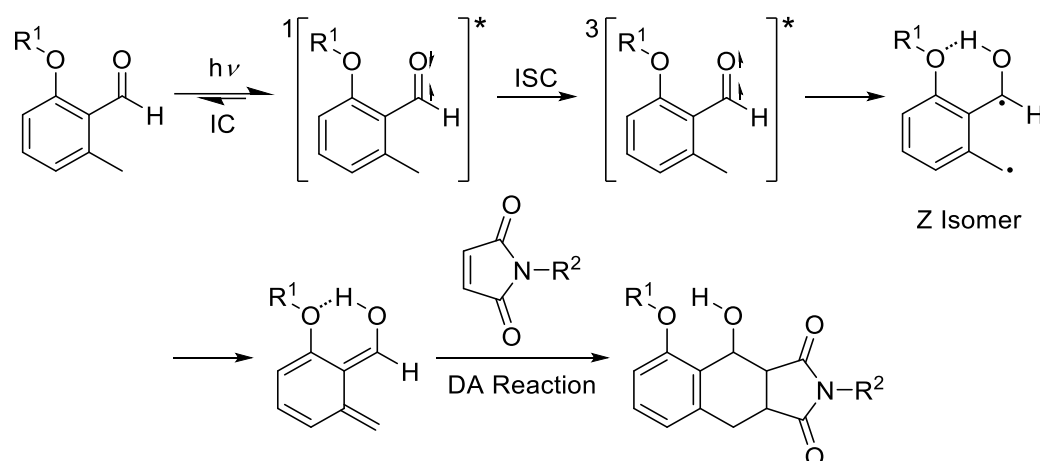
Mechanistically, the photoinduced rearrangement of *o*-alkylbenzophenone is a Norrish type II reaction. Upon irradiation, the 2-methylbenzophenone is excited from its singlet ground state S_0 to its electronically excited singlet state *via* an electronic n to π^* transition. Relaxation to the triplet state T_1 occurs *via* an ISC and subsequent hydrogen abstraction by rotation of the carbonyl group leads to the formation of two isomeric *o*-quinodimethanes. Herein, the (Z)-isomer, as it is depicted in **Scheme 5**, can undergo a 1,5-sigmatropic rearrangement resulting in the starting compound with a short lifetime of 4 s, whereas the (E)-isomer has the ability to perform DA cycloaddition trapping reactions because of steric reasons and its significantly longer lifetime of up to 250 s.^[135] Consequently, the (E)-isomer can be trapped *via* DA cycloaddition with electron poor dienophiles as demonstrated by Sammes and co-workers.^[136] In the absence of a reaction partner, the (E)-isomer undergoes a relaxation back to



Scheme 5. Mechanism and lifetimes of intermediates (for R = Ph) for the photoinduced enolization of *o*-alkylbenzophenones. Upon light absorption and the formation of excited singlet states, ISC occurs and leads to two isomeric *o*-quinodimethanes after hydrogen abstraction. The Z-isomer undergoes a 1,5-sigmatropic rearrangement to the starting material (singlet ground state), whereas the E-isomer is suitable as reactant for DA cycloadditions.^[135]

2. Theoretical Background

the ground state S_0 via hydrogen reversion. The lifetime of the (E)-isomer can be extended by exploiting stabilizing effects, i.e. hydrogen bonding in protic solvents. In addition, a stabilization effect of the isomer is achieved independent of solvent effects by a hydrogen accepting substituent in ortho position with regard to the aldehyde, which extends the lifetime by hydrogen bonding and therefore an increase in reaction rates can be observed (**Scheme 6**). DA cycloadditions carried out by employing *o*-MBAs as phototriggered dienes with dienophiles, such as maleimides, additionally benefit from the restoration of aromaticity. Thus, a reversed DA reaction is inhibited even at elevated temperatures, due to the fact that cycloreversion implies removing aromaticity and consequently, the DA reaction exhibits increased reaction rates towards [4+2] cycloadditions.



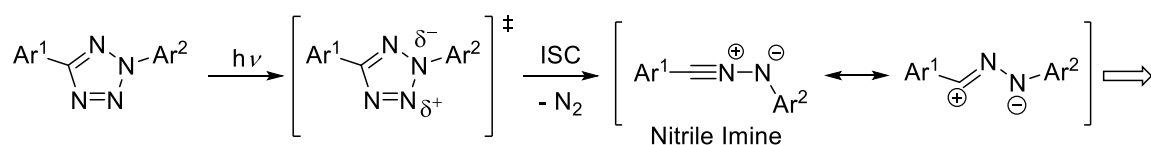
Scheme 6. Photoinduced transformation of an *o*-MBA into an *o*-quinodimethane intermediate (Norrish type II reaction) with stabilizing hydrogen bonding and subsequent DA trapping by a maleimide as dienophile resulting in a tetrahydro benzoisindole dione. Please note that the Z isomer, which is depicted in this scheme, possesses the same structural motif as the E isomer in **Scheme 5**. The categorization into E or Z isomers is derived from the Cahn-Ingold-Prelog priority rules and therefore no connection between reactivity and lifetimes can be drawn from the categorization into E or Z.^[135]

Interestingly, light driven *o*-MBA chemistry offers many advantages including high selectivity and orthogonality. Since the photochemical formation of reactive *o*-quinodimethanes is reversible, a transformation back to the electronic ground state is executed by both isomers, if no reaction partner is available. Thus, deactivation after irradiation is unnecessary because no unconverted *o*-quinodimethane moieties will remain after excitation and the starting compound will be regenerated. As a consequence, *o*-MBAs are a highly important photosensitive compounds as they can be combined with further photoresponsive groups, such as FAS or tetrazoles, enabling the generation of complex structures on demand – for example sequence-

defined macromolecules – *via* photochemical reactions in a λ -orthogonal manner.^[80, 137] The first photochemical attempt towards polymer conjugation using *o*-MBAs together with maleimides was reported by Barner-Kowollik and co-workers.^[138] Among other applications in functional polymers, a combination of *o*-MBA chemistry with thermally conducted ‘click’ reactions or supramolecular chemistry was exploited for the synthesis of triblock copolymers.^[77, 91] Moreover, the first attempt towards monodisperse macromolecules was demonstrated by Zydziak *et al.* with *o*-MBAs used in a combined approach by employing FAS groups as a second photosensitive moiety.^[60] Orthogonality, selectivity and efficiency of *o*-MBA ligation enables the straightforward synthesis of functional complex polymer architectures. Therefore, the UV-light triggered formation of *o*-quinodimethanes was investigated in the current thesis to obtain monodisperse sequence-defined macromolecules. Exploitation of *o*-MBAs as the single photoresponsive group as well as combined approaches together with Passerini multicomponent reactions and a λ -orthogonal approach with tetrazoles as the second photosensitive group were employed for the formation of sequence-defined macromolecules.

2.1.5. Photoinduced Release of Nitrile Imines from Tetrazoles

1,3-Dipolar cycloadditions find application in modern organic chemistry, especially in biochemistry 1,3-dipolar cycloadditions were found to be very efficient tools for bioconjugation. Already in 1959, the thermally induced decomposition of disubstituted tetrazole derivatives forming nitrile imine intermediates by the release of a nitrogen equivalent was reported.^[139] The highly efficient UV-light triggered formation of nitrile imines from 2,5-diphenyltetrazole was investigated by Huisgen and co-workers in 1967. A concerted reaction mechanism was proposed, where the 2,5-diphenyltetrazole is activated with UV-light between 280 - 320 nm generating a stable nitrile imine in-situ with quantum yields in the range between 0.5 and 0.9. The tetrazole moiety absorbs UV-light being excited to a higher singlet

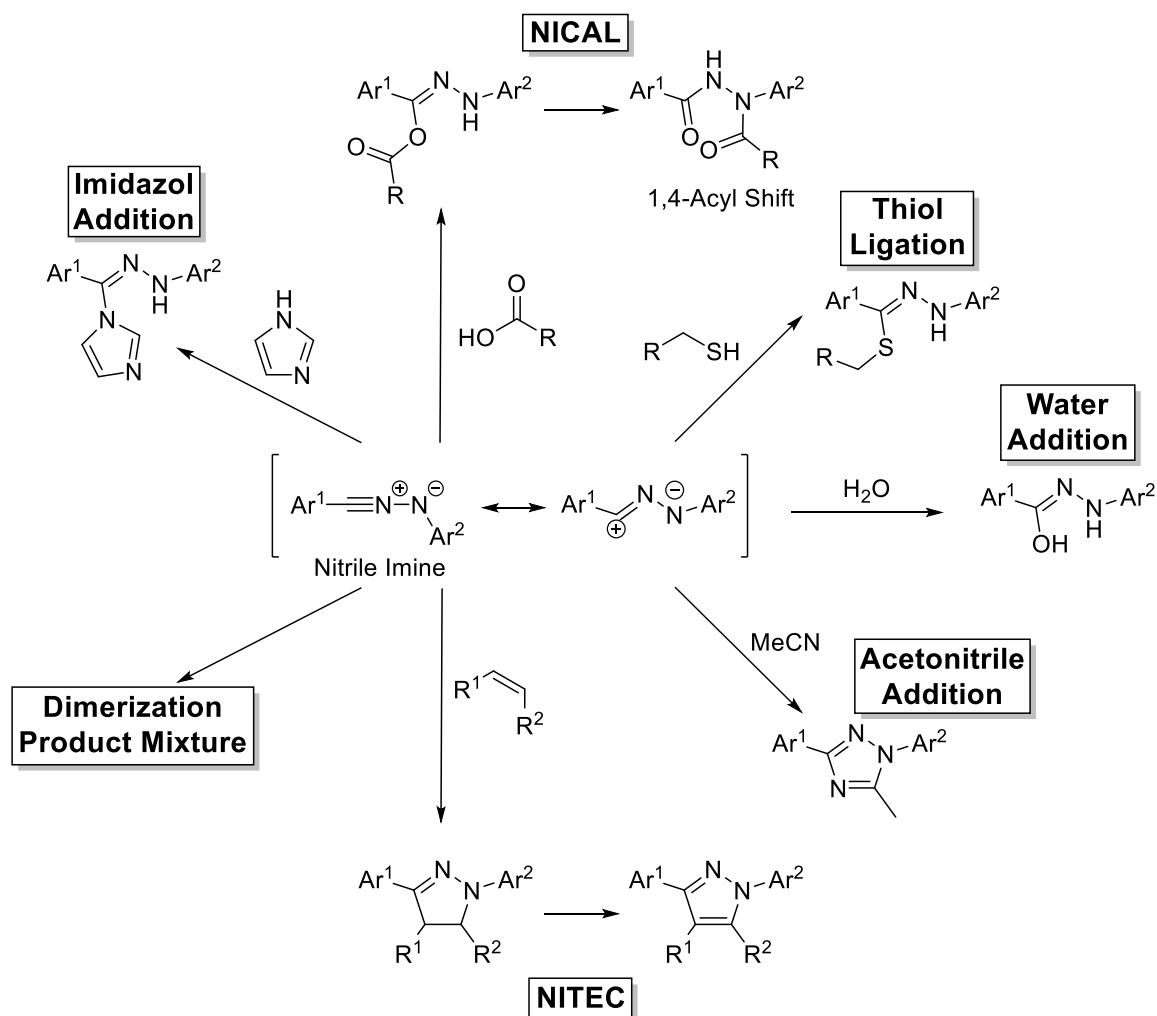


Scheme 7. Light induced decomposition of 2,5-disubstituted tetrazoles leading to the formation of nitrile imines, which can undergo subsequent reactions.^[140-142]

2. Theoretical Background

state. After ISC an equivalent of nitrogen is released and a nitrile imine is formed (**Scheme 7**).^[140-142]

The nitrile imine intermediate is reported to be a highly reactive 1,3-dipole (propargyl-allyl type) that can undergo ligation reactions with a wide range of reaction partners. The light induced 1,3-dipolar tetrazole-alkene cycloaddition was first reported in 2008 as a biorthogonal reaction and has been used in numerous chemical, biological, and material applications.^[143] Recent reports demonstrate the reaction between tetrazoles and various functional groups including electron-poor enes as well as reactions with nucleophiles, such as thiols,^[144] amines,^[145] water,^[146] acids,^[147-148] and heterocycles^[145] under similar conditions, questioning the orthogonality of tetrazoles. A brief reactivity overview of photogenerated nitrile



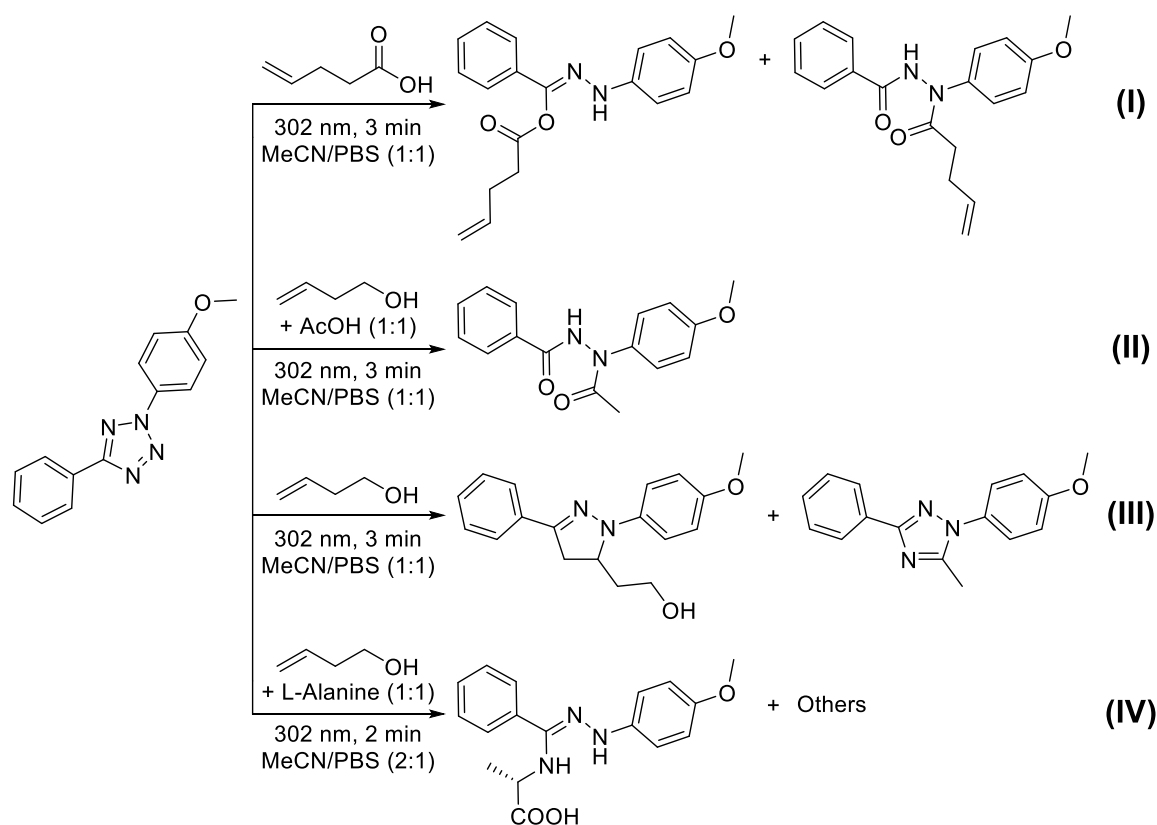
Scheme 8. Reaction overview of the intermediate 1,3-nitrile imine dipole generated by dissociation upon irradiation of tetrazoles. The adducts with imidazoles, carboxylic acids (NICAL), thiols, water, acetonitrile, double bonds, which are usually substituted with EWGs (NITEC), and self-dimerization, leading to a mixture of dimers, are depicted in clockwise order.^[143-149]

imines with various reaction partners is given in **Scheme 8**. The two most important ligation reactions in polymer chemistry are the so-called nitrile imine mediated tetrazole-ene cycloaddition (NITEC)^[149] and nitrile imine carboxylic acid ligation (NICAL).^[148] Upon the UV-light triggered release of nitrile imines, a [3+2]-cycloaddition reaction with an ene as dipolarophile is performed resulting in a fluorescent pyrazole adduct (NITEC reaction). The product of the reactive 1,3-dipolar intermediate and organic acids is a fluorescent mixture of a hydrazone anhydride and a hydrazide (1,4-acyl shift) after conducting the NICAL reaction.

Barner-Kowollik and co-workers introduced both ligation types for the precision design of polymer architectures. Employing both, a tetrazole and an *o*-MBA functional polymer, Hiltebrandt *et al.* introduced a strategy for λ -orthogonal photoligation in a one-pot reaction with maleimides or activated enes, which are selectively coupled to a photoenol moiety upon UV irradiation at 310 - 350 nm.^[80] Subsequent irradiation at 270 – 310 nm yields the NITEC adduct enabling a wavelength-orthogonal protocol for the synthesis of macromolecular architectures. Furthermore, the photochemistry of tetrazoles was exploited for the formation of fluorescent single chain nanoparticles. Small molecule studies were performed in order to establish both photoactivated nitrile imine reactions NICAL as well as NITEC ligation. The Tetrazole was activated at wavelengths close to 320 nm in the presence of a furan-protected maleimide and acetic acid as well as both reaction partners for comparison of the selectivity. As expected, the NITEC reaction leads to the formation of a pyrazoline adduct, whereas the nucleophile behavior of the acetic acid enables the NICAL ligation affording the tetrazole-acid adduct with high contribution of the acyl shifted product. If both reactants are present, the tetrazole-acid adduct is preferentially formed rather than the NICAL product with the non-activated alkene with a selectivity of 87 %.^[102, 148] Li *et al.* investigated the selectivity of photogenerated nitrile imines in nucleophilic reactions and cycloadditions with less activated enes to reassess its bioorthogonality.^[147] Therefore, a set of reactions was performed using 2-(4-methoxyphenyl)-5-phenyltetrazole in a mixture of acetonitrile and phosphate buffered saline (PBS) as illustrated in **Scheme 9**. First, the tetrazole was irradiated in presence of pent-4-enoic acid (100 eq.) resulting in the nucleophilic attack of the carboxylic acid forming the NICAL adduct with a selectivity of 71 %, while the expected 4,5-dihydro pyrazole conjugated product, originating from the NITEC reaction of the photogenerated nitrile imine and the ene, remained undetected (reaction I). Additionally, the selectivity between

2. Theoretical Background

NITEC and NICAL adduct formation was investigated employing a mixture of but-3-en-1-ol and acetic acid, which yielded the NICAL adduct (75 %) after irradiation exclusively (reaction II). Furthermore, the photoreaction of tetrazole and but-3-en-1-ol solely was carried out leading to the expected NITEC adduct formation as well as a NITEC adduct obtained from the cycloaddition of the nitrile imine intermediate and acetonitrile (reaction III). Moreover, the tetrazole was irradiated in a mixture of but-3-en-1-ol and L-alanine, whereas the nitrile imine-alanine adduct was obtained from the nucleophilic addition between the photo-generated intermediate and the N-terminus of L-alanine (reaction IV). In conclusion, it was demonstrated that tetrazoles undergo nucleophilic reactions potentially upon UV-irradiation, if the employed ene exhibits a low activation towards cycloaddition reactions. Nevertheless, the reaction behavior of tetrazoles in photoreactions can be readily tuned towards the intended adduct formation by the activity of the employed reaction partner.



Scheme 9. Overview of photoreactions carried out with a tetrazole and a mixture of a functionalized enes as well as nucleophiles in competition reactions in acetonitrile and PBS at 302 nm. It is demonstrated that the nitrile imine generated upon UV-irradiation favorably forms NICAL products or adducts obtained after a nucleophilic attack rather than a NITEC adduct with less activated enes.^[147]

Tetrazoles provide significant advantages since they are easily available by a straightforward synthesis and can readily be implemented into other systems. The tetrazole unit's absorption range can be tuned selectively between 254 - 410 nm by introducing appropriate substituents at the *N*-position of the tetrazole.^[150] Diaryl substituted tetrazoles, such as the 2,5-diphenyl tetrazole (290 nm) or 2-methoxyphenyl-5p-phenyl tetrazole (320 nm), require harsh UV-irradiation to release the reactive nitrile imine intermediate (refer to **Figure 9**). On the one hand, substitution with push-pull systems leads to a delocalization of the tetrazole π -electrons and thus to a red-shifting of the absorption (bathochromic shift). Accordingly, the substitution of tetrazoles with the push-pull substituent dimethylaniline, exploiting the delocalization of the tetrazole π -electrons, enables the light triggered release of nitrile imines at wavelengths of 365 nm.^[151] The absorption range can be shifted towards the visible light region by the utilization of larger delocalized π -systems, for instance pyrenes, decreasing the energy demand for the excitation of tetrazoles by irradiation as demonstrated by Lederhose *et al.*^[79] Consequently, the pyrene functional aryl tetrazole (PAT) can be excited at wavelengths in the visible light regime (410 - 460 nm) enabling NICAL ligation and NITEC reaction under mild conditions. Thus, the authors demonstrated polymer end-group modifications as well as block copolymer formation with visible light induced NITEC reactions. Profiting from the advantages of tetrazoles, visible light induced NICAL reactions using PAT were investigated in the current thesis for the protection-free wavelength-orthogonal formation of sequence-defined macromolecules by exploiting the excitation under mild conditions and selectivity of tetrazoles.

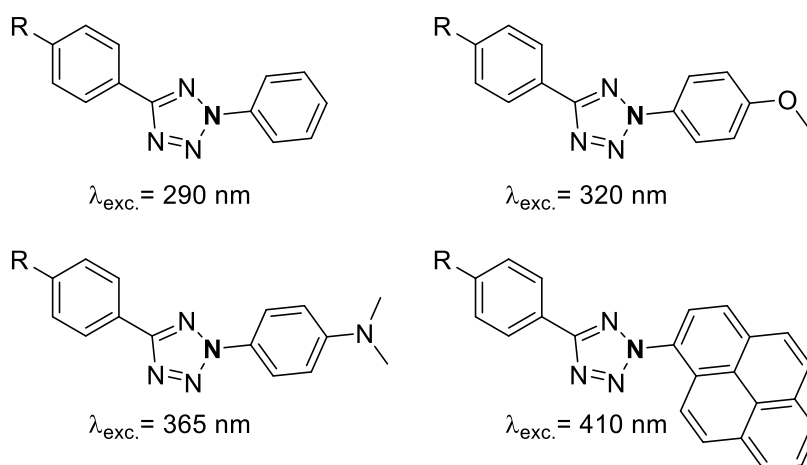
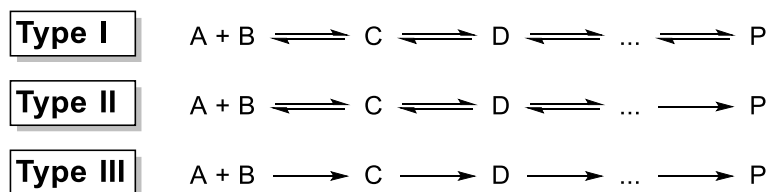


Figure 9. Tetrazoles with different substituents at their *N*-position and respective excitation wavelengths.^[79, 150-151]

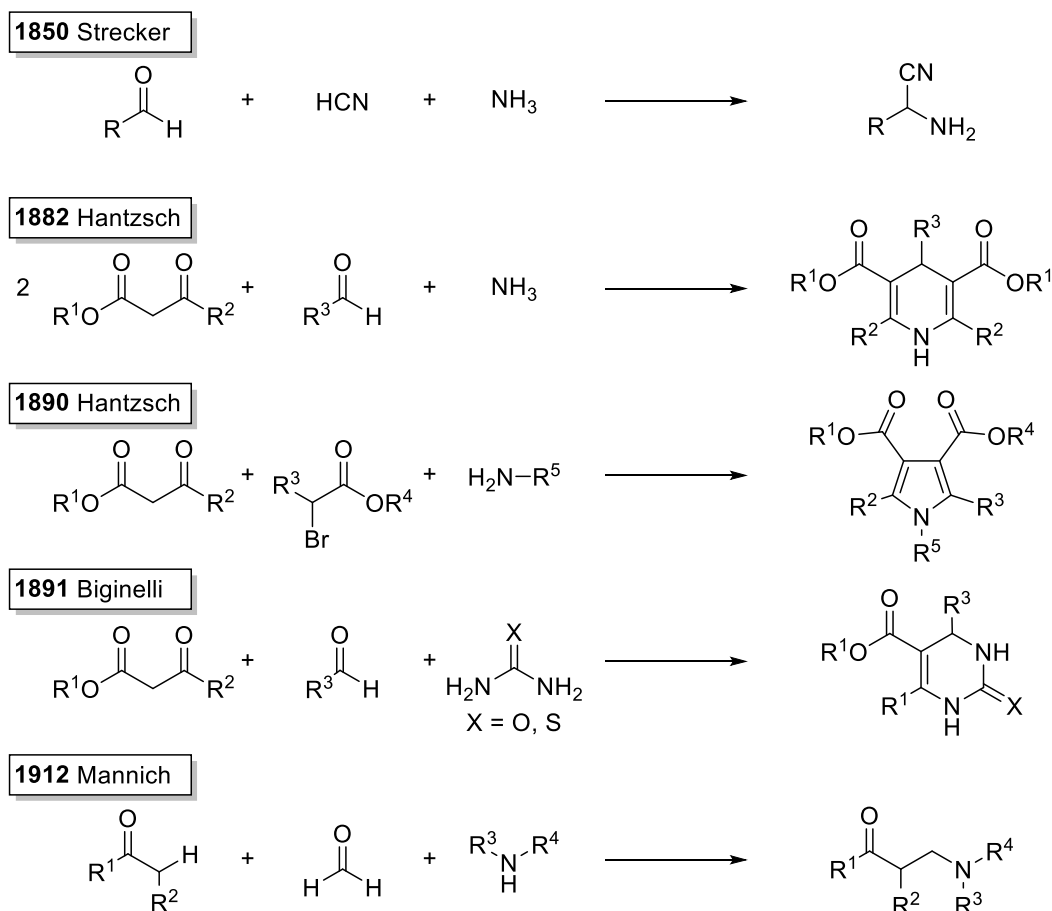
2.2. Multicomponent Reactions

In multicomponent reactions (MCRs), complex multifunctional structures are generated from three or more reactants in a one-pot reaction.^[152-153] Most atoms of the starting compounds are incorporated into the MCR adduct by the formation of covalent bonds with high yields, thus MCRs feature a high atom efficiency and enable the facile synthesis of highly functionalized compounds. Therefore, wide product libraries can potentially be obtained due to the high number of molecules that are incorporated in MCRs by simple variation of single reactants with molecules bearing the requested functionalities. Moreover, simple reaction conditions for most MCRs along with overall yields superior to multi-step reactions avoiding time consuming purification of intermediates enforce MCRs to be efficient tools for the synthesis of sequence-defined macromolecules. As illustrated in **Scheme 10**, Ugi and co-workers classified MCRs into three general reaction types with regard to their basic reaction mechanism.^[152] However, Ugi's differentiation is not strict and thus MCRs cannot always be categorized but rather occur in all the types as well as in smooth transitions between the three reaction types. Type I MCRs are characterized by equilibrium states of the single reaction steps leading to low yields as a function of the respective rate coefficients. In contrast, type III reactions completely consist of irreversible individual reactions and are mostly present in some naturally occurring biochemical reactions, however not in preparative organic chemistry. The type II MCR sequence consists of reversible as well as one last irreversible reaction step, which shifts the overall conversion towards the MCR-product and thus high yields are accomplished. The most popular examples for type II MCRs are the Passerini three-component reaction (P-3CR) and the Ugi four-component reaction (U-4CR), which have been employed for the synthesis of monodisperse macromolecules.^[55, 154]



Scheme 10. Classification of MCRs into three basic types with A and B as starting materials, C and D as intermediates, and P as final product. MCRs of type I are a combination of reversible equilibrium reactions. In type II MCRs the reaction step towards the final product is irreversible. Type III MCRs consist of a sequence of non-reversible individual reaction steps.^[152]

In **Scheme 11** the most important MCRs are depicted in chronological order. The first reported example of a MCR – published in 1850 – is the Strecker three-component reaction (S-3CR) for the synthesis of amino-acids being an example of a type I MCR.^[155] After imine formation of an aldehyde with ammonia followed by the addition of hydrogen cyanide yielding α -aminonitrile, a racemic mixture of amino acids is obtained by hydrolysis. In 1882, a condensation reaction of an aldehyde, ammonia, and two equivalents of a β -keto ester for the generation of dihydropyrimidines was reported by Hantzsch – the so-called Hantzsch four-component reaction (H-4CR).^[156] Hantzsch's discovery enabled the facile synthesis of Nifedipin – which is a commercially available drug sold under the brand name Adalat patented in 1967 – to manage hypertension, angina, or preterm birth. In addition, Hantzsch developed a three-component reaction (H-3CR) for the synthesis of pyrroles in 1890.^[157] Thus, pyrrole derivatives, featuring pharmacological properties for malaria treatment, can readily be obtained from β -keto esters, ammonia, and α -haloketones. Nearly simultaneously, Biginelli reported a three-component reaction (B-3CR) for the synthesis of aza-analogues of

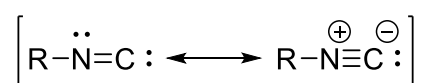


Scheme 11. Chronologically ordered important MCRs according to the reported synthetic routes from Strecker (1850), Hantzsch (1882 and 1890), Biginelli (1891), and Mannich (1912).^[155-160]

2. Theoretical Background

Hantzsch's dihydropyridines in 1891.^[158] The 3,4-dihydro-2(H)-pyrimidinone compounds are synthesized by the condensation of an aldehyde moiety with urea forming an imine, subsequently converted with a β -keto ester followed by intramolecular condensation. Likewise, B-3CR products exhibit biological properties for example as antitumor agents. Later, in 1912, the Mannich three-component reaction (M-3CR) was reported.^[159] The β -aminocarbonyl product is formed by the condensation of formaldehyde and an amine leading to the corresponding iminium-ion followed by the attack of an aldehyde or ketone moiety. M-3CR is employed for the synthesis of naturally occurring substances, for example in alkaloid syntheses.^[160] Due to the fact that MCRs are widely employed in the synthesis of pharmacologically active compounds, their crucial importance for past as well as contemporary chemistry is evident. In contrast to the MCRs introduced so far, there are two further important subclasses of MCRs, i.e. metal-catalyzed MCRs and isocyanide-based MCRs (IMCRs), where IMCRs pose a highly important class for the synthesis of monodisperse macromolecules. Thus, only IMCRs – namely the P-3CR and the U-4CR – will be discussed more detailed in the following section.

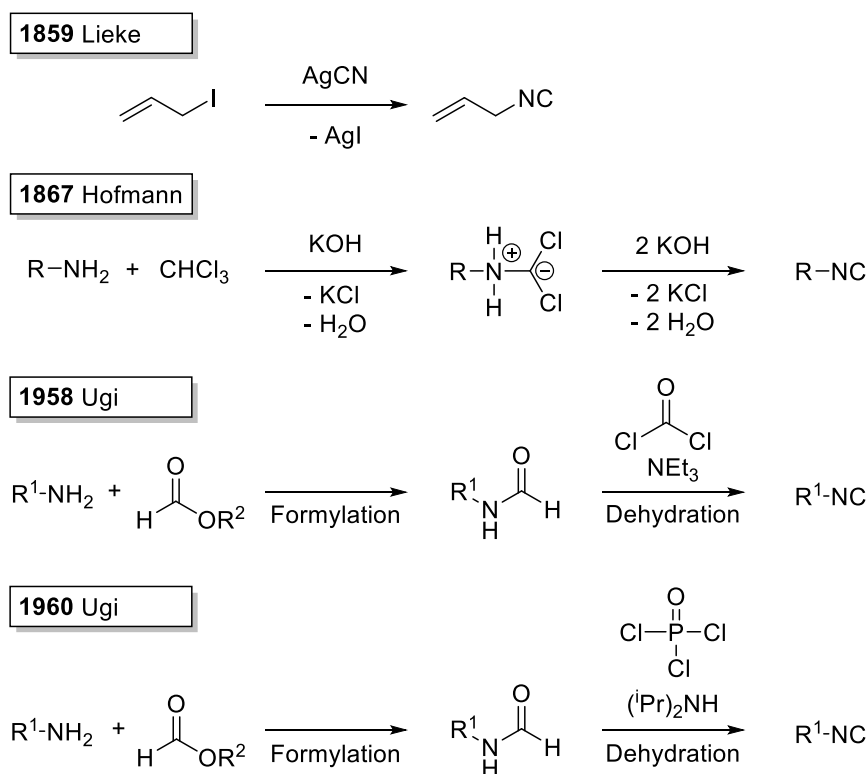
Due to the unique reactivity of isocyanides including α -acidity, zwitterionic, and carbene like behavior as well as the facile generation of radicals, IMCRs pose an interesting subclass of MCRs.^[153] In **Scheme 12**, two mesomeric resonance structures of isocyanides are illustrated, providing an explanation for their characteristic reaction behavior. One mesomeric structure of the isocyanide, also referred to as isonitrile, exhibits a carbene like configuration featuring a formally bivalent carbon atom, whereas the second structure describes a zwitterionic species. In comparison, only carbenes and carbon monoxide feature bivalent carbon atoms and have similar reactivity. Moreover, the ability to undergo nucleophilic reactions relies in the zwitterionic configuration while upon the nucleophilic attack the carbon is transferred into an electrophile subsequently allowing α -addition at the same position. Furthermore, isocyanides exhibit α -acidity and easily form radicals, which can be explained by the zwitterionic configuration displaying a positively charged nitrogen atom. Introduction of EWGs in α -position further increases α -acidity and the zwitterionic character. In addition,



Scheme 12. Mesomeric resonance structures of isocyanides are depicted including a carbene like and a zwitterionic configuration.^[153]

isocyanides are able to perform [4+1] cycloadditions with α,β -unsaturated carbonyls as reported by Chatani and co-workers.^[161] Interestingly, it was evidenced by high level valence bond calculations that the carbene like structure is the one predominantly responsible for the characteristic reaction behavior of isocyanides.^[162] Consequently, resting on the unique reactivity, isocyanides play a key role in MCRs and thus in the synthesis of versatile heterocyclic compounds.

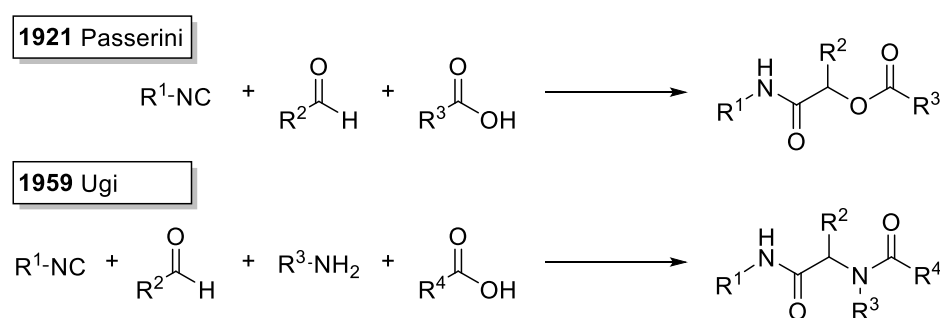
Already in 1859, Lieke developed a method to access isocyanides based on the substitution of allyl iodide with silver cyanide.^[163] However, the preparation requires heating of the reactants to 100 °C for three days and is therefore in any case unsuitable for achieving greater quantities. Lieke's target was the synthesis of allyl cyanide, only in 1868 Gautier verified the preparation of isocyanides by mesomeric structures formed between isocyanides and nitriles.^[164] Simultaneously, in 1867, Hofmann reported a method for the formation of primary isocyanides by the formation of phenylisocyanide from distillation of aniline, chloroform, and potassium hydroxide in alcoholic solution.^[165] Yet, it took almost 100 years until Ugi *et al.* developed a novel synthetic method towards isocyanides by dehydration of *N*-formamides by employing phosgene under basic conditions.^[166] Furthermore, Ugi *et al.* reported



Scheme 13. Overview of synthetic methods for the formation of isocyanides developed by Lieke (1859), Hofmann (1867), and Ugi (1958, 1960) in chronological order.^[163-167]

2. Theoretical Background

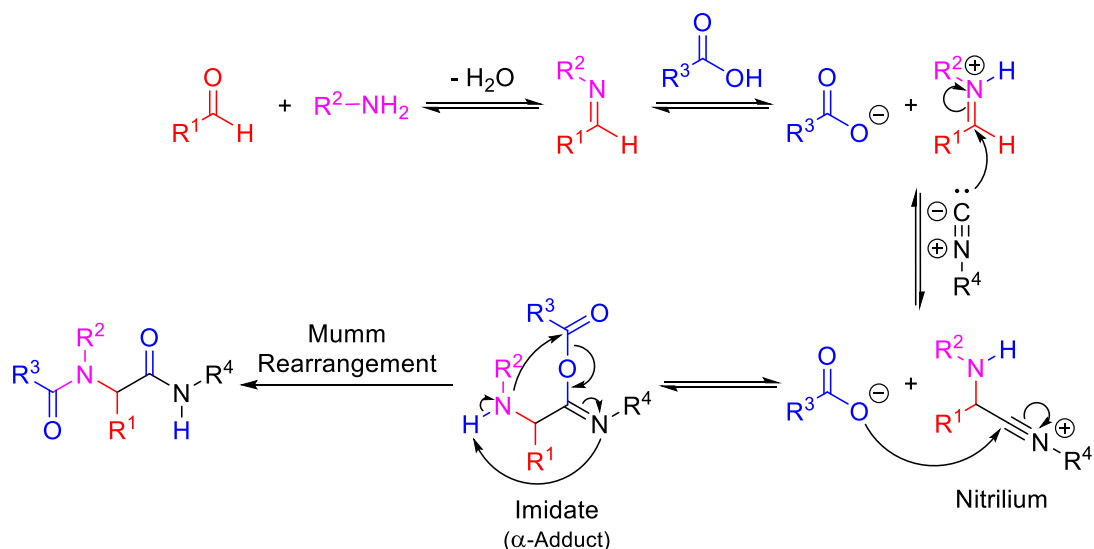
an alternative route by dehydration of the corresponding formamide utilizing phosphorous oxychloride in combination with secondary or tertiary amines as a base in 1960.^[167] Thus, the highly toxic phosgene was substituted while higher purity was achieved at comparable yields. Accordingly, a standard approach was established, still being used for the synthesis of isocyanides nowadays, although new methods have been developed. Nevertheless, the approach employing phosphorous oxychloride developed by Ugi was used for the synthesis of isocyanides in the current thesis.



Scheme 14. Overview of the IMCRs reported by Passerini (1921) and Ugi (1959).^[168-170]

The first IMCR was reported by Passerini in 1921 and will be discussed more detailed in Section 2.2.1. As depicted in **Scheme 14**, a carboxylic acid, an isocyanide, and a carbonyl compound (ketone or aldehyde) were employed to form an α -acyloxyamide under creation of a chiral center if a prochiral carbonyl compound is used.^[170] In 1959, Ugi investigated the U-4CR, one of the most common IMCRs, in which an amine moiety is added to the reactants that are employed in a P-3CR, additionally.^[168-169] Consequently, the amine allows the introduction of an additional functionality into the adduct in one step, leading to a wide range of substitution patterns. However, mechanistically, the U-4CR exhibits certain differences compared to the mechanism of the P-3CR (refer to **Scheme 15**). In the first step, the aldehyde and the amine moiety condensate to yield an imine followed by an imine activation *via* deprotonation of the carboxylic acid. Subsequently, α -addition of the isocyanide moiety is performed *via* a nucleophilic attack resulting in a nitrilium species. In the subsequent step, an imidate is formed by a nucleophilic attack of the deprotonated carboxylic acid. The desired product α -acylaminoamide is obtained in the final step after Mumm rearrangement. It is interesting to note that quantum mechanical calculations (modeling of energy and forces by density functional theory, DFT) revealed the nitrilium intermediate to be stable, which

was verified experimentally by the detection in electrospray ionization tandem mass spectrometry.^[171-173] In contrast to P-3CR, the U-4CR proceeds more efficiently in protic solvents, such as methanol. Nowadays, MCRs – IMCRs in particular – play an important role in preparative organic chemistry, since highly functionalized systems, heterocycles as well as pharmacological active compounds are readily accessible in a simple one-pot manner.^[174]



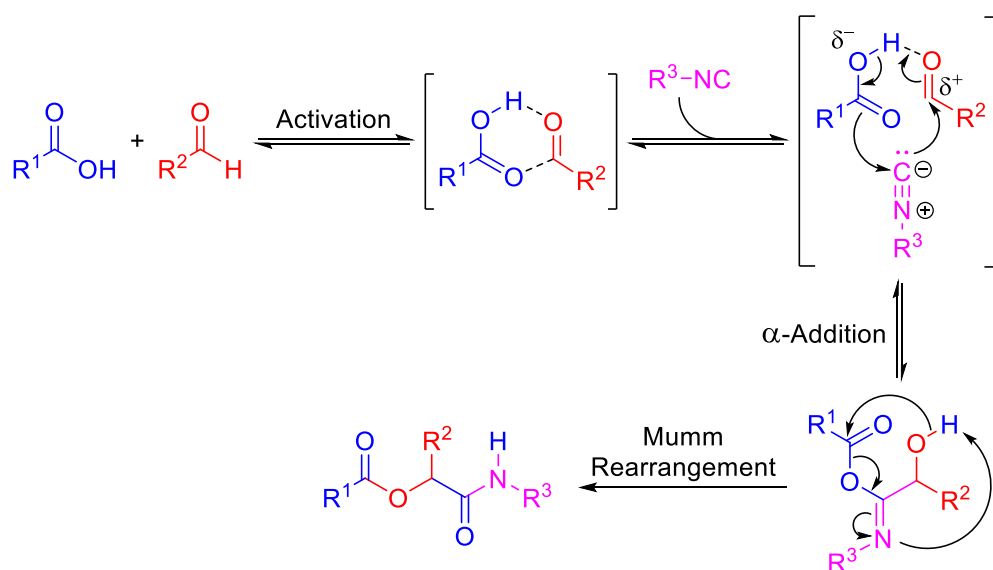
Scheme 15. Mechanism of the U-4CR as introduced by Ugi in 1961 and proposed by Fleurat-Lessard. After imine formation, a proton transfer proceeds from the carboxylic acid to the imine followed by an α -addition of the isocyanide. The α -acylaminoamide is formed after Mumm rearrangement.^[152, 171]

2.2.1. Passerini Three-Component Reaction

In 1921, Passerini developed an MCR in which a carboxylic acid, an isocyanide, and a carbonyl compound (aldehyde or ketone) was employed to synthesize an α -acyloxyamide under creation of a stereogenic center if a prochiral carbonyl compound is used.^[170] Even if the P-3CR was reported almost 100 years ago, the mechanism is not fully understood yet. Thus, various mechanisms have been discussed over the past decades. In **Scheme 16**, one plausible mechanism for the P-3CR is illustrated as investigated by Baker (1951) and Ugi (1961) in kinetic studies, whereas Passerini himself proposed a two-step mechanism.^[175-176] Thus, in the first step a six-membered transition state is formed leading to the activation of the aldehyde by the carboxylic acid. Subsequently, the isocyanide is inserted by a nucleophilic attack to the carbonyl group (α -addition). Thus, a hydroxylimine is formed leading to the desired α -acyloxyamide after Mumm rearrangement. In the proposed mechanism, only the final re-

2. Theoretical Background

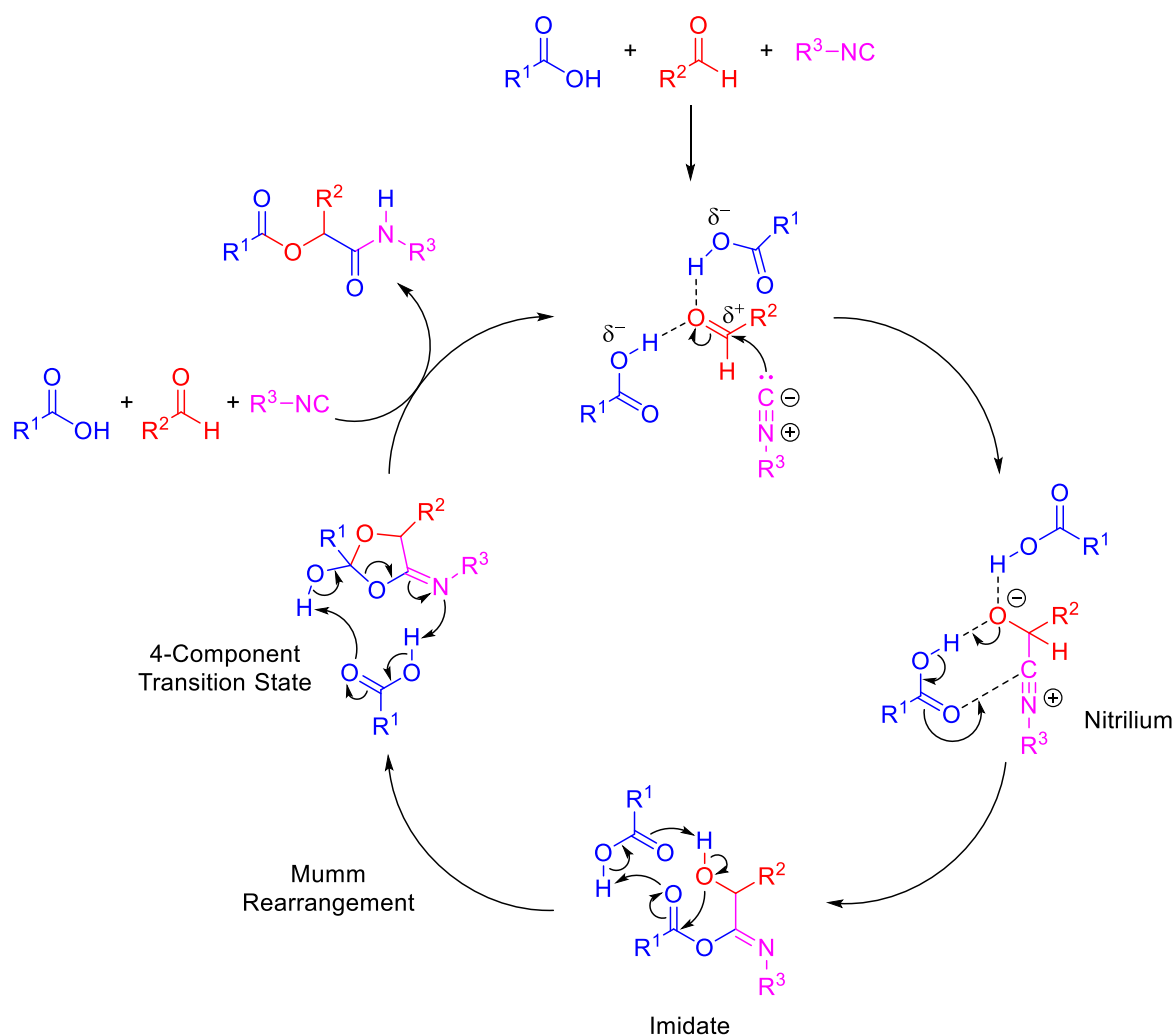
arrangement step is irreversible, therefore P-3CR is an example for type II MCRs. Commonly, the P-3CR shows highest conversions if conducted in aprotic solvents, such as dichloromethane (DCM), usually performed at ambient temperature and high reactant concentrations. The higher rates in aprotic solvents are in accordance with the proposed mechanism due to the fact that protic solvents interfere with the hydrogen bond formation of the six-membered transition state in the first step. In addition, the formation of a highly polar nitrilium species is prevented in aprotic solvents.



Scheme 16. Mechanism of the P-3CR proposed by Baker and Ugi. In the first step, a six-membered transition state is formed followed by the α -addition of an isocyanide species leading to the α -acyloxyamide after Mumm rearrangement.^[175-176]

Quantum chemical calculations *via* the artificial force induced reaction (AFIR) method in gas-phase performed by Maeda *et al.* suggest a four-component mechanism for the P-3CR in which a second carboxylic acid is involved as an organic catalyst in the final Mumm rearrangement step.^[177] In 2015, Morokuma and co-workers reported a revised mechanism based on high-level density functional theory (DFT) calculations as depicted in **Scheme 17**.^[178] In a first step, the aldehyde is activated by hydrogen bonding to carboxylic acids as already suggested by Passerini originally. Subsequently, the isocyanide is added in α -position of the aldehyde in a nucleophilic attack forming the nitrilium species. After one equivalent of the carboxylic acid is cleaved off, the imidate species is obtained. Due to a significantly lower energy of the transition state (TS) based on a second carboxylic acid, the Passerini adduct is formed in the final acid-catalyzed Mumm rearrangement. Since most of the

proposed mechanistic steps describe equilibria and only the final Mumm rearrangement is irreversible, the P-3CR can be regarded as type II MCR. The calculations carried out by Morokuma confirmed a second acid molecule as an organo-catalyzed P-3CR, however, it was postulated that the imidate formation is a stepwise process and not concerted as earlier reported. For a long time, the formation of the highly polar nitrilium species was questioned being in contrast with high yields obtained in aprotic solvents as the nitrilium formation is expected in protic solvents. In fact, aprotic solvents support the hydrogen bond formation between the carboxylic acid moieties and the aldehyde resulting in higher yields for the P-3CR. Even though Morokuma and co-workers reported the nitrilium to be stable in solution, based on their theoretical calculations, an experimental verification is still outstanding.



Scheme 17. P-3CR mechanism based on the DFT calculations of Morokuma and co-workers. Aldehyde activation by hydrogen bonding and subsequent nucleophilic addition of an isocyanide equivalent leading to a nitrilium species. The Passerini adduct is obtained after the addition of a carboxylic acid moiety and Mumm rearrangement.^[178]

2. Theoretical Background

Although the P-3CR mechanism is still under investigation, P-3CRs are widely employed in preparative chemistry, since highly functional products can be obtained in one-pot approaches. Pharmacologically active compounds are accessible through P-3CRs and therefore the reaction is often employed for the synthesis of pharmaceuticals in medicinal chemistry. Many P-3CR variants have been reported so far including substitution of the carboxylic acids by Lewis acids yielding α,β -unsaturated oxocarboxylic amides or Passerini-Smiles couplings employing electron poor phenols for the formation of α -hydroxyamides.^[153, 179]

In summary, structurally diverse P-3CR products are accessible in one-pot based on a wide range of commercially available starting materials. Consequently, the P-3CR represents a potential tool enabling the synthesis of monodisperse macromolecules exhibiting sequence-definition, additionally accomplishing the straightforward introduction of functional groups into the backbone of the macromolecules. P-3CRs were already employed for the formation of sequence-defined macromolecules by Meier and co-workers and thus the P-3CR is investigated with photochemistry as a combined approach in the current thesis.^[55, 180]

2.3. Sequence-Definition in Polymer Chemistry

A century after Staudinger understood macromolecules to consist of covalently bound monomer units, various scientific achievements have been made in modern polymer chemistry.^[181] Importantly, polymers were defined as “a substance composed of macromolecules” by the international union of pure and applied chemistry (IUPAC).^[182] Yet, naturally occurring polymers, such as specific proteins and deoxyribonucleic acid (DNA), are not only composed of macromolecules, however remain monodisperse and require a defined monomer order to fulfill the strict restrictions for their biological functionality. Consequently, such types of polymers are termed monodisperse sequence-defined macromolecules. Ever since, scientists keenly developed methods to mimic nature and achieve its precision in synthetic chemistry. One pathway was the development of reversible-deactivation radical polymerization (RDRP) techniques, for instance the atom transfer radical polymerization (ATRP), the nitroxide-mediated radical polymerization (NMP), or the reversible addition fragmentation chain transfer (RAFT) polymerization.^[183-187] A combination of controlled polymerization techniques not only enables the control over molecular weight, functionality, polymer topology, and dispersity, but also the synthesis of sequence-controlled polymers. Thus, narrow molecular weight distributions close to 1.0 can be achieved and precise block copolymers can be designed. Yet nature’s precision remained unachieved.

Lutz, Ouchi and Sawamoto defined **sequence-controlled** polymers to have monomer units, which are arranged in an ordered fashion.^[36] However, **sequence-defined** macromolecules additionally feature monodispersity ($\mathcal{D} = 1.00$) with a perfectly defined primary structure. Still, the terminology in the area of sequence-defined macromolecules is under discussion.^[188-189] Further, monodisperse macromolecules are also referred to as sequence-ordered polymers, yet both terms, i.e. sequence-ordered and sequence-defined, describe polymers with a precisely defined chain length and monomer sequence.^[190] Nevertheless, synthetic monodisperse macromolecules have been introduced to the scientific community by many working groups including biopolymers, such as peptides, peptoids, or oligonucleotides. In the current thesis, monodisperse sequence-defined macromolecules are investigated employing advanced photochemical protocols. In the following section, an overview about the state of the art is given and selected examples of monodisperse macromolecules are presented.

2.3.1. Biopolymers: The Foundation for Synthetic Monodisperse Macromolecules

From a historical point of view, the field of synthetic sequence-defined macromolecules was firstly approached through the pioneering work of Merrifield in 1963^[10] by the introduction of solid-phase peptide synthesis (SPPS) for which he was awarded the Nobel prize in 1984.^[11] The method allowed the synthesis of biopolymers, such as oligomeric peptides, and enabled the succeeding automation of the biopolymer synthesis process. The concept was later applied for the synthesis of natural and non-natural peptides,^[12] glycopeptides,^[15] oligonucleotides,^[16] and peptoids.^[14]

Peptide synthesis on a solid support offers significant advantages, for example the simple purification by filtration and washing off the solid support, minimizing the loss of product and intermediates during purification.^[19] However, the reagents need to be employed in high excess in order to ensure complete conversion. As solid support, a resin consisting of cross-linked copolymerized styrene and 1,4-vinyl benzene can be employed. After swelling in organic solvents, the linker units are accessible for post modification. In **Figure 10**, an overview of frequently employed resins and the respective linker units are depicted. Solid-phase based synthesis of peptides requires a carefully selected protecting group protocol, in which the respective amino acids are equipped with orthogonal protecting groups to avoid undesired cleavage from the resin, or coupling reactions yielding unintended product mixtures. Therefore, the amino acids are protected at the *N*-terminus to enable peptide synthesis by the successive addition of *N*-protected amino acids. The first amino acid is introduced with the *C*-terminus of the amino acid being covalently linked to the linker unit at the solid

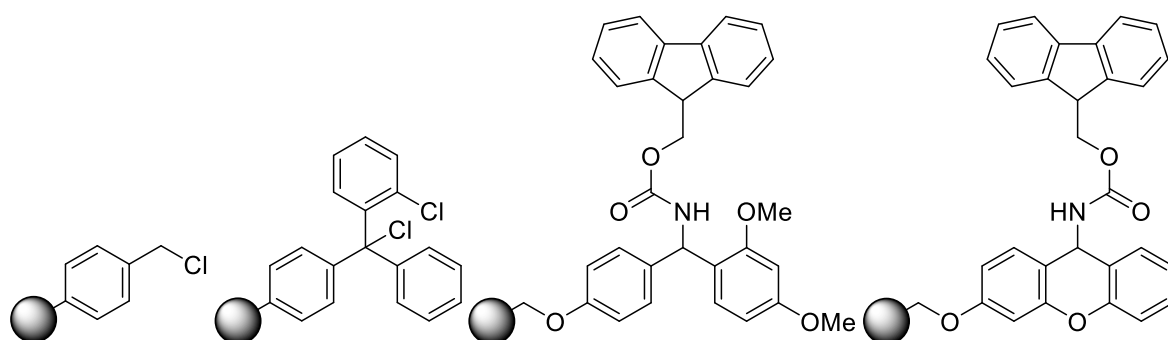
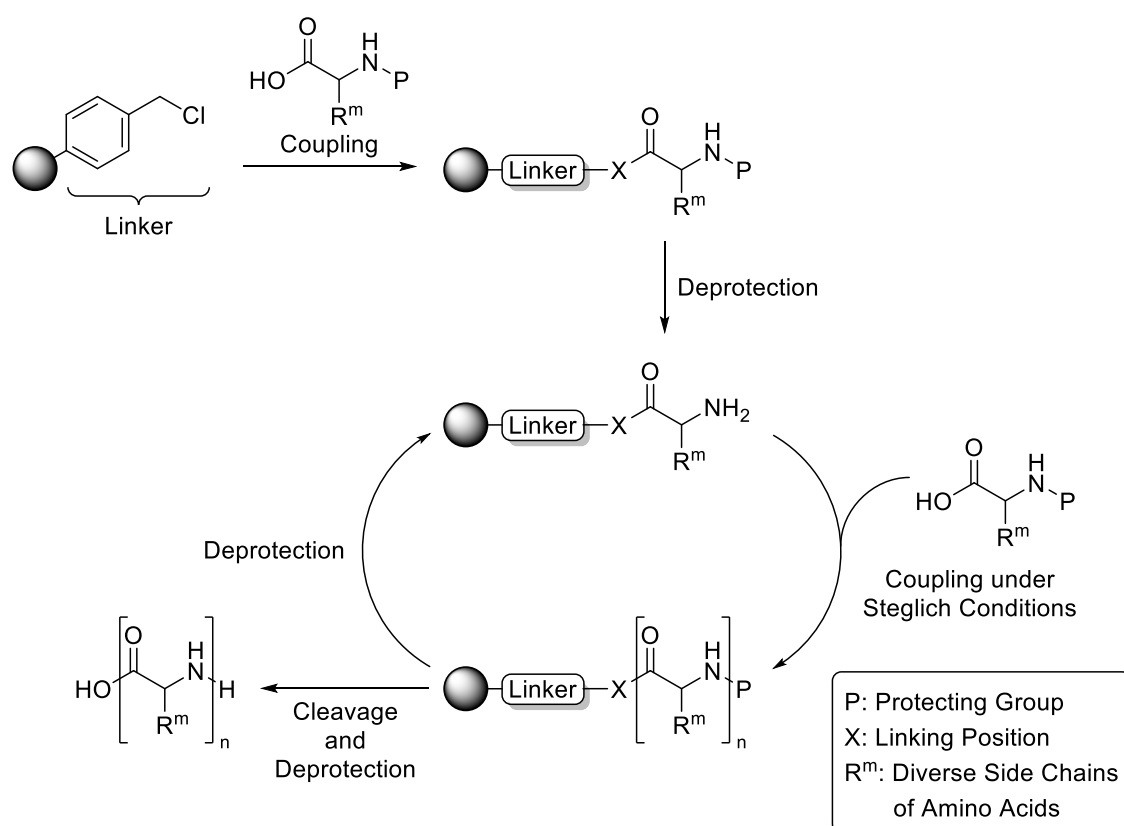


Figure 10. Overview of resins employed as solid support in solid-phase synthesis. From left to right: chloromethyl resin (Merrifield resin), 2-chlorotrityl chloride resin, Rink amide resin, Sieber amide resin.^[19]

support as presented in **Scheme 18**. Next, the SPPS cycle is continued by the deprotection at the *N*-terminus enabling the subsequent addition of the following amino acid. After washing the resin, chain extension can be performed *via* amidation under Steglich conditions, for example using *N,N'*-dicyclohexylcarbodiimide (DCC) as coupling agent. Other coupling agents are e.g. phosphonium- or uronium-based activating agents, for instance benzotriazol-1-yl-oxytripyrrolidino phosphonium hexafluorophosphate (PyBOP) and 2-(1*H*-benzotriazol-1-yl)-1,1,3,3-tetramethyluronium hexafluorophosphate (HBTU), allowing mild reaction conditions by activation of the carboxyl group. The SPPS cycle can be continued yielding the desired polypeptide after cleavage from the resin *via* iterative deprotection and coupling of amino acids. Rapid and highly efficient reactions with high conversions (ideally $\geq 99\%$) are required for the SPPS in order to enable the formation of synthetic peptides maximizing the number of repeating units. However, byproducts and incomplete conversion for each iterative cycle leading to defective sequence orders have to be prevented, since separation of



Scheme 18. Schematic overview of SPPS with the Merrifield resin. First an amino acid is coupled to the linker by S_N2 followed by a deprotection step. Chain extension is performed by coupling under Steglich conditions. The final peptide is obtained after cleavage from the solid support and deprotection of the *N*-terminus.^[10,191]

2. Theoretical Background

the targeted peptide from byproducts after cleavage from the solid support can be challenging. Therefore, SPPS cycles also include capping steps to block the ends of unreacted amino acids from reacting.^[191] In the first approach, Merrifield accomplished the preparation of a tetrapeptide *via* the presented route.^[10] Later, Merrifield and co-workers presented the synthesis of bovine insulin^[192] (51 amino acids) and ribonuclease A^[193] (124 amino acids) by determined optimization of the method. SPPS automation introduced by Merrifield in 1965 allowed a fully automatic protocol including all iterative operations of the polypeptide synthesis on solid support.^[194] Employing SPPS, numerous biologically active proteins were obtained from synthetic polypeptides after an induced or spontaneous folding process, leading to the defined tertiary structure of the protein/peptide.^[195] Thereafter developed coupling methods for protein synthesis, such as the Staudinger ligation,^[196-197] accomplished the synthesis of HIV-1 protease^[198] (approx. 22 000 g mol⁻¹) with 198 amino acids or erythropoietin^[199] (approx. 50 000 g mol⁻¹) containing 166 amino acid units. Consequently, solid-phase synthesis and highly efficient ligation methods play an important role not only in peptide synthesis but also in the synthesis of artificial monodisperse macromolecules that are described in the following sections.

A second important class of biopolymers are oligopeptoids (oligomers of *N*-substituted glycines) being the *N*-substituted analogues of peptides (peptidomimetics). A comparison is depicted in **Figure 11**. Synthesis of peptoids relies on the SPPS developed by Merrifield with *N*-glycines substituting amino acids. In contrast to peptides, the monomer units *N*-substituted glycines are much more complex in their synthesis and less abundant than amino acids. In addition, glycines bear a secondary amine after deprotection of the *N*-terminus that is more sterically demanding than primary amines resulting in a decrease of overall reaction efficiency.^[191] Therefore, Zuckermann developed a sub-monomer method for the iterative construction of oligopeptoids on solid supports in which the protected *N*-glycine building

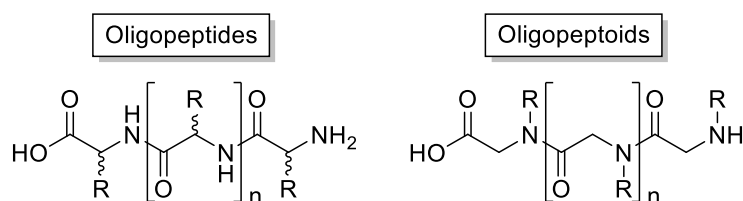
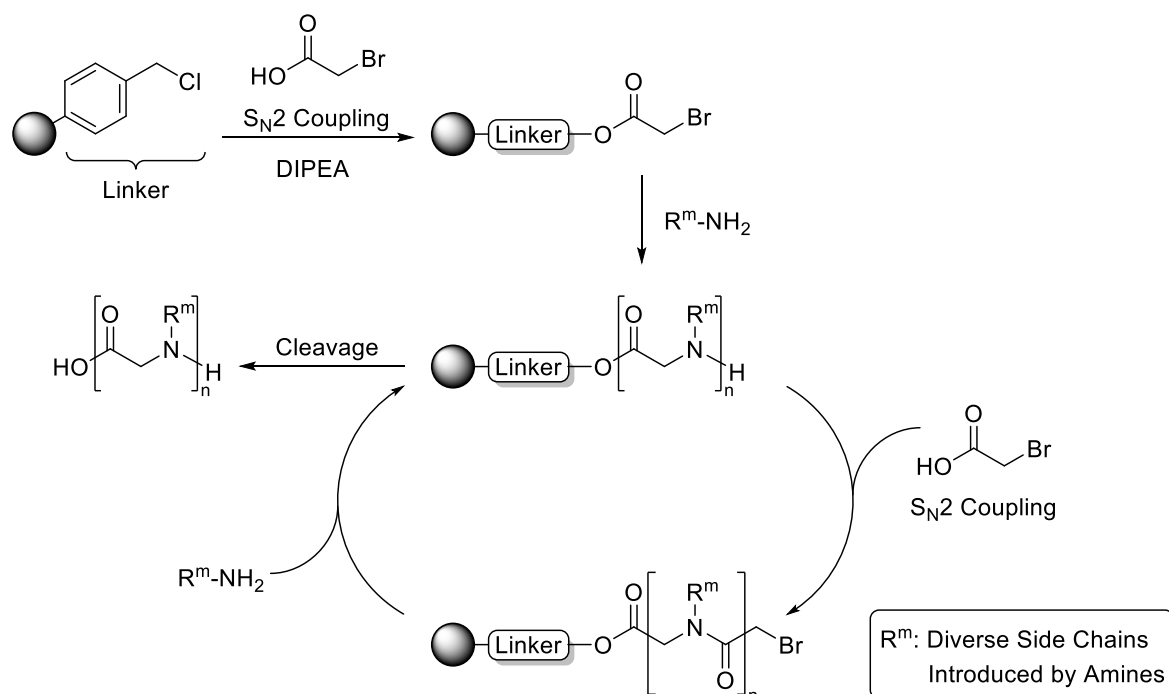


Figure 11. General structures of peptides (amino acid backbone) and peptoids (*N*-glycine backbone).^[191,200]

blocks are substituted with so-called sub-monomers (haloacetic acids and amines).^[200] In **Scheme 19**, the sub-monomer approach is illustrated. The oligopeptoid is generated by acylation of the resin with a halogenated acetic acid in the first step, followed by a S_N2 reaction employing primary amines, introducing side chain functionalities. Consequently, protecting group chemistry of the monomer building blocks is obsolete due to the fact that each sub-monomeric step is self-regulating and enables conversions of $\geq 99\%$.^[191, 201] The reaction rate of the S_N2 reactions depends on the nature of the employed amines and for aromatic as well as sterically demanding amines the reaction rate decreases significantly. In addition, it needs to be considered that other nucleophilic centers, such as a second amine functionality in diaminoalkanes, require protecting groups during the chain extension cycles. Thus, the sub-monomer method opens up a diverse synthesis of oligopeptoids with more readily available amines instead of employing *N*-glycine derivatives.^[191] One of the biological properties of oligopeptoids is the functionality as an excellent molecular transporter for pharmacologically active compounds, when corresponding side chains, for example diaminoalkanes, are employed.^[14, 202] In contrast to oligopeptides, peptoids are more resistant to enzymatic degradation in cells due to their *N*-substitution of side chains. Furthermore, peptoid transporters



Scheme 19. Sub-monomer method developed by Zuckermann. Acylation in a S_N2 reaction and subsequent S_N2 reaction addition of amines to the resin results in the targeted oligopeptoid after cleavage from the solid support.^[191,200]

2. Theoretical Background

are absorbed more quickly in the cell than their peptide based analogues. The secondary and tertiary structure as well as the physiological properties, such as lipophilic or hydrophilic solubility, or molecular transporting properties can be influenced by the side chains.^[201, 203-204] Polypeptoids of up to 50 glycine monomer units have been prepared relying on Zuckermans sub-monomer method on a solid support. Based on the non-challenging synthesis, the secondary structure of polypeptoids by self-assembly and the influence of side chains in relationship with the sequence order was investigated.^[202, 205-207] Peptoid ordering is stabilized by avoiding steric hindrance and by electrostatic repulsion between the backbone carbonyls and the side chains. It was demonstrated that helices are developed driven by α -chiral side chains in solution and loop structures are generated by intramolecular hydrogen bonding between side chains functionalities and backbone carbonyls.^[208] β -Sheet formation can be obtained by an introduction of two oppositely charged oligopeptoids bearing a defined sequence. The sequences are leading to a two-dimensional nanosheet formation, highlighting the sequence order and side chain related properties.^[209] Consequently, polypeptoids exhibit a very interesting class of non-naturally occurring sequence-defined macromolecules.

Polynucleotides, such as DNA, are another important class of sequence-defined monodisperse biopolymers profiting from automated solid-phase synthesis strategies introduced by Merrifield. In **Figure 12**, a basic structure of a synthetic oligonucleotide is depicted carrying the nucleobases adenine (A), cytosine (C), thymine (T), and guanine (G). Nucleotide units consist of a nitrogen-containing nucleobase and a deoxyribose (monosaccharide) unit linked by a phosphate group at the 3' and the 5' position of the sugar. Polynucleotides are composed of nucleotide units resulting in a sugar-phosphate backbone. Two separate polynucleotide

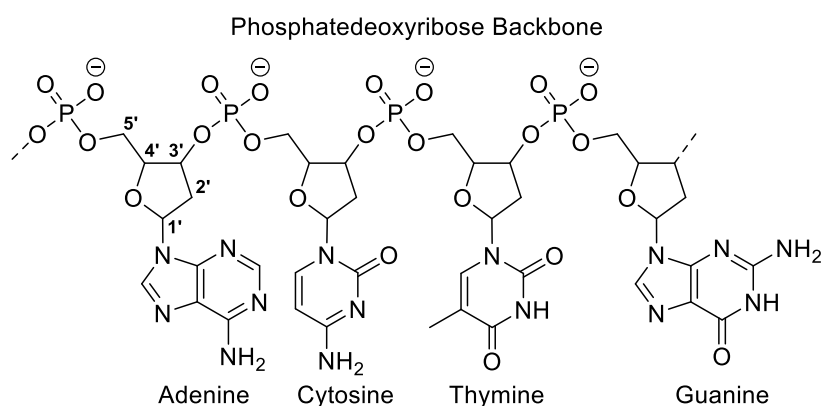


Figure 12. Exemplary structure of a synthetic oligonucleotide applying the phosphoramidite strategy with the DNA-bases adenine, cytosine, thymine, and guanine.^[210-211]

strands form double-stranded DNA by hydrogen bonding according to the base pairing rules (A with T and C with G). For the synthesis of polynucleotide strands, a highly orthogonal protecting group strategy is required for the hydroxyl groups of the deoxyribose, the amine groups of the DNA bases, and the phosphate group linker. In addition, the protecting groups need to be orthogonal regarding their cleaving conditions from the solid support. Commonly, the nucleobases are protected with base labile benzyl groups, the deoxyribose with acid labile dimethoxytrityl groups, and the phosphate groups as base labile phosphotriester, carrying a diisopropylamino group.^[210-211] Since the automated synthesis of DNA was first reported in 1985,^[212] continuous progress allowed the synthetic fabrication of DNA up to 98 or even 120 repeating units.^[213-214]

More importantly, nucleobases encoded in DNA are carrying the genetic code, which is vital to all aspects of life, such as self-replication. Regarding applications, data storage in synthetic polynucleotide strands is of high interest and is intensively investigated as potential information storage medium.^[215-220] Today's electronic data storage is based on a binary system, thus one bit can be coded per repeat unit. Coding of information using four nucleobases in a quaternary system allows the storage of two bits per repeating unit with 4^n permutations, increasing the density of information. For instance, the storage of one byte (8 bits) requires 256 permutations that can be accomplished by a tetramer in a quaternary system ($4^4 = 256$), whereas an octamer is required in a binary system ($2^8 = 256$) to achieve the same information density. In the M^n notation, M describes the number of employed fundamental information fragments (i.e. repeating unit or monomer unit) and n describes the degree of polymerization, hence the 2^8 notation is equal to an octamer with two different monomer units enabling 256 different permutations. In 2017, Erlich reported a DNA fountain encoding system for efficient information storage.^[50] A total of $2.14 \cdot 10^6$ bytes was encoded in oligonucleotides and retrieval was performed to perfectly encode the stored information. Thus, an information density of 215 petabytes per gram of DNA with 72 000 oligonucleotides, featuring 32 bytes each and 1.57 bits per nucleotide, was achieved with a perfect retrieval.

2.3.2. Artificial Sequence-Defined Macromolecules for Encoding

The synthesis of artificial sequence-defined macromolecules is described as the next “holy grail” in polymer science and therefore presents one of the major challenges in current re-

2. Theoretical Background

search.^[9] In contrast to artificial sequence-defined materials, naturally occurring monodisperse macromolecules are well investigated. In nature, sequence-definition is essential for information storage, i.e. folding of macromolecules into complex structures, such as enzymes, or the storage of genetic information in DNA. Non-natural systems allow for a wide range of synthetic protocols independent from natural macromolecules thereby extending limitations of DNA-based data storage systems. Hence, it is attractive to investigate sequence-defined macromolecules as a medium for coding and decoding of information.^[38, 221] Trinh *et al.* reported a chemoselective “AB + CD” iterative method to access molecularly encoded oligomers. A library of eight trifunctional macromolecules was prepared based on a (0,1) binary code through amidification and copper-catalyzed alkyne-azide cycloaddition reactions on solid support. Two monomers of AB-type, i.e. 4-pentynoic acid (encoding 0) and 2-methyl-4-pentynoic acid (encoding 1), and a CD-type building unit – an amino-azido component – were employed as complementary spacer blocks. Consequently, a set of eight pentamers was synthesized with all possible permutations exhibiting three encoded monomer units. The same group reported several approaches based on phosphoramidite to access artificial sequence-defined macromolecules in a highly efficient manner.^[46, 56, 222-226] Distinct fragmentation of the sequenced macromolecules and the erasing of codes was targeted to accomplish practical application possibilities.^[226] Furthermore, sequence-coded macromolecules were prepared by selective iterative approaches based on successive phosphoramidite

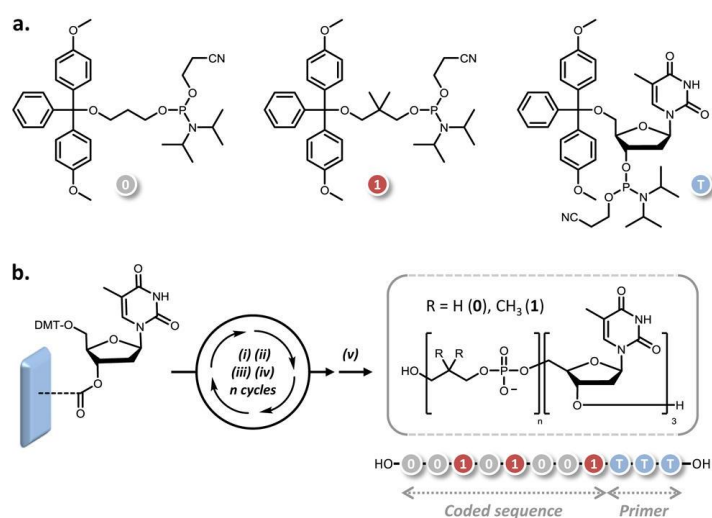


Figure 13. (a) Phosphoramidite based monomer units for the synthesis of sequence-encoded macromolecules. (b) Iterative approach using a solid support starting after the TTT sequence introduction with i) DMT deprotection, ii) coupling step, iii) oxidation, iv) capping, and v) cleavage. Reprinted with permission from A. A. Ouahabi *et al.*, *ACS Macro Lett.* **2015**, *4*, 1077-1080. Copyright 2015 American Chemical Society.^[56]

chemistry and radical-radical coupling steps yielding poly(alkoxyamine phosphodiester)s for the coding of 16 bits in total.^[222] Herein, the information read-out process was optimized by the introduction of fragment formation containing two bytes during tandem MS analysis. In a different report, the synthesis of non-natural sequenced macromolecules of DP > 100 based on phosphoramidite chemistry, employing a solid support strategy on an automated DNA synthesizer, was approached.^[56] Automated synthesizers in combination with SPPS strategies allow for the straightforward preparation of long sequence orders with a minimum of synthetic effort. Therefore, two phosphoramidite monomers were used to generate binary-based information encoding. In the first step, a primary sequence was introduced using thymine based nucleotides to allow purification by HPLC and analysis *via* UV spectroscopy. Subsequently, the phosphoramidite based monomer units for encoding have been polymerized iteratively using an automated DNA synthesizer as illustrated in **Figure 13**. Following the phosphoramidite cycles, sequence-encoded macromolecules consisting of up to 104 monomer units were obtained, allowing 2^{104} possible permutations. Consequently, with 2^{104} possible permutations a decabyte of information can be potentially incorporated into a single chain. Besides storing of information on the molecular level, the read-out of the stored information is of critical importance. Comparable to mass sequencing of peptides or DNA, tandem MS techniques are exclusively described so far for information read-out by Lutz and co-workers.^[30, 39, 48-49, 227-230] An automated computer assisted information read-out by MS/MS sequencing was developed allowing for precise decryption of sequence-coded polymers.^[30] Recently, the read-out *via* tandem mass spectroscopy of 64 bit encoded within one macromolecule was demonstrated by employing a binary system (depicted in **Figure 14**).^[229] Specifically, inter-byte fragmentation by exactly positioned mass tags along the chain was introduced in order to simplify the read-out process *via* collision-induced dissociation (CID). Alkoxyamine groups placed between the single bytes allowed the desired fragmentation, since the weak NO-C bonds are selectively cleaved first, leading to a fragmentation pattern consisting of intact bytes. The respective bytes were labeled with identification tags resulting in a tag-shifted mass spectrum after fragmentation. In the next step, the tagged bytes were analyzed by collision experiments to identify the sequence order of the respective byte fragments. Furthermore, an ASCII-coded sentence of 160 bytes in total was demonstrated by Lutz and co-workers.^[231] The data was embedded in a defined sequence of layers into

2. Theoretical Background

nanofabricated multilayered thin films. Therefore, a library of 16 sequence-defined polyanions were employed in layer-by-layer (LbL) deposition in order to form segregated layers of digitally encoded films. The respective sequence-defined polyanions contained 10 bytes of information each resulting in 160 bytes of information in total. However, read-out of the digitally encoded layers was not reported. In addition to coding information into sequence-defined macromolecules and the information read-out, applications beyond data storage have been reported. For instance, long-term stable sequence-defined macromolecules were

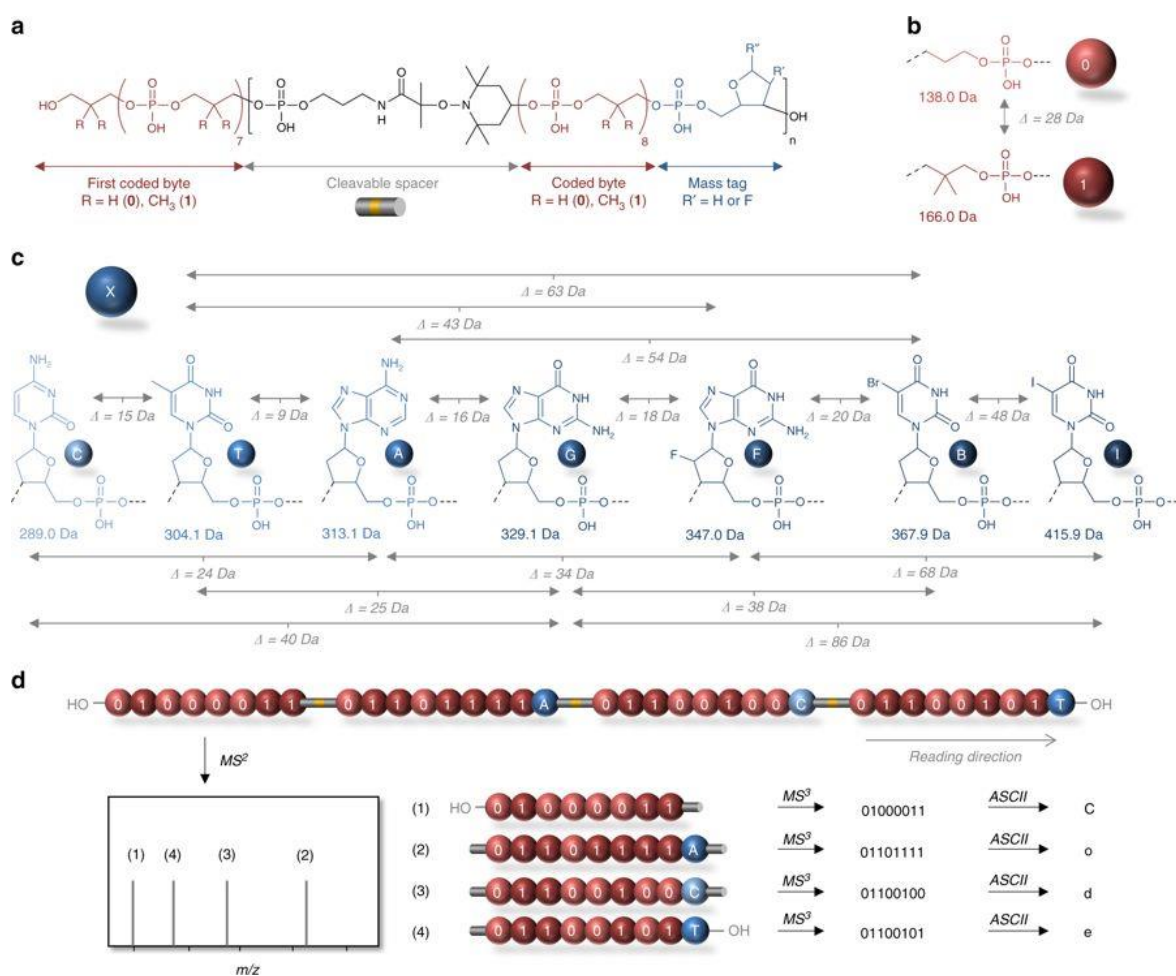
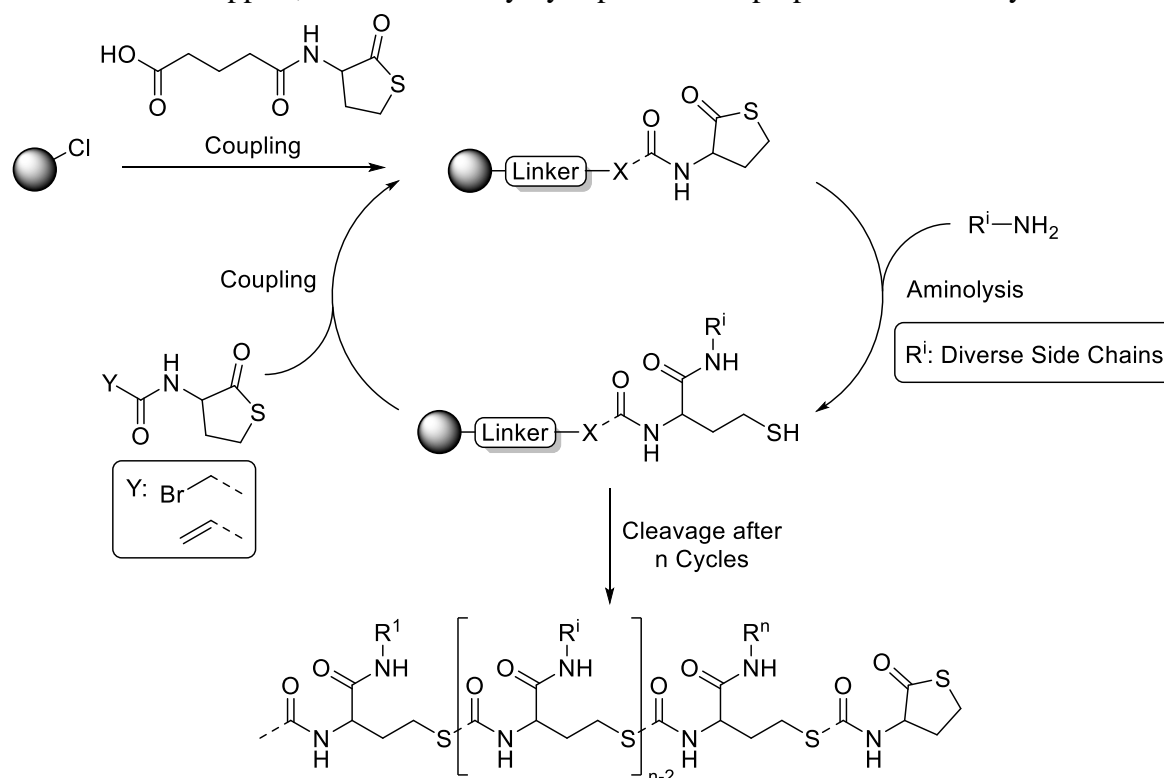


Figure 14. (a) Basic structure of the sequence-defined macromolecule synthesized by an automated phosphoramidite chemistry approach. Two bytes are linked with an alkoxyamine containing a NO-C bond for tandem MS fragmentation. The single bytes contain a mass tag for identification after CID fragmentation. (b) Structure of the monomer units employed for binary coding of information into the macromolecule. (c) Structure of the respective mass tags. (d) Schematic representation of the read-out of a 4 bytes containing macromolecule by tandem MS under CID conditions. In the first step, the macromolecule undergoes fragmentation at the NO-C bonds (depicted in yellow inside the grey spacers) resulting in the single byte fragments. Based on the mass tag the single byte fragments are sorted out by mass. In the next step, the single bytes are analyzed to identify their sequence order. The figure was reprinted from a publication of Al Ouahabi *et al.* licensed under a Creative Commons Attribution license.^[229]

discussed for applications in cryptography.^[51] Furthermore, applications of digital macromolecules as barcodes were demonstrated employing sequence-coded oligourethanes for labeling of polymeric materials^[232] as well as 3D-printed objects.^[233] In addition, abiotic sequence-defined oligourethanes were tested for *in vivo* tagging of implanted materials.^[234] The respective sequence-coded macromolecules were incorporated into their host materials as taggant. After extraction from the host materials, the encoded oligourethanes taggants were identified by MS/MS experiments revealing their sequence code. Consequently, the potential application for anti-counterfeiting or other tracking applications have been successfully demonstrated.

2.3.3. Thiolactone-Based Synthesis on Solid Support

Inspired by the SPPS, solid supported synthesis of sequence-defined macromolecules found application in the synthesis of artificial monodisperse polymers, exploiting simple product isolation by filtration. Yet, the obtained macromolecules have to be purified after cleavage from the solid support, most commonly by separation on preparative HPLC systems. Even



Scheme 20. Iterative two-step approach for the synthesis of sequence-defined oligomers based on thiolactones on a solid support. Side chain functionalization is introduced by aminolysis using amine components.^[27]

polymers since protecting groups can be avoided. The concept was later extended by Du Prez and co-workers for the preparation of macromolecules up to decamers with functional groups incorporated by acrylics during aminolysis. Additionally, an automation of the synthetic steps was introduced simultaneously.^[26, 235] An approach based on a four-step iterative protocol was further investigated for the preparation of sequence-defined oligomers utilizing thioacrylates.^[236] Furthermore, the protocol was adapted for the conjugation of thiolactone-based sequence-defined oligomers to poly(ethylene glycol) (PEG).^[237-238] Hence, a combined approach based on thiolactones as well as P-3CR was developed for the scalable and convergent synthesis of sequence-defined macromolecules with a molecular weight of up to 4629.73 g mol⁻¹ (1.37 g) including 15 individually selectable side chains.^[239] In 2018, the application of thiolactone-based sequence-defined macromolecules for chemical data storage was demonstrated by encoding a simple sentence or a 33 × 33 QR (Quick Response) code into a collection of oligomers.^[42] First, chemical writing and reading was automated by software tools: a Chemreader algorithm using tandem MS techniques for reconstructing oligomer sequences as well as Chemcoder for encoding/decoding of binary data as multifunctional macromolecules were established. As depicted in **Figure 15**, a QR code represents a two-dimensional binary string, which can be converted into a sequence of functionalities. The sequence to encode the QR code leading to the Wikipedia page of August Kekulé would require a single macromolecule being too long to be synthesized efficiently. Therefore, the code was split into short fragments with a fixed length containing an index for reassignment after decoding. In consequence, a collection of 71 short oligomers, i.e. 1 monomer, 11 pentamers, and 59 hexamers, were synthesized representing the coded fragments. Hence, a library of 15 acrylate monomers was employed to introduce side chain functionalization. After synthesis of the single oligomers following the thiolactone strategy, decoding was performed with tandem MS experiments (**Figure 16**). The mass spectra were analyzed automatically by the Chemreader, identifying the characteristic fragmentation patterns of the single oligomers. Based on the index, the Chemcoder sorted the sequenced fragments in their original order. Thus, the original bit string could be reconstructed and transferred into the original QR code. Consequently, the method demonstrates perfectly the advantages of protection free thiolactone chemistry with a facile introduction of side chain functionalization even in combination with an automated process to synthesize sequence-defined macromolecules highly efficiently.

2. Theoretical Background

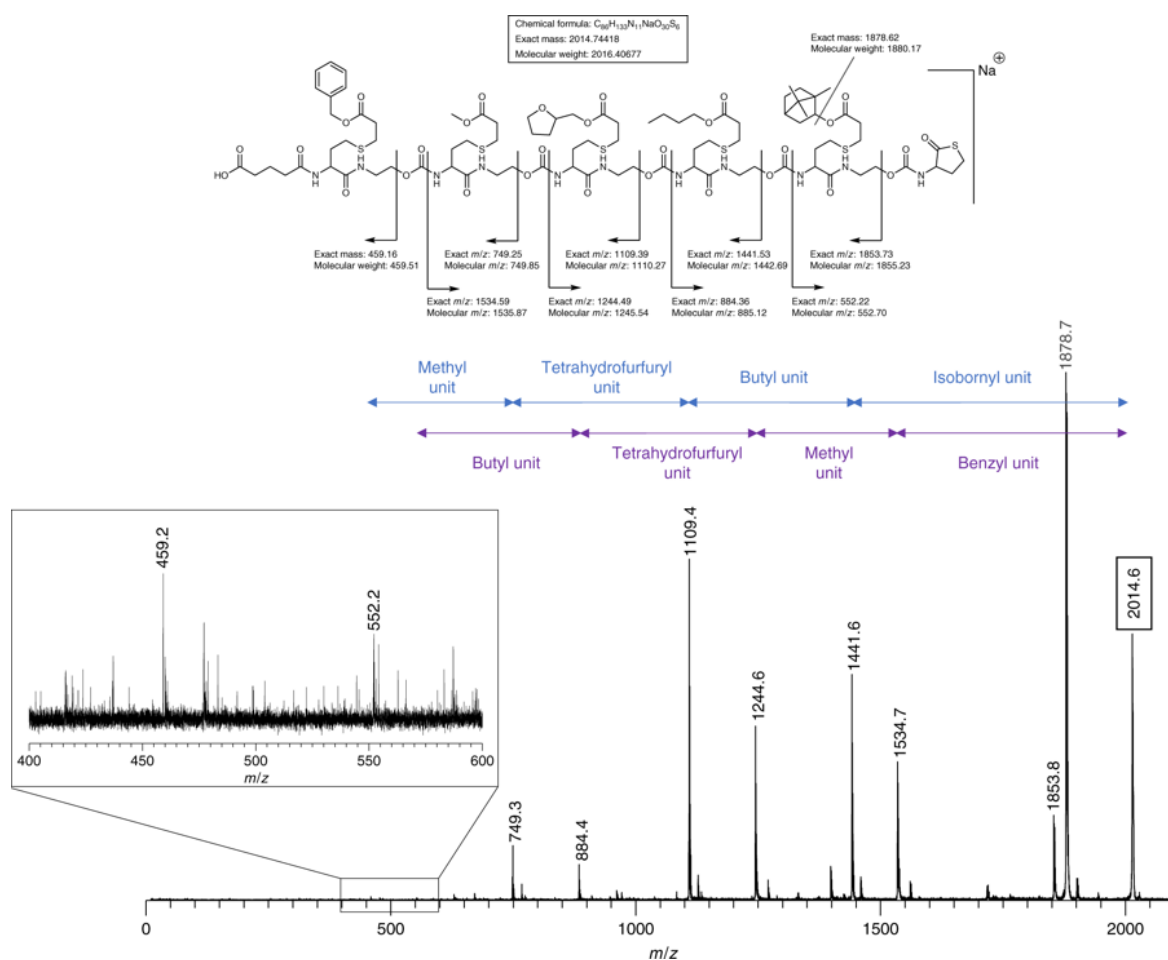
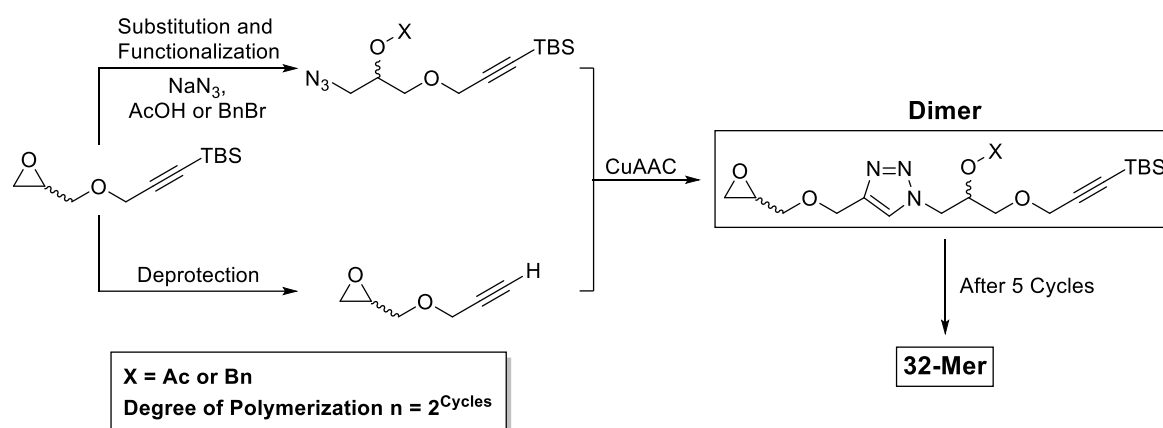


Figure 16. Sequence readout using tandem MS (MALDI-MS/MS) of a pentamer with different side chain functionalities. Fragmentation pattern and recurrence of the encoded oligomer is highlighted from right to left in blue and from left to right in purple. The figure was reprinted from a publication of Martens *et al.* licensed under a Creative Commons Attribution license.^[42]

2.3.4. Iterative Exponential Growth by Copper-Catalyzed Azide-Alkyne Cycloaddition

Huisgen was the first to describe the mechanism of dipolar cycloadditions and their synthetic applications.^[240] The copper-catalyzed version of the 1,3-dipolar azide-alkyne cycloaddition (Huisgen reaction) forming triazoles is a representative of the ‘click’ reaction concept. Being a highly efficient coupling method with mild reaction conditions and high chemical yields, copper-catalyzed azide-alkyne cycloadditions (CuAAC) present a possible tool for the synthesis of sequence-defined macromolecules. In 2015, Johnson and co-workers reported a new iterative exponential growth (IEG) approach employing the CuAAC as a coupling reaction for the synthesis of monodisperse polymers.^[23] In an IEG approach monomers react

to dimers, dimers to tetramers, tetramers to octamers, and further allowing for an exponential growth of the chain length with each coupling cycle. Hence, orthogonally protected monomer units have to be provided for an IEG strategy to enable chain extension by coupling reactions *via* deprotection or activation steps. Furthermore, in the approach of Johnson and co-workers, side chain functionalization was introduced employing enantiopure monomer units equipped with chiral epoxides and a TBDMS protected alkyne group. They accomplished varying sequences and stereoconfiguration in a monodisperse macromolecule up to 6 kDa featuring high yields and scalability. In **Scheme 21**, the IEG strategy is illustrated starting from the enantiopure monomer. In the first step, the side chain functional groups are introduced by a ring-opening reaction of the epoxide moiety with sodium azide generating a secondary alcohol, which was subsequently functionalized with acetic acid or benzyl bromide. Additionally, an equivalent of the TBDMS protected monomer is deprotected. In the following step, the modified monomer, carrying the functional group, and the deprotected monomer are combined in a CuAAC yielding a dimer in the first chain extension step. A 32-mer is generated after conducting five cycles by employing the respective intermediates (i.e. dimer, tetramer, octamer, and 16-mer) as starting material for the successive steps. Thus, following the iterative strategy, 170 milligrams of a sequence-defined homo-R-configured 32-mer with alternating benzyl ether and acetyl side chains was synthesized in an overall yield of 15 %. Furthermore, the concept was transferred to a semi-automated flow system

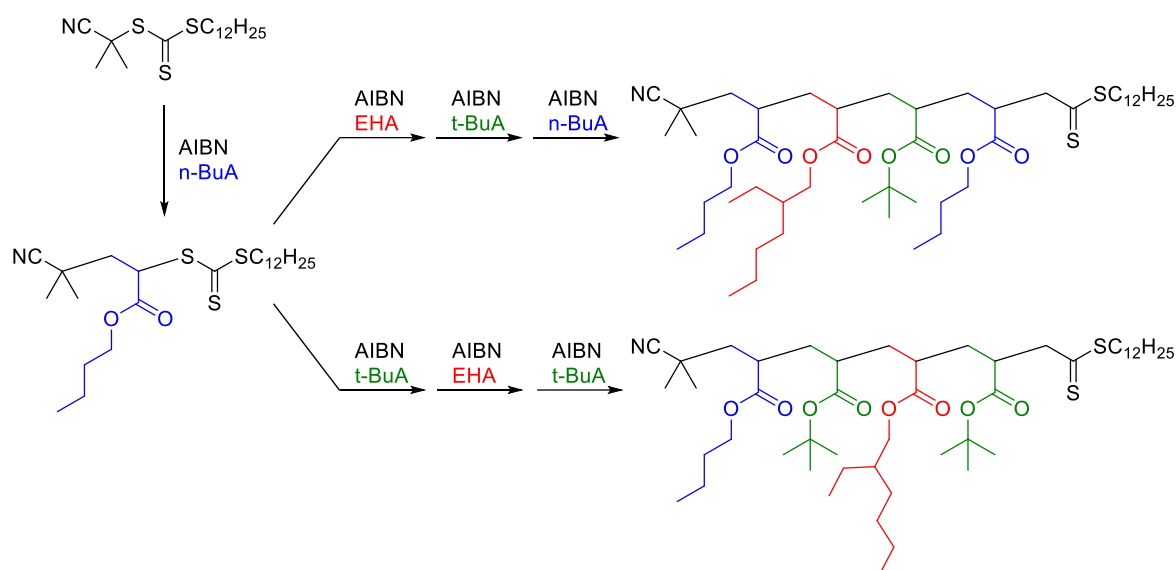


Scheme 21. Strategy of an IEG approach for the synthesis of sequence-defined macromolecules as reported by Johnson and co-workers. The cycle is depicted starting from the chiral key monomer equipped with an epoxide and a protected alkyne group. Ring opening with sodium azide enables subsequent functionalization with acetic acid or benzyl bromide. The combination of a deprotected and a functionalized building block generates monodisperse macromolecules *via* exponential chain growth by CuAAC.^[23-24]

providing a straightforward scalable synthesis of monodisperse unimolecular macromolecules.^[24] Therefore, three reactions are performed in the flow-IEG as already depicted in **Scheme 21** using the same monomers. Additionally, an in-line purification before the Cu-AAC step and after functionalization and deprotection of the respective building units was introduced. Thus, it was demonstrated how the molecular weight of an oligomeric species can be exponentially increased in an uninterrupted reaction sequence with a total residence time under 10 min per cycle. A molecular weight of 4 kDa was achieved allowing a throughput of 2.75 grams coupled product per hour. Furthermore, the post-functionalization of the side chains was demonstrated in order to synthesize diblock copolymers up to 12.1 kDa. In addition, phase segregation into hexagonal cylinder morphologies resulting from self-assembly of the amorphous block copolymer was investigated.^[25] In conclusion, IEG strategies provide one important advantage, i.e. a fast growth in molecular weight, and employing flow conditions enables scalability of the reaction. However, variation in the side chains is difficult as the method is limited to repetitive sequence orders in their side chain functionalization.

2.3.5. Sequence-Defined Oligomers *via* Radical Single Unit Monomer Insertion

Commonly, highly efficient ‘click’ reactions are employed for the synthesis of monodisperse sequence-defined macromolecules. Thus, monodisperse oligomers are obtained with a unique backbone different from common polymers, such as polyacrylates. Junkers and co-workers introduced a strategy employing SUMI for the formation of monodisperse oligomers exhibiting an acrylate backbone.^[19-20, 241] In a first approach, two different tetramers with defined sequence have been prepared by RAFT polymerization as depicted in **Scheme 22**. Therefore, a commercially available chain transfer agent for the polymerization of *n*-butyl acrylate (nBuA) was employed. The polymerization was kept in a time scale of 10 minutes to ensure the insertion of only one monomer unit. Purification was carried out by recycling SEC, enabling automated purification of the monodisperse macromolecules. Repeating of the polymerization cycle yielded two tetra-functional macro-RAFT agents after the insertion of four different monomer units into the chain transfer agent. Later the strategy was extended for the formation of linear monodisperse 18- and 20-mer acrylates *via* RAFT polymerization.^[241] First, two sequence-defined acrylate nona- and decamers were obtained

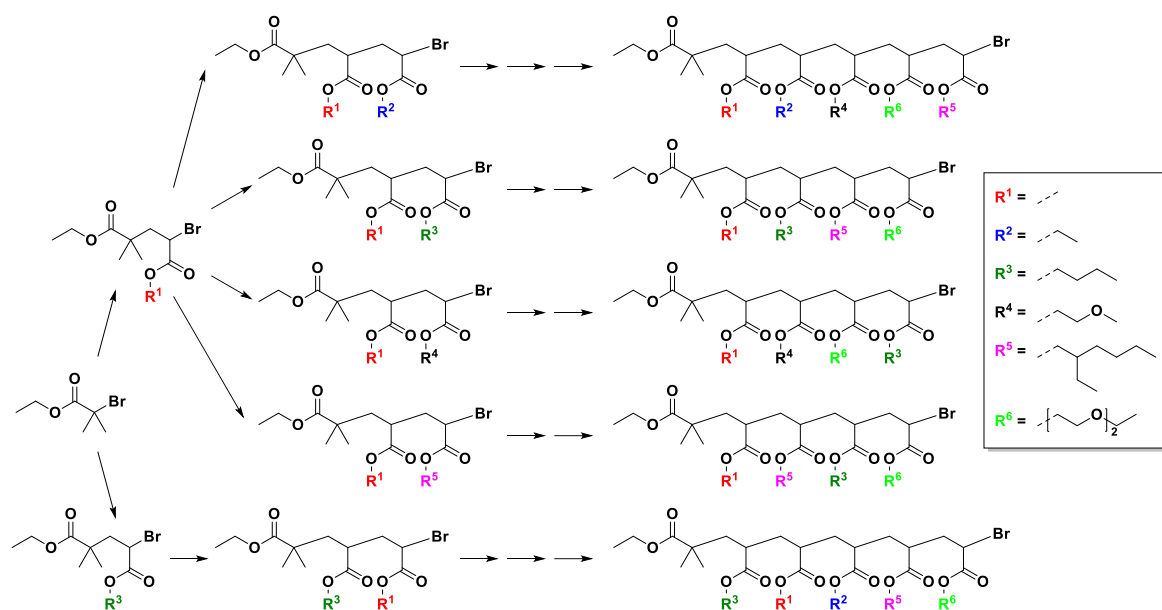


Scheme 22. Preparation of two sets of sequence-defined oligoacrylate RAFT agents by insertion of four single monomer units. Published by The Royal Society of Chemistry, licensed under a Creative Commons Attribution license.^[19]

by SUMI and multiple unit monomer insertions (MUMI) strategies starting from a RAFT agent. The purification of the single intermediates was performed by automated flash column chromatography. Subsequently, aminolysis of the trithiocarbonate end-group of the respective nona- and decamers was performed to enable disulfide bridge formation leading to the symmetrical sequence-defined 18- and 20-mer polyacrylates exhibiting a molecular weight of up to $2280.14 \text{ g mol}^{-1}$.

Furthermore, the sequential SUMI strategy for the synthesis of sequence-defined macromolecules entailing an acrylate based backbone was demonstrated *via* ATRP as depicted in **Scheme 23**.^[20] Therefore, a common ATRP initiator was employed together with copper(II)-bromide and tris[2-(dimethylamino)ethyl]amine (Me_6TREN). The polymerization was conducted under UV irradiation yielding the SUMI adduct as the main product, since turning off the light source also stopped the polymerization immediately enabling the insertion of a single monomer unit. The SUMI can be monitored online by Fourier transformed infrared spectroscopy (FT-IR). A decreasing signal at 1640 cm^{-1} , which is assigned to the vinyl bond of the acrylate, indicates consumption of the monomer. Thus, by repeating the SUMI cycles combined with automated recycling SEC or column chromatography purification steps, a set of sequence-defined tetra- and pentamers was obtained with different side groups. Compared

2. Theoretical Background



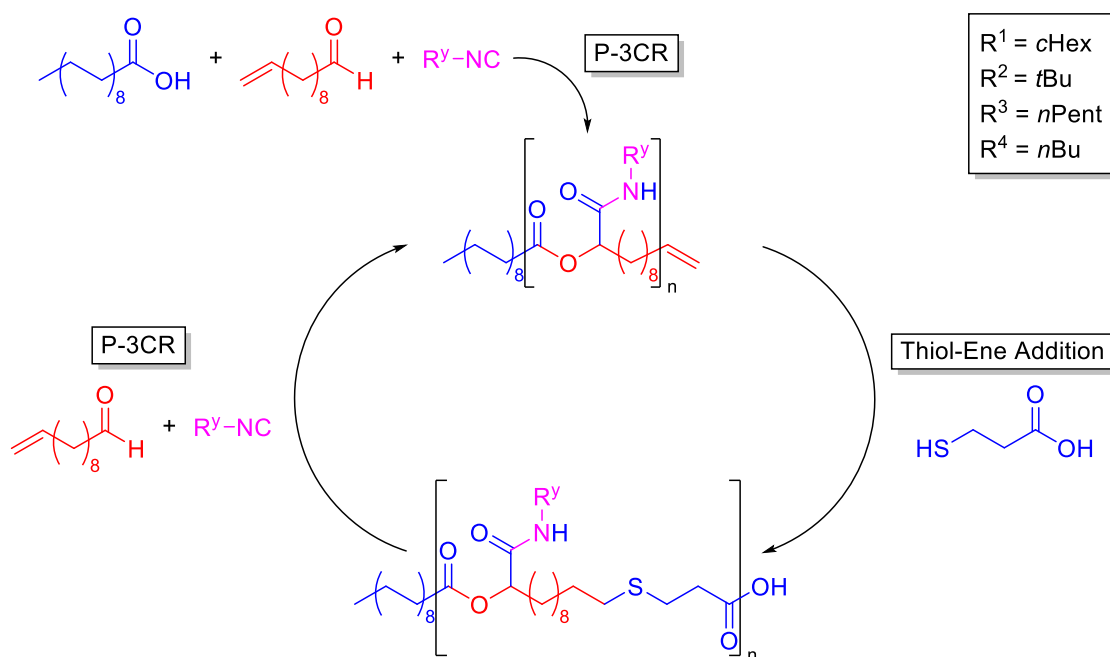
Scheme 23. A library of monodisperse sequence-defined macromolecules prepared by photoinduced ATRP *via* SUMI reactions. Published by The Royal Society of Chemistry, licensed under a Creative Commons Attribution license.^[20]

to the RAFT process, photoinitiated ATRP offers an additional advantage as it can be carried out at ambient temperature to avoid side product formation resulting from radical transfer reactions.

Nevertheless, an effective and flexible route for the synthesis of sequence-defined acrylate based macromolecules was established using reversible deactivation radical polymerizations (RDRP) techniques, standing in competition with iterative synthesis strategies. Different sets of sequence-defined polymer structures were presented exhibiting a precise sequence order of monomers. SUMI or the insertion of several monomer units in one reaction step could be accomplished with a large tolerance towards functional groups. Monomers for RDRP approaches are accessible in a facile fashion with a wide range of functional side groups due to the fact that they are commercially available. Thus, RDRP techniques allow access to common polymer structures, such as polyacrylates, entailing sequence-definition, and enable the possibility to create highly tunable materials.

2.3.6. Sequence-Defined Macromolecules by Multicomponent Reactions

Stepwise approaches allow for the large-scale synthesis of sequence-defined macromolecules. Therefore, a high overall yield is required to enable the preparation of longer sequences efficiently. For instance, IMCRs provide straightforward scalable reaction conditions along with overall yields superior to multi-step reactions and thus represent an ideal tool for the synthesis of monodisperse macromolecules equipped with functional side chains. Although the first MCR was reported more than 150 years ago, they found application in polymer chemistry only recently.^[155, 242-244] For mechanistic details about multicomponent reactions refer to Section 2.2. In 2014, Meier and co-workers reported the first strategy for sequence-defined macromolecules in an iterative approach using a combination of P-3CR and thiol-ene addition.^[55] As depicted in **Scheme 24**, stearic acid, undecenal, and an isonitrile have been employed for the first Passerini adduct. Subsequently, thiol-ene addition was performed with 3-thiopropionic acid under UV irradiation introducing a carboxylic acid group to enable further P-3CR cycles. Thus, a tetramer was prepared with an overall yield of 26 %. Additionally, a soluble polymer support was employed in the same iterative strategy

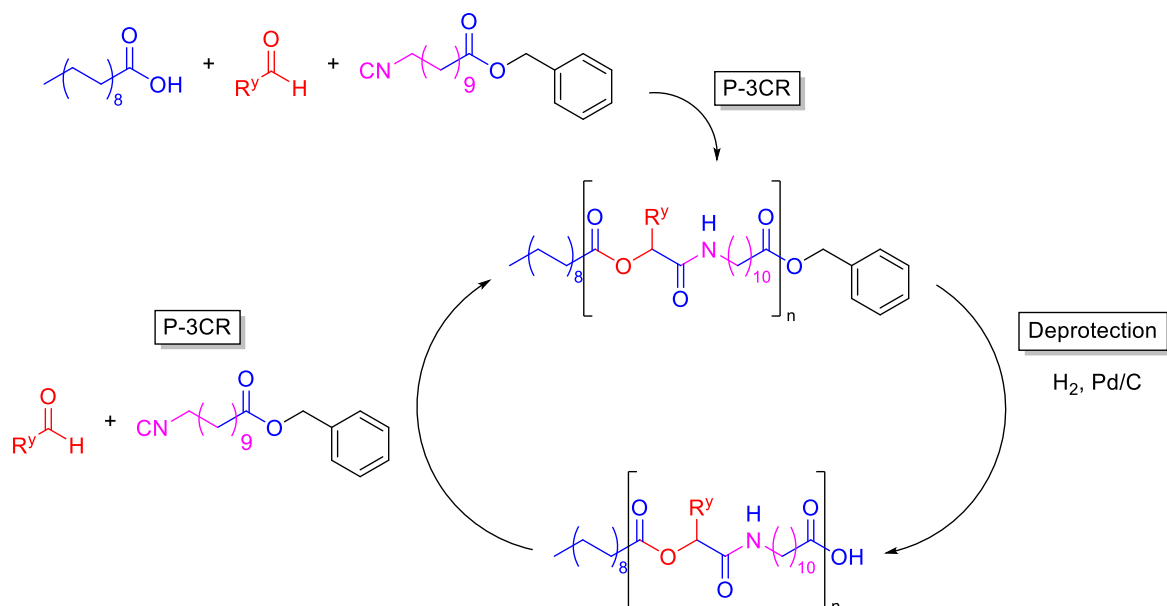


Scheme 24. Synthesis of sequence-defined macromolecules using an iterative two-step strategy combining P-3CR and the thiol-ene addition reaction. Adapted from a report of Solleder *et al.* with permission from Wiley.^[55]

2. Theoretical Background

using PEG bearing an acid functionality instead of stearic acid. The introduction of the support simplified the purification process since the intermediates were precipitated rather than purified by column chromatography. Hence, a pentamer was synthesized exhibiting five Passerini repeating units with an overall yield of 34 %. The reported avenue avoids protection groups as well as coupling agents, which is contributing to the overall yield. Moreover, a high variety of side groups can be achieved by exchanging of the isocyanide and facile up-scaling is feasible. In addition, a combination of the P-3CR thiol-ene addition approach and thiolactone chemistry was reported for the synthesis of monodisperse macromolecules.^[239] Thus, oligomers with a molecular weight up to 4629.73 g mol⁻¹ were generated bearing up to 15 independently selectable side chains evidencing the efficiency of the approach.

Furthermore, sequence-defined macromolecules have been prepared by Meier and co-workers using a U-4CR based strategy.^[154] Therefore, oligomers have been prepared *via* iterative U-4CR and thiol-ene addition in an approach similar to the P-3CR strategy being depicted in **Scheme 24**. The U-4CR enables the introduction of two different side groups per chain extension cycle. However, only the amine component was employed for the introduction of side chain groups while a *t*Bu-functionalized isocyanide was used as the isonitrile component. An overall yield of 15 % was achieved in the synthesis of a tetramer. In the last step of



Scheme 25. Two-step iterative P-3CR approach by employing protection chemistry. An isocyanide monomer that carries a benzyl protected acid functionality reacts with an aldehyde and stearic acid in a P-3CR. After deprotection of the acid functionality by hydrogenation with a palladium based catalyst, chain extension *via* P-3CR can be performed.^[180]

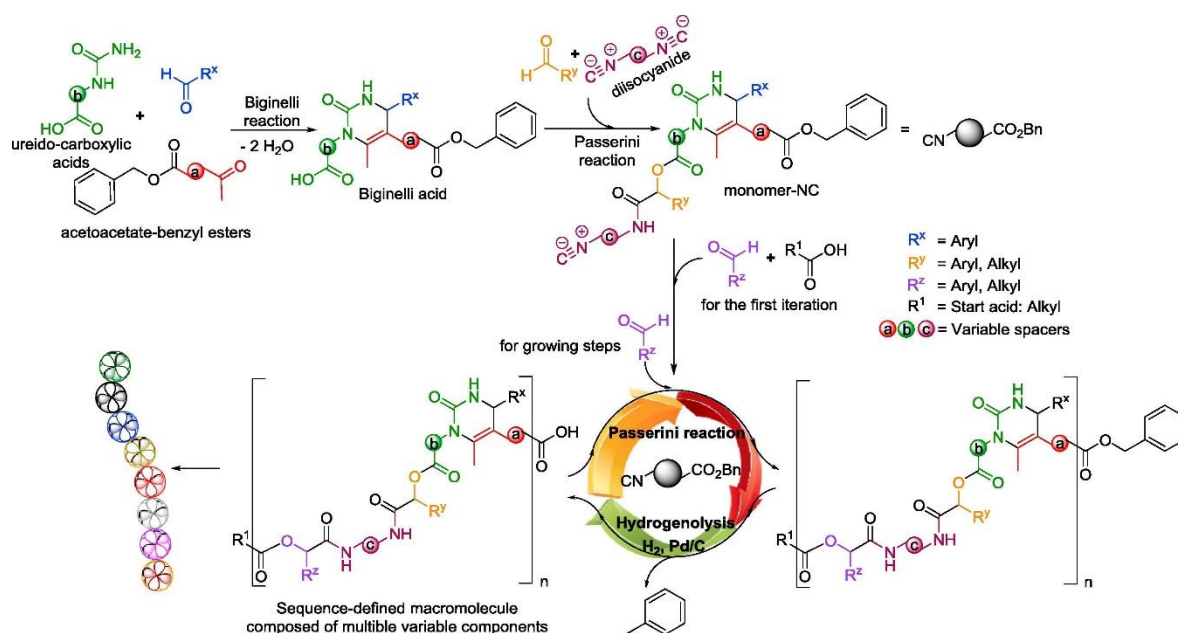
the cycle, ethanolamine was employed as amine component decreasing the yield (48 % rather than 76 to 94 % in the steps before). Consequently, protecting groups should be employed for the introduction of functional side chains as the alcohol interferes with the U-4CR. In addition, a second approach was performed varying both, the isonitrile and the amine components, to introduce functional side chain groups. Thus, a pentamer with an overall yield of 15 % was synthesized entailing ten different side chains in total. Hence, the U-4CR presents a truly powerful tool for the introduction of functional side groups in sequence-defined macromolecules.

In 2016, the P-3CR concept was further developed towards a scalable high yield approach by combining the P-3CR with protection chemistry.^[180] Therefore, an AB-type monomer equipped with both an isocyanide and a benzyl ester protected carboxylic acid was designed. Thus, in contrast to the P-3CR thiol-ene approach, the side group was introduced *via* the aldehyde instead of the isocyanide moiety. After the formation of the Passerini adduct using the isocyanide monomer, an aldehyde, and stearic acid, the benzyl protecting group was removed by hydrogenation employing palladium as catalyst. The deprotection enabled a subsequent chain extension *via* P-3CR (**Scheme 25**). Owing to almost quantitative deprotection in each step, the overall yield increased drastically to 44 % providing 2.4 g of the sequence-defined decamer exhibiting ten different side chains. In the last chain extension step an olefin was introduced as side chain. Subsequently, the decamer was combined in a self-metathesis reaction to yield a symmetrical 20-mer with a molecular weight of 7046.40 g mol⁻¹ and an overall yield of 21 %. Accordingly, Meier and co-workers demonstrated a scalable high yield strategy for sequence-defined macromolecules, which allowed the introduction of functional side groups employing P-3CR. Moreover, the same group investigated the formation of sequence-defined macrocycles by ring-closing metathesis of a symmetrical monodisperse polymer precursor.^[245]

In 2018, Meier and co-workers reported a combined MCR approach using the Biginelli and the Passerini reaction to synthesize sequence-coded macromolecules for data storage.^[41] The structural variety that can be introduced into a macromolecule by both MCRs allows coding of a high information density. Up to six different functional components can be introduced per repeating unit. Consequently, storage of up to 24 bits (3 bytes) per repeating unit can be

2. Theoretical Background

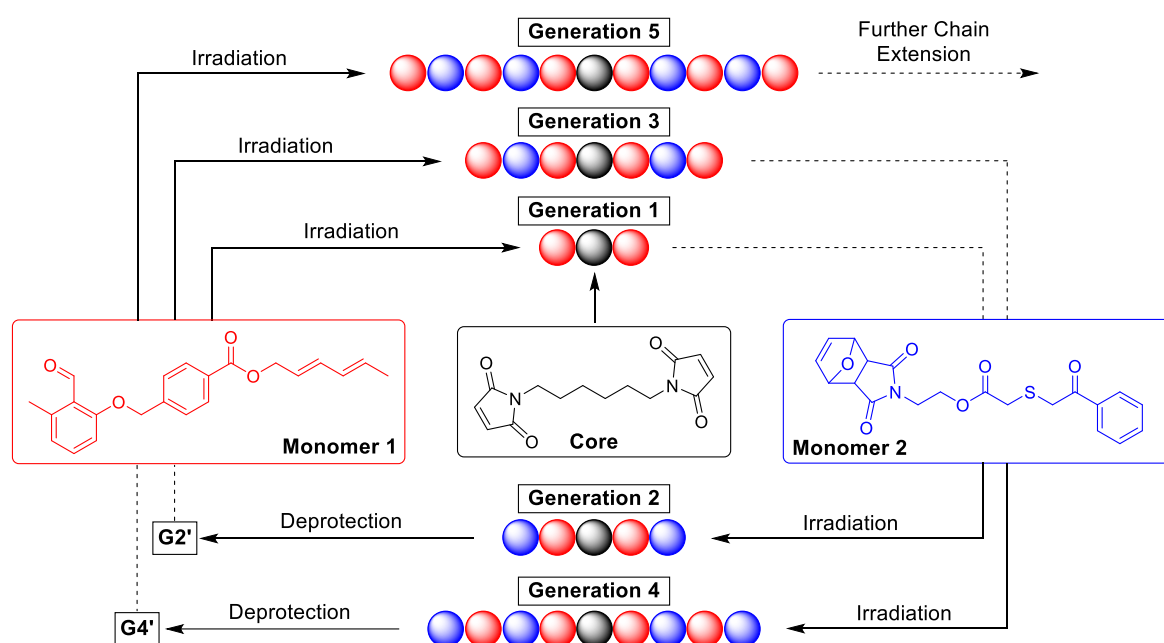
accomplished considering a large base of more than 100 compounds, which can be potentially incorporated. First, a Biginelli acid was synthesized with ureido-carboxylic acid (green), an aromatic aldehyde (blue), and an acetoacetate-benzyl ester (red) as depicted in **Scheme 26**. In the subsequent step the Biginelli acid was employed in a P-3CR using an aldehyde (orange) and a diisocyanide (purple) yielding a dimer (monomer-NC). The monomer-NC is functionalized with an isocyanide group, enabling further P-3CRs for iterative chain extension using the two-step strategy combining the P-3CR with protection chemistry. Thus, tetramers were obtained formally encoding 97 bit, respectively. The read-out was carried out *via* tandem mass spectrometry by identification of the characteristic fragmentation patterns to reconstruct the sequence of the macromolecules. Additionally, Meier and co-workers demonstrated the synthesis of Ugi adducts as molecular encryption keys by employing tandem mass spectrometry for read-out.^[51] Therefore, molecular steganography was combined with advanced encryption cryptography. Resting on the U-4CR, multifunctional Ugi adducts starting from perfluorinated acids, incorporating various side groups of 130 commercially available compounds, were presented. Accordingly, synthesis of 500,000 molecular keys can be accomplished in one synthetic step considering all possible permutations.



MCRs clearly present a powerful tool for incorporating various functional groups into a monodisperse macromolecule in one step. Hence, multifunctional sequence-defined oligomers are synthesized and can even be employed for coding of information into the sequence, which can be read *via* tandem mass spectrometry. The information density that can be stored in MCR-macromolecules is superior to biomacromolecules, such as DNA or RNA, due to the high number of side groups introduced per repeating unit. Even different chemical approaches can be combined with MCRs for the preparation of sequence-defined macromolecules to exploit all combined methodological benefits.

2.3.7. Methylbenzaldehydes and Phenacyl Sulfides in the Synthesis of Sequence-Defined Macromolecules

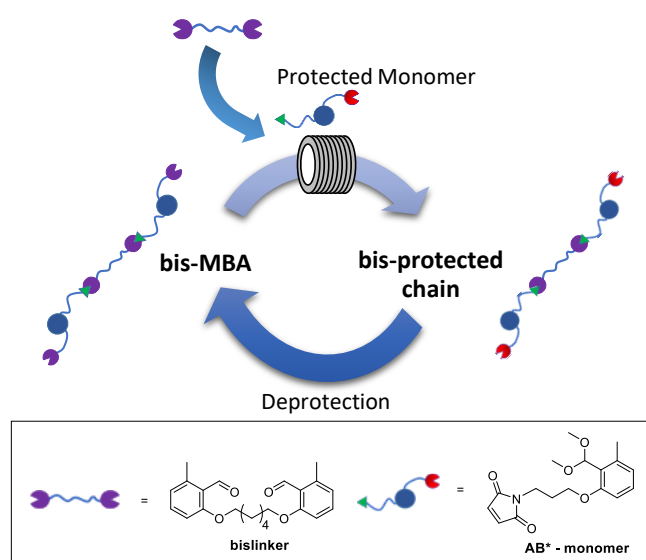
In Section 2.1 photochemical approaches have been introduced underpinning their advantages, which are temporal and spatial control over the reaction. Consequently, photoreactions are versatile tools for introducing sequence order and functionality within the chains. Photoligation protocols including MBAs and phenacyl sulfides have been developed for the construction of macromolecular architectures as well as surface modifications with spatial



Scheme 27. Schematic overview of the synthesis of sequence-defined oligomers reported by Barner-Kowollik and co-workers. The MBA bearing monomer unit is coupled to the core unit *via* an irradiation step. Subsequently, the second monomer unit is added under irradiation to form a tetramer. Thermal treatment releases the furan protecting groups and yields the maleimide group on either chain end enabling further chain extension.^[60]

2. Theoretical Background

resolution.^[138, 143, 246] The combination of photochemistry and ‘click’ reactions, such as the DA cycloaddition using MBAs for example, affords a highly efficient tool for the generation of sequence-defined macromolecules. Our team, Zydziak *et al.*, reported the first example of sequence-defined oligomers employing photoligation techniques as illustrated in **Scheme 27**.^[60] Herein, two hetero bifunctional monomer units were used, one carrying a MBA group (refer to Section 2.1.4) as well as a diene and the second equipped with a furan protected maleimide as well as a phenacyl sulfide moiety (refer to Section 2.1.3). In the first step, the MBA containing monomer was coupled to a bifunctional maleimide core unit by irradiation at 355 nm resulting in a dimer exhibiting dienes at both chain ends. The chain was further extended *via* irradiation of the second monomer unit releasing a highly reactive thioaldehyde that can undergo a DA cycloaddition with the diene end-groups of the dimer. In the following step, the symmetric tetramer was deprotected *via* thermal treatment leading to a macromolecule that is functionalized with maleimide groups on both chain ends. Further chain extension was achieved by repeating the cycle of irradiation and deprotection affording a decamer (3231.58 g mol⁻¹) with a perfectly defined monomer sequence and monodispersity. Furthermore, Barner-Kowollik and co-workers demonstrated a practical route for the synthesis of sequence-defined materials on multi-gram scales as depicted in **Scheme 28**.^[61] Here, a commercially available continuous flow setup was employed based on a sequential two-step approach using maleimides and MBAs as photocaged dienes. In the first step, an AB-type



Scheme 28. Two-step iterative approach based on *o*-MBAs as photocaged dienes. Symmetrical monodisperse macromolecules are obtained starting from a bifunctional core unit exploiting acetals as protection group for the *o*-MBAs. Reprinted with the permission from the authors.^[61]

monomer equipped with a maleimide and a dimethyl acetal protected MBA was synthesized. The sequence-defined macromolecules were generated starting from a bifunctional MBA core unit, being extended on both chain ends using the AB-monomer under irradiation of UV-light, yielding the symmetrical product with acetal protected chain ends. Subsequently, the protection groups were removed to enable consecutive chain extension. Thus, a monodisperse octamer could be prepared providing 800 mg of the final product.

Consequently, it was demonstrated that photochemical ligation protocols, resting on the photoinduced 'click' reaction of maleimides and MBAs, represent an efficient tool for the synthesis of monodisperse macromolecules. The approach of synthesizing a symmetrical macromolecule leads to a significant increase in molecular weight per chain extension step as two monomer units are added at a time. In addition, the high increase in molecular weight per chain extension step simplifies the purification of the respective generations. Although side chain groups can be introduced straightforward by employing functional spacer units to generate functionalized sequence-defined macromolecules, the demonstrated synthesis affords symmetrical macromolecules. However, it needs to be noted that employing degradable core units could yield non-symmetrical monodisperse macromolecules by cleavage of the core unit after the desired sequence order is obtained. Therefore, photochemical ligation protocols are investigated within the current thesis by exploiting the advantages of photochemistry in combination with 'click' reactions using symmetrical core units to efficiently construct sequence-defined macromolecules.

3

Results and Discussion

As described in Section 2.1, highly efficient coupling reactions play a fundamental role in the synthesis of sequence-defined macromolecules. In particular, DA cycloadditions appear to be highly suitable for the formation of monodisperse materials as DA reactions can be executed at ambient temperature providing high conversions. Moreover, photochemically driven reactions enable spatial and temporal control over the reaction accomplishing precise reaction conduction. Therefore, the main objective of the current thesis is the conceptual application of photochemical approaches for the synthesis of sequence-defined macromolecules. The work is focusing on photoinduced DA cycloadditions of *o*-MBAs investigated for efficient coupling of building units in a sequence-defined manner. In Section 3.1, the combination of *o*-MBAs and the P-3CR is presented since MCRs contribute to the facile synthesis of highly functionalized compounds in one-pot reactions. Furthermore, the photoinduced release of nitrile imines from tetrazoles as well as *o*-MBA based cycloadditions are introduced to provide sequence-defined macromolecules (Section 3.2). It is demonstrated that tetrazoles and *o*-MBAs can be activated selectively at distinct wavelengths in a λ -orthogonal manner. In Section 3.3, the synthesis of sequence-defined macromolecules is accomplished using only *o*-MBAs based coupling reactions. A library of sequence-encoded and multifunctional oligomers is prepared, demonstrating the read-out of the encoded macromolecules by tandem mass experiments.

3.1. A Combined Photochemical and Multicomponent Approach

Parts of this chapter, the following subchapters, and the associated parts in the experimental section were adapted with permission from a publication written by the author.^{[247-248],a}

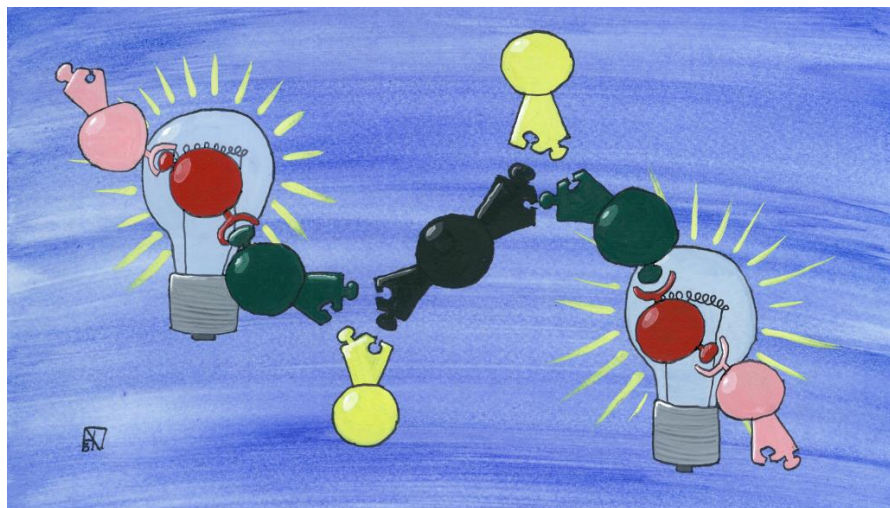
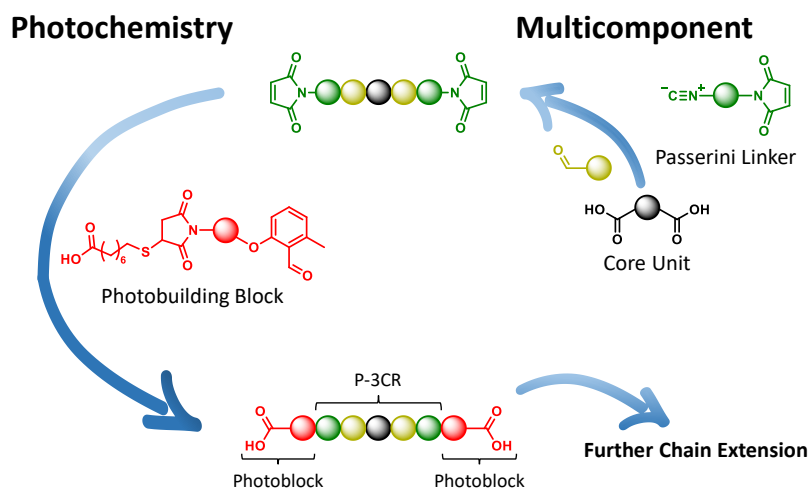


Figure 17. Graphical abstract for the combination of the P-3CR and photoinduced *o*-MBA conjugation. The aquarelle was prepared by Fabian Blößer.

In this section, the synthesis of sequence-defined macromolecules, combining the P-3CR and *o*-MBA conjugation iteratively, is discussed (**Scheme 29**). Therefore, a set of *o*-MBA containing monomer units and building blocks for the P-3CR were prepared in the first step. Afterwards, various Passerini linkers have been synthesized carrying an isocyanate group in order to enable modular chain extension *via* P-3CR (Section 3.1.1). Furthermore, the Passerini linker unit is equipped with a maleimide moiety to allow for subsequent photoinduced *o*-MBA conjugation. Sebacic acid, as core unit, enables the synthesis of a library of symmetric sequence-defined oligomers. Switching between both reaction types, monodisperse macromolecules are accessible in a modular approach. Thus, the strategy yields sequence-defined oligomers up to a molecular weight of 3532.16 g mol⁻¹ alternatingly consisting of

^a Parts of the current section were subject of the master thesis of Fabian Blößer conducted under supervision of the author. Fabian Blößer performed the synthesis of the Passerini building units and all Passerini reactions.

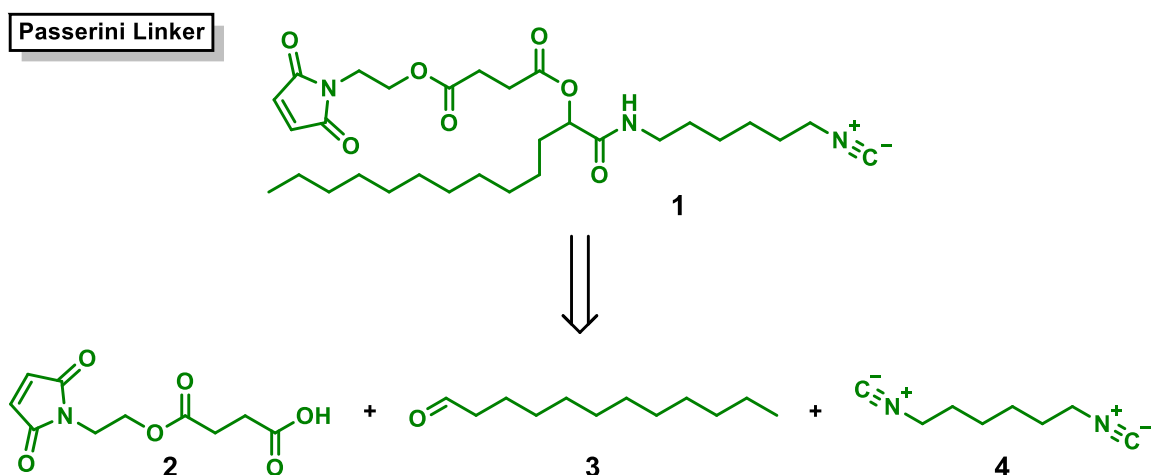
P-3CR and photoblocks. The in-depth characterization was carried out *via* SEC, ESI-MS, and NMR in order to evidence the monodisperse nature of the prepared oligomers.



Scheme 29. Schematic illustration of the consecutive chain extension switching between P-3CR and photochemistry. Starting from a bifunctional core unit, symmetrical sequence-defined macromolecules consisting of Passerini- and photoblocks are obtained.^[247]

3.1.1. Synthesis of the Passerini Linkers

For the combination of the Passerini reaction and photochemical *o*-MBA conjugation to synthesize sequence-defined macromolecules, a linking unit for both chemistries had to be developed. Therefore, in the first step, a Passerini linker **1** was designed carrying a maleimide group as well as an isocyanide moiety (**Scheme 30**). The maleimide group is introduced to

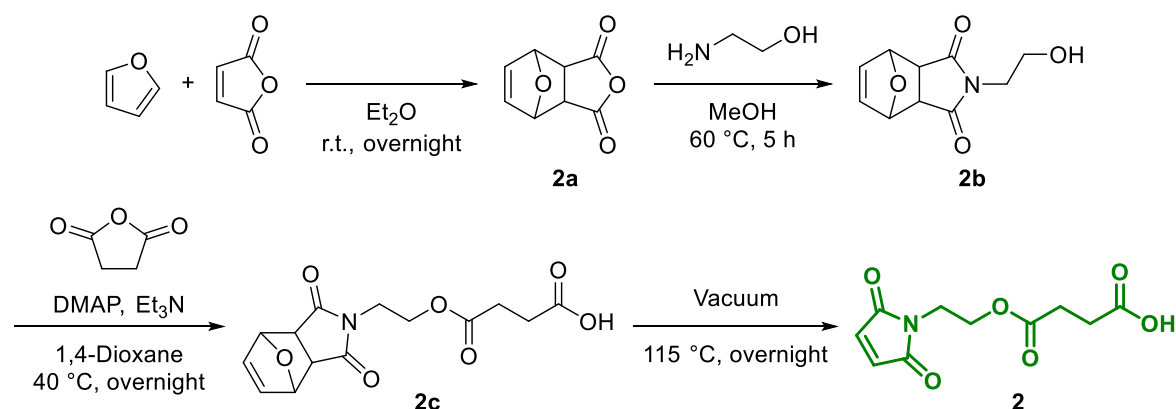


Scheme 30. Retrosynthetic analysis of the Passerini linker **1**. The linker can be prepared from a maleimide carrying carboxylic acid **2**, an aldehyde **3**, and an isocyanide **4**.

3. Results and Discussion

enable a DA cycloaddition in a photochemical approach, whereas the isocyanide group allows the conduction of further P-3CRs to grow macromolecules in as few chain extension steps as possible. As MCRs allow the introduction of multiple groups under simple conditions in a one-pot reaction, linker **1** was prepared *via* a P-3CR. For a Passerini reaction, a carboxylic acid, an aldehyde, and an isocyanide have to be provided and furthermore a maleimide group has to be introduced as linking point towards photochemistry. Therefore, a carboxylic acid **2**, carrying a maleimide moiety for DA reactions, and a bifunctional isocyanide **4** were designed, whereas the commercially available aldehyde **3** was used for the introduction of side chain functionalities.

The maleimide carboxylic acid **2** was prepared starting from furan and maleic anhydride in four steps as depicted in **Scheme 31**.^[249-250] Due to the EWGs, the maleic anhydride double bond is highly prone towards nucleophilic attacks as well as cycloadditions. Therefore, protection of the dienophile had to be performed prior to maleimide formation with furan *via* DA cycloaddition. The resulting cycloadduct **2a** bears a double bond exhibiting an increased electron density and thus shows drastically reduced sensitivity to nucleophilic attacks or cycloadditions. In the consecutive step, the maleimide alcohol **2b** was obtained *via* a nucleophilic reaction by employing ethanolamine and subsequent nucleophilic ring opening of succinic anhydride with the alcohol **2b** yielded the maleimide acid **2c**. In the last step, the furan protecting group was removed prior to the Passerini linker formation to enable DA cycloaddition with *o*-MBAs in a photochemical step. Deprotection was achieved under thermal conditions yielding the target compound **2**. Successful formation of the maleimide **2** and the



Scheme 31. Preparation of the maleimide-acid **2** as building unit for the synthesis of the Passerini linker **1**. Protection of maleic anhydride with furan, maleimide formation with ethanolamine, ring-opening of succinic anhydride and subsequent deprotection of the furan-protected maleimide intermediate **2c** yielded the maleimide acid **2**.

3.1. A Combined Photochemical and Multicomponent Approach

precursors **2a-c** was confirmed by ^1H nuclear magnetic resonance (NMR) spectroscopy as depicted in **Figure 18**. The magnetic resonances at 6.58 (1), 5.46 (2), and 3.18 ppm (3) are resulting from the furan protection group (**Figure 18a-c**). Successful retro-DA reaction yielding the maleimide-acid **2** was confirmed by the absence of magnetic resonances arising from the protection group at 6.50 (1) and 5.26 ppm (2) as well as the resonance shift of proton 3 from 2.87 to 6.72 ppm evidencing the deprotection. The emerging signals of two triplets at 3.73 (4) and 3.67 ppm (5) stemming from the two methylene groups introduced by ethanolamine confirm the formation of the maleimide intermediates. Additionally, the proton resonances between 2.66 and 2.62 (6) as well as between 2.61 and 2.56 ppm (7) were detected as multiplets underpinning the successful formation of the maleimide-acid **2**.

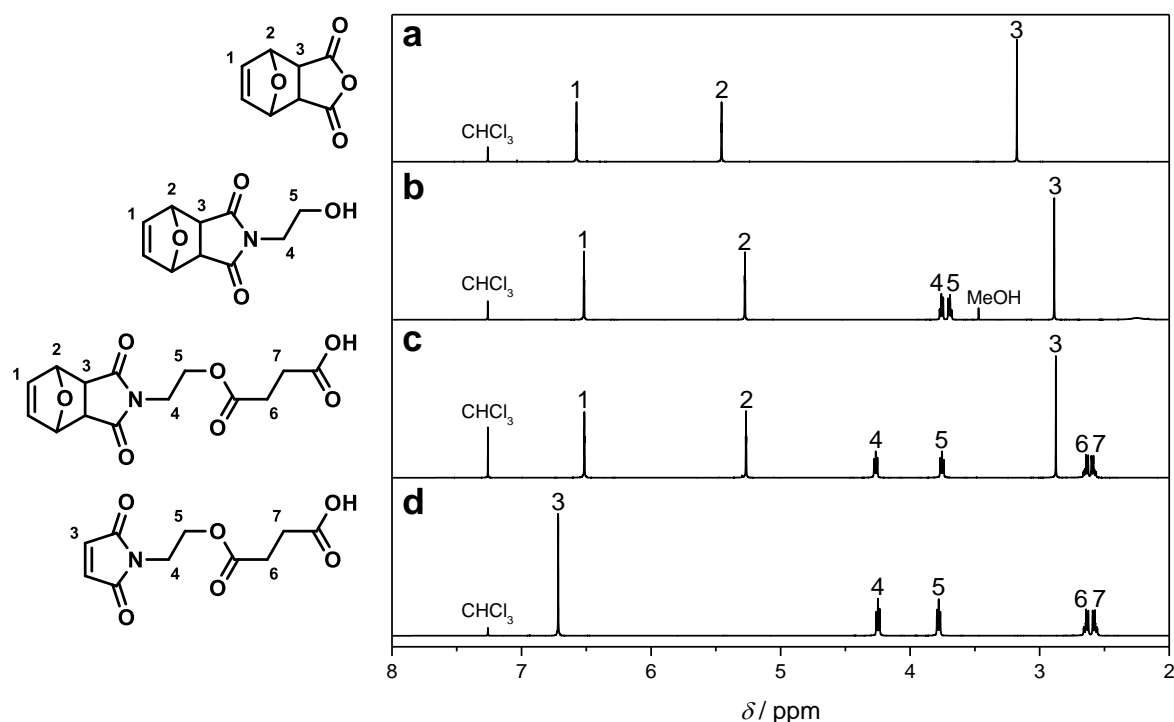
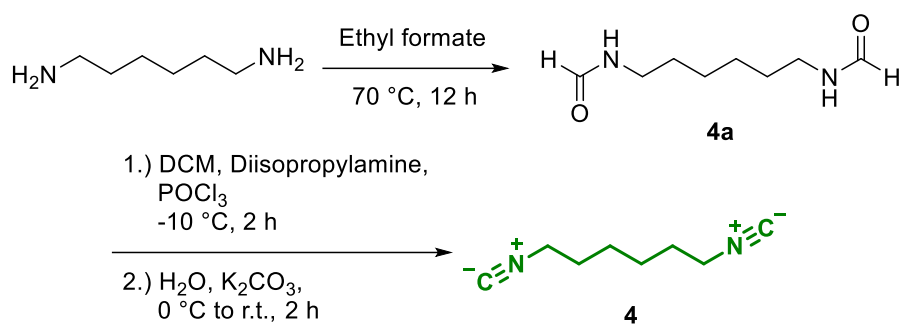


Figure 18. ^1H NMR spectra of the maleimide-acid **2** and its precursors **2a-c** recorded in CDCl_3 at 400 MHz. For the signal assignments refer to the depicted structures.

Apart from the maleimide-acid **2**, a bifunctional isocyanide had to be prepared as building unit for the formation of the Passerini linker enabling further chain extension in consecutive P-3CRs. Therefore, hexamethylenediamine was used as starting material for the synthesis of 1,6-diisocyanohexane **4** as depicted in **Scheme 32**, performed by Fabian Blöber.^[243] In the first step, hexamethylenediamine was refluxed overnight in ethyl formate leading to the

3. Results and Discussion



Scheme 32. Synthesis of 1,6-diisocyanohexane **4** starting from 1,6-diaminohexane. The diamine was converted into the corresponding formamide **4a** by refluxing in ethyl formate. Dehydration in basic medium employing phosphorous oxychloride yielded the desired diisocyanohexane **4**.

formation of the bifunctional formamide **4a** as an intermediate. Subsequently, **4a** was transformed into the diisocyanohexane **4** by dehydration of the formamide below $0\text{ }^\circ\text{C}$ under basic conditions to prevent degradation of the isocyno groups. Characterization of the diisocyanohexane **4** by ^1H NMR spectroscopy is challenging due to the fact that only three multiplets

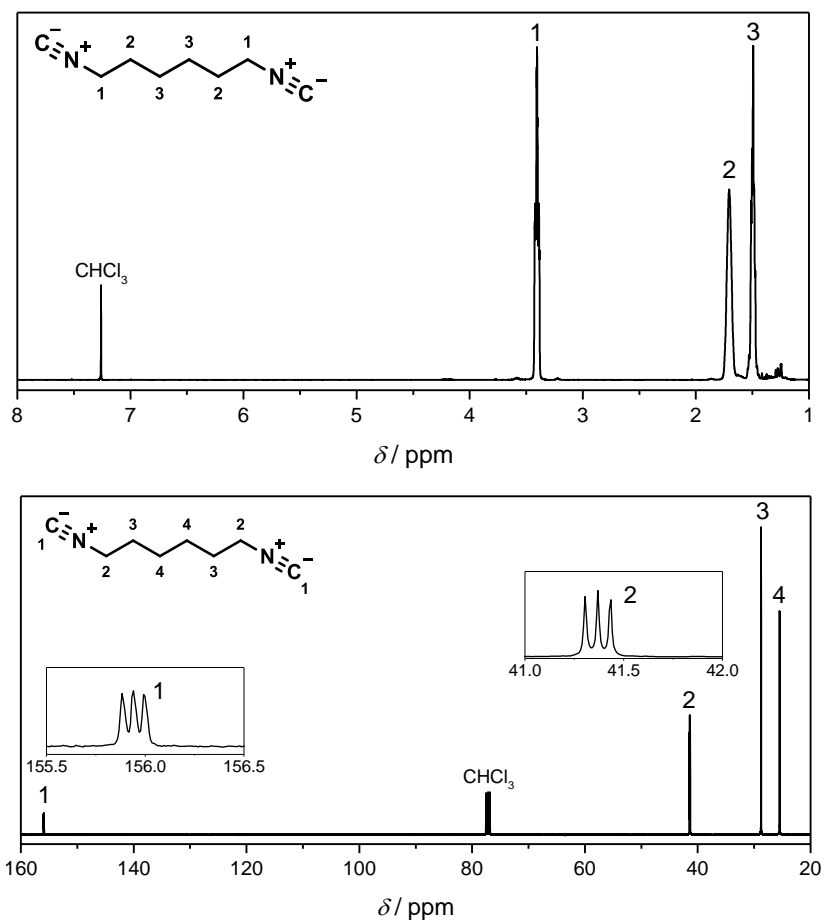
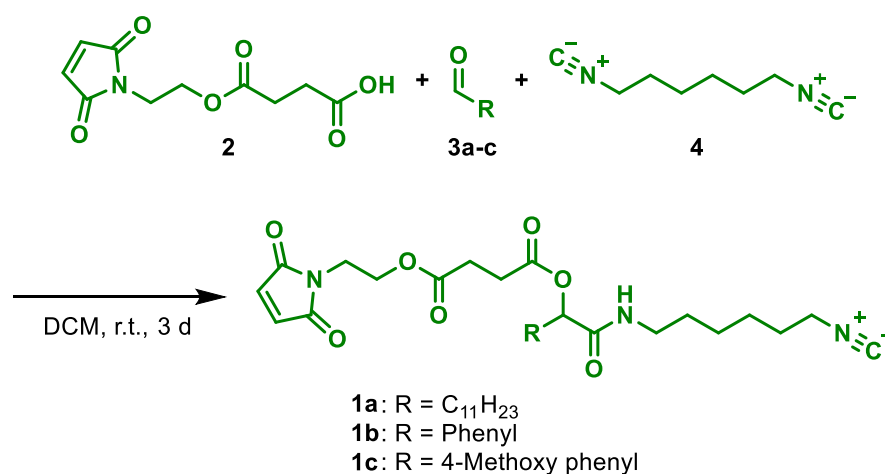


Figure 19. ^1H NMR (top) and ^{13}C NMR (bottom) spectrum of 1,6-diisocyanohexane **4** recorded in CDCl_3 at 400 and 101 MHz, respectively. For the signal assignments refer to the depicted structure.

3.1. A Combined Photochemical and Multicomponent Approach

ranging from 3.50 to 3.33 (1), 1.80 to 1.62 (2), and 1.57 to 1.42 ppm (3) are detected (refer to **Figure 19** top). Therefore, additional confirmation of the isonitrile formation were carried out by ^{13}C NMR characterization recording a ^{13}C - ^{14}N -coupled carbon spectrum as depicted in **Figure 19** (bottom).^[251] Due to ^{13}C - ^{14}N -coupling the carbon resonances at 155.94 ppm (1) as well as 41.37 ppm (2), deriving from the isonitrile group and from the carbon atom adjacent to the isonitrile group, are detected as triplets. Moreover, magnetic resonances of the central methylene groups were recorded at 28.73 (3) and 25.44 ppm (4) evidencing successful formation of the 1,6-diisocyanohexane **4**.

To achieve a high molecular weight in as few chain extension steps as possible, the Passerini linker units **1a–c** were prepared equipped with a maleimide moiety and a isocyanide group providing modular chain growth. The isocyanide group enables chain extension *via* consecutive P-3CRs introducing two Passerini units into the growing chain in a single step while the maleimide group allows the attachment of photoblocks *via* DA cycloaddition. For the synthesis of the desired Passerini linkers **1a–c**, the previously synthesized maleimide-acid **2**, the diisocyanide **4**, and commercially available aldehydes were employed in a P-3CR (**Scheme 33**). Three aldehyde components, i.e. lauric aldehyde **3a**, benzaldehyde **3b**, and methoxybenzaldehyde **3c**, were used for the P-3CR to introduce various side chain substituents. To prevent consumption of both isocyanide groups of the diisocyanide **4**, a fourfold excess of the starting component was added to the reaction mixture. The excess of diisocyanide **4** could be recovered from the reaction mixture by column chromatography (up to



Scheme 33. Synthesis of the Passerini linkers **1a–c** *via* a P-3CR using 1,6-diisocyanohexane **4**, the maleimide-acid **2**, and a commercially available aldehyde **3a–c**.

3. Results and Discussion

65 %). DCM was employed to dissolve the starting material due to the fact that Passerini reactions show higher reaction rates and conversions in aprotic unipolar solvents.^[252] However, the maleimide-acid **2** exhibits a low solubility in DCM, therefore dimethyl sulfoxide (DMSO) was added additionally. The reaction time was of crucial interest, since Passerini reactions need reaction times of up to several days to result in nearly quantitative conversions and high yields. However, the isocyanide group of the Passerini linkers **1a-c** is prone towards hydrolysis already at ambient temperature. Therefore, all operations were conducted under nitrogen atmosphere and the reaction time of three days prevented the isocyanide groups from degradation. Successful formation of the corresponding Passerini linkers **1a-c** was confirmed by ¹H NMR spectroscopy (**Figure 20**). In the ¹H NMR spectrum of the lauric

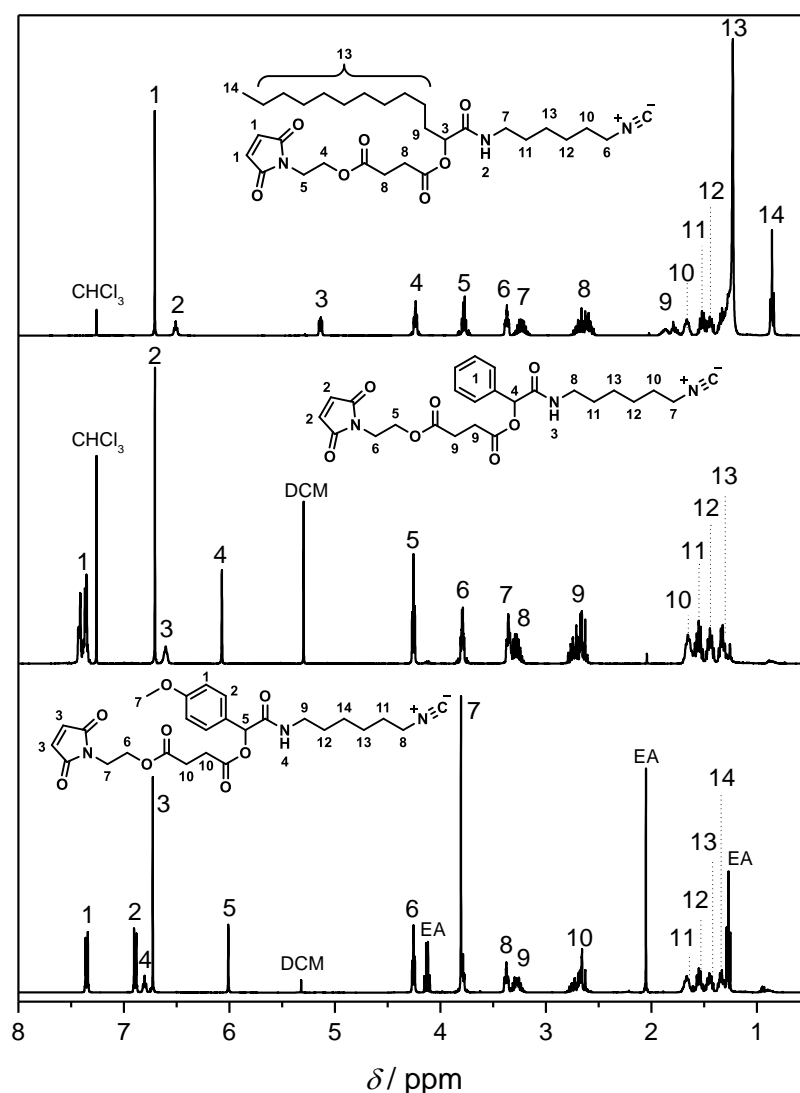
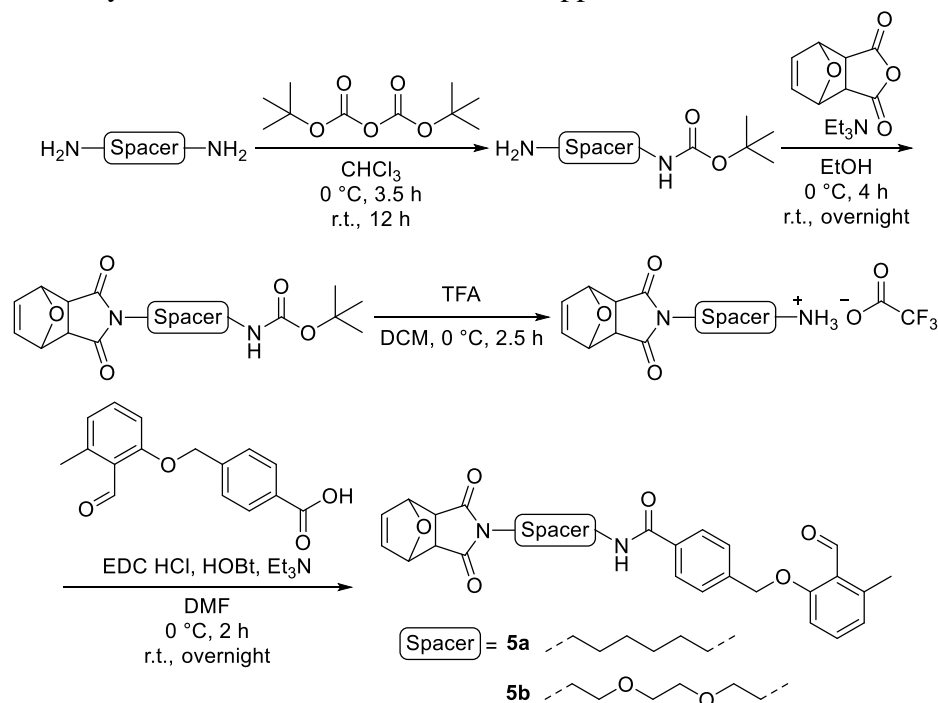


Figure 20. ¹H NMR spectra of the Passerini linker units **1a-c** (top to bottom) recorded in CDCl₃ at 400 MHz. For the signal assignments refer to the depicted structures.

aldehyde Passerini linker **1a** (refer to **Figure 20**, top), a magnetic resonance is observed at 6.51 ppm (2) as a triplet arising from the newly formed amide group. Additionally, the magnetic resonance at 5.14 ppm (3), deriving from the chiral methine group, evidences successful formation of the Passerini adduct **1a**. Furthermore, the adjacent methylene group at 1.92 to 1.73 ppm (9) exhibits characteristic splitting due to coupling with the chiral methine proton as well as the adjacent methylene group 13. Analogous characteristic resonances are recorded for the benzaldehyde Passerini linker **1b** (refer to **Figure 20**, middle). A singlet at 6.60 ppm (3) arising from the amide functionality and the magnetic resonance of the chiral methine proton (4) at 6.07 ppm evidence successful formation of the Passerini linker **1b**. Accordingly, the ^1H NMR spectrum of the methoxybenzaldehyde Passerini linker **1c** (refer to **Figure 20**, bottom) exhibits magnetic resonances at 6.63 ppm stemming from the amide formation (4) and a proton resonance resulting from the chiral methine proton at 6.00 ppm (5). Moreover, the magnetic resonances associated with the maleimide moiety are detected around 6.7 ppm in all ^1H NMR spectra. Consequently, the successful formation of the Passerini linkers **1a–c** exhibiting three functional anchor sides is confirmed by ^1H NMR spectroscopy. The linkers exhibit three functional units. First, the isocyanide side allows consecutive Passerini reactions *via* chain extension of an oligomer species. Second, the maleimide side enables attachment of photoblocks *via* DA cycloaddition with *o*-MBAs and third, a variable side chain substituent can be introduced by different aldehydes. Introduction of functional groups to the Passerini linker might be challenging, since carboxylic acids, aldehydes, ketones, amines, and isocyanides are competing with the starting material in a P-3CR and will lead to side products. The aldehyde moieties employed for the synthesis of the Passerini linkers **1a–c** offer two advantages. First, they provide relatively high molecular weights (up to 184 g mol^{-1}), leading to a higher increase in molecular weight of the oligomers. A significant increase of molecular weight facilitates purification since the chromatographic separation of the single generations is more efficient. Secondly, large aliphatic substituents increase the solubility in organic solvents. The photobuilding blocks used for the synthesis of sequence-defined macromolecules exhibit a high difference in polarity within the building units themselves and thus display decreased solubility in organic solvents with increased number of sequence orders. Therefore, large aliphatic moieties, such as lauric aldehyde, should increase the solubility in organic solvents with increasing repeating units.

3.1.2. Synthesis of the Photobuilding Blocks

Three different types of photobuilding blocks were prepared in total. First, as depicted in **Scheme 34**, two types of photomonomers **5a-b** were synthesized equipped with two different spacer units based on 1,6-hexamethylenediamine (**5a**) and 2,2'-(ethylenedioxy)bis(ethylamine) (**5b**) to provide variation of the polymer backbone. Starting from the two spacer units, the monomers have been obtained in a four-step synthesis approach by protection of one amine side, maleimide formation, deprotection, and attachment of an *o*-MBA *via* amidification. Each of the units exhibit a benzaldehyde moiety that undergoes photoenolization when irradiated as well as a furan-protected maleimide for DA trapping. In the ^1H NMR spectrum depicted in **Figure 21**, characteristic resonances at 6.5, 5.2, and 2.8 ppm evidence the successful introduction of the furan protected maleimide. In addition, the proton resonance at 10.7 ppm deriving from the *o*-MBA group verifies the formation of the target compounds **5a-b**. However, a functional group for the conduction of consecutive P-3CRs is missing in the photomonomers **5a-b**. Therefore, a carboxylic acid had to be introduced to the monomer units providing an anchor point for Passerini reactions (second photobuilding block). The maleimide moiety of the monomers offers a facile approach for the introduction of an acid



Scheme 34. Synthesis of the photomonomers **5a-b**. First the spacer units were equipped with a tert-butyloxycarbonyl protecting group on one side followed by the maleimide formation. The Boc protecting group was removed under acidic conditions prior to the amidification of the *o*-MBA moiety.

3.1. A Combined Photochemical and Multicomponent Approach

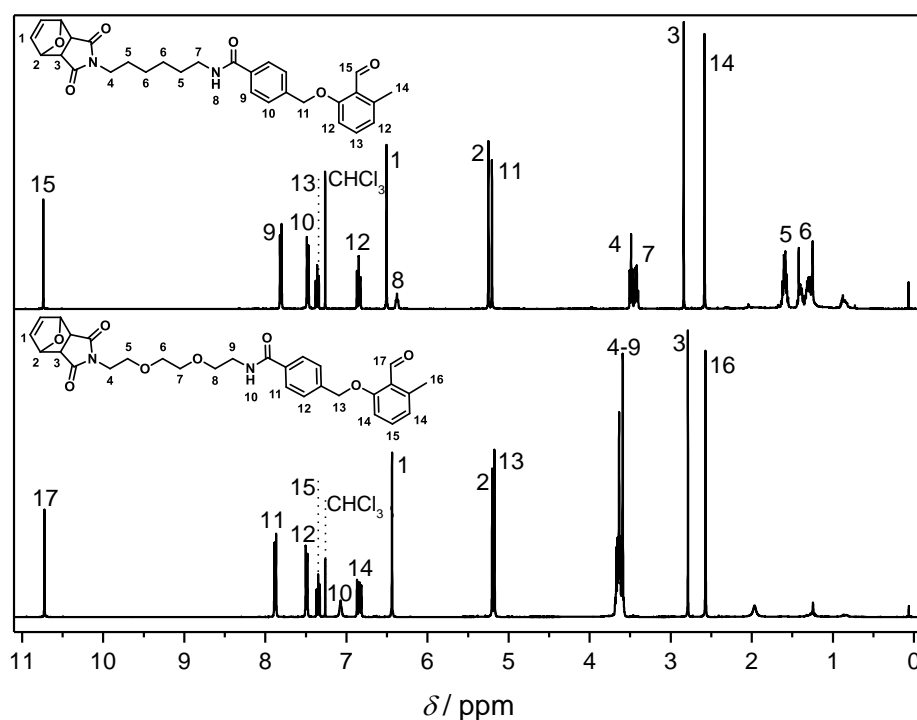
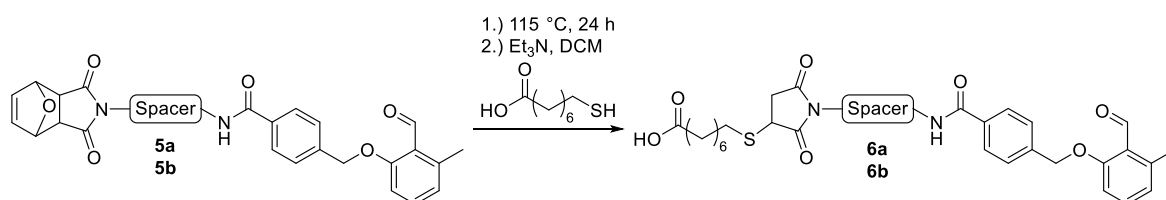


Figure 21. ^1H NMR spectra of the photomonomer units **5a–b** (top to bottom) recorded in CDCl_3 at 400 MHz. For the signal assignments refer to the depicted structures.

functionality *via* base-catalyzed thiol-Michael addition using mercaptooctanoic acid (refer to **Scheme 35**). However, deprotection of the maleimide is necessary prior to the thiol-Michael addition. The furan protecting group of the photomonomers **5a–b** was removed by thermal treatment at 115 °C for 24 hours in order to initiate the retro DA reaction. In addition, high vacuum was employed in order to remove the released furan from the reaction mixture and shift the DA reaction equilibrium towards cycloreversion. Successful formation of the photomonomer acids **6a–b** was evidenced *via* ^1H NMR spectroscopy as depicted in **Figure 22**. First, the proton resonances deriving from the furan protecting group at 6.50, 5.25, and 2.84 ppm could not be detected after deprotection (compare with protons 1,2, and 3 in **Figure 21**). Due to the thiol-Michael addition, no olefinic proton resonances arising from the



Scheme 35. Synthesis of the photomonomer acids **6a–b**. The furan protecting group was first removed by thermal treatment under vacuum. Thiol-Michael addition using mercaptooctanoic acid yielded the target compounds.

3. Results and Discussion

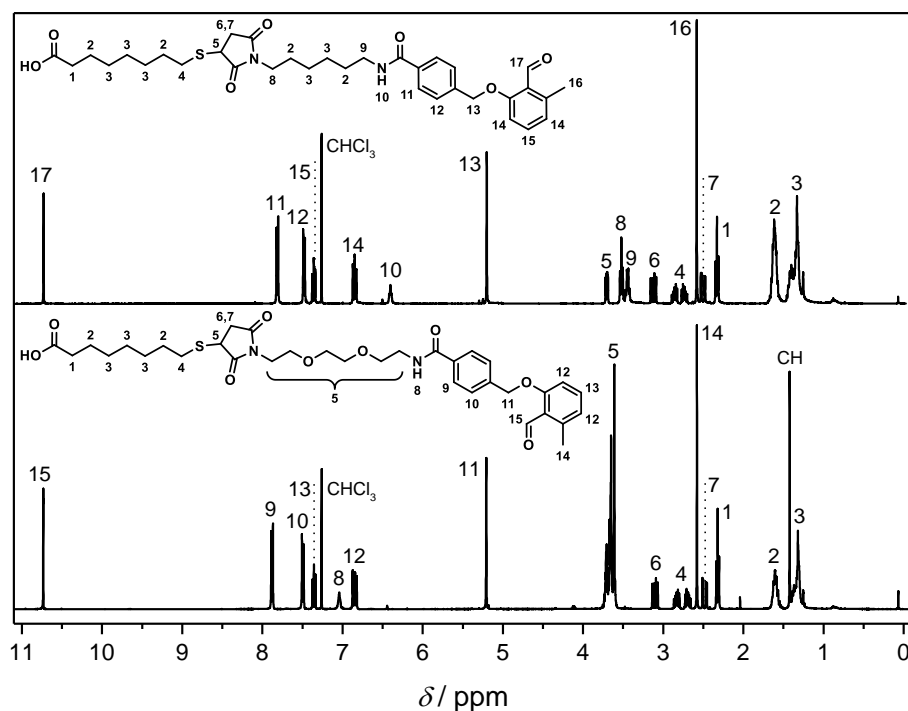
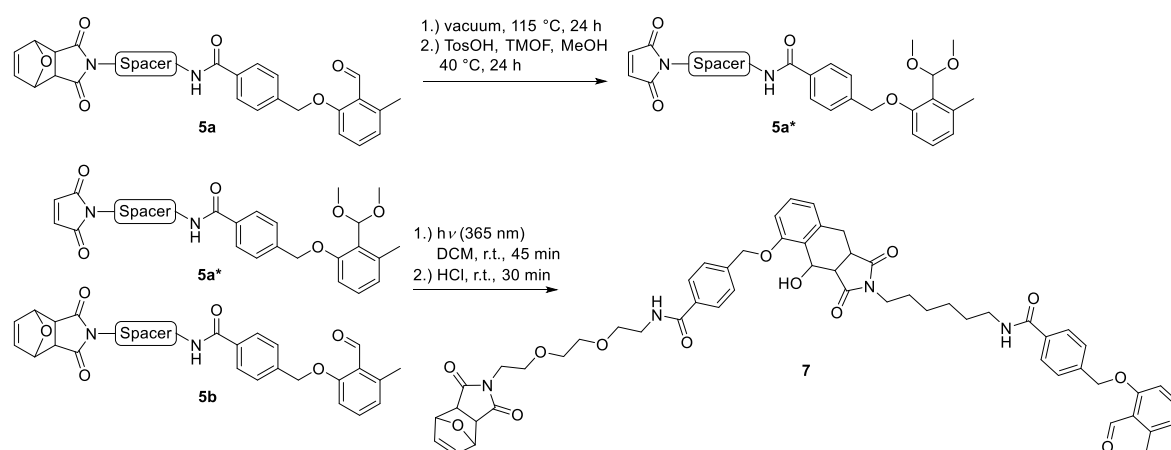


Figure 22. ^1H NMR spectra of the photomonomer acids **6a–b** (top to bottom) recorded in CDCl_3 at 400 MHz. For the signal assignments refer to the depicted structures.

deprotected maleimide group were recorded around 6.7 ppm, indicating the formation of the thiol-Michael adduct. Moreover, a magnetic resonance at 3.7 ppm (5) resulting from the methine group adjacent to the thioether is detected with a doublet of doublets coupling. In addition, two doublet of doublets observed at 3.12 (6) and 2.50 ppm (7) are deriving from



Scheme 36. Synthesis of photodimer **7**. In a first step photomonomer **5a** was deprotected on the maleimide side and a dimethyl acetal protecting group was introduced to prevent the benzaldehyde from reacting. The photodimer **7** was obtained under irradiation of UV-light at 365 nm using the monomers **5a*** and **5b**.

the methylene group of the five-membered ring in *cis* and *trans*-position, respectively. Furthermore, a multiplet (4) was recorded at 2.95 to 2.66 ppm, stemming from the methylene group adjacent to the thioether, evidencing the formation of the thiol-Michael adduct. The methylene group adjacent to the introduced carboxylic acid results in a magnetic resonance in the ^1H NMR spectrum at 2.33 ppm (1) – introduced by the thiol-Michael addition – evidencing successful functionalization of the photomonomers.

The modular strategy in which a symmetric linear molecule is ligated with a previously synthesized block, is an efficient way for increasing the molecular weight in sequence-defined macromolecules. Therefore, a third photobuilding block, a dimer consisting of two photomonomers was prepared as illustrated in **Scheme 36**. In the first step, the furan protecting group was removed by thermal treatment on the maleimide side of the photomonomer unit **5a** and the photoreactive aldehyde functionality was locked as a dimethyl acetal in order to

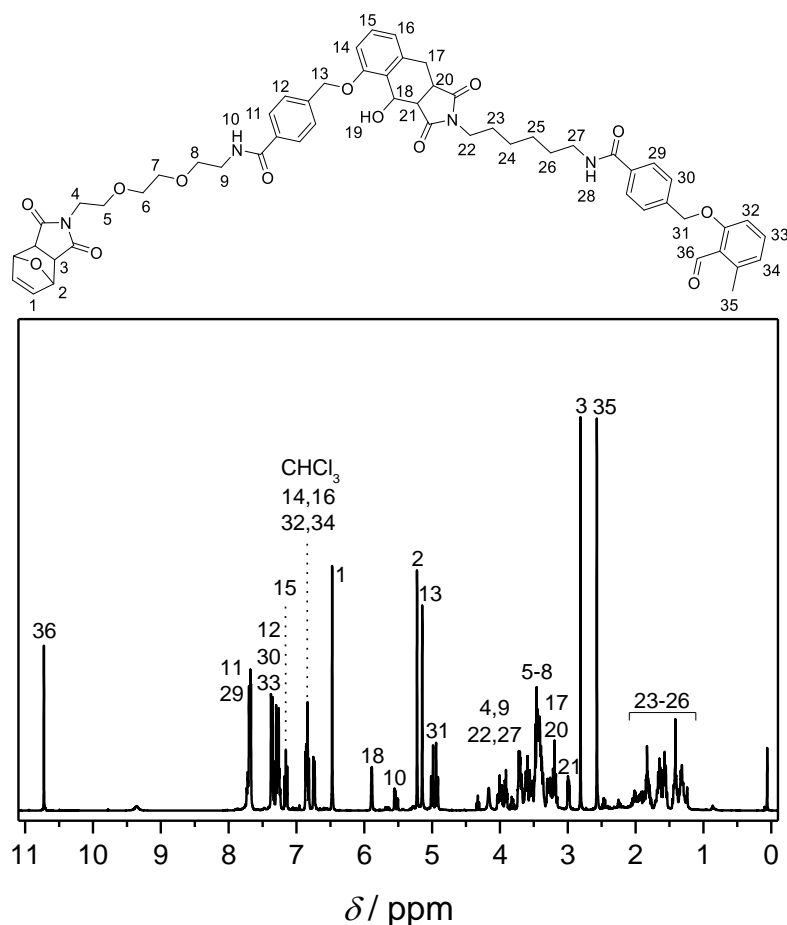
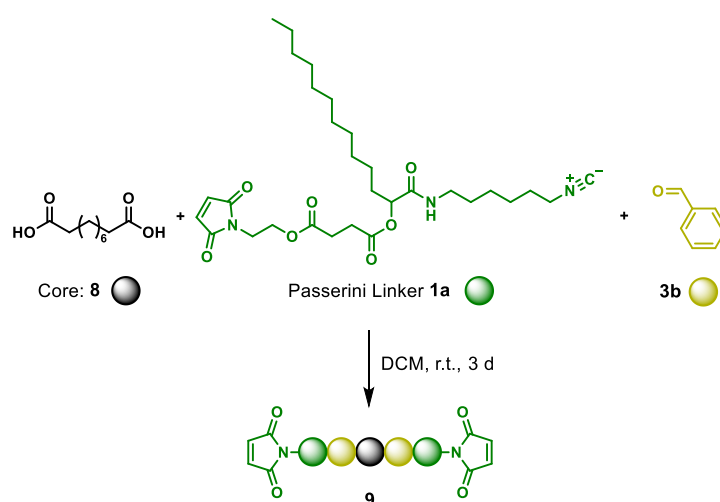


Figure 23. ^1H NMR spectrum of the photodimer **7** recorded in CDCl_3 at 400 MHz. For the signal assignments refer to the depicted structure.

3. Results and Discussion

prevent unintended photopolymerization of the monomer. The acetal was formed in dry methanol using trimethyl orthoformate (TMOF) and *para*-toluenesulfonic acid (*p*-TsOH) as catalyst. Since the dimethyl acetal is sensitive to hydrolysis, purification was carried out by filtration of the crude mixture over silica gel with DCM and 1 % of triethylamine under continuous nitrogen flow. Photomonomer **5b** was employed for the formation of the dimer without any further modifications. The two monomers **5a*** and **5b** were transferred into nitrogen flushed headspace vials, due to the fact that residual oxygen quenches the transition of the *o*-MBA into its triplet state T_1 and thus prevents formation of the DA adduct. Under irradiation of UV-light at 365 nm, the dimer was obtained by photoinduced DA cycloaddition of the *o*-MBA moiety of the PEG derived monomer **5b** and the deprotected maleimide of **5a***. After converting the labile dimethyl acetal by acidic hydrolysis to an aldehyde functionality, the dimer **7** carries a furan-protected maleimide and a benzaldehyde group enabling chain extension *via* photoinduced [4+2] cycloaddition. The ^1H NMR spectrum of dimer **7** is depicted in **Figure 23**. Importantly, the three functional groups, i.e. furan protected maleimide, *o*-MBA, and the benzo isoindole, formed upon DA cycloaddition, are identified in the proton spectrum. Proton resonances at 10.72 (36) and 2.57 ppm (35) were assigned to the carbonyl proton and the methyl group of the *o*-MBA moiety, respectively. The magnetic resonances verifying the presence of the furan protecting group are recorded at 6.47 (1), 5.22 (2), and 2.81 ppm (3). Upon irradiation with UV-light, *o*-MBAs form an isoindole structure when reacted with maleimides. Characteristic resonances are detected arising from the new



Scheme 37. Synthesis of the symmetrical tetramer **9** in a Passerini reaction starting from the symmetrical core unit sebacic acid **8** and the Passerini linker **1a**. Benzaldehyde **3b** was employed for the introduction of side chain substituents.

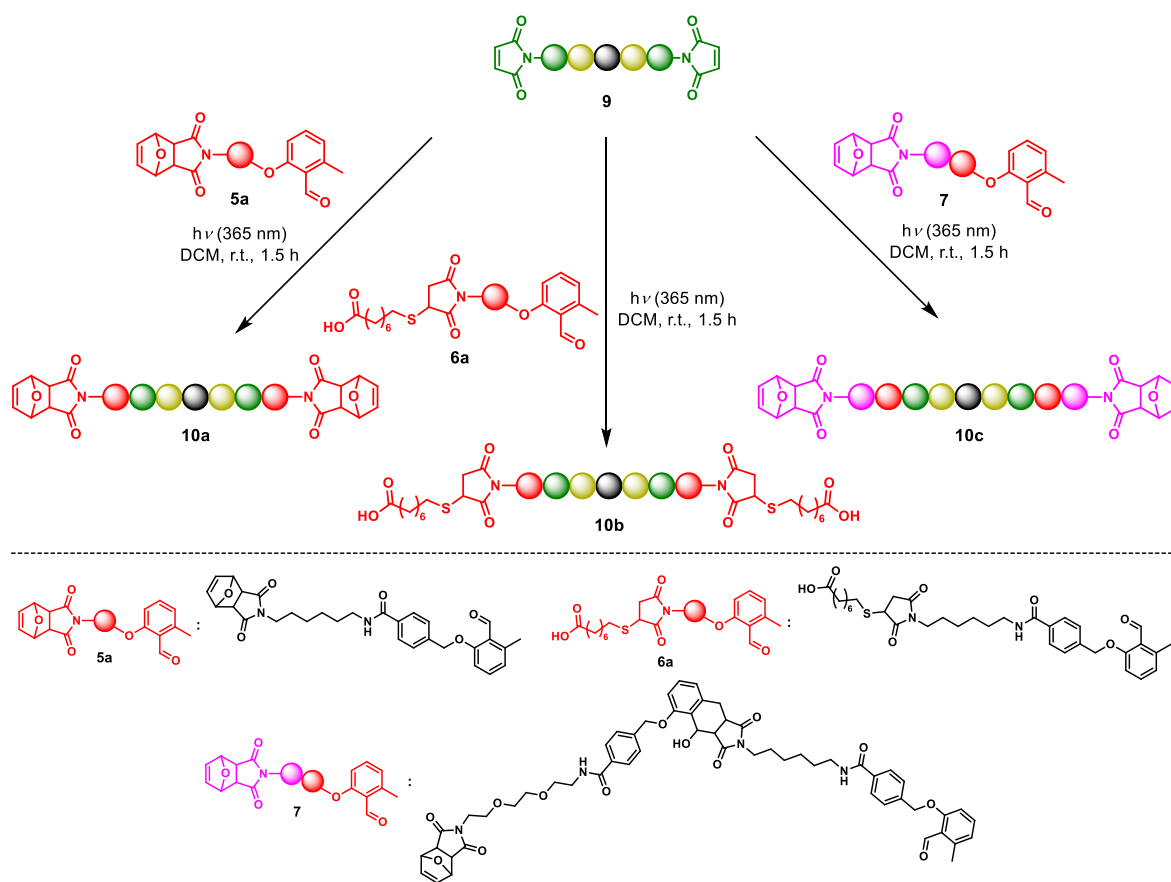
bond formation at 5.89 (18), 3.31 - 3.12 (17 and 20), and 2.99 ppm (21) verifying the successful DA cycloaddition.

3.1.3. Combining Photochemistry and Passerini Reactions for Sequence-Defined Macromolecules

As illustrated in the introductory **Scheme 29**, the sequence-defined macromolecules have been prepared starting from a symmetrical core unit. Therefore, the bifunctional sebacic acid **8** was employed as core unit for the synthesis of linear oligomers leading to a bidirectional growth, significantly increasing the molecular weight per chain extension step and thus resulting in symmetric macromolecules. In the first step, a P-3CR was carried out using the Passerini linker **1a** and the core unit **8** yielding the symmetric tetrafunctional macromolecule **9** by introducing two Passerini substituents into the growing oligomer on each side in a single step (**Scheme 37**). The formation of the tetra-substituted macromolecule **9** was conducted under similar reaction conditions applied for the synthesis of the Passerini linkers **1a-c** using benzaldehyde **3b** for the introduction of a side chain group. To drive the reaction towards high yields, the linker **1a** was employed in a 3.6-fold excess, whereas benzaldehyde **3b** was added in a threefold excess. After stirring the Passerini reaction in DCM (0.5 M relative to sebacic acid **8**) for three days at ambient temperature, the crude product was purified by flash chromatography with a gradient of cyclohexane/ethyl acetate yielding 67 % of the desired symmetric sequence-defined oligomer **9**. Furthermore, up to 45 % of the excess of the Passerini linker **1a** could be recovered.

In general, modular strategies provide a powerful tool to design complex sequence-defined macromolecules using building blocks with different functional groups and thus achieving variation of the oligomer backbone functionalization. For the chain extension using photochemistry after P-3CR, three different types of α,ω -functionalized photobuilding blocks were employed. First, the non-modified photomonomer **5a** equipped with an *o*-MBA unit (photo-caged diene) and a furan caged maleimide was applied for the photoreaction. Second, the modified monomer **6a** exhibiting an *o*-MBA on the one side, and on the other side a carboxylic acid was used in order to conduct chain extension *via* P-3CR in further chain extension steps. An efficient approach for increasing molecular weight is the addition of

3. Results and Discussion



Scheme 38. Sequential and modular strategies for the synthesis of sequence-defined oligomers alternatingly consisting of Passerini and photoblocks. The tetramer **9** was extended with the photomonomer **5a**, a modified photomonomer **6a**, and a photodimer **7** to afford the functional oligomers equipped with furan capped maleimides (**10a** and **10c**) or a terminal carboxylic acid group at both chain ends (**10b**).

larger building blocks, such as dimers. Therefore, as a third photobuilding block, the photodimer **7** functionalized with an *o*-MBA group and a furan protected maleimide was employed for the synthesis of sequence-defined macromolecules. Based on the three building blocks **5a**, **6a**, and **7**, the macromolecular backbone structure can be varied diversifying the composition of the symmetrical sequence-defined oligomers. The photoinduced DA cycloaddition between the Passerini tetramer **9** and the photobuilding blocks **5a**, **6a**, and **7** were conducted under batch conditions in headspace vials employing a PL-L lamp ($\lambda_{\text{max}} = 365 \text{ nm}$) as irradiation source as depicted in **Scheme 38**. Upon irradiation, macromolecules alternatingly consisting of P-3CR and photoblocks were obtained, i.e. the symmetric hexamers **10a** ($2571.13 \text{ g mol}^{-1}$) and **10b** ($2851.52 \text{ g mol}^{-1}$) as well as the symmetric octamer **10c** with a molecular weight of $3532.16 \text{ g mol}^{-1}$. From the building blocks to the final octamer, an isolated overall yield of 55 % was achieved. Since the Passerini reaction requires reactants in

3.1. A Combined Photochemical and Multicomponent Approach

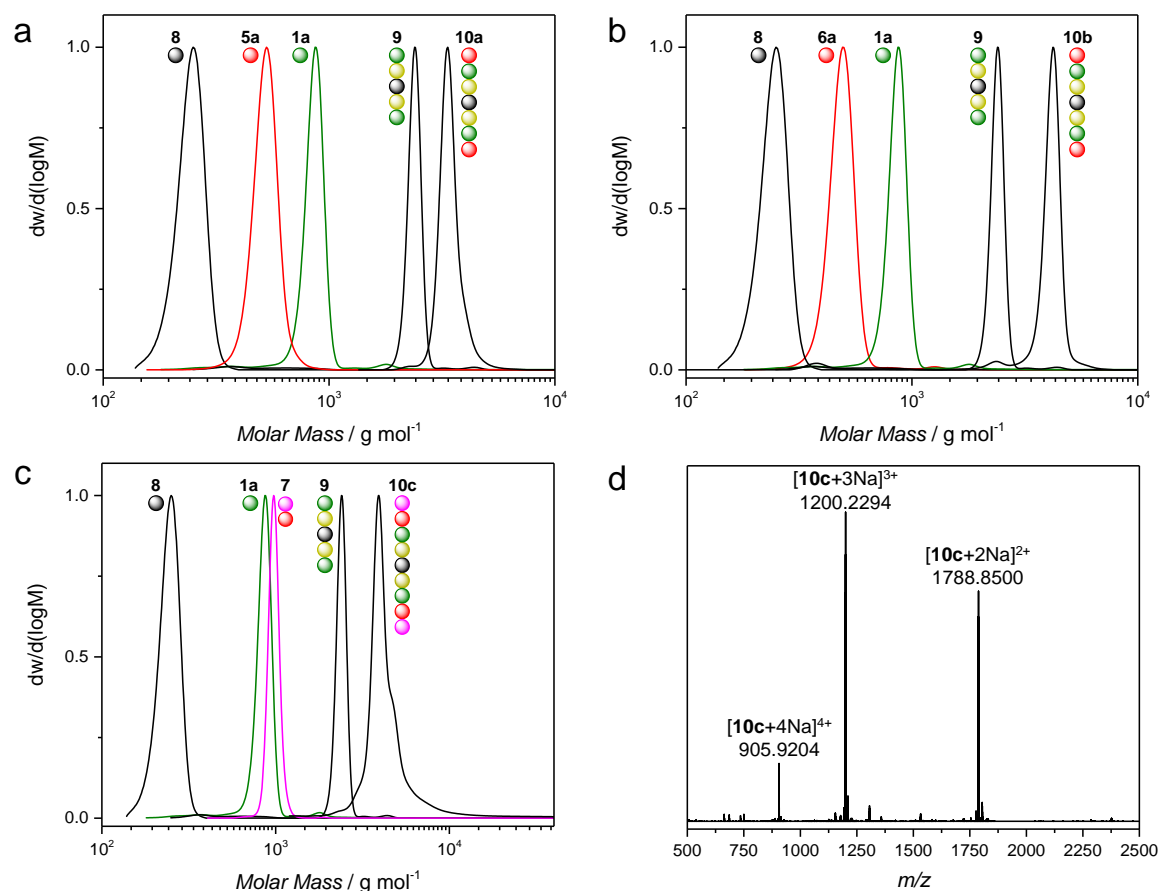


Figure 24. (a-c) SEC traces of the synthesized sequence-defined macromolecules **10a-c** alternately consisting of Passerini and photoblocks. Additionally, the core unit sebacic acid **8**, the building blocks **1a**, **5a**, and **6a** as well as the tetramer **9** are depicted. All SEC traces were recorded on a THF based SEC system. (d) Full MS spectrum of **10c** in the mass range of m/z 500 to 2500 recorded in positive ion mode.

excess and the photoreaction demands equimolar stoichiometry, the intermediates and target compounds need to be purified *via* flash chromatography resulting in a decrease of the overall yield. Additionally, bidirectional growth starting from a symmetrical core unit contributes to a certain loss in overall efficiency since quantitative conversion of the chain ends has to be ensured. Anything but quantitative conversion of the chain ends leads to a single side chain extension of the sequence-defined macromolecules resulting in reduced overall yields. It is interesting to note that the hexamer **10b** exhibits a carboxylic acid at both chain ends offering an anchor point for a consecutive Passerini reaction to extend the chain length further. In contrast, the hexamer **10a** and the octamer **10c** are equipped with furan capped maleimides. In order to conduct chain extension *via* a Passerini reaction, the furan protection group has to be removed and a carboxylic acid has to be introduced as it was presented in

the synthesis of the photomonomers **6a-b** in Section 3.1.2. Furthermore, the oligomers **10a** and **10c** could be extended in subsequent photoreactions after a deprotection step using the photobuilding blocks **5a**, **6a**, or **7**.

Successful formation of the successively synthesized sequence-defined macromolecules was verified by SEC, high resolution Orbitrap ESI-MS, and NMR spectroscopy. The SEC traces were recorded on a THF based SEC system and are depicted in **Figure 24a-c** including the core unit **8**, Passerini linker **1a**, Passerini tetramer **9**, photomonomers **5a** and **6a**, photodimer **7**, and the targeted sequence-defined oligomers **10a-c**. The molecular weights have been obtained relative to a polystyrene (PS) calibration. After the formation of the Passerini tetramer **9**, a shift indicating an increase in molecular weight by 1500 g mol^{-1} (corresponding to a decrease in retention volume) is observed, starting from the core unit **8** and the Passerini linker **1a**, by inspecting their SEC traces. Additionally, an increase in molecular weight by 1000 g mol^{-1} (**5a**), 1200 g mol^{-1} (**6a**), and 2000 g mol^{-1} (**7**) is detected for the formation of the consecutive symmetrical sequence-defined oligomers **10a-c** using the respective photobuilding units **5a**, **6a**, and **7** for chain extension. Consequently, the SEC analysis confirms the successful modular chain extension with an increase of molecular weight after the addition of each of the respective building blocks. For the macromolecules **10a** and **10b** chromatographically determined dispersities of $D = 1.01$ have been obtained, whereas **10c** shows a dispersity of $D = 1.03$ due to a shoulder. Nevertheless, the increase of molecular weight resulting from the sequential approach confirms the success of the successive multicomponent reaction and photochemical synthetic strategy. In addition, the traces are verifying the monodisperse nature of the synthesized sequence-defined oligomers **10a-c**. In **Figure 24c**, a shoulder towards higher molecular weight is determined for the SEC trace of **10c** leading to a slight increase of the dispersity going from tetramer **9** to the octamer **10c**. In addition, the trace of **10c** displays a broadening compared to the traces of **10a** and **10b** increasing the dispersity further. One explanation for the broadening could be associated with a higher adsorption driven column interaction with the column material since **10c** features a higher amount of the polar photomonomers incorporated into the macromolecule. **10c** also shows reduced solubility in organic solvents as the photomonomers exhibit a higher difference in polarity in contrast to the Passerini blocks. Yet, the high resolution ESI-MS spectrum of the

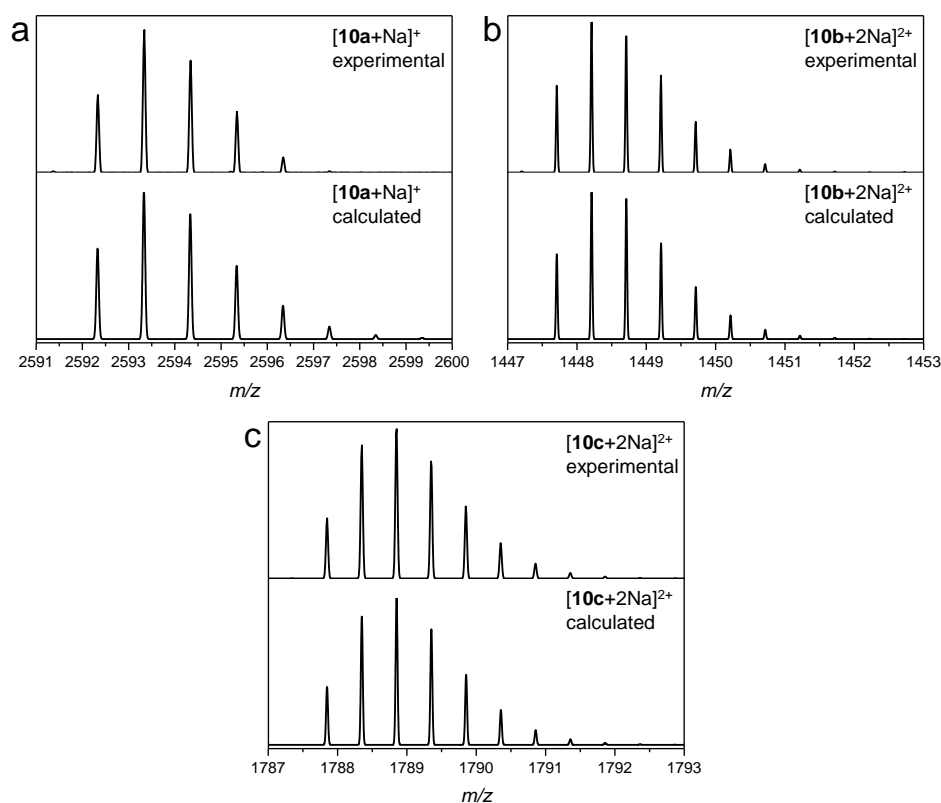


Figure 25. Recorded (top) and calculated (bottom) ESI-MS spectra of the oligomers isotopic pattern **10a** (a), **10b** (b), and **10c** (c).

sequence-defined macromolecule **10c** depicted in **Figure 24d** only reveals mass signals arising from the macromolecule itself (full mass spectra of **10a** and **10b** can be found in Section 5.3.5). Mass signals have been recorded as the respective charged sodium adducts at m/z 1788.8500 ($[10c+2Na]^{2+}$, $m/z_{\text{calc.}}$ 1788.8516, $\Delta m/z$ 0.0016), m/z 1200.2294 ($[10c+3Na]^{3+}$, $m/z_{\text{calc.}}$ 1200.2308, $\Delta m/z$ 0.0014), and m/z 905.9188 ($[10c+4Na]^{4+}$, $m/z_{\text{calc.}}$ 905.9204, $\Delta m/z$ 0.0016) being in excellent agreement with the resolution limits of the employed Orbitrap mass analyzer. The characterization *via* SEC evidences the monodisperse character of the synthesized sequence-defined oligomers **10a-c** as well as the mass spectrum of **10c** clearly indicates its monodispersity. Furthermore, the in positive mode recorded as well as the calculated mass spectra of **10a-c** are depicted in **Figure 25a-c**. In the ESI-MS spectrum, a single charged sodium adduct of the sequence-defined macromolecule **10a** was recorded at m/z 2593.3369 ($m/z_{\text{calc.}}$ 2593.3317, $\Delta m/z$ 0.0052). It is important to note that during ESI-MS analysis the symmetric hexamer **10b** was oxidized. Therefore, a double charged signal detected at m/z 1448.2110 could be assigned to the sulfone adduct of **10b** containing two sodium cations ($m/z_{\text{calc.}}$ 1448.2111, $\Delta m/z$ 0.0001). In **Figure 25c**, **10c** was recorded as a

3. Results and Discussion

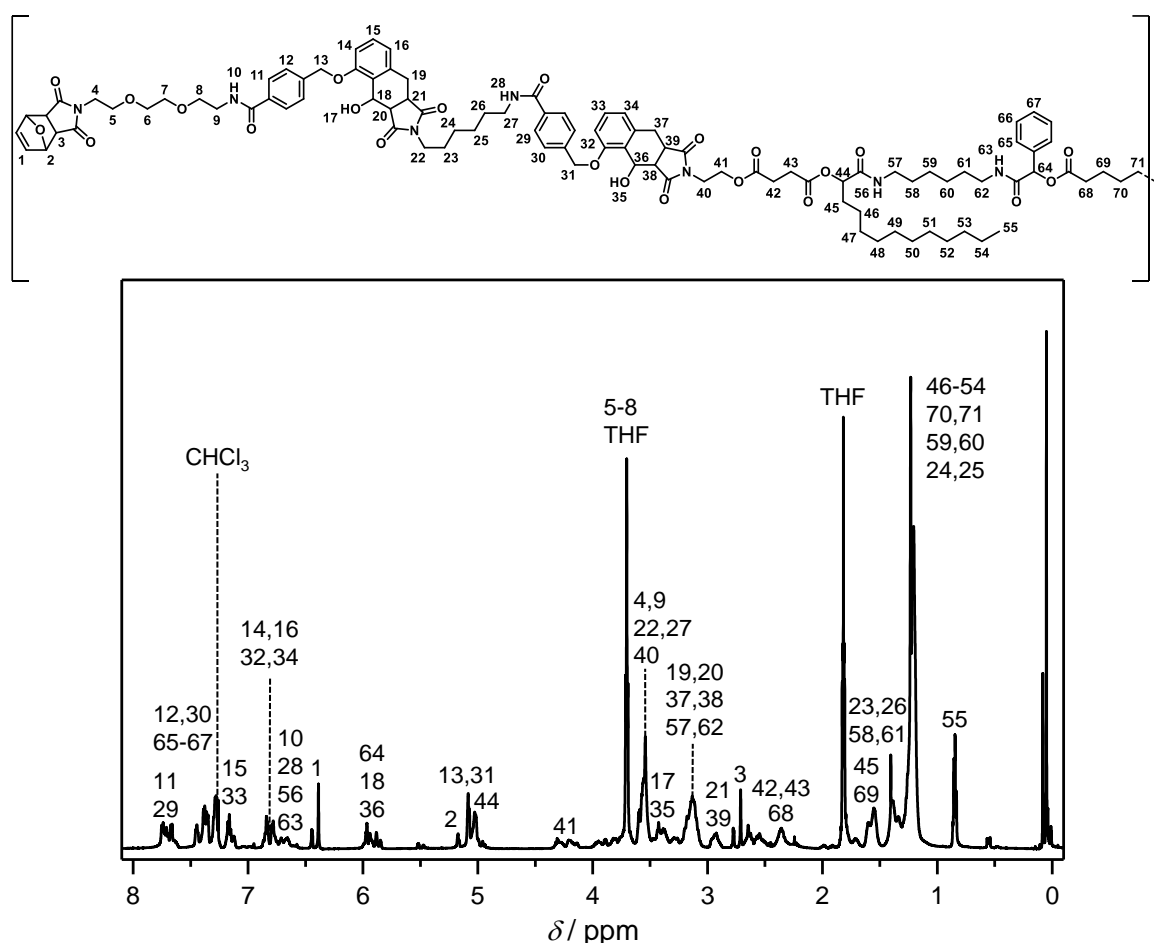


Figure 26. ^1H NMR spectrum of the sequence-defined octamer **10c** recorded in CDCl_3 at 400 MHz. For the signal assignments refer to the depicted structure.

double charged species with two sodium counter ions at m/z 1788.8500 ($m/z_{\text{calc.}}$ 1788.8516, $\Delta m/z$ 0.0016). The isotopic pattern of the in **Figure 25a-c** presented mass spectra of the sequence-defined oligomers **10a-c** are in excellent agreement with the calculated isotopic pattern verifying the successful synthesis and the monodisperse character of the linear sequence-defined macromolecules.

Additionally, characterization of the respective sequence-defined macromolecules was carried out *via* NMR spectroscopy. In **Figure 26** the ^1H NMR spectrum of the octamer **10c** is depicted (for ^1H NMR spectra of **10a** and **10b** refer to the Section 5.3.5). Three characteristic functional groups are identified in the macromolecule **10c**. First, two chiral methine groups are indicating the formation of Passerini adducts. One methine group (64) is introduced during the Passerini linker **1a** formation and one adjacent to the phenyl ring (44) is introduced upon the formation of the tetra-substituted oligomer **9**. The recorded magnetic resonances

between 6.00 - 5.84 (64) and 5.04 - 5.00 ppm (44), deriving from the chiral methine groups, indicate the successful formation of Passerini blocks. Second, the isoindole structure, formed upon irradiation during DA cycloaddition of *o*-MBA and maleimide, evidences the successful formation of the octamer, which is confirmed by magnetic resonances recorded at 6.00 - 5.84 (18/36), 3.20 - 3.06 (19/20/37/38) as well as 2.96 - 2.88 ppm (21/39) as already detected in the photodimer **7**. Third, the sequence-defined macromolecule **10c** exhibits furan caged maleimides on both chain ends as verified by proton resonances at 6.39 (1), 5.17 (2), and 2.77 ppm (3).

MCRs and photoconjugation methods are very efficient tools for providing precision oligomers alternatingly consisting of P-3CR and photoblocks. Furthermore, P-3CRs provide a straightforward approach for the chain extension and the introduction of functional side chains in one step, while photochemical methods allow temporal and spatial control over reactions. Therefore, the combination of both ligation techniques, i.e. P-3CR and DA cycloaddition with *o*-MBAs, was demonstrated in this section confirming the versatility of the combination of P-3CRs and photoreactions. Starting from sebacic acid symmetric sequence-defined macromolecules have been prepared based on a Passerini linker and photobuilding units. A modular approach was applied for the consecutive chain extension leading to the desired symmetric sequence-defined macromolecules with molecular weights of up to 3532.16 g mol⁻¹. The synthesis of symmetric macromolecules based on a modular approach leads to a significant increase of molecular weight per chain extension step. The current convergent approach combining P-3CRs and photoconjugation allows for straightforward synthesis of monodisperse sequence-defined macromolecules exhibiting absolute chain-end fidelity and functional monomers placed at exact positions along the chain. In conclusion, the toolbox was extended towards precision macromolecules with potential applications in mimicking complex features of naturally occurring macromolecules or data storage materials.

3.2. Protection-free Sequence-Defined Macromolecules via λ -Orthogonal Photochemistry

Parts of this chapter, the following subchapters, and the associated parts in the experimental section were adapted with permission from a publication written by the author.^{[253-255],b}

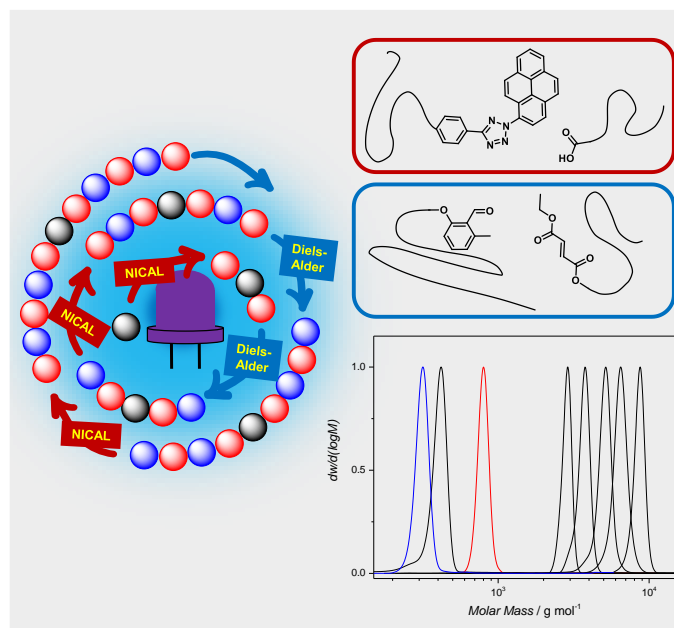
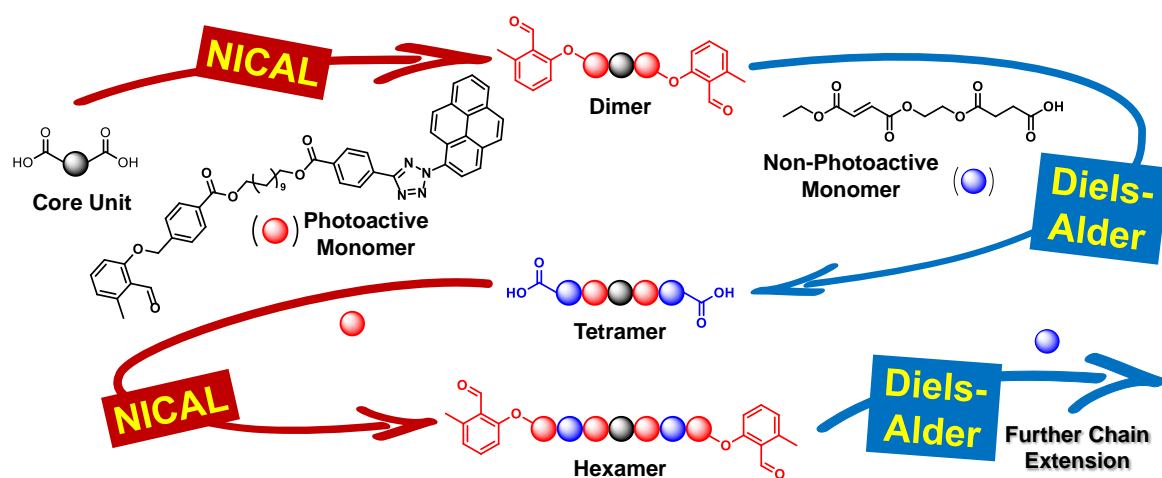


Figure 27. Graphical abstract for the synthesis of sequence-defined macromolecules *via* the combination of two photoinduced conjugation methods, i.e. NICAL ligation and DA cycloaddition based on fumarates and *o*-MBAs.

In the current section, the synthesis of sequence-defined macromolecules *via* an advanced light induced avenue is presented based on the convergent iterative combination of NICAL ligation and DA cycloaddition (**Scheme 39**). Therefore, two complementary monomer units were prepared to conduct the NICAL ligation and DA reaction: one monomer was equipped with a visible light responsive pyrene aryl tetrazole (PAT) as well as an UV responsive *o*-MBA and the second unit carries a carboxylic acid as well as a fumarate. Furthermore, a symmetric core unit was synthesized exhibiting excellent solubility in DCM. The core unit enables the synthesis of symmetric sequence-defined macromolecules (Section 3.2.1). In the

^b The synthesis of sequence-defined macromolecules, i.e. the symmetrical dimer and tetramer, performed under flow conditions using a commercially available Vapourtec photoflow reactor was subject of the Vertiefearbeit of Christian Fengler conducted under supervision of the author. The Vertiefearbeit was performed at the Queensland University of Technology (QUT) in Brisbane, Australia.

next step, monodisperse macromolecules were accessed in a modular approach by switching between NICAL ligation and DA cycloaddition. Hence, the respective photosensitive groups were selectively excited at distinct wavelengths to conduct the chain extension (Section 3.2.2). The λ -orthogonal strategy enables the protecting-free synthesis of sequence-defined macromolecules with a molecular weight of $6257.10 \text{ g mol}^{-1}$. The in depth characterization was carried out *via* SEC, ESI-MS, and NMR spectroscopy in order to evidence the monodisperse nature of the prepared macromolecules.



Scheme 39. Synthesis of sequence-defined macromolecules by chain extension of a symmetrical core unit circumventing protection group strategies. The sequential light induced chain extension is carried out by switching between NICAL ligation and DA cycloaddition. Reprinted with permission from a publication of W. Konrad *et al.*^[253]

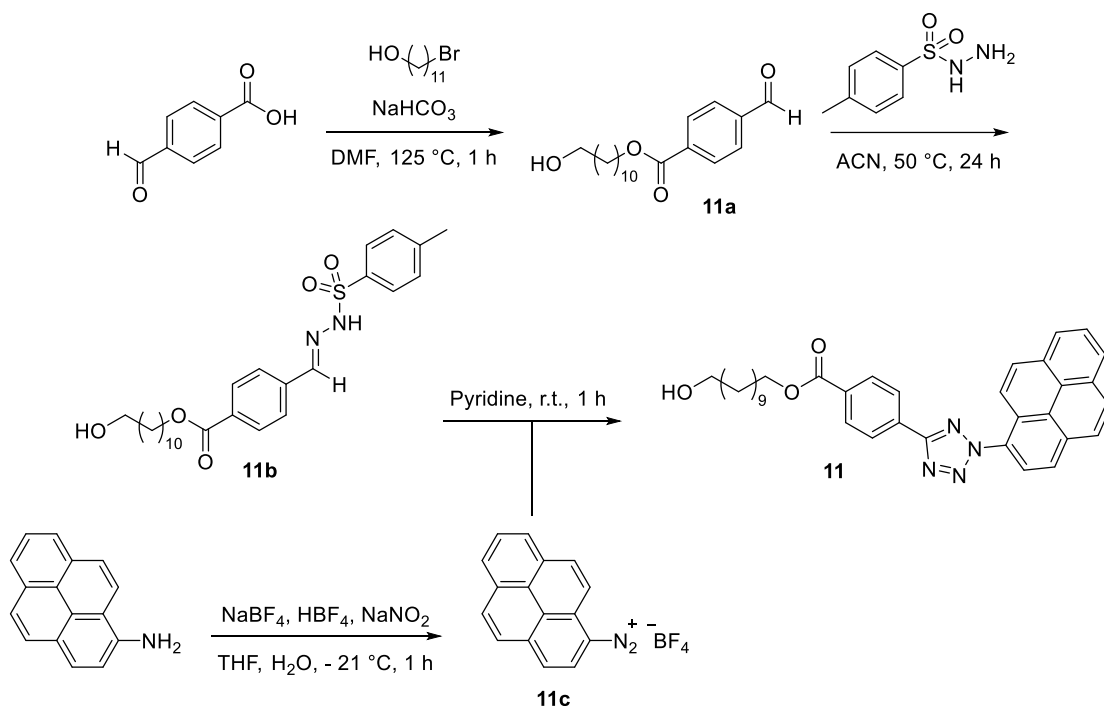
3.2.1. Synthesis of the Building Units

In Chapter 3.1, an approach for the synthesis of sequence-defined macromolecules is presented with a photochemical protocol relying on *o*-MBAs and furan caged maleimides. Consequently, the oligomers need to be thermally deprotected after each chain growth step prior to chain extension. However, modifications carried out with the macromolecules themselves decrease overall efficiency and yield of the synthesis. Therefore, it is important to avoid protection group chemistry in order to reduce the total number of reaction steps in synthetic approaches for sequence-defined macromolecules. For instance, protection groups can be circumvented by the selective excitation of photolabile moieties by irradiation at different wavelengths. As described in Section 2.1.5, pyrene-functionalized tetrazoles respond to visible light and form nitrile imines upon irradiation at 410 – 420 nm. The nitrile imines can be

3. Results and Discussion

employed for NICAL ligation in a subsequent reaction step with carboxylic acids. In the presence of dienophiles, such as fumarates, [4+2] DA cycloadditions can be carried out with photocaged dienes, for example with *o*-MBAs, in the UV region at 365 nm. The combination of both photoresponsive groups in one molecule (photomonomer unit) allows the photoinduced chain extension by selective excitation of the respective light sensitive group. While the activated moiety proceeds in the photochemical coupling reaction, the non-activated group is not participating in the photoreaction and remains in its ground state, thus protection chemistry can be avoided. Iterative chain extension is accomplished through a two-monomer system. The first monomer designed for this purpose exhibits a PAT unit that undergoes a NICAL reaction when exposed to visible light and a UV-light responsive *o*-MBA for DA cycloadditions, wherein the second monomer is equipped with complementary groups, i.e. a carboxylic acid and a fumarate.

In the first step, the two light sensitive groups, i.e. PAT and *o*-MBA, were prepared prior to the formation of a photomonomer. The synthesis of the visible light sensitive pyrene-func-



Scheme 40. Synthesis of PAT **11** starting from 4-formylbenzoic acid and aminopyrene. First, formylbenzoate **11a** is formed with bromo undecanol under basic conditions. The tosylhydrazone **11b** is obtained from the hydrazone formation by employing tosylhydrazide. In the last step, PAT **11** is synthesized from tosylhydrazone **11b** and pyrene diazonium tetrafluoroborate **11c** in pyridine.

tionalized tetrazole **11** was already demonstrated by Lederhose *et al.*^[79] Two major advantages can be identified for the pyrene tetrazole. First, the tetrazole enables rapid chain growth directly *via* the formation of a nitrile imine after the photoinduced release of an equivalent of nitrogen. Second, the pyrene moiety acts as a photosensitizer by expansion of the conjugated system. The expansion leads to a bathochromic shift resulting in a tetrazole moiety with the ability to perform NICAL reactions at higher wavelengths (410 nm). Lederhose *et al.* investigated the absorbance of PAT **11** exhibiting an absorption maximum at 345 nm to demonstrate that the pyrene functional tetrazole can be activated by light at higher wavelengths. Even though PAT exhibits an absorbance maximum in the UV region, an absorbance tail was observed beyond 400 nm. The fluorescence quantum yield of PAT **11** at 410 nm was found to be 0.17, which means that a part of the absorbed energy from light is not being reemitted as fluorescence, giving the potential ability for the molecule to convert the absorbed energy into photochemical reactions. However, Lederhose *et al.* reported a low reaction yield of 32 % in the final step and a limited scalability were reported providing 171 mg of PAT **11**. Since PAT **11** is employed for monomer synthesis, the synthetic procedure had to be modified in order to provide sufficient amounts of the visible light responsive tetrazole. Therefore, the tosylhydrazone **11b** was prepared starting from 4-formylbenzoic acid by esterification with bromo undecanol yielding formylbenzoate **11a** as intermediate (**Scheme 40**). As a spacer unit the undecanol moiety separates the tetrazole from adjacent groups and introduces an alcohol functionality enabling coupling *via* Steglich esterification. In addition, the ester in the para-position of the phenyl ring increases reaction rates for the light induced formation of nitrile imines. Furthermore, electron donating groups in *para*-position increase reaction rates of cycloadditions with electron deficient alkenes.^[143] As presented by Lederhose *et al.*, **11b** was obtained *via* hydrazone formation by employing tosylhydrazone. Lederhose *et al.* reported that the formation of the pyrene diazonium tetrafluoroborate **11c** needs to be carried out on a low scale in order to generate the diazonium salt efficiently. For large scale synthesis of the salt, parallel batches of the diazotization reaction were performed and afterwards combined for the formation of the targeted PAT **11**. Nonetheless, the pyrene diazonium tetrafluoroborate **11c** can also be prepared in a single batch by

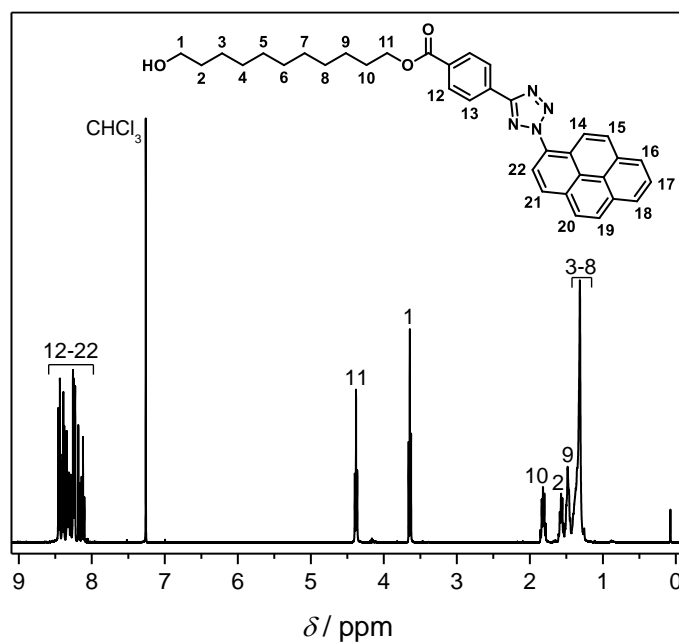
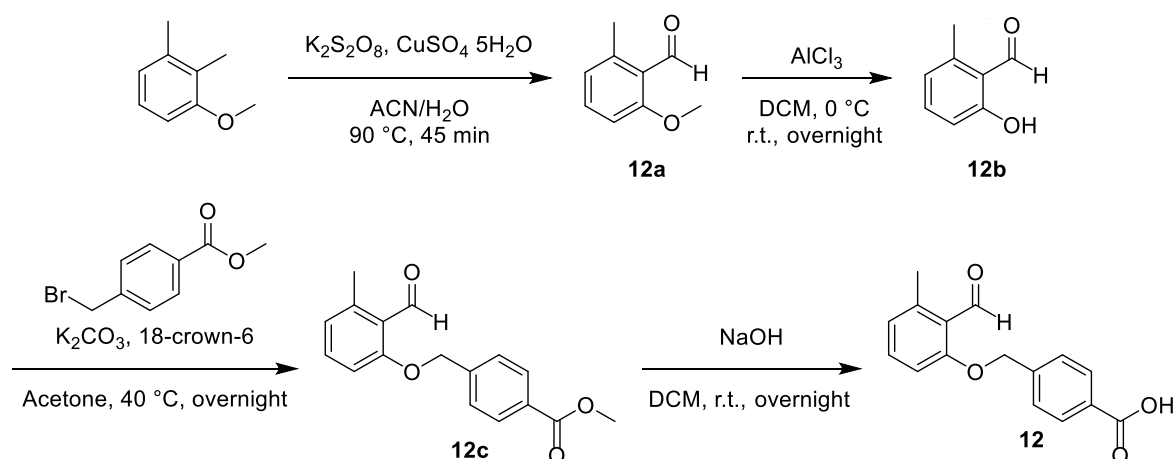


Figure 28. ^1H NMR spectrum of the PAT **11** recorded in CDCl_3 at 400 MHz. For the signal assignments refer to the depicted structure.

upscaling – contrary to the previous report – an improved reaction protocol was suitable for single batch synthesis. Therefore, the aminopyrene was dissolved in dry THF, cooled to $-21\text{ }^\circ\text{C}$, and degassed with nitrogen carefully. Afterwards the orange diazonium salt was formed by the addition of sodium tetrafluoroborate and sodium nitrite under nitrogen atmosphere. Furthermore, the diazonium salt was kept stirring at room temperature to ensure complete conversion. The tetrazole itself was obtained in pure pyridine from the pyrene diazonium salt **11c** and the tosylhydrazone **11b**. Precipitation in aqueous 1M hydrochloric acid afforded 1.19 g of PAT **11** with a yield of 55 % after a single recrystallization step in ethanol. Hence, sufficient amounts of PAT **11** can be provided in order to synthesize a photomonomer efficiently. The successful formation of the PAT **11** and the obtained purity was verified *via* ^1H NMR spectroscopy (refer to **Figure 28**). A characteristic triplet at 4.38 ppm (11) provides evidence for the formation of the benzoate and the triplet detected at 3.64 ppm (1) confirms the methylene unit adjacent to the hydroxyl group. The magnetic resonances recorded between 8.50 to 8.00 ppm (12-22) further indicate the successful incorporation of the pyrene functionality. Additionally, the ^{13}C NMR spectrum and the recorded mass spectrum underpin the successful synthesis of the target compound **11** (refer to **Figure S35** and **Figure S36** in Section 5.3.2).



Scheme 41. Synthesis of the *o*-MBA **12** starting from dimethyl anisole by oxidation. Afterwards, **12b** was obtained by methyl ether cleavage followed by ether formation under Williamson conditions leading to **12c**. The target compound **12** was formed by saponification in the final step.

An efficient wavelength-orthogonal system to circumvent protection chemistry requires the respective photochemical reaction paths to be activated independently of one another. Therefore, the activation wavelength gap between the light sensitive groups has to be sufficient to prevent the unintended excitation of the photoactive moieties. The introduced PAT **11** can be activated upon irradiation at 410 nm, wherein *o*-MBAs exhibit no significant absorption at the same wavelength. Thus, a λ -orthogonal reaction sequence can be accomplished by the activation of the tetrazole at 410 nm and an *o*-MBA at 365 nm allowing independent photo-

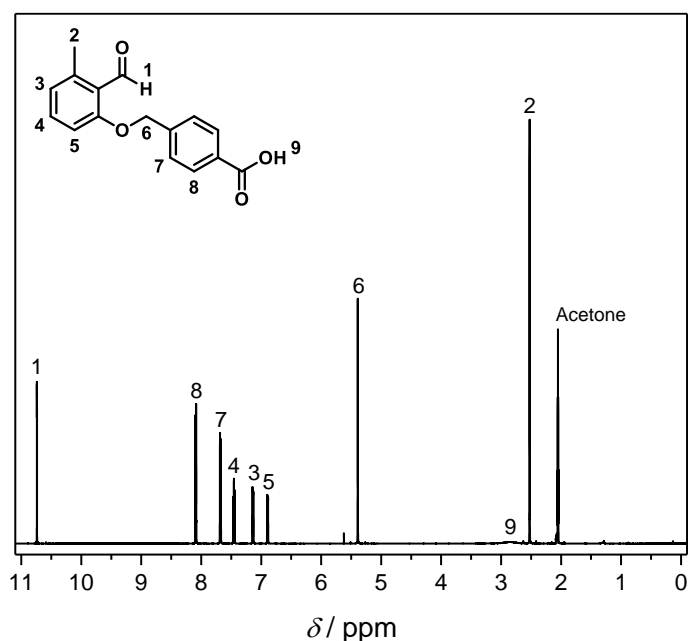
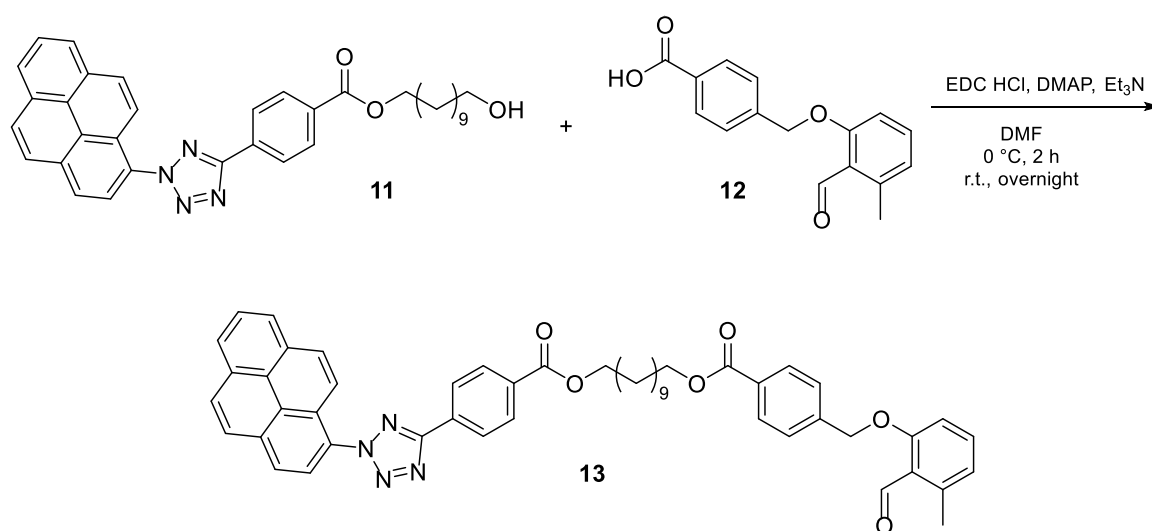


Figure 29. ^1H NMR spectrum of the *o*-MBA **12** recorded in acetone at 600 MHz. For the signal assignments refer to the depicted structure.

3. Results and Discussion

chemical reaction pathways. Therefore, an *o*-MBA unit was synthesized as the second photoactive moiety prior the formation of a photomonomer. Hence, the *o*-MBA synthesis was adapted with slight modifications from a report of Pauloehrl *et al.*^[246, 256-257] The synthetic approach is illustrated in **Scheme 41**. In the first step, dimethyl anisole was oxidized to yield the *o*-MBA **12a**. Subsequently, the crude mixture of **12a** was employed directly in an ether cleavage reaction prior purification leading to **12b**. The *o*-MBA **12** was obtained after etherification under Williamson conditions (**12c**) and saponification. Successful formation of the benzaldehyde was confirmed *via* ¹H NMR spectroscopy as depicted in **Figure 29**. A singlet recorded at 10.74 ppm (1) indicates the presence of the aldehyde moiety. Furthermore, the doublet of doublets at 7.45 ppm (4) as well as the doublets at 7.13 (3) and 6.89 ppm (5) arising from the aromatic protons introduced by the dimethyl anisole additionally verify the successful formation of the benzaldehyde **12**. A characteristic magnetic resonance is recorded at 5.39 ppm (6) deriving from the methylene group introduced by the Williamson ether formation. In addition, the magnetic resonances from 8.12 to 8.07 as well as from 7.71 to 7.65 ppm stemming from the aromatic protons introduced by the bromo benzoate underpin the formation of the UV-light reactive unit **12**.

In order to accomplish the photochemical formation of sequence-defined macromolecules without protection chemistry by selective excitation of light sensitive groups, both photoreponsive groups, i.e. PAT **11** and *o*-MBA **12**, have to be combined in one molecule to afford



Scheme 42. Formation of the photomonomer **13** by esterification of PAT **11** and *o*-MBA **12** under Steglich conditions using EDC·HCl and DMAP.

a photomonomer (**Scheme 42**). The undecanol spacer moiety of the PAT **11** offers a straightforward attachment point for the combination of the two light sensitive groups. Therefore, the two moieties, PAT **11** and *o*-MBA **12**, were combined in an esterification under Steglich conditions by employing EDC·HCl and DMAP as reagents leading to the photomonomer **13** achieving an isolated yield of 60 %. The purification was performed *via* flash chromatography using a gradient of CH/EA. Importantly, the UV detector was deactivated to prevent the light induced degradation of the tetrazole moiety forming the reactive nitrile imine intermediate while purification. Considering the ^1H NMR spectrum depicted in **Figure 30**, it was determined that the characteristic resonances of the starting materials **11** and **12** are also detected for the formed photomonomer **13**. A singlet recorded at 10.63 ppm (30) is arising from the aldehyde unit introduced by the *o*-MBA. Furthermore, the two doublets at 6.70 ppm (26, 28), the doublet of doublets at 7.21 ppm (27), and the two singlets at 5.05 (25) and 2.47 ppm (29) deriving from the *o*-MBA indicate successful introduction of the benzaldehyde moiety **12**. Moreover, the proton resonances ranging from 8.38 to 7.89 ppm (1-11) stemming from the aromatic region represent the pyrene moiety. The shift of the methylene protons adjacent to the alcohol group of PAT **11** from 3.64 ppm to 4.25 ppm, upon esterification, evidences the successful formation of the photomonomer **13** (refer to **Figure 28**, resonance 1).

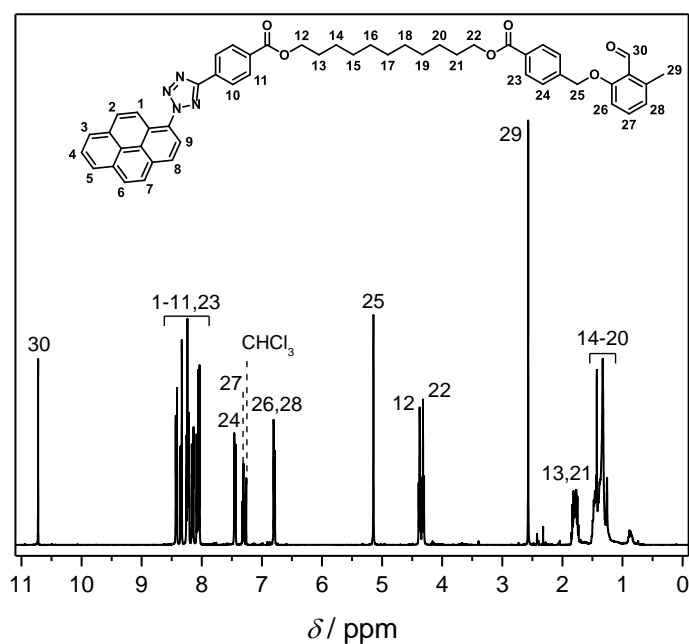
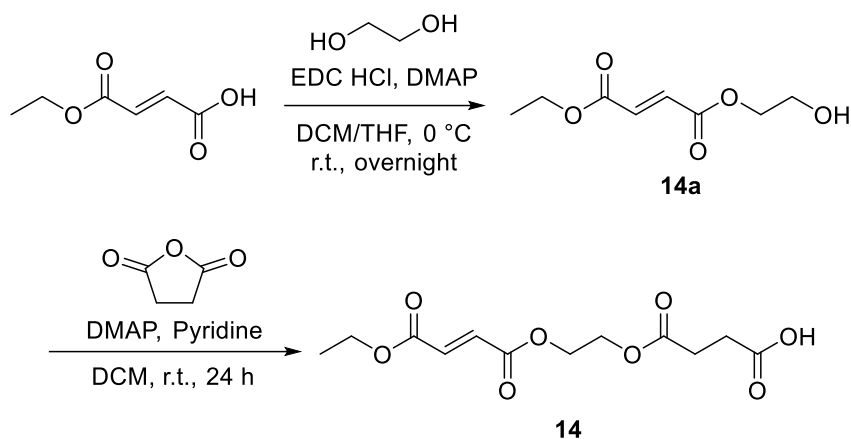


Figure 30. ^1H NMR spectrum of the photomonomer **13** recorded in CDCl_3 at 400 MHz. For the signal assignments refer to the depicted structure.

3. Results and Discussion



Scheme 43. Synthesis of monomer **14** starting from mono-ethyl fumarate by esterification with an excess of glycol under Steglich conditions and subsequent nucleophilic ring-opening of succinic anhydride.

In order to conduct chain extension for the formation of sequence-defined macromolecules by switching between NICAL ligation and DA cycloaddition, a complementary monomer unit had to be synthesized. Therefore, a monomer was designed carrying a carboxylic acid for NICAL ligation and fumarate as dienophile for DA reactions as depicted in **Scheme 43**. In the first step, the hydroxyl fumarate **14a** was obtained in a Steglich esterification of monoethyl fumarate with an excess of glycol in order to avoid conversion of both hydroxyl groups of the alcohol component. The targeted monomer was obtained using hydroxyl fumarate intermediate **14a** in a nucleophilic ring-opening reaction of succinic anhydride with DMAP as catalyst in anhydrous DCM resulting in the monomer **14** achieving an isolated yield of 90 %. The ¹H and ¹³C NMR spectra presented in **Figure 31** confirm the purity of the monomer **14**. A characteristic doublet at 6.85 ppm (3,4) is assigned to the olefin moiety of the fumarate. The methylene protons between the ester bonds resulting from the esterification of glycol are visible as multiplet ranging from 4.42 to 4.33 ppm (5,6). Furthermore, the proton resonances associated with the methylene protons adjacent to the carbonyl groups introduced by the nucleophilic ring-opening reaction exhibit a characteristic multiplet ranging from 2.71 to 2.62 ppm (7,8). **Figure 31** further displays a ¹³C NMR spectrum for the additional verification of the successful synthesis of **14** since the ¹H NMR spectrum of monomer **14** only exhibits methylene groups at expected magnetic resonances. Characteristic magnetic resonances at 134.5 and 132.9 ppm (4,5) derive from the carbon atoms of the double bond of the fumarate. Furthermore, the resonances of the carbonyl carbons are detected as singlets at 177.7 (12), 172.0 (9), as well as 165.0, and 164.8 ppm (3,6) underpinning the

successful formation of monomer **14**. The monomer exhibits an electron deficient alkene enabling a selective DA cycloaddition. More importantly, monomer **14** introduces carboxylic acid as end-groups *via* DA reactions and thus accomplishing consecutive chain extension by NICAL ligation.

The synthesis of sequence-defined macromolecules described in the current section is based on a two-monomer system by chain extension of a symmetrical core unit. Symmetrical core

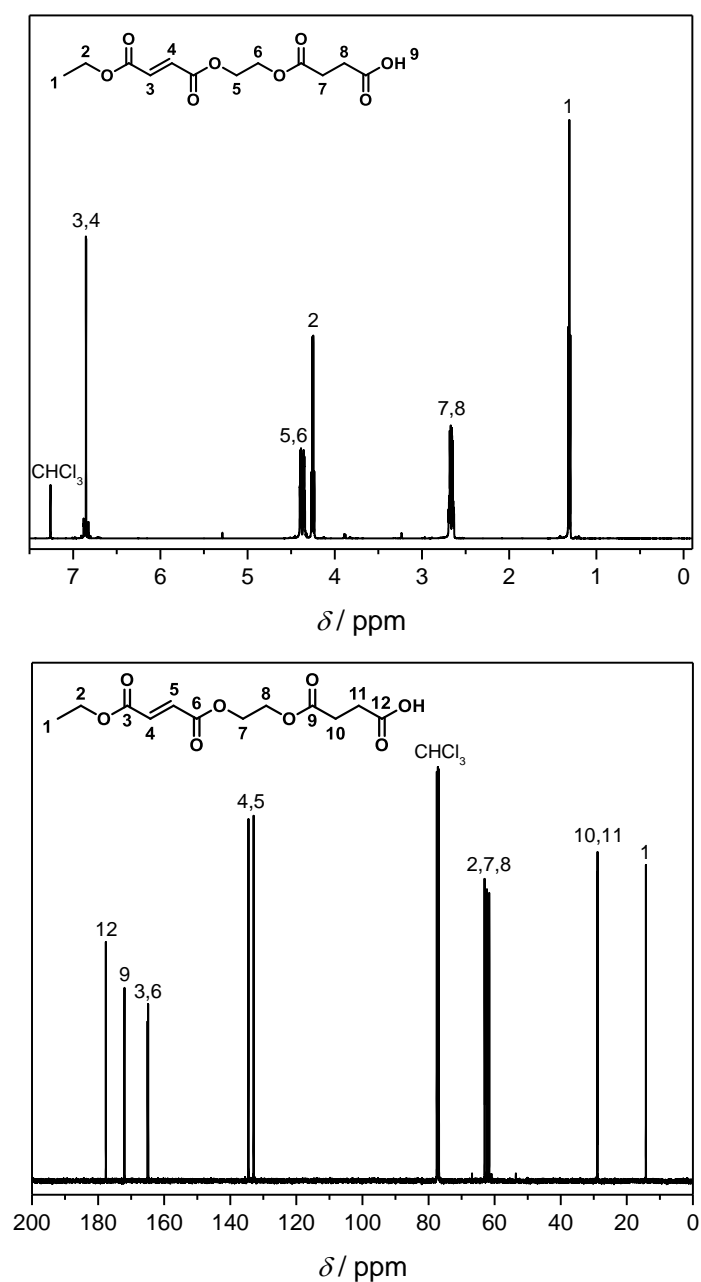
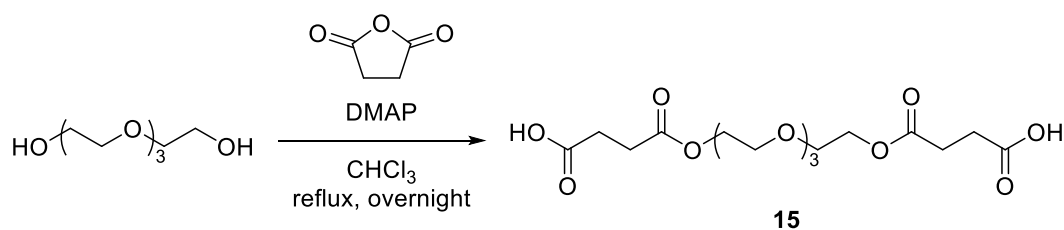


Figure 31. ^1H NMR (top) and ^{13}C NMR (bottom) spectrum of the monomer **14** recorded in CDCl_3 at 400 MHz and 101 MHz, respectively. For the signal assignments refer to the depicted structure.

3. Results and Discussion



Scheme 44. Synthesis of the symmetric bifunctional carboxylic acid **15** by a nucleophilic ring-opening reaction starting from tetraethylene glycol.

units enable bidirectional growth for sequence-defined macromolecules, thereby achieving high molecular weights in as few reaction steps as possible by a significant increase in molecular weight per chain extension step since two monomer units are added simultaneously. However, bidirectional growth reduces the overall efficiency as incomplete monomer addition leads to product mixtures. Nevertheless, a symmetric dicarboxylic acid was designed as a core unit due to the fact that two highly efficient coupling reactions, i.e. NICAL ligation and DA cycloaddition, are employed for chain extension. The core unit **15** was obtained by a nucleophilic ring-opening reaction of succinic anhydride using tetraethylene glycol and a catalytic amount of DMAP, resulting in the target compound **15** with an isolated yield of 75 % (**Scheme 44**). In contrast to various commercially available bifunctional carboxylic acids, such as sebacic acid as it was employed in Section 3.1 as core unit, the herein synthesized symmetric acid **15** exhibits excellent solubility in organic solvents, for example in DCM. In addition, tetraethylene glycol acts as a spacer unit minimizing steric demands and thus enhancing the formation of symmetric sequence-defined macromolecules. Moreover, polyethylene glycols generate complexes with alkali metals being analogous to complexes formed by crown ethers. The formation of alkali metal complexes can be exploited for mass analysis *via* ESI-MS as the complex formation enhances the ionization probability of the macromolecules. The ^1H and ^{13}C NMR spectra presented in **Figure 32** confirm the purity of the core unit **15**. In total three characteristic proton resonances are recorded for the core unit **15** because it only exhibits methylene protons in ester or ether positions. First, the methylene groups adjacent to the ester units are detected as multiplet ranging from 4.31 to 4.22 ppm (3,10). Furthermore, the magnetic resonances of the methylene groups in ether position exhibit a multiplet ranging from 3.73 to 3.60 ppm (4-9). A magnetic resonance ranging from 2.72 to 2.58 ppm (1,2,11,12), stemming from the methylene groups between the carboxylic acid and the ester group, indicate the successful formation of the core unit **15**. **Figure 32**

further displays a ^{13}C NMR spectrum for the additional verification of the successful synthesis of **15**. A characteristic magnetic resonance at 177.0 ppm (1,16) is associated with the carboxylic acids at the chain ends of the symmetric core unit **15**. Furthermore, the resonances of the carbonyl carbons of the ester groups are detected as a signal at 172.3 ppm (4,13) additionally verifying the successful formation of the core unit **15**.

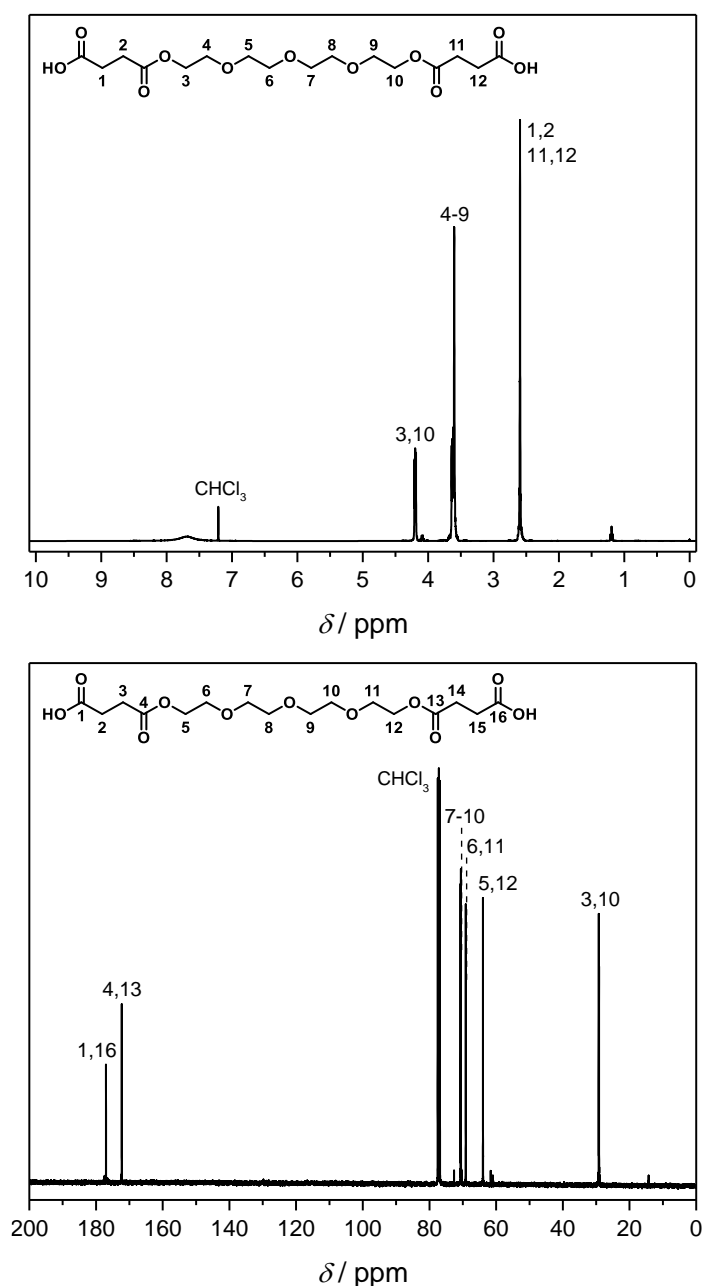


Figure 32. ^1H NMR (top) and ^{13}C NMR (bottom) spectrum of the symmetrical core unit **15** recorded in CDCl_3 at 400 MHz and 101 MHz, respectively. For the signal assignments refer to the depicted structure.

3.2.2. Preparation of the Sequence-Defined Macromolecules by NICAL Ligation and DA Cycloaddition

Starting from a symmetrical core unit **15**, the synthesis strategy of the sequence-defined macromolecules is based on two monomers, i.e. photomonomer **13** and a complementary monomer **14**, avoiding protection chemistry in-between the chain extension steps by switching from NICAL ligation (carried out at an excitation wavelength of 410-420 nm) and DA cycloaddition (365 nm). The sequence-defined macromolecules described in Section 3.1 were obtained by irradiation of headspace vials under batch conditions. However, batch reactions are hardly scalable and provide limited amounts of the target compounds. In order to contribute to a facile scalability, the photoreactions discussed in the current section are supposed to be carried out under flow conditions, since flow reactions can be easily scaled up by simply increasing the reaction time and simultaneously maintaining reaction conditions

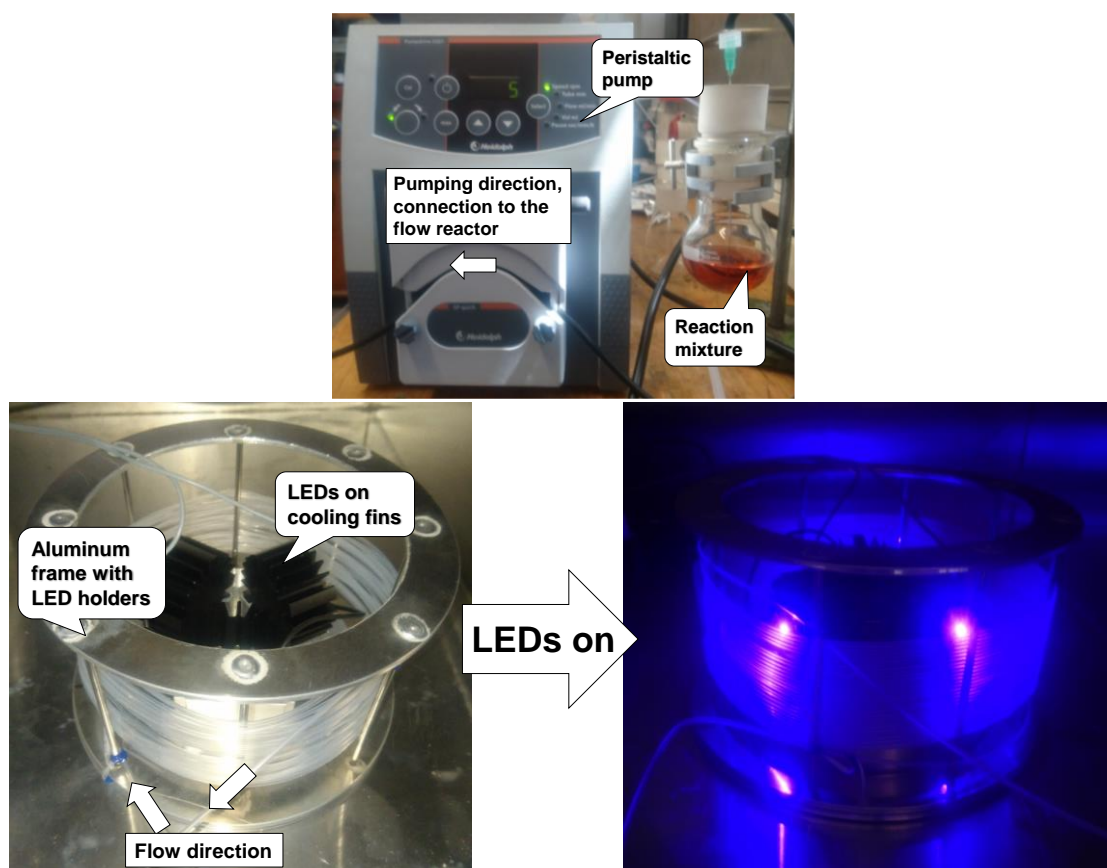
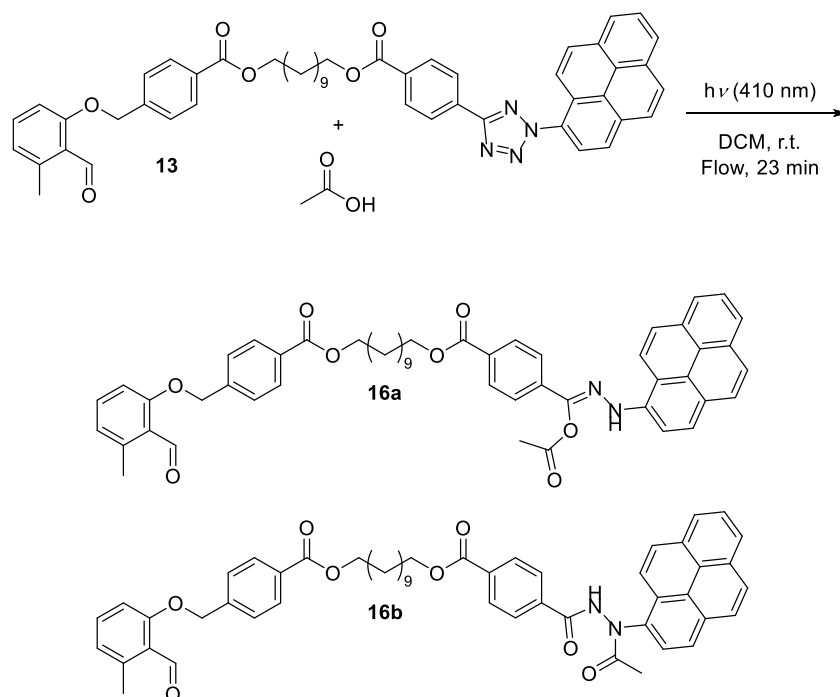


Figure 33. Peristaltic pump with a viton (0.8 mm ID) tubing for transporting the reaction mixture into the flow reactor (top). Perfluoroalkoxy alkane (PFA) polymer tubing wrapped around an aluminum carousel (reactor volume 7.5 mL) standing on an aluminum plate with LED holders and LEDs (410-420 nm) as radiation source (bottom left). Flow reactor in operation mode (bottom right).

including concentration and exposure time. Moreover, flow reactions exhibit an additional significant advantage over conventional batch reactions. According to the Beer-Lambert's law, equipping flow reactors with reactor tubes with a low diameter contributes to a maximum of light penetration and thus increases the reaction efficiency. Therefore, a custom mode flow reactor was designed. In **Figure 33** the flow setup is illustrated. An aluminum carousel on an aluminum plate with LED holders in its center was custom made and the carousel was wrapped with a high purity PFA tubing (0.50 mm inside and 1.55 mm outside diameter) with a total length of 15 m resulting in a total reactor volume of 7.5 mL. A setup of three LEDs on cooling ribs was placed in the center of the carousel as radiation source. The reaction mixture was transported from a flask into the reactor *via* a peristaltic pump controlling the residence and exposure time of the reaction mixture as depicted in **Figure 33** (top).

Initially, the NICAL ligation and DA cycloaddition have been investigated by employing test systems to simulate the reaction conditions in the flow reactor. Tetrazoles can be used for cycloadditions or NICAL ligation under atmosphere as they exhibit a high reactivity, since the reactive nitrile imine intermediate is formed irreversibly. In the first approach, the



Scheme 45. NICAL test reaction conducted under flow conditions with the photomonomer **13** and acetic acid at residence times of 10, 15, and 23 min. Adduct **16a** is obtained *via* reaction of the nitrile imine and the acid derivative, whereas rearrangement of the photoadduct leads to the hydrazide **16b**.

NICAL ligation was investigated with the photomonomer **13** and acetic acid as depicted in **Scheme 45**. The monomer **13** was used to investigate two effects in-depth. Namely, the formation of the NICAL adduct upon irradiation with a wavelength of 410 nm as well as the behavior of the aldehyde under the given conditions. Therefore, the monomer **13** and acetic acid were dissolved in DCM with a concentration of 12.3 mmol L⁻¹. Afterwards, the reaction mixture was irradiated in the flow reactor at different residence times of 10, 15, and 23 min. It was found that with a residence time of 23 min the NICAL adduct is obtained quantitatively. It is interesting to note that two NICAL adducts are formed by intramolecular rearrangement from the initially obtained hydrazoneic anhydride **16a** leading to the hydrazide **16b**. As a result, the ¹H NMR spectrum of the irradiated crude reaction mixture in **Figure 34** reveals complex magnetic resonances due to the fact that the rearrangement equilibrium favors the hydrazide species in a ratio of 2:1. Most importantly, the magnetic resonances deriving from the benzaldehyde moiety at 10.73 ppm (32) and the aromatic resonances at 7.46 (26), 7.84 (29), and 6.83 ppm (28,30) are detected after the irradiation with 410 nm indicating that the *o*-MBA remained in its ground state and thus did not participate in the reaction. The aromatic resonances associated with the pyrene substituent are shifted from 8.44 - 8.04 to 8.28 - 7.86 ppm (1-9) upon NICAL adduct formation. Additionally, a charac-

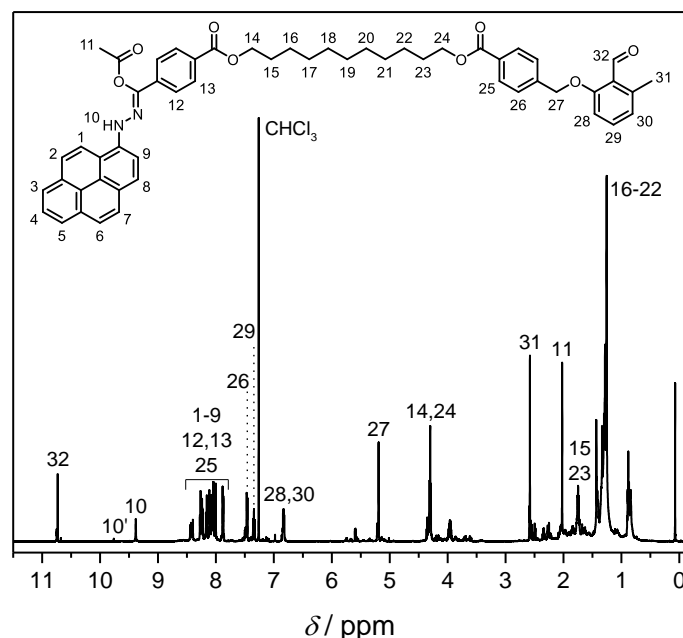
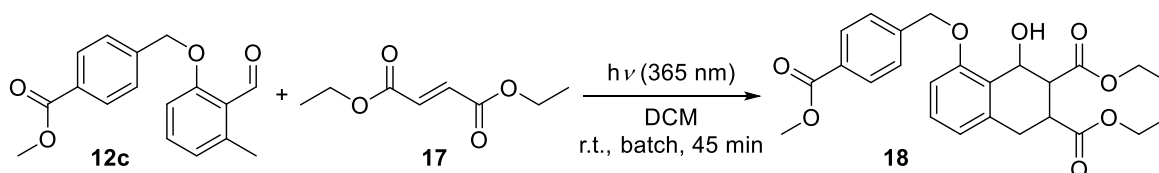


Figure 34. ¹H NMR spectrum of the reaction mixture described in **Scheme 45** after irradiation in a flow reactor, recorded in CDCl₃ at 400 MHz. For the signal assignments refer to the depicted structure.

teristic multiplet is visible ranging from 8.45 to 8.40 ppm arising from the pyrene moiety. The methyl group introduced by the acetic acid is detected at 2.02 ppm (11). Moreover, a singlet is observed at 9.45 ppm (10,10') stemming from the formation of hydrazone anhydride **16a** and hydrazide **16b** verifying the successful NICAL adduct formation under flow conditions in the custom made flow reactor.

Since NICAL ligation was successfully conducted in the flow reactor using the photomonomer **13** and acetic acid, the DA reaction was investigated under flow conditions by employing an *o*-MBA and a dienophile. However, the photomonomer **13** is unsuitable for the investigation of the DA cycloaddition of the *o*-MBA moiety, since both photosensitive groups are activated at wavelength around 365 nm and undergo a cycloaddition in presence of dienophiles. Therefore, the benzaldehyde **12c** and diethyl fumarate **17** were used as a test system. It is important to note that *o*-MBAs have to be irradiated under inert atmosphere to ensure complete conversion, since molecular oxygen can quench the excited triplet state of the benzaldehyde.^[258] Consequently, the *o*-MBA **12c** and an excess of diethyl fumarate **17** were dissolved in dry DCM under nitrogen atmosphere with a concentration of 10.0 mmol L⁻¹. Before the reaction mixture was transferred into the flow reactor via the peristaltic pump, the reactor was flushed with nitrogen and dry DCM. Afterwards, the reaction mixture was irradiated with a residence time of 23 min by employing three LEDs with an emission maximum at 365 nm. However, the analysis *via* ¹H NMR spectroscopy revealed the presence of starting material and only 5 % of DA cycloadduct after irradiation. Moreover, the experiment was repeated in the flow reactor in a steady state with irradiation times up to 3 h leading to a conversion of 5 % as calculated *via* ¹H NMR spectroscopy. Therefore, it is assumed that an inert atmosphere free of oxygen cannot be established in the custom made flow reactor. As a consequence, the DA cycloaddition between the *o*-MBA **12c** and diethyl fumarate **17** is not feasible under the presented conditions using the custom made flow reactor. Thus, the



Scheme 46. DA cycloaddition of the *o*-MBA **12c** and an excess of diethyl fumarate **17** as test system conducted under conventional batch conditions employing nitrogen-flushed headspace vials and a PL-L lamp ($\lambda_{\text{max}} = 365$ nm) as irradiation source.

3. Results and Discussion

DA cycloaddition was conducted under conventional batch conditions in headspace vials flushed with nitrogen (compare with Section 3.1). A PL-L lamp ($\lambda_{\max} = 365$ nm) was employed for irradiation with exposure times of 45 min, as displayed in **Scheme 46**. The characterization was carried out by ^1H NMR as depicted in **Figure 35**. Upon irradiation *o*-MBAs are transformed into *o*-quinodimethanes performing the DA reaction with dienophiles. Consequently, a cycloadduct, tetrahydronaphthalene **18** is generated forming four isomers with characteristic chemical shifts in the ^1H NMR spectrum. In **Figure 35**, magnetic resonances between 3.32 and 2.67 ppm (8-10) are detected deriving from the methylene group 8 as well as the two chiral methine groups 9 and 10. Furthermore, the chiral methine group 11 adjacent to the hydroxyl moiety is recorded as doublet at 5.44 and 5.30 ppm with a ratio of 2 to 1 verifying the successful formation of the tetrahydronaphthalene cycloadduct **18**. Moreover, no resonances deriving from the *o*-MBA starting material is detected in the ^1H NMR spectrum indicating quantitative conversion upon irradiation. Nevertheless, it is important to highlight that the DA cycloaddition of *o*-MBAs and fumarates can be carried out under flow condition employing a commercially available flow reactor in general. Christian Fengler conducted flow experiments using *o*-MBAs and fumarates in a Vapourtec photoflow reactor as part of his advanced lab course supervised by the author.^[255] It was found that an inert

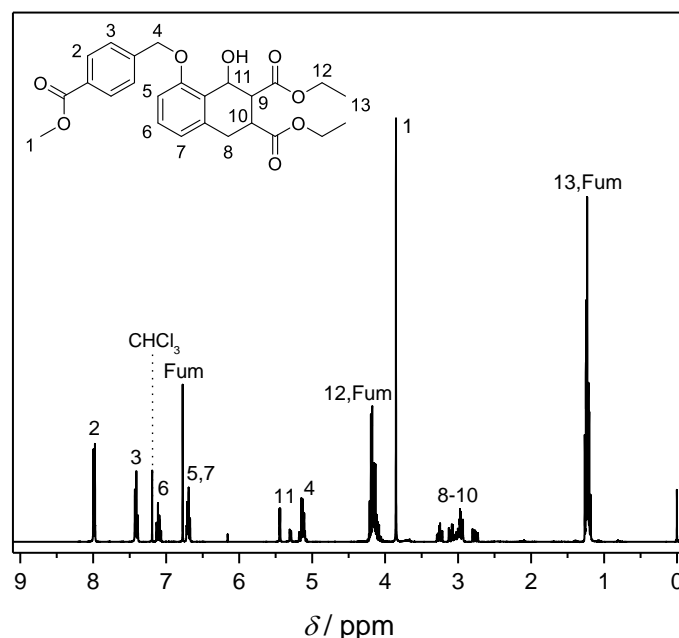
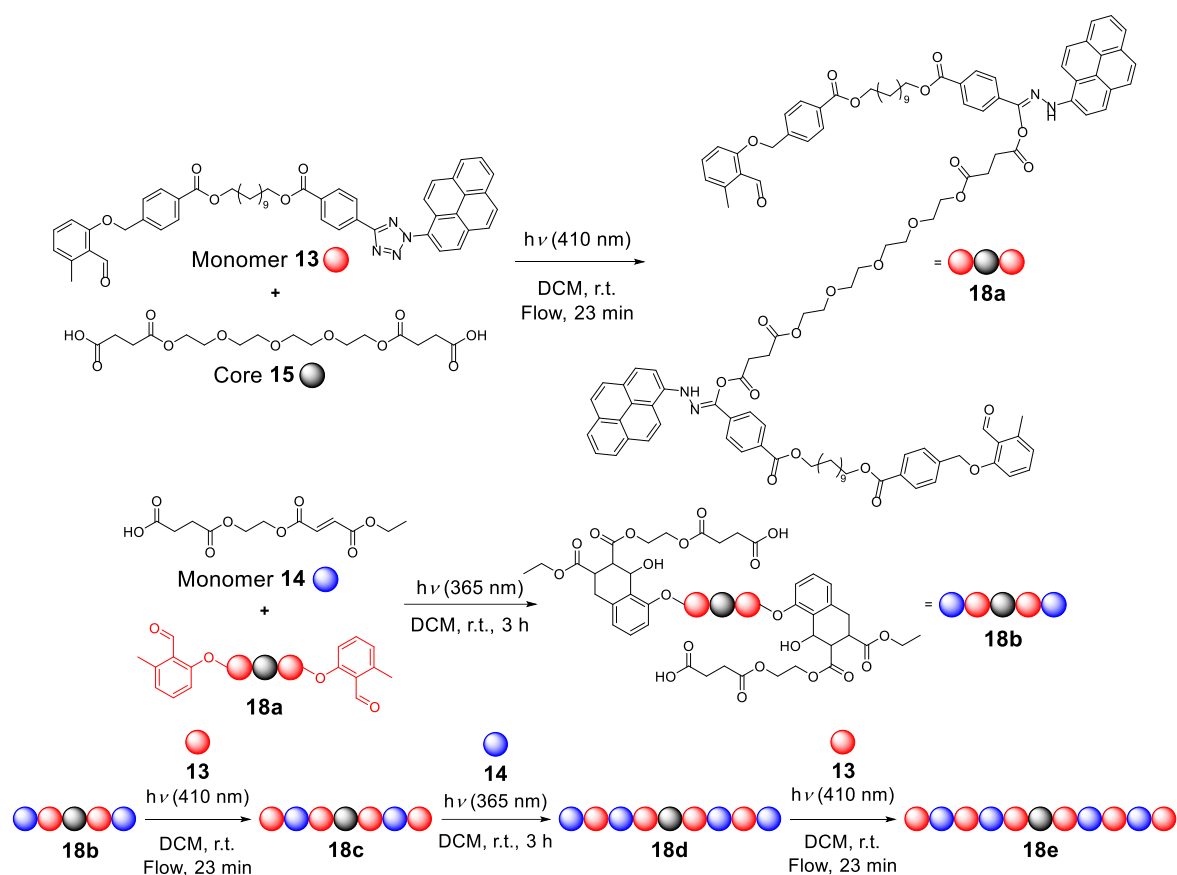


Figure 35. ^1H NMR spectrum of the reaction mixture described in **Scheme 46** after irradiation in a batch reactor, recorded in CDCl_3 at 400 MHz. For the signal assignments refer to the depicted structure.

3.2. Protection-free Sequence-Defined Macromolecules via λ -Orthogonal Photochemistry

atmosphere free of oxygen can be accomplished enabling the DA cycloaddition between *o*-MBAs and fumarates yielding a tetrahydronaphthalene cycloadduct quantitatively under flow conditions.

In conclusion, the initial investigations revealed that the NICAL ligation can be successfully performed under flow conditions in the custom made photoflow reactor at residence times of 23 min and LEDs with an emission maximum at 410 – 420 nm. Moreover, it was demonstrated that the tetrazole moiety of the photomonomer **13** can be selectively activated for NICAL ligation, while the monomer's *o*-MBA group remains in its ground state not participating in the photoreaction. However, *o*-MBAs moieties require an inert atmosphere free of oxygen to ensure quantitative conversion in a photoreaction. Yet, oxygen-free conditions



Scheme 47. Sequential approach for the photochemical synthesis of sequence-defined macromolecules avoiding protection chemistry by wavelength selective switching between NICAL ligation and DA cycloaddition. Starting from the core unit **15**, a symmetrical decamer **18e** was synthesized using the monomers **13** and **14** iteratively by bidirectional chain extension. The NICAL chain extension yielded macromolecules with benzaldehydes as end-groups (**18a**, **18c**, and **18e**), while DA cycloaddition afforded terminal carboxylic acids (**18b** and **18d**).

could not be established in the photoreactor designed by the author and thus the photoinduced DA cycloaddition of *o*-MBA and fumarate has to be conducted under conventional batch conditions as already presented in Section 3.1.

The aim of the present work is to investigate the formation of sequence-defined macromolecules by a combinatorial approach employing NICAL ligation and *o*-MBA conjugation in a wavelength-orthogonal fashion. Therefore, the bifunctional carboxylic acid **15** was prepared as a core unit as well as the two complementary monomers **13** and **14**. In the first step, a symmetrical dimer **18a** was synthesized in a NICAL ligation step using the core unit **15** and a slight excess of the photomonomer **13** (2.3 eq.) in anhydrous DCM employing the custom made photoflow reactor as depicted in **Scheme 47**. Irradiation of the photomonomer **13** excited the molecule and transformed the tetrazole moiety into the reactive nitrile imine irreversibly while the benzaldehyde group remained in its ground state not participating in the photoreaction. The dimer **18a** (1964.28 g mol⁻¹) was obtained with a yield of 89 % after a purification step *via* flash chromatography using a gradient of CH/EA. Due to the fact that a symmetrical carboxylic acid was employed as core molecule, the bidirectional growth affords macromolecules end functionalized with α -methylbenzaldehyde at both chain ends enabling the consecutive chain extension *via* DA cycloaddition. Subsequently, the symmetrical carboxylic acid functionalized tetramer **18b** (2540.79 g mol⁻¹) was obtained by irradiation of to the dimer **18a** and an excess of monomer **14** (4.0 eq.) using a PL-L lamp ($\lambda_{\text{max}} = 365 \text{ nm}$) as light source under conventional batch conditions. It is interesting to note that the carboxylic acid functionalized tetramer **18b** is purified by simple extraction of the reaction mixture. The excess of monomer **14** is selectively extracted with diluted bicarbonate solution, while the tetramer **18b** is obtained purely by extraction with saturated bicarbonate solution achieving a yield of 85 %. In addition, Christian Fengler conducted the synthesis of the carboxylic acid functionalized tetramer **18b** successfully in a commercially available Vapourtec flow reactor proving that the current strategy for the formation of monodisperse macromolecules can be fully performed under flow conditions in principle.^[255] The symmetric sequence-defined hexamer **18c** (4110.69 g mol⁻¹) was prepared by applying same reaction conditions as for the dimer formation in the flow reactor, employing tetramer **18b** and the visible light responsive photomonomer **13**. Purification *via* flash chromatography using a gradient of

CH/EA yielded 79 % of the macromolecule. As the hexamer **18c** exhibits benzaldehyde moieties at both chain ends, further chain extension was executed under batch conditions by the addition of an excess of monomer **14** introducing carboxylic acids as end-groups after UV-light induced cycloaddition resulting in the symmetric octamer **18d** ($4687.20 \text{ g mol}^{-1}$). The excess of the employed monomer was extracted under basic conditions and the targeted octamer **18d** was obtained after purification *via* flash chromatography with a yield of 65 %. In the last step, the octamer **18d** was further extended under flow conditions with photomonomer **13** resulting in the targeted symmetrical sequence-defined macromolecule **18e** ($6257.10 \text{ g mol}^{-1}$) with a yield of 75 % after purification *via* flash chromatography. Importantly, **18e** exhibits benzaldehyde units at both chain ends enabling further chain extension towards monodisperse macromolecules with higher molecular weights. Altogether, an overall yield of 30 % was achieved for the formation of the decamer **18e**. Since the photoreactions require equimolar stoichiometry and an excess of monomers was employed, purification of the intermediates and target compounds resulted in a reduced yield. Although symmetrical core molecules provide a significant increase of molecular weight by bidirectional growth, they also reduce the synthetic overall efficiency since quantitative conversion of the chain ends has to be ensured. The loss in overall efficiency can be compensated by employing powerful coupling methods, such as the NICAL ligation or the DA cycloaddition.

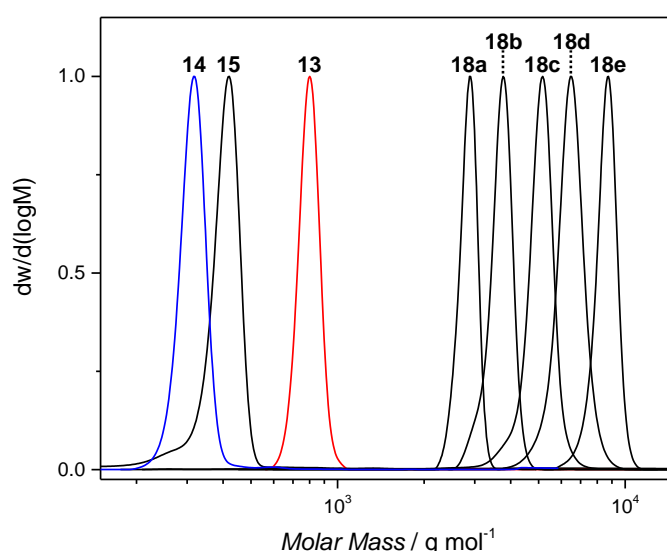


Figure 36. SEC traces of the synthesized sequence-defined macromolecules **18a-e** alternately chain end functionalized with benzaldehydes or carboxylic acids. Additionally, the core unit **15**, the photomonomer **13**, and monomer **14** are depicted. All SEC traces were recorded on a THF based SEC system.

Nevertheless, symmetrical core units will always exhibit reduced synthetic efficiency. Therefore, the monodisperse macromolecules in the current section were designed with a drastically changing polarity of the macromolecule after each chain extension step by the introduction of carboxylic acids at both chain ends. Compared to the sequence-defined macromolecules presented in Section 3.1, the polarity difference of the macromolecules in-between the formation of each generation improves purification of the respective macromolecules. Thus, the introduced carboxylic acids at the macromolecules chain ends facilitates the chromatographic separation of each macromolecular generation.

Successful formation of the successively synthesized sequence-defined macromolecules was verified by SEC, high resolution Orbitrap ESI-MS, and NMR spectroscopy. The SEC traces were recorded on a THF based SEC system and are depicted in **Figure 36** including the core unit **15**, photomonomer **13**, monomer **14**, and the targeted sequence-defined oligomers **18a-e**. The molecular weights have been obtained relative to a polystyrene calibration. Starting from the bifunctional core unit **15** a shift of the SEC trace towards increased molecular weight is obtained after the addition of two equivalents of photomonomer **13** leading to the formation of dimer **18a**. Additionally, an increase in molecular weight is detected for the formation of the consecutive symmetrical sequence-defined macromolecules **18b-e** by employing the two monomers **13** and **14** alternately for chain extension. Consequently, the SEC analysis confirms the successful iterative chain extension by an increase of molecular weight after the addition of the respective building blocks using different wavelengths of light to initiate chain growth. Additionally, the SEC traces depicted in **Figure 36** approve the purity of the macromolecules as well, since only narrow monomodal distribution were recorded. For all SEC traces representing the macromolecules **18a-e** and the building blocks **13-15** depicted in **Figure 36**, dispersities of $D < 1.01$ have been determined against a PS calibration verifying the monodispersity of the synthesized sequence-defined macromolecules. In addition, in **Figure 37a** the high resolution ESI-MS spectrum is displayed in the m/z range from 1500 to 5000 obtained from the targeted symmetrical sequence-defined macromolecule **18e**. As illustrated, only mass signals of the respective charged sodium adduct, assigned to the sequence-defined macromolecule **18e**, are revealed in the recorded spectrum at m/z 3151.3119 ($[\mathbf{18e}+2\text{Na}]^{2+}$, $m/z_{\text{calc.}}$ 3151.2924, $\Delta m/z$ 0.0195), m/z 2108.5312 ($[\mathbf{18e}+3\text{Na}]^{3+}$, $m/z_{\text{calc.}}$ 2108.5247, $\Delta m/z$ 0.0065), and m/z 1587.1443 ($[\mathbf{18e}+4\text{Na}]^{4+}$,

$m/z_{\text{calc.}}$ 1587.1408, $\Delta m/z$ 0.0035). The calculated molecular mass is in excellent agreement with the recorded molecular mass as indicated by the low $\Delta m/z$ values. Furthermore, **Figure 37b** also displays both the simulated and experimentally recorded isotopic pattern deriving from the macromolecule **18e** as doubly charged species containing two sodium counter ions. Both the simulated and experimentally recorded isotopic pattern are in excellent agreement. The full mass spectra and isotopic patterns of **18a-d** can be found in Section 5.3.5. In conclusion, SEC analysis as well as mass spectroscopic methods, including the evaluation of the full mass spectrum in regard to the conformity of the recorded and calculated isotopic patterns, are verifying the successful synthesis of the sequence-defined decamer **18e** and the monodisperse nature.

Additional characterization of the respective sequence-defined macromolecules was carried out *via* ^1H NMR spectroscopy. In **Figure 38** the ^1H NMR spectrum and structure of the decamer **18e** is depicted with signal highlighting (for ^1H NMR spectra of **18a-d** refer to the Section 5.3.5). It is important to note that broad magnetic resonances are expected for the analysis *via* ^1H NMR spectroscopy due to three effects. First, hydrazonic anhydride initially formed after NICAL ligation is transferred into a hydrazide by intramolecular rearrangement

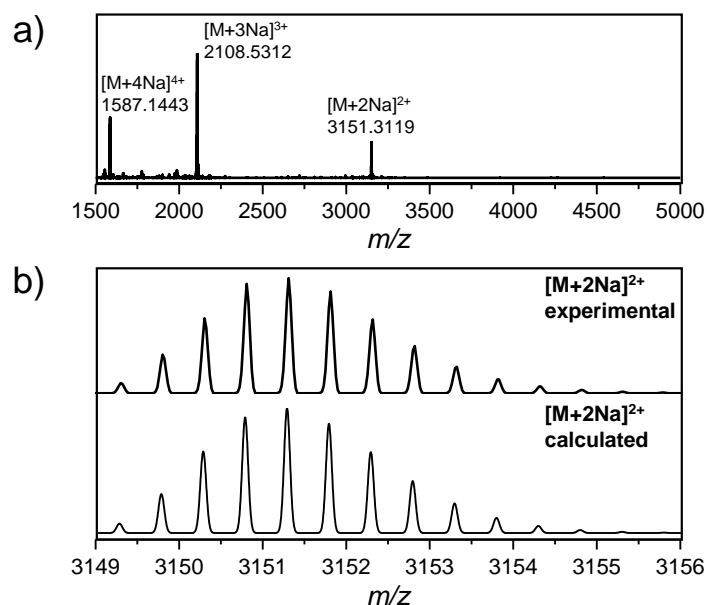


Figure 37. (a) Full MS spectrum of **18e** in the mass range of m/z 1500 to 5000 recorded in positive ion mode. (b) Recorded (top) and calculated (bottom) ESI-MS spectrum of the oligomer's **18e** isotopic pattern.

3. Results and Discussion

leading to a complex ^1H NMR spectrum. Additionally, up to four different isomers of tetrahydronaphthalene are obtained by the DA cycloaddition of *o*-MBAs and fumarates. Moreover, the in general for macromolecules typical signal broadening further complicates the analysis *via* ^1H NMR spectroscopy (compare with ^1H NMR spectrum of the octamer **10c** depicted in **Figure 26**, Section 3.1.3). Nevertheless, the decamer **18e** reveals characteristic resonances in the recorded ^1H NMR spectrum, such as the magnetic resonance deriving from the aldehyde unit of the *o*-MBA moiety at 10.73 ppm (a), indicating the successful chain extension by employing the photomonomer **13** in the final extension step. Moreover, the *o*-MBA group enables the option for further chain extension with monomer **14**. The formation of hydrazonic anhydride after the NICAL ligation and hydrazide rearrangement adduct are detected as broad singlets at 11.06 and 10.84 ppm (a). Furthermore, aromatic resonances, arising from the introduction of pyrene rings into the backbone of the sequence-defined oligomers, are identified by the characteristic magnetic resonances visible as multiplets ranging from 8.80 to 7.50 ppm (b). The successful formation of the tetrahydronaphthalene structure formed upon DA cycloaddition is indicated by the magnetic resonances recorded between 5.60 - 4.90 (d) and 3.50 - 2.50 ppm (e). For more detailed resonance assignments please refer to Section 5.3.5.

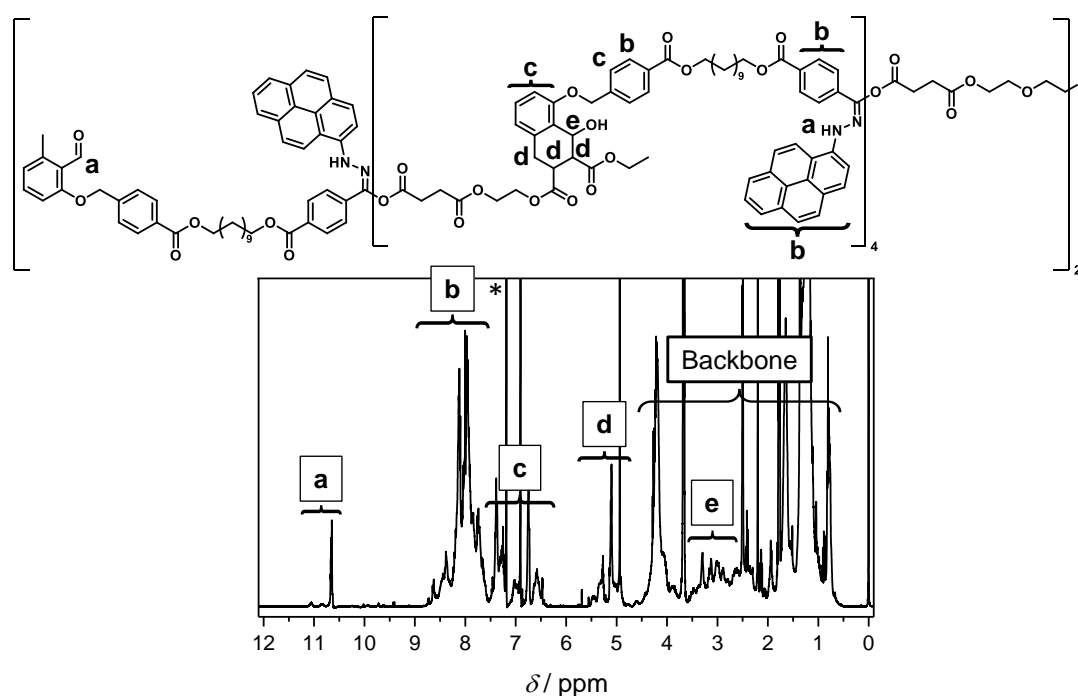


Figure 38. ^1H NMR spectrum of the sequence-defined decamer **18e** recorded in CDCl_3 at 400 MHz. For the signal assignments refer to the depicted structure. The CHCl_3 resonance is marked with a star (*).

Photochemical conjugation methods provide highly efficient tools for the precise synthesis of sequence-defined macromolecules. On the one hand, photochemistry provides temporal and spatial control over reactions, on the other hand photochemistry allows selective triggering of reaction channels by wavelength-orthogonal excitation. Therefore, the selective wavelength dependent activation of tetrazoles and *o*-MBAs carried out in a λ -orthogonal fashion was demonstrated for the protection-free synthesis of sequence-defined macromolecules in the current section. As the key molecule, a photomonomer unit carrying two photosensitive groups, i.e. PAT and *o*-MBA, was employed for chain extension upon irradiation at distinct wavelengths. Starting from a bifunctional carboxylic acid as a core unit, symmetrical sequence-defined macromolecules have been prepared with a molecular weight up to $6257.10 \text{ g mol}^{-1}$ by bidirectional chain growth. The synthesis of symmetric macromolecules based on a modular approach leads to a significant increase of molecular weight per chain extension step. The current iterative approach allows for the synthesis of monodisperse sequence-defined macromolecules featuring absolute chain-end fidelity with monomers placed at exact positions along the chain, thus evidencing the efficiency of the λ -orthogonal photochemical protocol.

3.3. Multifunctional Sequence-Defined Macromolecules *via* Photoligation

Parts of this chapter, the following subchapters, and the associated parts in the experimental section were adapted with permission from a publication co-wrote by the author.^{[29].c}

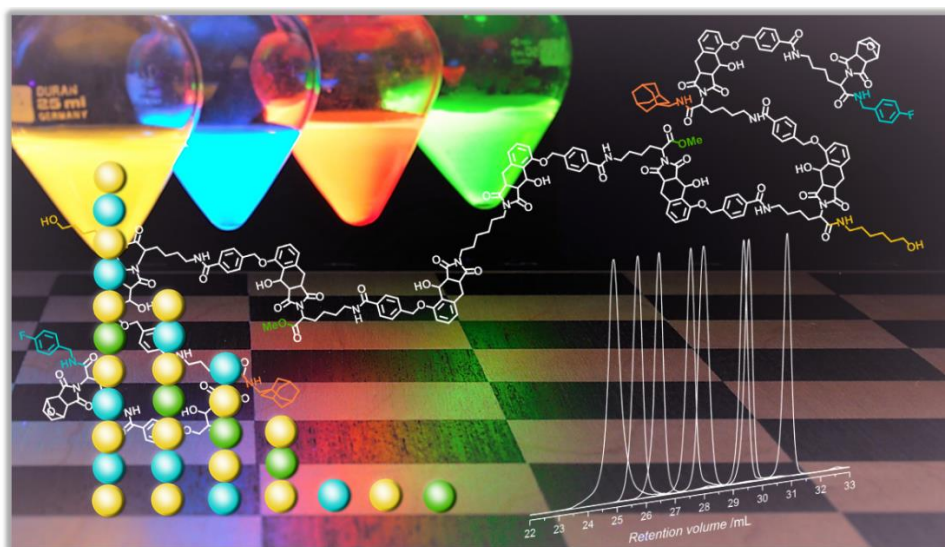


Figure 39. Graphical abstract for the synthesis of sequence-defined macromolecules *via* photoinduced DA cycloaddition based on maleimides and *o*-MBAs. The abstract was prepared by Florian Feist.

In the current section, the synthesis of sequence-defined macromolecules *via* a light induced avenue based on a convergent iterative DA cycloaddition is presented. Therefore, a library of functionalized monomers equipped with a furan protected maleimide and *o*-MBAs was prepared (refer to Section 3.3.1), which in turn were employed for the synthesis of α,ω -functionalized building blocks consisting of up to five monomer units (refer to Section 3.3.2 and 3.3.3). The symmetrical monodisperse macromolecules varying in chemical constitution were obtained starting from a bifunctional maleimide core unit by the combination of sequential and modular chain extension steps (refer to Section 3.3.4). Hence, specific side groups could be placed at any desired position along the chain *via* the iterative addition of

^c Nicolas Zydziak, Florian Feist, and the author conducted the synthetic experiments and analyzed the data. Sergii Afonin performed the MALDI–ToF spectrometry experiments and Steffen Weidner (BAM-Federal Institute for Materials Research and Testing, Berlin) conducted the MALDI–ToF–ToF spectrometry experiments.

the respective building units leading to a library of functional macromolecules with diverse monomer sequences. Sequence-defined macromolecules with a molecular weight of up to $4897.54 \text{ g mol}^{-1}$ were enabled by the synthesis strategy. The in depth characterization was carried out *via* SEC, ESI-MS, and NMR spectroscopy in order to evidence the monodisperse nature of the prepared macromolecules. Moreover, tandem mass spectrometry (MALDI-ToF-ToF) was conducted with the macromolecules for decoding of the monomer sequence order.

3.3.1. Synthesis of a Photomonomer Library

Highly efficient reaction systems are necessary for the synthesis of sequence-defined macromolecules under batch conditions. Therefore, a single photochemical reaction was employed relying on benzaldehydes as before mentioned in Section 3.1 and 3.2. Upon irradiation the *o*-MBA is transformed into its reactive diene structure (so-called photocaged dienes) undergoing DA cycloadditions with electron deficient dienophiles. The monodisperse macromolecules are generated based on a one monomer strategy, i.e. merely one type of monomer with two different functional groups is required for the synthesis of sequence-defined

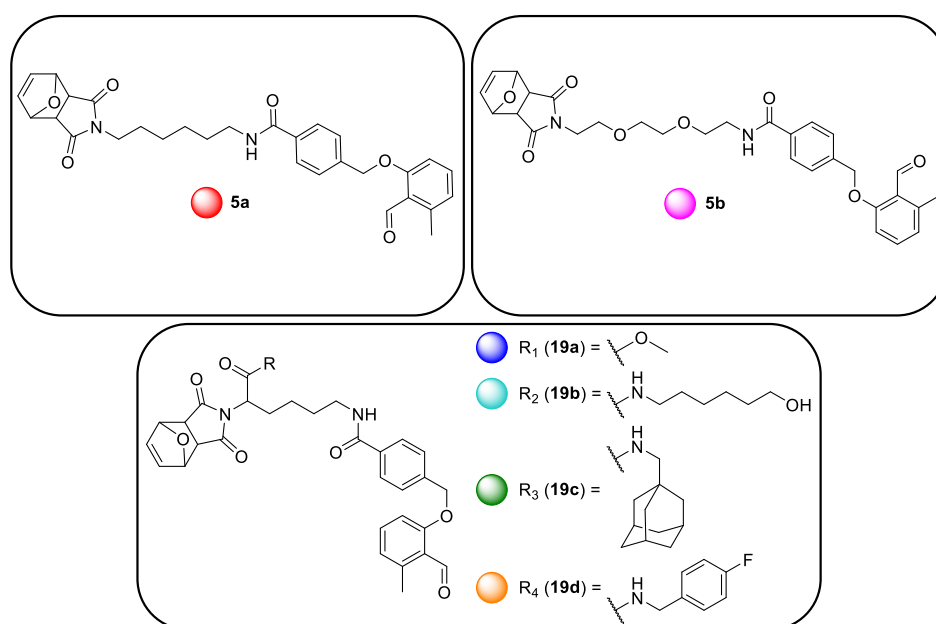
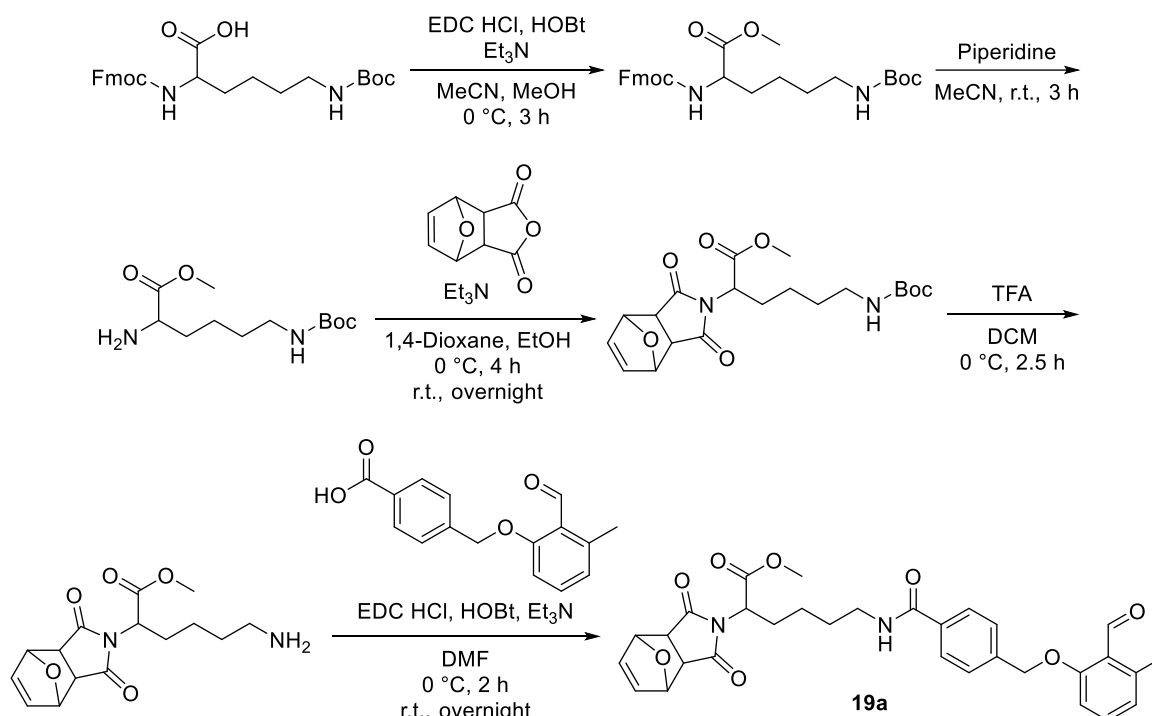


Figure 40. Photomonomers including an *o*-MBA and a furan protected maleimide employed for the synthesis of functional linear sequence-defined macromolecules. The monomers **5a** and **5b** were equipped with a hexane and a PEG based spacer unit, whereas the photomonomers **19a-d** were prepared based on a lysine spacer unit functionalized with a methyl ester, hexanol, adamantly, and a fluorobenzyl moiety.

3. Results and Discussion

macromolecules in contrast to the alternating approach discussed in Section 3.2. In order to synthesize a library of sequence-defined macromolecules varying in their chemical constitution, a set of six functional monomers was introduced as depicted in **Figure 40**. The monomers were equipped with a photoreactive benzaldehyde as well as an maleimide functionality required for the photochemically induced DA reaction. An alkyl as well as a PEG derived spacer unit was employed in the monomer synthesis of **5a** and **5b**. In Section 3.1.2, the synthesis of the two photomonomers **5a** and **5b** was already discussed and employed within the context of the preparation of sequence-defined macromolecules by combining photochemistry and Passerini reactions. Furthermore, side chain groups were introduced relying on a lysine derived spacer unit, which was used for the synthesis of the monomers **19a-d**. The photomonomers **19b-d** equipped with a hexanol, adamantyl, and a fluorobenzyl moiety were synthesized by Florian Feist. Albeit, the photomonomer **19a**, carrying a methyl ester as side chain group, was prepared by the author relying on the same synthetic concept as described in **Scheme 48**. In detail, the different side chain groups were incorporated based on an α,ω -caged lysine precursor carrying orthogonal fluoromethoxycarbonyl (Fmoc) and *tert*-butyloxycarbonyl (Boc) protecting groups. In the first step, the side chain groups were



Scheme 48. The photomonomer **19a** was prepared starting from a α,ω -Fmoc-Boc protected lysine spacer unit. Selective deprotection and introduction of the side chain functional group, i.e. furan protected maleimide and benzaldehyde, lead to the targeted compound **19a**.

tethered to the lysine derivative by esterification under Steglich conditions. After selective deprotection of the Fmoc protected amine group in basic medium, the lysine spacer was equipped with a furan protected maleimide group. Subsequently, the Boc protecting group was removed under acidic conditions prior to the esterification under Steglich conditions introducing a benzaldehyde moiety affording the photomonomer **19a** (23 % overall yield). In the ^1H NMR spectrum of the photomonomer **19a** depicted in **Figure 41**, characteristic magnetic resonances deriving from the *o*-MBA moiety, furan protected maleimide, and the methyl ester are identified. Singlets recorded at 10.66 (aldehyde proton 18), 5.12 (methylene group 13), and 2.51 ppm (methyl group 17) associated with the *o*-MBA group verify the successful incorporation of the benzaldehyde into the monomer unit. Furthermore, the functionalization of the monomer with the furan protected maleimide moiety is evidenced by the magnetic resonances visible at 6.41 (1), 5.12 (2), and 2.81 ppm (3). The magnetic resonance at 3.65 ppm (5) is assigned to the protons of the methyl ester confirming the successful synthesis of the targeted photomonomer **19a**.

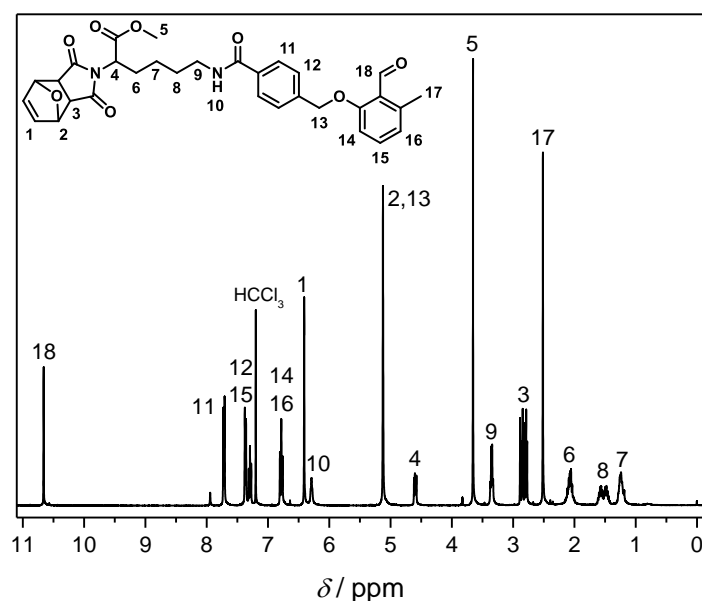


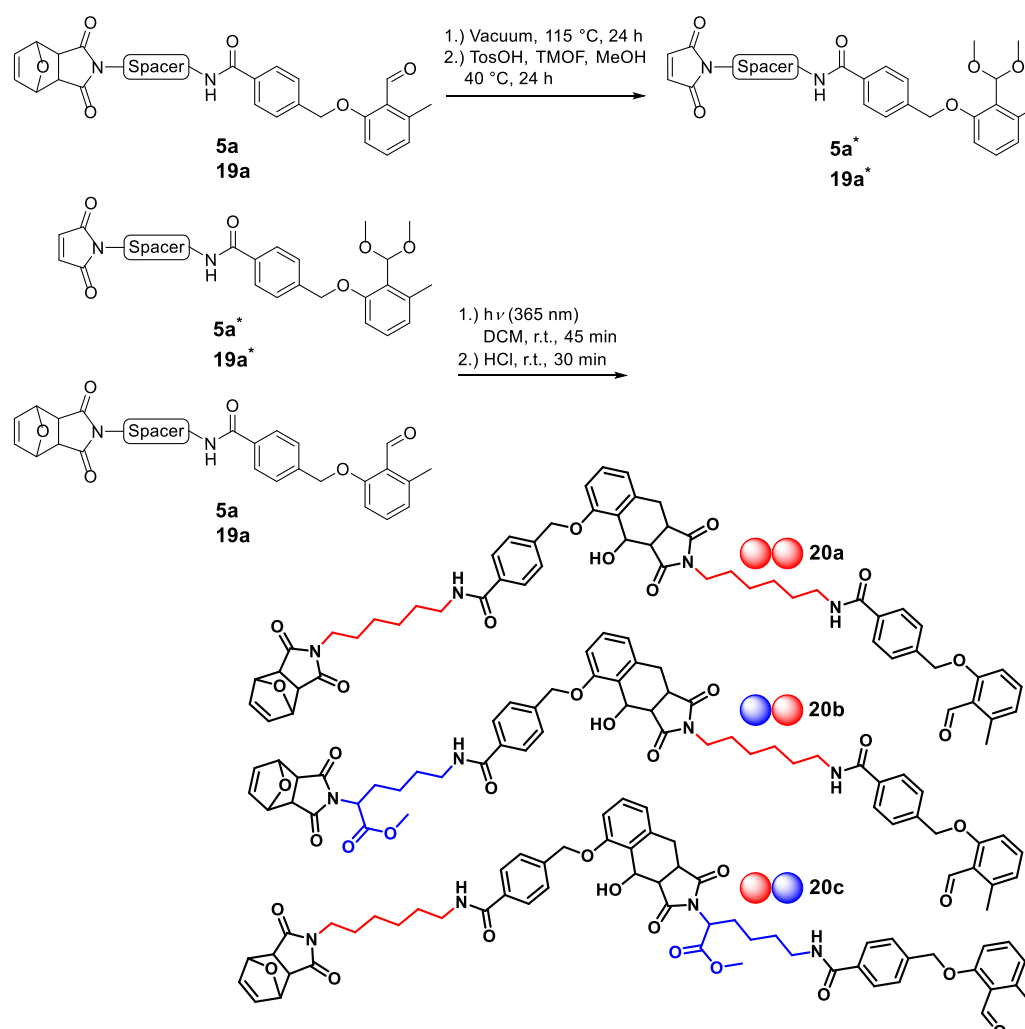
Figure 41. ^1H NMR spectrum of the photomonomer **19a** recorded in CDCl_3 at 400 MHz. For the signal assignments refer to the depicted structure.

3.3.2. α,ω -Functionalized Macromolecules as Building Blocks

High molecular weights can be achieved most efficiently by a combination of sequential and modular strategies. In general, modular strategies provide an advanced tool to design com-

3. Results and Discussion

plex sequence-defined macromolecules using building blocks of different chemical composition and thus achieving variation of the oligomer backbone functionalization. In addition, a modular approach leads to a significant increase of molecular weight per chain extension step reducing the total number of reactions. A significantly higher increase of molecular weight also contributes to the purification of the macromolecules as the feasibility of the chromatographic separation of the respective generations is increased. Therefore, a set of three non-symmetric α,ω -functionalized dimers **20a-c** were synthesized by employing the photomonomers **5a** and **19a** as depicted in **Scheme 49**. In the first step, selective transformation of the end-groups was performed. Consequently, the furan protecting group of the respective photomonomer **5a** or **19a** was removed by thermal treatment at 115 °C under



Scheme 49. Selective end-group transformation of the monomers **5a** and **19a** by thermal treatment for unlocking of the maleimide and following acetalization resulted in the modified monomers **5a*** and **19a***. The photoreaction between the modified and non-modified monomers yielded the dimers **20a-c**.

3.3. Multifunctional Sequence-Defined Macromolecules via Photoligation

vacuum. Subsequent locking of the photosensitive benzaldehyde as dimethyl acetal resulted in the modified monomers **5a*** and **19a*** equipped with an unlocked maleimide and a protected benzaldehyde. The combination of the complementary unlocked groups by irradiation with UV-light at $\lambda_{\max} = 365$ nm and subsequent mild acidic hydrolysis of the labile acetal group yielded the targeted dimers **20a-c**. A combination of **5a** and **5a*** lead to dimer **20a**, the combination of **19a** and **5a*** resulted in dimer **20b**, and **5a** combined with **19a*** afforded dimer **20c**, all bearing a furan-protected maleimide and a benzaldehyde group at the chain ends. Characterization of the dimers **20a-c** was carried out *via* SEC (depicted in **Figure 45a-**

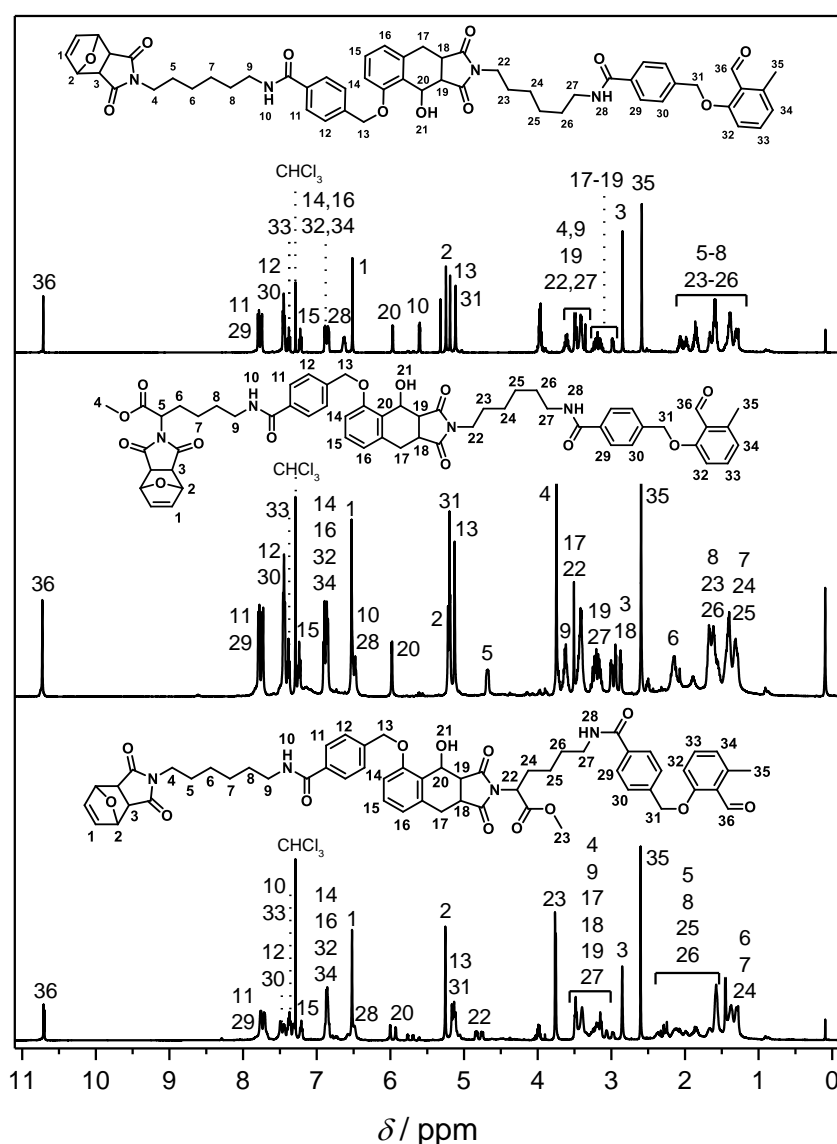
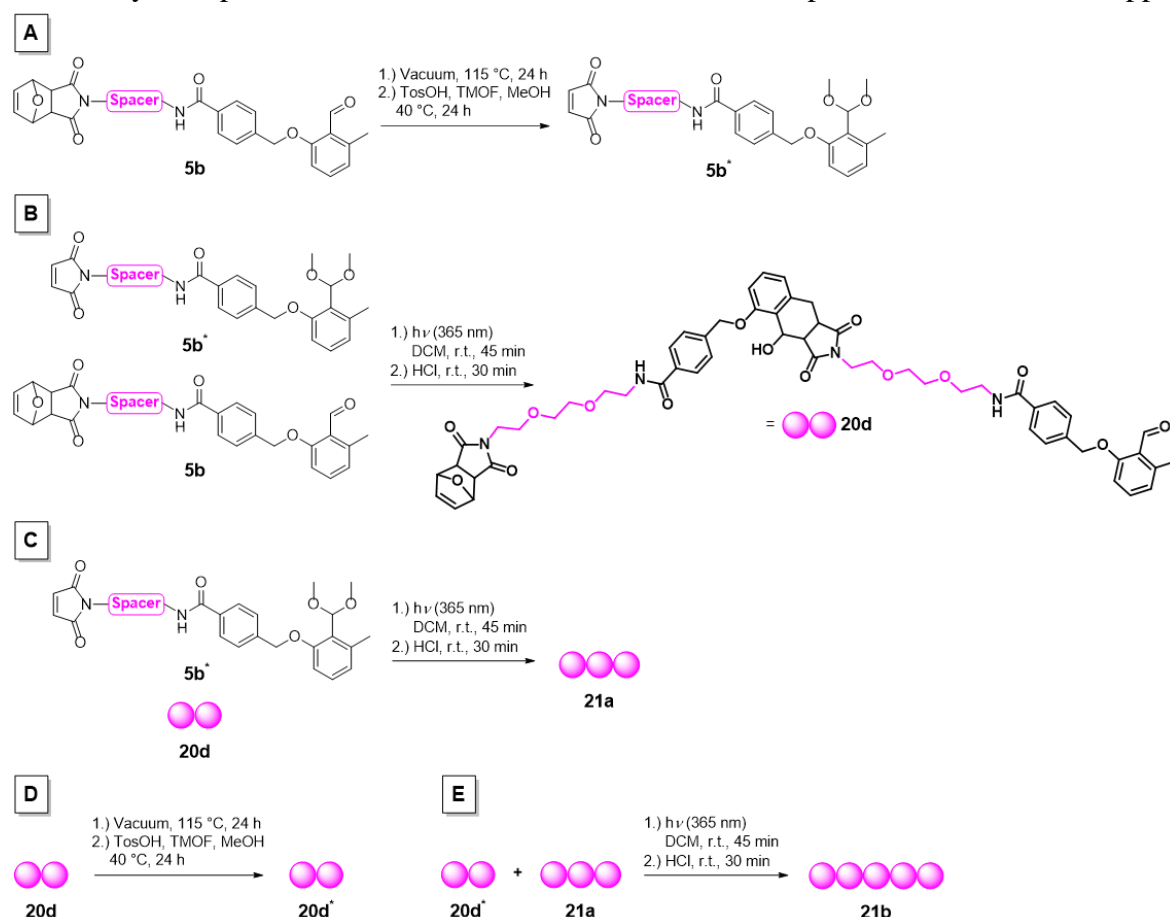


Figure 42. ¹H NMR spectrum of the dimers **20a-c** (top to bottom) recorded in CDCl₃ at 400 MHz. For the signal assignments refer to the depicted structures.

3. Results and Discussion

d, Section 3.3.4), MALDI-ToF mass spectrometry (depicted in **Figure 46**, Section 3.3.4), and NMR spectroscopy. In **Figure 42** the ^1H NMR spectra of the dimers **20a-c** are illustrated. Characteristic magnetic resonances of the protons of the *o*-MBA moiety, the furan protected maleimide, and the tetrahydronaphthalene structure formed by the DA cycloaddition are identified. The magnetic resonances at 10.71 (aldehyde proton 36), 5.12 (methylene group 31), and 2.58 ppm (methyl group 35) associated with the *o*-MBA moiety are detected in the ^1H NMR spectra of all three dimers. Singlets recorded at 6.52 (1), 5.24 (2), and 2.85 ppm (3) result from the furan caged maleimide end-group. The successful DA cycloaddition formation is evidenced by the characteristic magnetic resonance of the chiral methine group 20 located at 5.95 ppm. Additional magnetic resonances deriving from the methylene groups of the tetrahydronaphthalene structure 17-19 are visible as multiplets between 3.6 to 2.9 ppm



Scheme 50. (A) Maleimide deprotection by thermal treating and acetal formation starting from the photomonomer **5b** yielding the modified monomer **5b***. (B) Formation of the dimer **20d** employing the photomonomer **5b** and the modified monomer **5b***. (C) Formation of the trimer **21a** by combining dimer **20d** and the modified monomer **5b***. (D) Maleimide deprotection by thermal treating and acetal formation starting from the dimer **20d** yielding the modified dimer **20d***. (E) Synthesis of the pentamer **21b** employing the dimer **20d** yielding the modified dimer **20d***.

confirming the successful synthesis of the dimers **20a-c**. The synthesized dimers **20a-c** were subsequently employed as building blocks in the final modular chain extension step for the preparation of symmetrical sequence-defined macromolecules **23a-d** as discussed in Section 3.3.4.

3.3.3. Synthesis of α,ω -Functionalized Macromolecules

With the aim to expand the library of modular building blocks, the non-symmetric α,ω -functionalized pentamer **21b** was generated consisting of photomonomer **5b** units using the same synthetic modular concept as for the preparation of the dimers **20a-c** (refer to **Scheme 50**). Hence, the dimer **20d** was obtained by the irradiation of photomonomer **5b** and the modified monomer **5b**^{*} (which in turn was received after furan deprotection under thermal conditions and acetalization) and subsequent hydrolysis of the acetal group. In the next step, dimer **20d** was combined with another equivalent of the modified monomer **5b**^{*} for chain extension to yield the trimer **21a** after hydrolysis. Following the locking/unlocking strategy, the end-groups of the dimer **20d** were transformed resulting in the modified dimer **20d**^{*} after maleimide deprotection and acetalization. In the final step, the trimer **21a** was tethered to the modified dimer **20d**^{*} upon irradiation with UV-light at $\lambda_{\text{max}} = 365$ nm resulting in the non-symmetric α,ω -functionalized pentamer **21b** achieving a yield of 20 % and a molecular weight of 2470.62 g mol⁻¹.

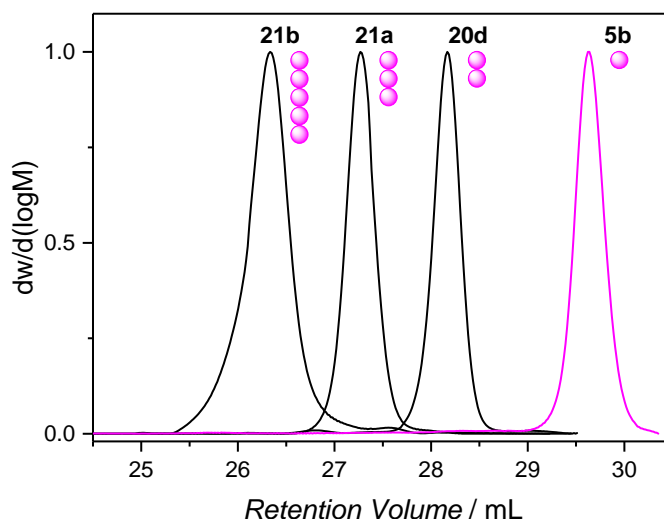


Figure 43. SEC traces of the synthesized non-symmetric α,ω -functionalized sequence-defined pentamer **21b** (26.3 mL) and its precursors the dimer **20d** (28.2 mL) and the trimer **21a** (27.3 mL). In addition, the SEC trace of the photomonomer **5b** (29.6 mL) is depicted. All SEC traces were recorded on a SEC system with THF as eluent.

The monodispersity of the sequence-defined macromolecule **21b** and the respective intermediates was underpinned *via* SEC and MALDI-ToF mass spectrometry confirming the versatility of the photoreactions yielding α,ω -functional linear macromolecules. In **Figure 43**, the SEC traces of α,ω -functionalized pentamer **21b** and its precursors, the dimer **20d** and the trimer **21a**, as well as the photomonomer **5b** recorded on a THF-based SEC system are displayed. The molecular weights and dispersities have been received relative to a polystyrene calibration. Starting from the photomonomer **5b** a shift of the SEC trace towards decreased retention volume (increased molecular weight) is detectable after the combination of two monomer equivalents. A further decrease in retention volume is detected for the formation of the trimer **21a**. The SEC trace of the α,ω -functional sequence-defined pentamer **21b** obtained by UV-irradiation of the trimer **21a** in the presence of the modified dimer **20d*** clearly exhibits a shift towards decreased retention time and thus increased molecular weight. Consequently, the SEC analysis confirms the successful iterative modular chain extension by an increase of molecular weight after each addition of the respective building block. Moreover, the SEC traces depicted in **Figure 43** confirm the purity of the macromolecules since only

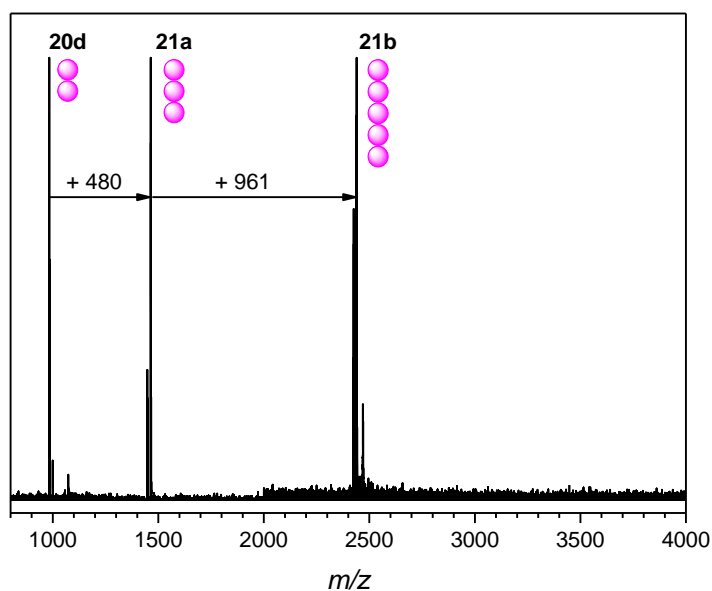


Figure 44. MALDI-ToF spectra of the α,ω -functionalized pentamer **21b** (depicted in the m/z range of 2000 to 4000) as well as of the dimer **20d** and the trimer **21a** (visible in the m/z range of 800 to 4000). The increase of m/z 480 corresponds to the addition of one equivalent of the photomonomer **5b**, whereas the increase of m/z 961 corresponds to the addition of one equivalent of the dimer **20d**. Dimer **20d**: m/z 983.69 ([**20d**-furan+Na]⁺, $m/z_{\text{calc.}}$ 983.37, $\Delta m/z$ 0.32). Trimer **21a**: m/z 1463.85 ([**21a**-furan+Na]⁺, $m/z_{\text{calc.}}$ 1463.56, $\Delta m/z$ 0.28). Pentamer **21b**: m/z 2424.95 ([**21b**-furan+Na]⁺, $m/z_{\text{calc.}}$ 2424.47, $\Delta m/z$ 0.48).

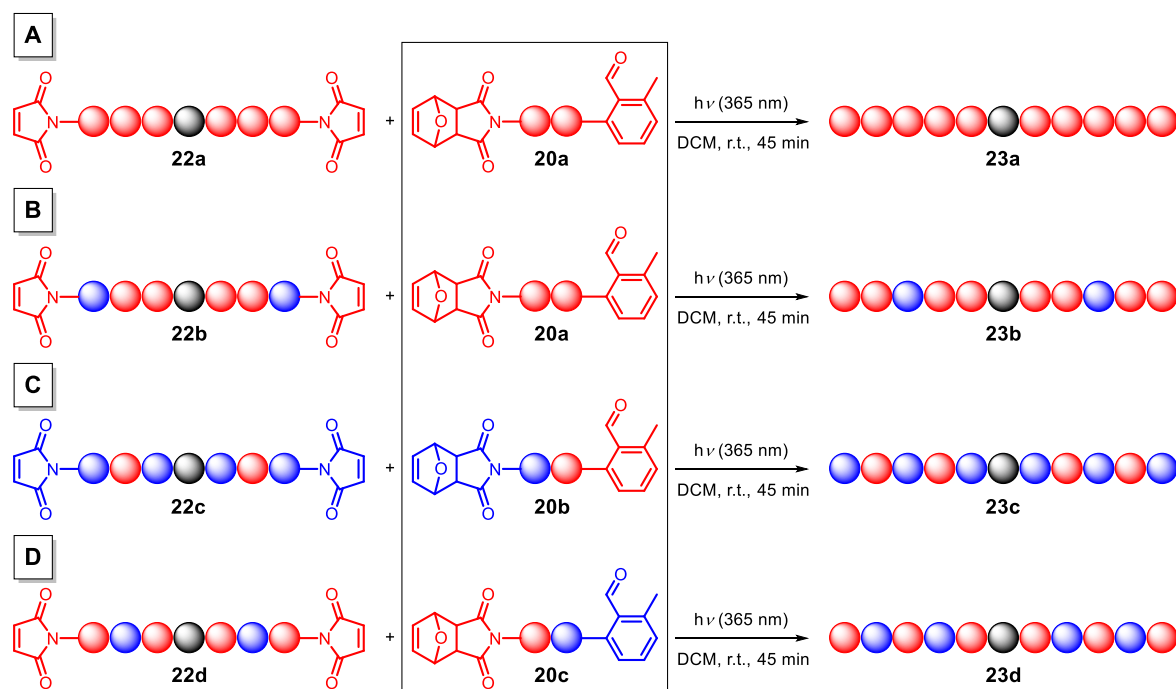
narrow monomodal distributions were recorded. For all SEC traces – from the α,ω -functionalized pentamer **21b** to its precursors – dispersities of $\mathcal{D} < 1.01$ have been determined chromatographically, which verifies the monodispersity of the synthesized non-symmetric sequence-defined macromolecules. The overlaid MALDI-ToF spectra of the α,ω -functionalized macromolecules **20d**, **21a**, and **21b** are depicted in **Figure 44**. Only mass signals of the respective charged counter ion adducts (H^+ , Na^+ , and K^+) assigned to the furan deprotected sequence-defined pentamer **21b** are revealed in the MALDI-ToF spectrum at m/z 2424.95 ($[\mathbf{21b}\text{-furan+Na}]^+$, $m/z_{\text{calc.}} 2424.47$, $\Delta m/z 0.48$). Consequently, furan deprotection of the maleimide occurred during the MALDI ionization process. The indicated increase of m/z 480 corresponds to the addition of one equivalent of photomonomer **5b** during the formation of the trimer **21a**, whereas the increase of m/z 961 corresponds to the chain extension of the trimer **21a** employing the modified dimer **20d***. In conclusion, the successful synthesis of the α,ω -functionalized sequence-defined pentamer **21b** and the monodisperse nature is verified by SEC analysis as well as MALDI-ToF mass spectrometry.

3.3.4. Modular Synthesis of Symmetric Sequence-Defined Macromolecules

The synthetic strategy for achieving sequence-defined macromolecules featuring high molecular weights is relying on the combination of an iterative and modular approach. Modular strategies drastically reduce the number of reactions that need to be carried out with the macromolecules themselves for achieving high molecular weight, comparable to IEG strategies (refer to Section 2.3.4). In addition, 1,6-hexylbismaleimide was employed as a symmetrical core unit contributing to an increased molecular weight growth as two building units are added to the growing macromolecule simultaneously in one reaction step. In **Scheme 51** the synthesis of four symmetrical sequence-defined decamers **23a-d** using modular building blocks, i.e. the dimers **20a-c**, starting from the symmetrical hexamers **22a-d** is illustrated. The respective modular building units **20a-c**, highlighted through a black colored frame, were prepared by the author by orthogonally locking and unlocking of the diene and dienophile groups of each photomonomer on demand as presented in Section 3.3.2 and 3.3.3. The formation of the hexamers **22a-d** and the symmetrical sequence-defined decamers **23a-d** was performed by Nicolas Zydziaik. Therefore, the core unit 1,6-hexylbismaleimide (denoted

3. Results and Discussion

as a black sphere in **Scheme 51**) was extended with two equivalents of the respective photomonomers **5a** (red sphere) and **19a** (blue sphere) in the first step resulting in a linear symmetrical dimer possessing furan protected maleimides on both chain ends. Subsequently, thermal treatment was performed removing the furan protecting group in order to enable consecutive photoligation with the monomers. Repeating the cycle of photoinduced iterative chain extension employing the photomonomers **5a** and **19a** followed by thermal deprotection of the maleimide afforded the third sequence order in which the hexamers **22a-d** exhibit different sequences of monomers. The sequential alternation of the two photomonomers diversifies the composition of the symmetrical macromolecules verifying the successful design of the complex copolymers. Since a modular strategy provides an efficient way in order to increase the molecular weight of sequence-defined macromolecules, the hexamers **22a-d** were extended by ligation with the previously synthesized dimers **20a-c** (refer to Section 3.3.2). The dimers **20a-c** are equipped with a furan protected maleimide and a benzaldehyde group and can be directly employed for chain extension. Consequently, the symmetrical sequence-defined decamers **23a-d** with molecular weights about 4900 g mol^{-1} were prepared by chain extension of the hexamers **22a-d** after a preliminary thermal treatment to remove



Scheme 51. Modular strategy for the synthesis of sequence-defined decamers **23a-d**. The hexamers **22a-d** were prepared by Nicolas Zydziak. The decamers **23a-d** varying in their chemical composition were obtained by chain extension employing, the in the black frame highlighted, α,ω -functionalized dimers **20a-c** synthesized by the author.

the furan protecting group. Isolated overall yields of 1.0 % from the monomer to the final decamer were obtained. The low yield can be explained by the purification *via* flash chromatography after every generation since slight excess of monomers was employed for the photoreactions. In addition, a photoinduced [2+2] cycloaddition of the maleimide core unit was observed during the formation of the first sequence order of the monodisperse macromolecules. As a result, the purification and side reactions lead to a certain loss of overall efficiency. It is interesting to note that the targeted decamers could be purified by selective precipitation as the solubility between the hexamers **22a-d** and decamers **23a-d** is changed significantly. Moreover, the synthesis of a symmetrical icosamer was performed by the author by employing the symmetrical decamer **23a** and the α,ω -functionalized pentamer **21b** (refer to Section 3.3.3). However, a precipitate was formed during UV irradiation of the

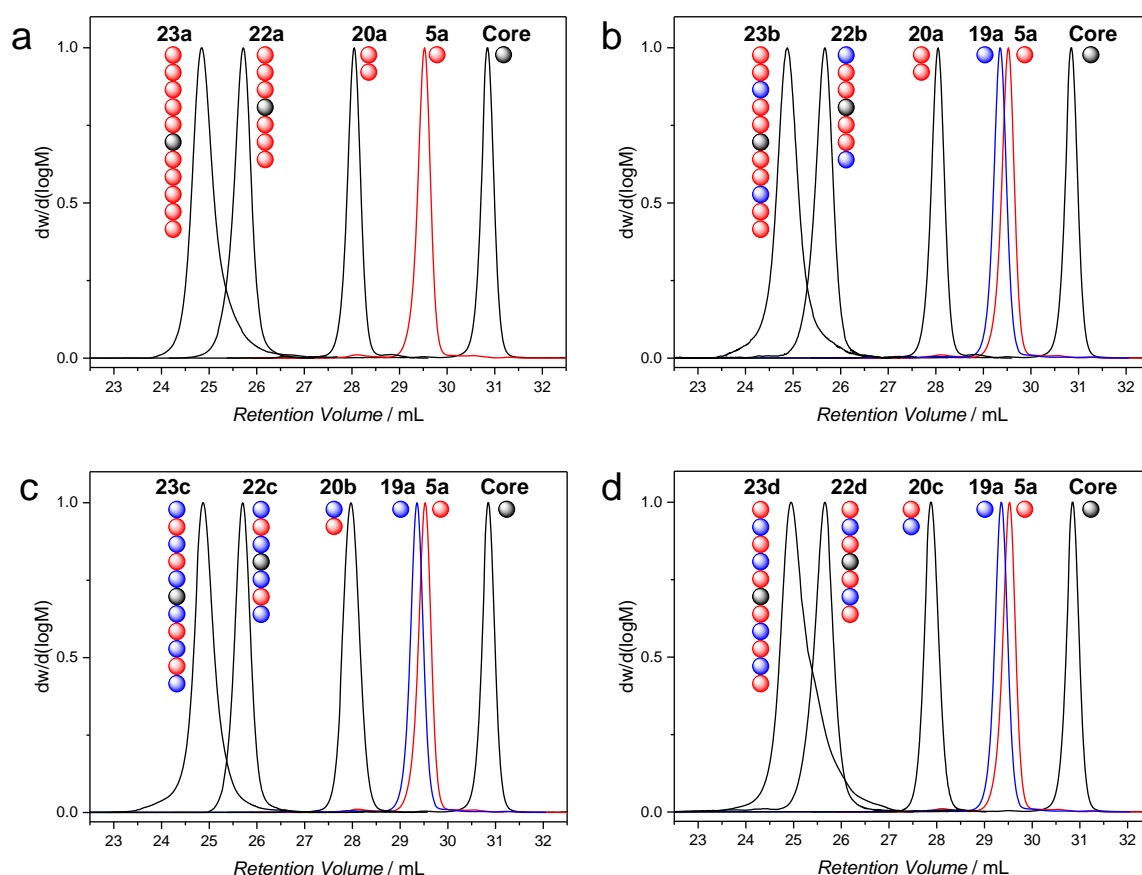


Figure 45. SEC traces of the successively synthesized sequence-defined decamers **23a-c** varying in their monomer sequence order. Additionally, the core unit, the photomonomers **5a** and **19a**, the α,ω -functionalized dimers **20a-c**, and the symmetrical hexamers **22a-d** are represented. All SEC traces were recorded on a THF based SEC system.

reaction mixture. Analysis of the material turned out to be challenging due to its low solubility. Hence, characterization was attempted on a dimethylacetamide (DMAc)-based SEC system and mass spectrometry. However, the targeted icosamer couldn't be identified or characterized in the reaction mixture after the irradiation at 365 nm.

Successful formation of the successively synthesized sequence-defined macromolecules was verified by SEC and MALDI-ToF mass spectrometry. The SEC traces were recorded *via* a THF-based SEC system and are depicted in **Figure 45a-d** including the core unit, the photomonomers **5a** and **19a**, the α,ω -functionalized dimers **20a-c**, the hexamers **22a-d**, and the targeted symmetrical sequence-defined decamers **23a-d**. The molecular weights and dispersities have been obtained relative to a polystyrene calibration. Starting from the bismaleimide core unit, a shift of the SEC trace towards decreased retention volume (corresponding to an increased molecular weight) is received after the addition of the photomonomers resulting in the formation of the hexamers **22a-d**. In addition, a significant decrease in retention time (increase in molecular weight) is detected for the symmetrical sequence-defined

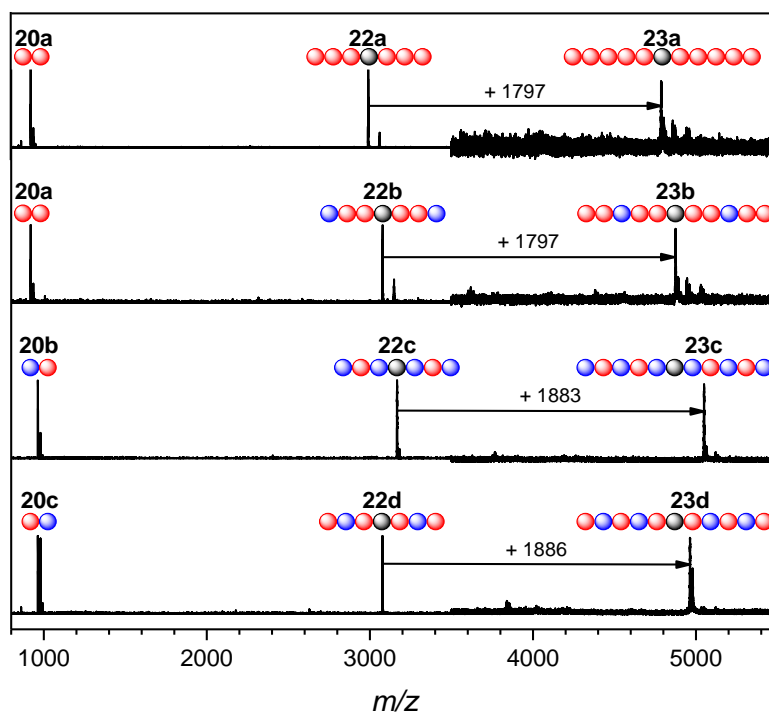


Figure 46. Overlaid MALDI-ToF mass spectra of the symmetric sequence-defined decamers **23a-d** and its precursors the hexamers **22a-d** as well as α,ω -functionalized dimers **20a-c**. The MALDI-ToF spectra are depicted in different m/z -ranges, 800–4000 for the dimers as well as hexamers and 3500–5500 for the decamers. The m/z -intervals between the hexamers and decamers are characteristic for the addition of two dimer blocks (m/z 1797 for **20a**, m/z 1883 for **20b**, and m/z 1886 for **20c**) at the chain termini.

decamers **23a-d** after the modular chain extension carried out by employing the α,ω -functionalized dimers **20a-c**. The SEC analysis confirms the successful iterative and modular chain extension by an increase of molecular weight after the addition of the respective building blocks. Furthermore, the SEC traces depicted in **Figure 45a-d**, underline the purity of the macromolecules since only narrow monomodal distribution were recorded. The SEC analysis of the α,ω -functionalized dimers **20a-c** and the symmetrical hexamers **22a-d** dispersities of $D < 1.01$ based on a PS calibration have been determined chromatographically, whereas dispersities between 1.02 and 1.03 were recorded for the symmetrical sequence-defined decamers **23a-d** confirming the successful photochemical synthetic strategy. Mass spectrometry enables the accurate identification of molecular weights of sequence-defined molecules and thus the verification of monodispersity and structural elucidation. Therefore, the MALDI-ToF mass spectra of the symmetrical sequence-defined decamers **23a-d** in the m/z range from 3500 to 5500 are additionally depicted in **Figure 46**. Mass signals of the respective charged adducts (H^+ , Na^+ , and K^+) assigned to the sequence-defined macromolecules **23a-d** are recorded and displayed in the spectra. The m/z -intervals between the hexamers and decamers are characteristic for the addition of two dimer blocks (m/z 1797 for **20a**, m/z 1883 for **20b**, and m/z 1886 **20c**) at the chain termini confirming the expected molecular weight increase as well as the monodispersity. Interestingly, the SEC trace of **23d** displays a shoulder towards lower molecular weight responsible for the slight increase of the dispersity from the hexamer to the decamer, from $D = 1.01$ to 1.03. However, the analysis by the mass spectrum of **23d** suggests monodispersity since only a single molecular peak is detected. The shoulder of the SEC trace recorded for **23d** may be explained by the particularly increased lysine content potentially leading to column interactions *via* adsorption of the amino acid motifs. In conclusion, the successful synthesis of the sequence-defined decamers **23a-d** and the monodisperse nature is verified by SEC analysis and MALDI-ToF mass spectrometry.

Moreover, supplementary tandem mass experiments of the symmetrical sequence-defined decamers **22a-d** were conducted by MALDI-ToF-ToF mass spectrometry (refer to **Figure 47**). The verification of the monomer sequence order itself represents a specific challenge as the molecular weight of isomers is exactly the same. Therefore, decoding of the chain structure becomes crucial to confirm the monomer sequence. Decoding was performed by Steffen

3. Results and Discussion

Weidner using the symmetric hexamers **22b** and **22d**. Both hexamers **22b** and **22d** possess the same molecular weight, yet the photomonomer **19a** (blue sphere) was placed at different sequence positions leading to both isomers. Tandem mass conducted by MALDI-ToF-ToF spectrometry allows access to the degradation fragmentation pattern of the isomers **22b** and **22d** leading to a distinct correlation between the sequence order and the monodisperse hexamers. Hence, the successful coding in the symmetrical hexamers **22b** and **22d** is confirmed by the characteristic fragmentation pattern of the respective isomer.

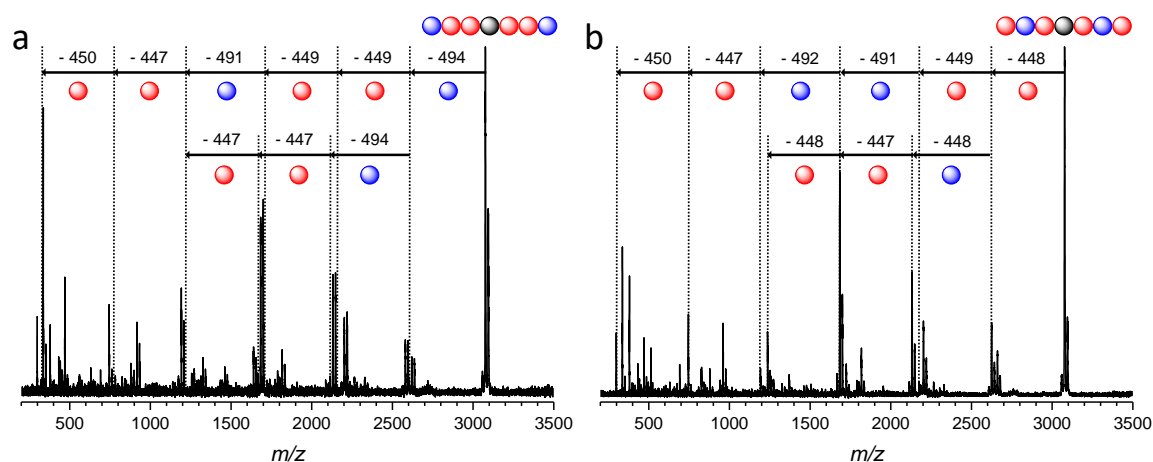


Figure 47. Tandem mass spectrometry *via* MALDI-ToF-ToF with the symmetrical hexamers **22b** (a) and **22d** (b).

Photochemistry provides a variety of efficient and orthogonal reactions offering accessible routes to sequence-defined macromolecules. In summary, a versatile photochemical strategy for the synthesis of a library of functional sequence-defined macromolecules, varying in chain length and monomer sequence order, was demonstrated relying on an iterative and modular chain extension. Moreover, α,ω -functionalized macromolecules have been prepared as building blocks for modular chain extension, ready to be combined on demand in order to achieve high molecular weights in as few reaction steps as possible. As a consequence of the sequential and modular light induced approach of adding every building unit successively, the macromolecules exhibit dispersities of $\mathcal{D} < 1.03$ and feature absolute chain-end fidelity. As a result, the current photochemical technology platform can be employed for mimicking selected features of Nature's macromolecules, such as coding and transcription of information. The in-depth characterization of the sequence-defined macromolecules and the investigation of the monomer sequence order require multiple analytical techniques including SEC and mass spectrometry in particular. Moreover, tandem mass spectrometry,

MALDI-ToF-ToF for instance, enables access to the monomer sequence order by the investigation of the characteristic degradation fragmentation pattern generated upon the mass analysis. Hence, a distinct assignment the monomer sequence order is ensured.

4

Conclusion and Outlook

Modular strategies in which a symmetric linear molecule is ligated with previously synthesized building blocks is an efficient way for increasing the molecular weight in sequence-defined macromolecules. In general, modular strategies provide an effective tool in designing complex sequence-defined macromolecules using building blocks with different functional groups and thus achieving variation in the functionalization of the oligomer backbone. In addition, a modular approach enables the combination of large building blocks, minimizing the synthetic steps required to create sequence-defined macromolecules with high molecular weights. A significantly higher increase of molecular weight also facilitates the purification of the macromolecules as the chromatographic separation of the respective generations is increased. Furthermore, the synthesis of macromolecules by bidirectional growth – employing symmetrical core units – also contributes to a significant increase of molecular weight per chain extension reaction due to the fact that two building units are added simultaneously in one step. High molecular weights can be achieved most efficiently by a combination of symmetrical molecules and modular strategies. However, the use of symmetrical core molecules results in restricting the level of freedom for the design of monodisperse polymers since only symmetric sequence-defined macromolecules are synthetically feasible. Nonetheless, cleavable core units can be employed for the synthesis of symmetric sequence-defined macromolecules leading to non-symmetric α, ω -functionalized macromolecules. Additionally, bidirectional growth starting from a symmetrical core unit contributes to a certain loss in overall efficiency since quantitative conversion of each chain end must be ensured. Anything but quantitative conversion of the chain ends leads to a single side chain extension of the sequence-defined macromolecules resulting in reduced overall yields. Hence, highly

efficient coupling methods, such as ‘click’ reactions, need to be employed to ensure quantitative conversion of chain ends and to increase the overall efficiency of the synthetic strategy.

In this context photochemistry provides a variety of efficient and, under certain conditions, orthogonal conjugation methods offering accessible routes to sequence-defined macromolecules. On the one hand, photochemistry provides temporal and spatial control over reactions, and on the other hand, it allows selective triggering of reaction channels by wavelength-orthogonal excitation. However, side chain functionalities need to be introduced into photobuilding units prior to light induced conjugation of the photomonomers to achieve multifunctional macromolecules. In contrast, MCRs, for example the Passerini reaction, enable the chain extension and the introduction of functional side chains in one step. Consequently, the combination of both, photoconjugation methods and MCRs, appears to be a very powerful tool for providing precision oligomers consisting of alternating P-3CR and photoblocks. Herein, the advantages of photochemistry and MCRs, namely the temporal and spatial control over reaction conditions and the introduction of functional side chains, were exploited. The combination of both ligation techniques, i.e. P-3CR and DA cycloaddition with *o*-MBAs, was demonstrated in Section 3.1, confirming the versatility of the combination of P-3CRs and photoreactions. A modular approach was applied in combination with bidirectional chain growth for the consecutive chain extension leading to the desired symmetric sequence-defined macromolecules with molecular weights of up to 3532.16 g mol⁻¹. Sebacic acid was used as the core unit, providing symmetric sequence-defined macromolecules based on a previously prepared Passerini linker and photobuilding units. The photobuilding units employed were based on a UV-light active benzaldehyde moiety, a photocaged diene, and furan protected maleimides. The convergent approach combining P-3CRs and photoconjugation allowed for straightforward synthesis of monodisperse sequence-defined macromolecules featuring absolute chain-end fidelity and functional monomers to be placed at exact positions along the chain.

In Section 3.1 and 3.3, the photoinduced DA reaction between a UV-light active benzaldehyde and a furan caged maleimide was exploited for the photochemical synthesis of sequence-defined macromolecules. Prior to further chain extension, the oligomers need to be thermally deprotected after each chain growth step. However, modifications carried out with

the macromolecules themselves decrease the overall yield of the synthesis and thus the efficiency of the strategy is decreased. Therefore, it is important to avoid protection group chemistry in order to reduce the total number of reaction steps. For instance, protecting groups can be circumvented by the selective excitation of photosensitive moieties by irradiation at different wavelengths. On the one side, pyrene-functionalized tetrazoles respond to visible light and form nitrile imines upon irradiation at 410 – 420 nm. The nitrile imines can be employed for NICAL ligation in a subsequent reaction step with carboxylic acids. On the other side, [4+2] DA cycloadditions can be carried out with photocaged dienes, such as *o*-MBAs, combined with dienophiles, for example fumarates, in the UV-light region at 365 nm. In Section 3.2, the combination of both photoresponsive groups in one molecule was utilized for the photoinduced chain extension by selective excitation of the respective light sensitive group. While the activated moiety proceeds in the photochemical coupling reaction, the non-activated group is not participating in the photoreaction and remains in its ground state. The synthesis of sequence-defined macromolecules described in Section 3.2 is based on a two-monomer system by chain extension of a symmetrical core unit. A photomonomer unit carrying two photosensitive groups, i.e. PAT and *o*-MBA, was employed for chain extension at distinct wavelengths and the second monomer was equipped with complementary groups, i.e. a carboxylic acid and a fumarate. A custom made photoflow reactor was designed for the NICAL reaction to provide straightforward scalability. Starting from a bifunctional carboxylic acid as a core unit, symmetrical sequence-defined macromolecules were prepared with a molecular weight up to 6257.10 g mol⁻¹ by bidirectional chain growth featuring absolute chain-end fidelity and monomer units placed at exact positions along the chain. Moreover, the polarity of the monodisperse macromolecules was changed significantly after each generation since every second chain extension step introduced carboxylic acids at the chain termini. Therefore, purification was straightforward. Hence, the efficiency of the λ -orthogonal photochemical protocol was evidenced in Section 3.2.

Based on the photoinduced DA reaction between UV-light active *o*-MBAs and furan caged maleimides, a library of functional sequence-defined macromolecules varying in chain length and monomer sequence order was created in Section 3.3. This versatile photochemical strategy relies on an iterative and modular chain extension. α,ω -functionalized macromolecules consisting of up to five monomer units were prepared in the first step as building blocks

for modular chain extension, ready to be combined on demand. Starting from a bismaleimide core unit, symmetrical sequence-defined decamers were obtained by the successive addition of the respective building units *via* UV-light. The macromolecules exhibit dispersities of $D < 1.03$ and feature absolute chain-end fidelity.

The distinct characterization and the investigation of the monomer sequence order of monodisperse macromolecules is challenging and requires multiple analytical techniques. In-depth characterization of the sequence-defined macromolecules was thus conducted *via* SEC, NMR spectroscopy and mass spectrometry techniques. SEC allows access for the determination of the macromolecular dispersity and additionally confirms the purity of the sequence-defined molecules. However, the determination of reliable molecular weights is nearly impossible since no suitable calibration data is available for most sequence-defined macromolecular systems. It is important to note that for comparison reasons the molecular weights of the monodisperse macromolecules, investigated in the current thesis, have been obtained relative to a polystyrene calibration. Because of this, high resolution Orbitrap ESI-MS measurements were performed in order to identify the exact molecular weights of the monodisperse macromolecules, synthesized in the current thesis. Additionally, precise determination of the isotopic pattern *via* analysis of MS spectra further highlights the precise confirmation of the successful synthesis of the sequence-defined macromolecules. Moreover, tandem mass spectrometry, such as MALDI-ToF-ToF, enables the determination of the monomer sequence order by the characteristic degradation fragmentation pattern generated upon tandem mass analysis. Furthermore, NMR spectroscopy is essential for complete characterization and was conducted to verify the structure and purity of the synthesized compounds. However, with increasing complexity of the proton spectra, the explicit assignment of magnetic resonances becomes imprecise since the typical broadening of proton resonances seen for macromolecular systems is observed. Furthermore, intramolecular rearrangement or the formation of different isomers leads to complex NMR spectra. Nevertheless, characteristic resonances stemming from end-groups can be unambiguously identified. Therefore, distinct characterization of sequence-defined macromolecules can only be accomplished by the combination of complementary analytical tools.

Nonetheless, one goal remains unachieved. Although the photochemical ligation methods exhibit quantitative conversions in small molecule test reactions, the isolated yields of the

respective generations of sequence-defined macromolecules is below 100 %. Furthermore, the photoligation reactions appear to lose efficiency with increasing molecular weight. One explanation for the low yields is the requirement to perform purifications that are carried out after each chain extension step. The photoreactions require stoichiometric equivalency, but an excess of monomers is employed, which ensures full conversion yet needs to be removed by purification. In addition, occurring side reactions, such as light induced [2+2] cycloadditions, and further photoinduced degradation can reduce the overall yield. Moreover, symmetrical core units were employed in order to achieve high molecular weight in as few reaction steps as possible. However, complete conversion of both chain ends needs to be guaranteed to provide precision monodisperse macromolecules. Without any doubt, the efficiency of photoreactions can be increased by employing a commercially available photoflow reactor, providing reaction conditions free of oxygen. The high intensity of the irradiation source in a Vapourtec reactor, for instance, and reactor tubes with a low diameter contribute to a maximum of light penetration according to the Beer-Lambert's law and thus increases the photoreaction efficiency. Therefore, future experiments have to be investigated using photoflow conditions.

The herein investigated photochemical ligation methods act as an efficient technology platform for the synthesis of sequence-defined macromolecules. As demonstrated in the current thesis, photochemistry can be combined with other highly efficient coupling methods, leading to versatile multifunctional macromolecules. Importantly, photochemical ligation methods can be carried out in a wavelength-orthogonal manner by selective excitation of the photolabile groups. Moreover, photoflow reactors can be employed for the formation of sequence-defined macromolecules providing straightforward scalability. In general, non-natural synthetic macromolecules can be designed offering an increased chemical stability compared to natural analogues, such as DNA for example, in which the phosphate esters exhibit hydrolysis sensitivity. However, the most important advantage of artificial macromolecules is achieved by the number of functionalities that can be incorporated in the backbone or side chains leading to a significantly higher functionalization density within few synthetic steps, compared to biomacromolecules. The combination of chemical methodologies further contributes to the rapid development of synthetic procedures towards sequence-defined macromolecules. Consequently, the current photochemical technology platform can be employed

4. Conclusion and Outlook

towards precision macromolecules with potential applications in mimicking complex features of naturally occurring macromolecules or data storage materials. Due to the fact that the sequence-defined macromolecules in the current thesis are symmetric, the application for data storage or mimicking biomolecules is restricted and future work has to address the synthesis of α,ω -functionalized macromolecules in particular. In addition, the development of the automation of the synthesis procedure and the purification process would contribute to a straightforward preparation of long sequences crucial for potential applications.

5

Experimental Section

The experimental section contains more detailed information about synthetic and analytic procedures. Details about the analytic instrumentation and methods are provided in Section 5.1 and a list of materials is given in Section 5.2. Finally, Section 5.3 contains the synthetic procedures together with the corresponding analytic data of the species discussed in the present thesis.

5.1. Instrumental Data and Methods

5.1.1. Nuclear Magnetic Resonance (NMR) Spectroscopy

Proton nuclear magnetic resonance (^1H NMR) spectra were recorded on a Bruker AM 400 (400 MHz) and on a Bruker AM 500 spectrometer (500 MHz). All spectra were measured at room temperature (298 K) in chloroform- d^1 . Chemical shifts δ are expressed in parts per million (ppm) downfield from tetramethylsilane (TMS) as internal standard and are referenced to chloroform- d^1 (^1H : $\delta = 7.26$ ppm, ^{13}C : $\delta = 77.16$ ppm), dimethylsulfoxide- d^6 (^1H : $\delta = 2.50$ ppm, ^{13}C : $\delta = 39.52$ ppm) or acetone- d^6 (^1H : $\delta = 2.05$ ppm, ^{13}C : $\delta = 29.84$ ppm).^[259-260] All coupling constants are absolute values and J values are expressed in Hertz (Hz). The following abbreviations were used to describe peak patterns when appropriate: s (singlet), d (doublet), dd (doublet of doublets), t (triplet), q (quadruplet), dt (doublet of triplet), td (triplet of doublet) and m (multiplet). Carbon nuclear magnetic resonance (^{13}C NMR) spectra were recorded on a Bruker AM 400 (100 MHz) and on a Bruker AM 500 spectrometer (125 MHz).

5.1.2. Electrospray Ionization Mass Spectrometry (ESI-MS)

Mass spectra were recorded on a Q Exactive (Orbitrap) mass spectrometer (Thermo Fisher Scientific, San Jose, CA, USA) equipped with an HESI II probe. The instrument was calibrated in the m/z range 74-1822 using premixed calibration solutions (Thermo Scientific). A

spray voltage between 3.6 and 4.5 kV, a dimensionless sheath gas of 5 to 10, a dimensionless auxiliary gas flow rate of 3 and a dimensionless sweep gas flow rate of 1 were applied. The capillary temperature and the S-lens RF level were set to 320 °C and 62.0, respectively. The samples were dissolved with a concentration of 0.05 mg mL⁻¹ in a mixture of THF and MeOH (3:2) containing 100 μmol of sodium trifluoroacetate or DCM and infused with a flow of between 5 and 10 μL min⁻¹.

5.1.3. Size Exclusion Chromatography – Electrospray Ionization Mass Spectrometry (SEC-ESI-MS)

Spectra were recorded on a Q Exactive (Orbitrap) mass spectrometer (*Thermo Fisher Scientific*, San Jose, CA, USA) equipped with an HESI II probe. The instrument was calibrated in the m/z range 74–1822 employing premixed calibration solutions (*Thermo Scientific*). A constant spray voltage of 4.6 kV, a dimensionless sheath gas of 8, and a dimensionless auxiliary gas flow rate of 2 were applied. The capillary temperature and the S-lens RF level were set to 320 °C and 62.0, respectively. The Q Exactive was coupled to an UltiMate 3000 UHPLC System (*Dionex*, Sunnyvale, CA, USA) consisting of a pump (LPG 3400SD), autosampler (WPS 3000TSL), and a thermostated column department (TCC 3000SD). Separation was performed on two mixed bed size exclusion chromatography columns (*Polymer Laboratories*, Mesopore 250 × 4.6 mm, particle diameter 3 μm) with a precolumn (Mesopore 50 × 4.6 mm) operating at 30 °C. THF at a flow rate of 0.30 mL·min⁻¹ was employed as eluent. The mass spectrometer was coupled to the column in parallel to a RI-detector (Refracto-Max520, ERC, Japan) in a setup described earlier. 0.27 mL min⁻¹ of the eluent were directed through the RI-detector and 30 μL min⁻¹ infused into the electrospray source after postcolumn addition of a 100 μM solution of sodium iodide in methanol at 20 μL min⁻¹ by a micro-flow HPLC syringe pump (Teledyne ISCO, Model 100DM). A 100 μL aliquot of a sample solution in THF with a concentration of 2 mg mL⁻¹ was injected into the HPLC system.

5.1.4. Matrix Assisted Laser Desorption Ionization – Time of Flight Mass-Spectrometry (MALDI–ToF-MS)

The mass-spectra were obtained using Matrix-Assisted Laser Desorption/Ionization with the Time of Flight detection (MALDI–ToF). An Autoflex III instrument (Bruker Daltonics, Bremen, Germany) equipped with a smartbeam Nd:YAG laser (355 nm, 200 Hz) was employed. A 1:1 mixture of 2,5-dihydroxybenzoic acid and 2-cyano-3-(4-hydroxyphenyl)acrylic acid, freshly dissolved in THF, was used as the matrix solution (40 mg mL⁻¹). Analyte samples were obtained as THF solutions without the concentration control. Analyte/matrix mixtures (1/3, v/v) were obtained immediately before the on-target deposition. The mixtures were applied on a stainless steel target, pre-washed with pure THF, in three successive deposition-air drying steps (0.3 μL each time). After the deposition, the entire target was additionally dried under the elevated air flow in the flow bench (15 min). All operations were performed at ambient temperature and extensive exposure to light was avoided at all stages. Depending on the required m/z range, both linear and reflection positive-ion measurement modes were

used. Calibration of the measurement methods prior to measurements was carried out following the manufacturer's procedures. The spectra were acquired and processed with the "Compass 1.3 for flex" software package from Bruker.

5.1.5. Matrix Assisted Laser Desorption Ionization – Time of Flight – Time of Flight (MALDI–ToF–ToF)

An Autoflex III MALDI–ToF mass spectrometer (Bruker Daltonic, Germany) was employed for the tandem MS/MS measurements. The system is equipped with a laser operating at 355 nm with a frequency of 200 Hz. Fragmentation was performed using the so-called LIFT™ mode. Precursor ions were selected and, after collision induced dissociation (CID) using argon as collision gas, formed fragment ions were accelerated in a second ToF unit. For sample preparation solutions of polymer (2 mg mL⁻¹) and DCTB (*trans*-2-[3-(4-*tert*-butylphenyl)-2-methyl-2-propenylidene]malononitrile) matrix (20 mg mL⁻¹) were mixed (1/10, v/v). 1 µL of the resulting solution was deposited on the stainless steel target plate and, after air drying, inserted into the mass spectrometer.

5.1.6. Size Exclusion Chromatography (SEC)

Size exclusion chromatography (SEC) was performed on an Agilent 1200 system, comprising an auto-sampler, a Plgel 5 µm bead-size guard column (50 × 7.5 mm), one Plgel 5 µm Mixed E column (300 × 7.5 mm), three Plgel 5 µm Mixed C columns (300 × 7.5 mm) and a differential refractive index detector as well as an UV detector using THF as eluent at 35 °C with a flow rate of 1 mL min⁻¹. The SEC system was calibrated using linear poly(styrene) standards ranging from 370 to 6 × 10⁶ g mol⁻¹ or poly(methyl methacrylate) standards ranging from 800 to 2.2 × 10⁶ g mol⁻¹. All SEC calculations were carried out relative to poly(styrene) calibration (Mark-Houwink-parameters for PS at 35 °C: K = 13.63 × 10⁻³ mL g⁻¹; a = 0.714). Typically, 100 µL of a 2.0 mg mL⁻¹ sample solution was injected onto the columns.

5.1.7. Spectrophotometry to Determine Source Emission Spectra

The source emission spectrum was measured in the range of 200-800 nm with a UV-VIS spectrometer SR600 (Model 840 320, Opystec Dr. Gröbel) calibrated to the National Metrology Institute of Germany (Physikalisch-Technische Bundesanstalt, PTB) and equipped with a linear silicon photodiode array. Measurements were performed with a resolution of 0.6 nm. The emission spectrum was registered after a dark measurement. The probe was placed at the identical distance employed for irradiating the reaction samples.

5.1.8. Custom Built Photoreactor Employed for Batch Reactions

Light triggered photoenol reactions were performed in a custom built photoreactor as presented in **Figure S1**. The reactor was equipped with three compact low-pressure lamps CLEO Compact PL-L (*Philips*, Amsterdam, Netherlands) emitting at $\lambda_{max} = 365$ nm (± 30 nm, 36 W, see **Figure S2** for emission spectrum). Reaction mixtures (5.0 mmol L⁻¹)

5. Experimental Section

were filled into head space vials (Pyrex, diameter 20 mm) with 5.0-10.0 mL solution containing a stirring bar, sealed with PTFE inner layer and were placed at a distance of 40–50 mm to the light source and exposed for irradiation over 3 hours. The reaction was performed with the vials being placed on a stirrer.

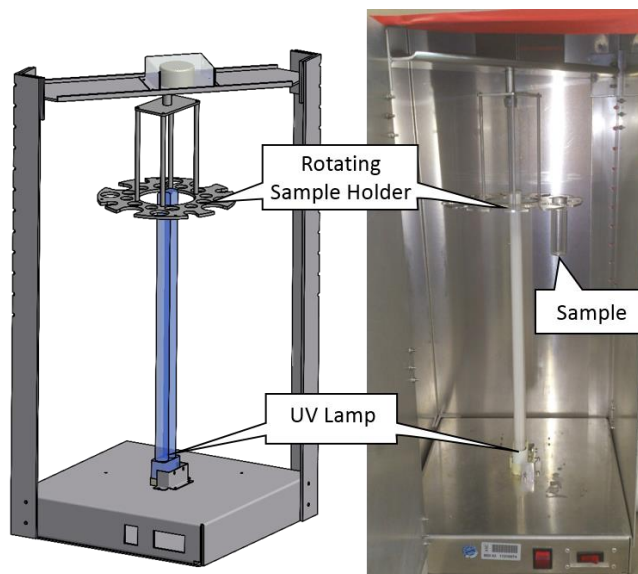


Figure S1. Illustration of the custom-built photoreactor employed for batch conditions in the current study.

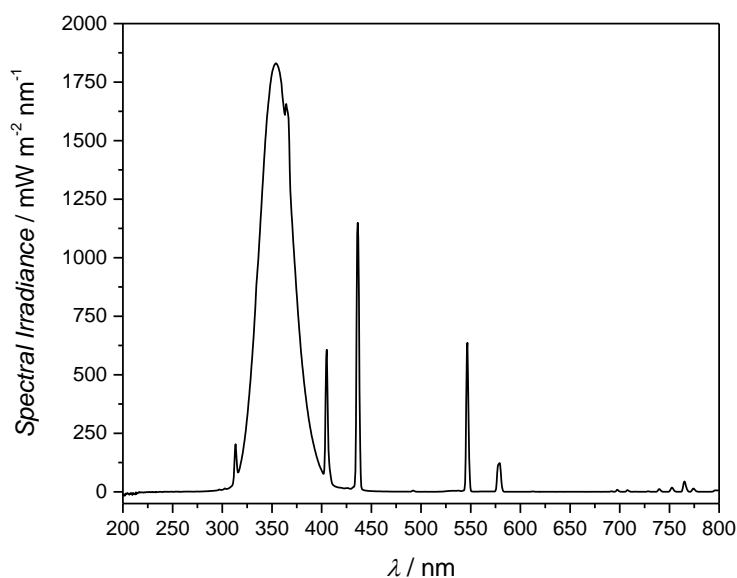


Figure S2. Emission spectrum of the employed PL-L lamps. The spectrum was recorded with the probe placed at a distance of 3.0 cm with an irradiance power of $8.6 \cdot 10^4 \text{ mW m}^2$ and results from averaging 100 spectra employing an integration time of 1109.9 ms.

5.1.9. Custom Built Photoreactor for Irradiation under Flow Conditions

Light triggered NICAL reactions were performed in a custom built photoflow reactor designed by the authors as presented in **Figure S3**. The reactor was equipped with three LED lamps (Avonec, on a star plate, 3 W, 750 mA, 3.5-4.5 V) emitting at $\lambda_{max} = 410-420$ nm (± 15 nm, see **Figure S4** for emission spectrum) on cooling elements (Avonec, Fischer Kühlkörper, SK577-25SA, 50 mm x 25 mm). A PFA tubing (Postnova, PFA HP Plus, length 15 m, OD: 1.55 mm, ID: 0.75 mm) was coiled around a custom build aluminum framework at a distance of 3 cm from the light source (7 cm frame radius) resulting in a reactor coil volume of 7 mL. Reaction mixtures (5.0 mmol L^{-1}) were pumped into the reactor coil using a peristaltic pump (Heidolph, PD 5201 Pump Drive, viton tube with 0.8 mm ID for pumping reaction mixtures) employing flow rates of 0.3 mL min^{-1} corresponding to approx. 23 min residence time.

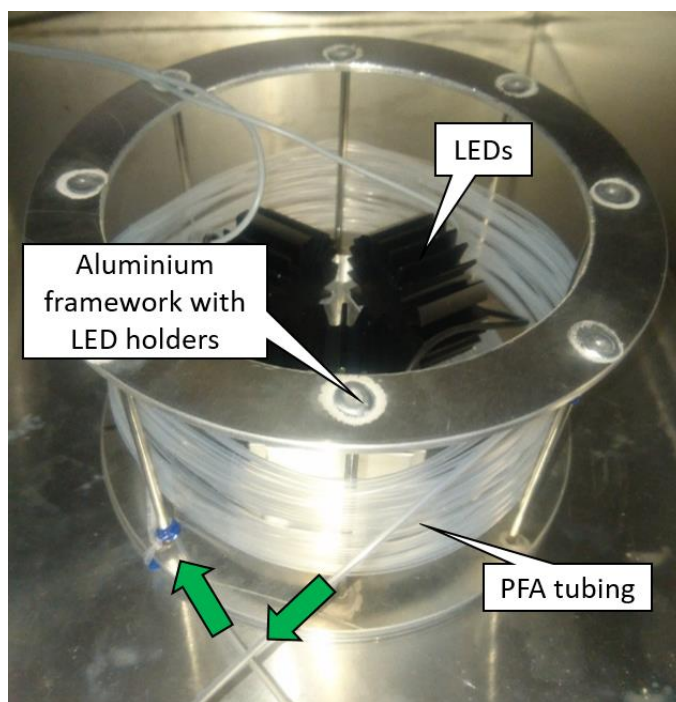


Figure S3. Illustration of the custom-built photoreactor employed for flow conditions in the current study.

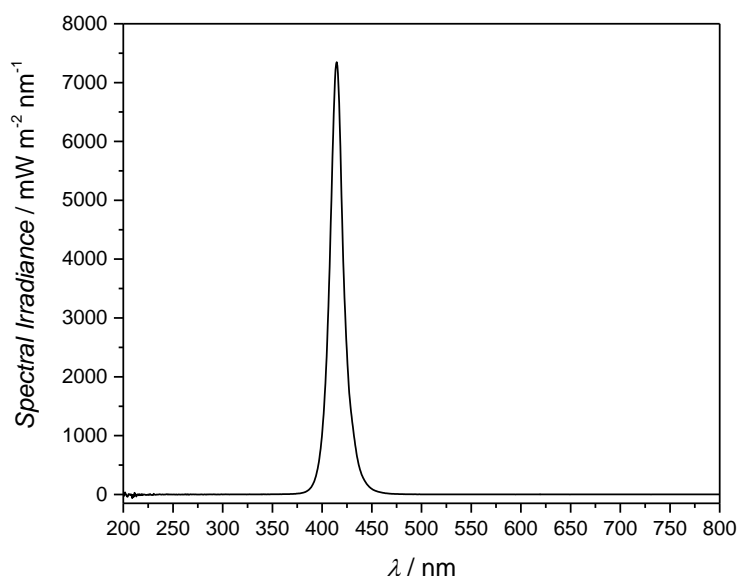


Figure S4. Emission spectrum of the employed LED lamps. The spectrum was recorded with the probe placed at a distance of 2.5 cm with an irradiance power of $1.3 \cdot 10^5$ mW m² and results from averaging 100 spectra employing an integration time of 197.3 ms.

5.1.10. Vapourtec E2 Flow Reactor

Photoreactions under flow conditions were performed using a Vapourtec E-series platform (peristaltic pumps) in combination with the UV-150 module and the VSD006 cooling module. The module consists of a temperature controlled irradiation chamber, a transparent fluorinated ethylene polymer (FEP) reactor coil (1.3 mm inner diameter, 0.15 mm wall thickness, 10 mL reactor volume) and a LED assembly (360 to 390 nm, peak 365 nm, total power output of 16 W and 390 to 420 nm, peak 410 nm, total power output of 12 W). The temperature is controlled employing pre-cooled nitrogen (heat exchange in the cooling module).

5.1.11. Flash Column Chromatography

Flash chromatography was performed on a CombiFlash Rf+ (Teledyne ISCO). Fractions were collected *via* a UV detector (254, 280, 320 or 344 nm and detection of the full UV-Vis spectrum). Puriflash cartridges of 12, 25, 40 and 120 g (interchim, F0012, F0025, F0040, F0120, 30 μ m, SI-HP) or an Uptisphere Strategy silica column (100 Å, 15 μ m, interchim) were employed for the purification in direct mode and puriflash C18-HP cartridges of 12 and 40 g (interchim, F0012, F0040, 15 μ m) for the reverse mode. The analyte was dried on celite and was transferred into an adapted pre-column prior to purification.

Flash chromatography was performed on an Isolera Biotage One (OS 578). The fractions were collected *via* a UV detector (254 nm). A SNAP Ultra (10 g) cartridge was employed for the purification in direct mode, and a SNAP C18 (12 g) cartridge for the reverse mode (both column volume of 15 mL). The analyte was dried on an adapted short pre-column prior to purification.

5.1.12. UV-VIS Spectroscopy (UV-VIS)

The UV-Vis spectra were recorded on a Cary 100 UV-Visible Spectrophotometer (Agilent Technologies, USA) equipped with a tungsten halogen light source (190 to 900 nm, accuracy ± 2 nm) and a R928 PMT detector. Spectra were recorded in DCM at 20 °C and collected between 200 and 800 nm. Samples were baseline corrected with respect to the pure solvent. The sample concentration is given in the description of the respective spectrum.

5.1.13. Fluorescence Spectroscopy

Fluorescence spectra were measured on a Varian Cary Eclipse Fluorescence Spectrometer using quartz cuvettes loaded with 700 μ L of sample solution. All spectra were recorded in DCM at 20 °C. The excitation wavelength and sample concentration is given in the description of the respective spectra.

5.2. Materials

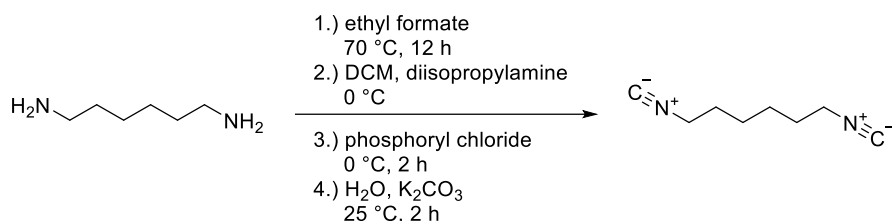
Acetic anhydride (Ac_2O , >99 %, *Merck*), aluminum chloride (AlCl_3 , anhydrous, 99 %, *Roth*), 1-aminopyrene (> 99 %, *TCI*), benzaldehyde (99 %, *Alfa Aesar*), 11-bromoundecan-1-ol (> 97 %, *TCI*), Celite® 545 (*VWR*), copper sulfate pentahydrate ($\text{CuSO}_4 \cdot 5\text{H}_2\text{O}$, 99 %, *Acros Organics*), 18-crown-6 (95 %, *VWR*), diethyl fumarate (98 %, *Alfa Aesar*), diisopropylamine (99.5 %, *Sigma-Aldrich*), 2,3-dimethylanisole (97 %, *Alfa Aesar*), 4-dimethylaminopyridine (DMAP, 99 %, *Acros Organics*), dimethyl sulfoxide (DMSO, 99 %, *Fischer Scientific*), 1,4-dioxane (99 %, *Acros Organics*), di-tert-butyl dicarbonate (Boc_2O , 98 %, *Novabiochem*), ethanol (EtOH , 99.5 %, *Merck*), ethanolamine (99 %, *Acros Organics*), 1-ethyl-3-(3-dimethylaminopropyl)-carbodiimid hydrochloride ($\text{EDC} \cdot \text{HCl}$, 98 %, *Alfa Aesar*), 2,2-(ethylenedioxy)bis(ethylamine) (98 %, *Sigma Aldrich*), ethylene glycol (99 %, *Alfa Aesar*), ethyl formate (98 %, *Acros Organics*), 4-formylbenzoic acid (98 %, *TCI*), furan (99 %, *Acros Organics*), hexamethylenediamine (98 %, *Alfa Aesar*), hydrochloric acid (37 %, *Carl Roth*), 1-hydroxybenzotriazole (HOBt, 97 %, *Sigma-Aldrich*), lauric aldehyde (97 %, *Sigma-Aldrich*), lysine-Fmoc-NBoc (98 %, *Sigma-Aldrich*), magnesium sulfate (MgSO_4 , 99 %, *Carl Roth*), maleic anhydride (99 %, *Acros Organics*), 8-mercaptooctanoic acid (99 %, *Sigma-Aldrich*), 4-methoxybenzaldehyde (99 %, *abcr*), 4-methylbenzenesulfonohydrazide (97 %, *Acros Organics*), methyl-4-(bromomethyl)benzoate (97 %, *ABCR*), monoethyl fumarate (95 %, *Sigma Aldrich*), phosphorous oxychloride (99 %, *Sigma-Aldrich*), piperidine (98 % for synthesis, *Merck*), potassium carbonate (K_2CO_3 , 99 %, *Carl Roth*), potassium peroxodisulfate ($\text{K}_2\text{S}_2\text{O}_8$, 97 %, *Sigma Aldrich*), pyridine (99 %, *Acros Organics*), p-toluenesulfonic acid (pTsOH , 99 %, *Merck*), sebacic acid (99 %, *Sigma-Aldrich*), silica gel (*Merck*), sodium acetate (NaAc , 99 %, *Alfa Aesar*), sodium carbonate (Na_2CO_3 , 99 %, *Carl Roth*), sodium chloride (NaCl , 99.5 %, *Fluka*), sodium hydrogen carbonate (NaHCO_3 , 99 %, *Carl Roth*), sodium hydroxide (NaOH , 99 %, *Carl Roth*), sodium nitrite (NaNO_2 , 97 %, *Acros Organics*), sodium tetrafluoroborate (NaBF_4 , 97 %, *Sigma Aldrich*), sorbic aldehyde (95 %, *Alfa Aesar*), succinic anhydride (99 %, *Acros Organics*), tert-butyl isocyanide (98 %, *Sigma-Aldrich*), tetraethylene glycol (99 %, *Alfa Aesar*), tetrafluoroboric acid (HBF_4 , 50 % solution in water, *Alfa Aesar*), triethylamine (TEA, 99 %, *Fischer Scientific*), trimethyl orthoformate (TMOF, 99 %, *Sigma-Aldrich*) and trifluoroacetic acid (TFA, 99 %, *ABCR*) were employed without further purification.

Acetone, acetonitrile (ACN), chloroform, cyclohexane (CH), dichloromethane (DCM), diethyl ether (Et_2O), ethanol (EtOH), ethyl acetate (EA), methanol (MeOH), tetrahydrofuran (THF) and toluene were purchased as analytical grade (99 %, *VWR*). DCM, *N,N*-dimethylformamide (DMF), dioxane, methanol and THF (>99.9 %, extra dry, *AcroSeal*, *Acros Organics*) were purchased and employed as dry solvents. For photoreactions DCM (>99.9 %, extra dry, *AcroSeal*, *Acros Organics*) was used as solvent as received. For GPC measurements tetrahydrofuran (THF, multisolvent, stabilized with BHT, *Scharlau*) was used. Acetone- d^6 (99.8 %, *EURISO-TOP*), chloroform- d^1 (CDCl_3 , 99.8 %, *EURISO-TOP*) and dimethyl sulfoxide- d^6 ($\text{DMSO-}\text{d}^6$, 99.8 %, *EURISO-TOP*) were utilized as solvent for NMR measurements. Dichloromethane (DCM, ROTISOLV HPLC ultra gradient grade, *Carl Roth*), tetrahydrofuran (THF, *Scharlau*, multisolvent GPC grade, 250ppm BHT) and methanol (MeOH, ROTISOLV HPLC ultra gradient grade, *Carl Roth*) were employed as solvents and sodium trifluoro acetate (NaTFA , 98 %, *Sigma Aldrich*) was employed as doping agent (5 μmol) for ESI-MS measurements as received.

5.3. Synthesis Procedures and Analytical Data

5.3.1. Synthesis of Passerini Linker

Synthesis of 1,6-diisocyanohexane 4^[243]



A solution of hexamethylenediamine (10.0 g, 86.1 mmol, 1.00 eq.) in ethyl formate (163 mL, 150 g, 2.02 mol, 23.5 eq.) was heated under reflux overnight. The reaction mixture was concentrated *in vacuo*. The resulting formamide was suspended in dichloromethane (175 mL) without additional purification and diisopropylamine (72.6 mL, 52.2 g, 516 mmol, 6.00 eq.) was added. The mixture was cooled to 0 °C and phosphoryl chloride (22.0 mL, 36.9 g, 241 mmol, 2.80 eq.) was added dropwise at such a rate that the reaction temperature remained below 0 °C. The mixture was stirred for 2 h, then poured into ice-water (500 mL) containing K₂CO₃ (100 g) maintaining the reaction temperature below 25 °C. The resulting emulsion was stirred at room temperature for 1 h. The organic layer was separated, the aqueous layer extracted three times with dichloromethane (50 mL) and the combined organic layers were dried with K₂CO₃. Purification was performed *via* flash column chromatography (Puriflash, 12 g, 30 mL min⁻¹) with CH and a EA gradient of 1.7 % per column volume (CV). Isocratic phases of a constant EA content were applied at 0 % (5 CV), 17, 33, 50 % (10 CV, respectively) and 100 % (5 CV). The target compound was obtained as a yellow oil (8.39 g, 71.6 %).

¹H NMR (400 MHz, CDCl₃): δ = 3.50–3.33 (m, 2H, CH₂-NC), 1.80–1.62 (m, 2H, CH₂), 1.57–1.42 (m, 2H, CH₂) ppm. ¹³C NMR (100 MHz, CDCl₃): δ = 155.9 (N≡C⁻), 41.4 (CH₂-N⁺), 28.7 (CH₂), 25.4 (CH₂) ppm. MS (ESI) *m/z*: [M + Na]⁺ calcd. for C₈H₁₂N₂, 159.0893; found, 159.0888. Details of the ¹H NMR and ¹³C NMR chemical shift assignments can be found in **Figure 19** (Section 3.1.1).

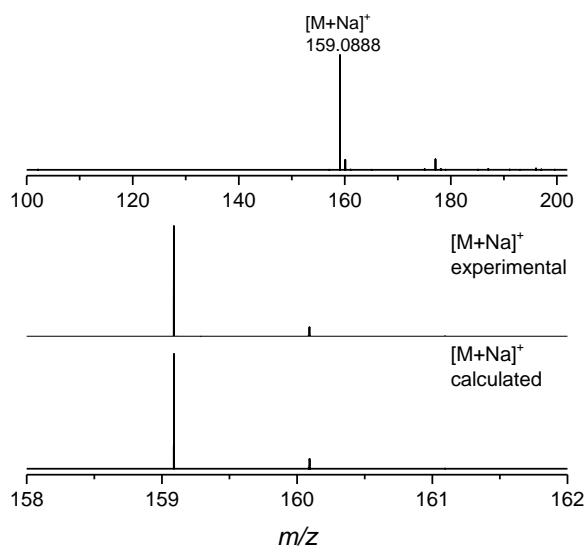
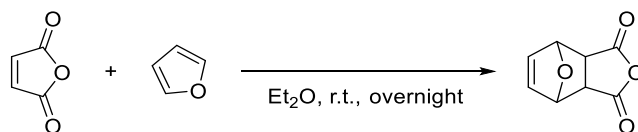


Figure S5. Full ESI-MS spectrum of the diisocyanohexane **4** (top) recorded in THF/MeOH (3:2). ESI-MS spectra of the diisocyanohexane **4** isotopic pattern (bottom). Recorded mass spectra shown are in excellent agreement with the calculated isotope pattern.

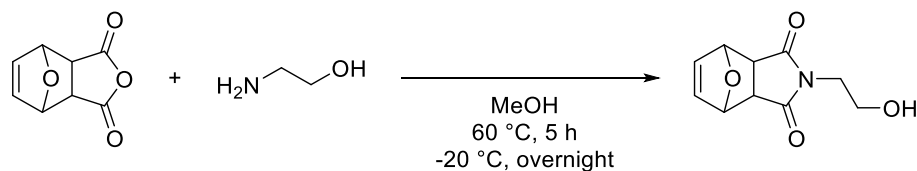
Synthesis of 3a,4,7,7a-tetrahydro-4,7-epoxyisobenzofuran-1,3-dione **2a**



Maleic anhydride (20.00 g, 204 mmol, 1.00 eq.) was dispersed in diethyl ether (100 mL). Subsequently, furan (74.1 mL, 69.4 g, 1020 mmol, 5.00 eq.) was added to the suspension and the reaction mixture was stirred at ambient temperature overnight. The product was filtered and rinsed with ether. Drying of the product yielded 29.6 g of a white solid (87.2 %).

$^1\text{H NMR}$ (400 MHz, CDCl_3): δ = 6.58 (t, J = 1.0 Hz, 2H, CH=CH), 5.46 (t, J = 1.0 Hz, 2H, CH-O), 3.18 (s, 2H, CH-CO) ppm. $^{13}\text{C NMR}$ (100 MHz, CDCl_3): δ = 170.1 (C=O), 136.9 (CH=CH), 82.3 (CH-O), 48.8 (CH) ppm. **MS** (ESI) m/z : $[\text{M} + \text{Na}]^+$ calcd. for $\text{C}_8\text{H}_6\text{O}_4$, 189.0158; found, 189.0156. Details of the $^1\text{H NMR}$ chemical shift assignments can be found in **Figure 18** (Section 3.1.1).

Synthesis of 2-(2-hydroxyethyl)-3a,4,7,7a-tetrahydro-1H-4,7-epoxyisindole-1,3(2H)-dione **2b**

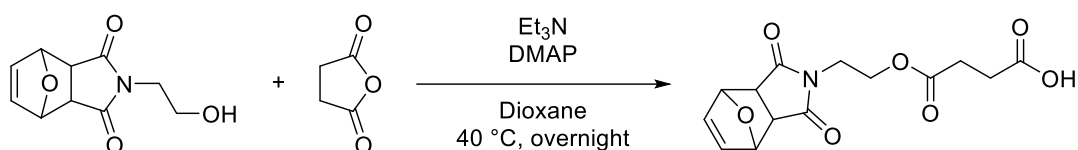


Furan-protected maleic anhydride **2a** (29.6 g, 178 mmol, 1.00 eq.) was dispersed in methanol (120 mL) and ethanolamine (10.9 mL, 11.1 g, 181 mmol, 1.02 eq.) was added to the flask. The solution was heated to 60 °C for 5 h. After heating, the mixture was stored in a cooling bath of isopropanol and liquid nitrogen overnight. After crystallization, the solid was filtered and washed with cold methanol. The filtrate was concentrated and cooled to -20 °C

to recover more product from the solution. The reaction yielded 13.3 g of white crystals (35.9 %).

¹H NMR (400 MHz, CDCl₃): δ = 6.50 (t, *J* = 1.0 Hz, 2H, CH=CH), 5.26 (t, *J* = 1.0 Hz, 2H, CH-O), 3.73 (t, *J* = 5.0 Hz, 2H, CH₂-O), 3.67 (t, *J* = 5.8 Hz, 2H, CH₂-N), 2.87 (s, 2H, CH-CO), 2.54 (bs, 1H, OH) ppm. **¹³C NMR** (100 MHz, CDCl₃): δ = 176.9 (C=O), 136.6 (HC=CH), 81.1 (CH-O), 60.2 (CH₂-O), 47.6 (CH₂), 41.8 (CH₂-N) ppm. **MS** (ESI) *m/z*: [M + Na]⁺ calcd. for C₁₀H₁₁NO₄S, 232.0580; found, 232.0578. Details of the ¹H NMR chemical shift assignments can be found in **Figure 18** (Section 3.1.1).

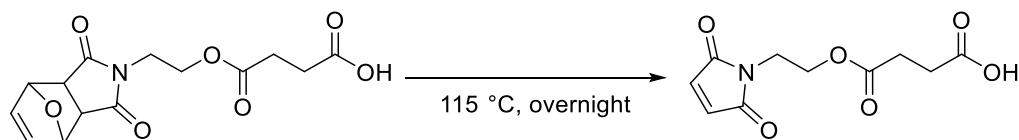
Synthesis of 4-(2-(1,3-dioxo-1,3,3a,4,7,7a-hexahydro-2H-4,7-epoxyisoindol-2-yl)ethoxy)-4-oxobutanoic acid **2c**



Furan-protected maleimide-alcohol **2b** (13.3 g, 63.8 mmol, 1.00 eq.) was dissolved in dioxane (150 mL). TEA (44.2 mL, 319 mmol, 5.00 eq.) and DMAP (11.7 g, 99.1 mmol, 1.50 eq.) were added. Subsequently, succinic anhydride (25.5 g, 255 mmol, 4.00 eq.) was added and the reaction mixture was allowed to stir overnight at 40 °C. The solution was poured into ice-cold 1 M HCl and extracted with DCM. The organic phase was washed with 1 M HCl and dried over Na₂SO₄. The solvent was removed under reduced pressure. Recrystallization from ethanol yielded 10.5 g of a white solid (53.2 %).

¹H NMR (400 MHz, CDCl₃): δ = 6.51 (t, *J* = 1.0 Hz, 2H, CH=CH), 5.27 (t, *J* = 1.0 Hz, 2H, CH-O), 4.26 (t, *J* = 5.8 Hz, 2H, CH₂-O), 3.75 (t, *J* = 5.8 Hz, 2H, CH₂-N), 2.87 (s, 2H, CH-CO), 2.66–2.62 (m, 2H, CH₂-COO), 2.61–2.56 (m, 2H, CH₂-COO) ppm. **¹³C NMR** (100 MHz, CDCl₃): δ = 177.1 (COOH), 176.3 (N-C=O), 172.0 (COO), 136.7 (CH=CH), 81.1 (CH-O), 61.1 (CH₂-O), 47.6 (CH), 38.0 (CH₂-N), 28.9 (CH₂-COO), 28.8 (CH₂-COO) ppm. **MS** (ESI) *m/z*: [M + Na]⁺ calcd. for C₁₄H₁₅NO₇, 332.0741; found, 332.0735. Details of the ¹H NMR chemical shift assignments can be found in **Figure 18** (Section 3.1.1).

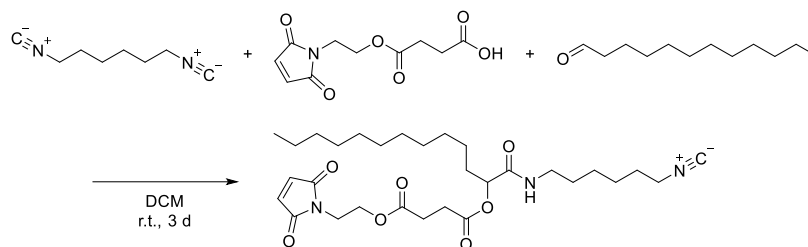
Synthesis of 4-(2-(2,5-dioxo-2,5-dihydro-1H-pyrrol-1-yl)ethoxy)-4-oxobutanoic acid **2**



Furan-protected maleimide-acid **2c** (641 mg, 2.07 mmol, 1.00 eq.) was heated to 115 °C for 24 h *in vacuo* to provide the bare maleimide-acid **2** quantitatively.

¹H NMR (400 MHz, CDCl₃): δ = 6.72 (s, 2H), 4.25 (dd, *J* = 5.7, 4.7 Hz, 2H), 3.82–3.75 (m, 2H), 2.64 (ddd, *J* = 7.0, 5.6, 1.5 Hz, 2H), 2.57 (ddd, *J* = 7.7, 5.7, 1.6 Hz, 2H) ppm. Details of the ¹H NMR chemical shift assignments can be found in **Figure 18** (Section 3.1.1).

Synthesis of the Passerini linker **1a**



In a 50 mL round-bottom flask 1,6-diisocyanohexane **4** (1228 mg, 9.02 mmol, 4.35 eq.) was stirred in 5 mL DCM, subsequently lauric aldehyde **3a** (1528 mg, 8.29 mmol, 4.00 eq.) was added. Finely powdered maleimide-acid **2** (500 mg, 2.07 mmol, 1.00 eq.) was added in small portions to the stirring isocyanide/aldehyde mixture. The resulting reaction mixture was stirred at ambient temperature for 3 d. The crude mixture was concentrated under reduced pressure. Purification was performed *via* flash column chromatography (Puriflash, 12 g, 30 mL min⁻¹) with CH and a EA gradient of 1.7 % per column volume (CV). Isocratic phases of a constant EA content were applied at 17, 33, 50, 67 and 100 % (10 CV, respectively). The target compound was obtained as a yellow oil (659 mg, 56.6 %).

¹H NMR (400 MHz, CDCl₃): δ = 6.71 (s, 2H, CH=CH), 6.51 (t, J = 5.9 Hz, 1H, NH), 5.14 (dd, J = 7.7, 4.2 Hz, 1H, CH=O), 4.30–4.19 (m, 2H, CH₂-O), 3.85–3.68 (m, 2H, CH₂-N), 3.42–3.32 (m, 2H, CH₂-N⁺), 3.32–3.14 (m, 2H, CH₂-NH), 2.76–2.51 (m, 4H, CH₂-COO), 1.92–1.73 (m, 2H, CH₂), 1.73–1.61 (m, 2H, CH₂), 1.61–1.49 (m, 2H, CH₂), 1.49–1.39 (m, 2H, CH₂), 1.39–1.16 (m, 20H, CH₂), 0.90–0.80 (m, 3H, CH₃) ppm. **¹³C NMR** (100 MHz, CDCl₃): δ = 172.9 (COO), 171.3 (COO), 170.5 (N-C=O), 169.9 (HN-C=O), 155.9 (t, N \equiv C⁻), 134.4 (CH=CH), 74.6 (O-CH-CO), 62.1 (CH₂-O), 41.5 (t, CH₂-N⁺), 39.1 (CH₂-NH), 36.8 (CH₂), 31.9 (CH₂), 29.7 (CH₂), 29.6 (CH₂), 29.5 (CH₂), 29.4 (CH₂), 29.3 (CH₂), 29.3 (CH₂), 29.2 (CH₂), 29.1 (CH₂), 29.0 (CH₂), 26.1 (CH₂), 26.0 (CH₂), 25.0 (CH₂), 22.8 (CH₂), 14.2 (CH₃) ppm. **MS** (ESI) m/z : [M + Na]⁺ calcd. for C₃₀H₄₇N₃O₇, 584.3306; found, 584.3309. Details of the ¹H NMR chemical shift assignments can be found in **Figure 20** (Section 3.1.1).

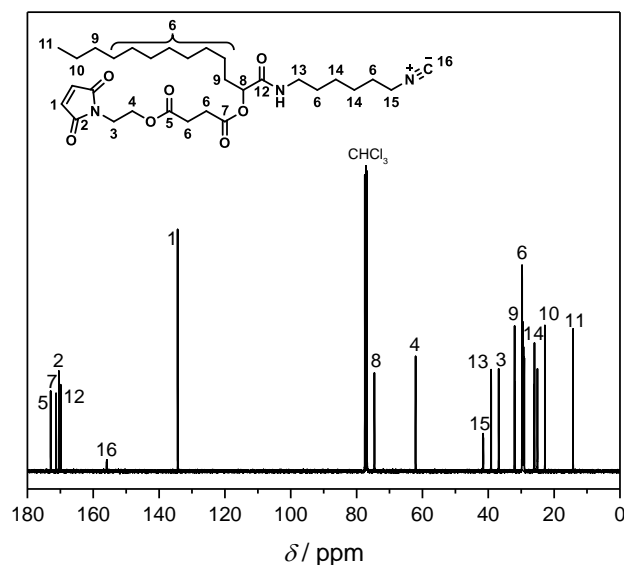


Figure S6. ¹³C NMR spectrum of the Passerini linker **1a** recorded in CDCl₃ at 101 MHz. For the resonance assignments refer to the depicted structure.

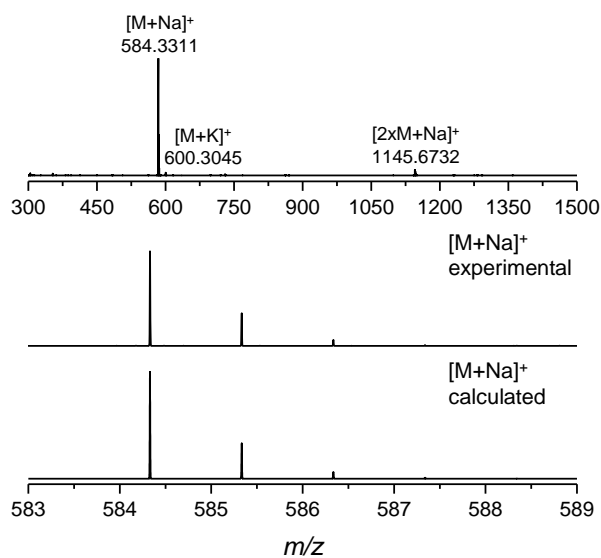


Figure S7. Full ESI-MS spectrum of the Passerini linker **1a** (top) recorded in THF/MeOH (3:2). ESI-MS spectra of the Passerini linker **1a** isotopic pattern (bottom). Recorded mass spectra shown are in excellent agreement with the calculated isotope pattern.

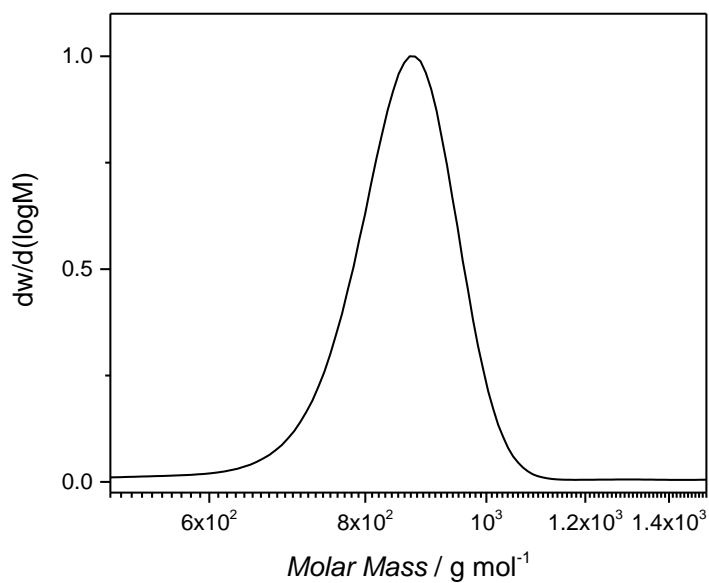
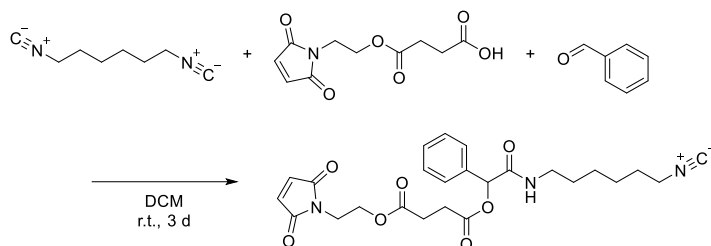


Figure S8. SEC trace of the Passerini linker **1a** recorded in THF at 35 °C. ($D = 1.01$, $M_n = 870 \text{ g mol}^{-1}$).

Synthesis of 2-(2,5-dioxo-2,5-dihydro-1H-pyrrol-1-yl) ethyl (2-((6-isocyanoethyl) amino)-2-oxo-1-phenylethyl) succinate **1b**



In a 50 mL round-bottom flask 1,6-diisocyanohexane **4** (1179 mg, 8.66 mmol, 4.35 eq.) was stirred in 5 mL DCM, subsequently benzaldehyde **3b** (845 mg, 7.96 mmol, 4.00 eq.) was added. Finely powdered maleimide-acid **2** (480 mg, 1.99 mmol, 1.00 eq.) was added in small portions to the stirring isocyanide/aldehyde mixture. The resulting reaction mixture was stirred at ambient temperature for 3 d. The crude mixture was concentrated under reduced pressure. Purification was performed *via* flash column chromatography (Puriflash, 12 g, 30 mL min⁻¹) with CH and a EA gradient of 1.7 % per column volume. Isocratic phases of a constant EA content were applied at 17, 33, 50, 67 and 100 % (10 CV). The target compound was obtained as 686 mg of a yellow oil (61.4 %).

¹H NMR (400 MHz, CDCl₃): δ = 7.48 – 7.31 (m, 5H, ArH), 6.71 (s, 2H, CH=CH), 6.60 (bs, 1H, NH), 6.07 (s, 1H, Ar-CH), 4.25 (t, ³J = 5.3 Hz, 2H, CH₂-O), 3.79 (tt, ³J = 5.1, 3.1 Hz, 2H, CH₂-N), 3.35 (tt, ³J = 6.7, 1.9 Hz, 2H, CH₂-N⁺), 3.27 (dt, ³J = 13.2, 6.7 Hz, 2H, CH₂-NH), 2.84 – 2.57 (m, 4H, CH₂-COO), 1.72 – 1.61 (m, 2H, CH₂), 1.55 (p, ³J = 7.1 Hz, 2H, CH₂), 1.44 (td, ³J = 9.5, 8.9, 4.6 Hz, 2H, CH₂), 1.39 – 1.20 (m, 2H, CH₂) ppm. **¹³C NMR** (100 MHz, CDCl₃): δ = 172.78 (COO), 170.73 (COO), 170.52 (N-C=O), 168.36 (HN-C=O), 155.85 (t, N≡C⁻), 135.68 (C_{Ar}), 134.39 (CH=CH), 129.06 (C_{Ar}H), 128.83 (C_{Ar}H), 127.51 (C_{Ar}H), 76.03 (O-CH-CO), 62.14 (CH₂-O), 41.55 (t, CH₂-N⁺), 39.30 (CH₂-NH), 36.86 (CH₂-N), 29.33 (CH₂), 29.17 (CH₂), 29.04 (CH₂), 26.04 (CH₂), 25.92 (CH₂) ppm. **MS** (ESI) *m/z*: [M + Na]⁺ calcd. for C₂₅H₂₉N₃O₇, 506.1898; found, 506.1904. Details of the ¹H NMR chemical shift assignments can be found in **Figure 20** (Section 3.1.1).

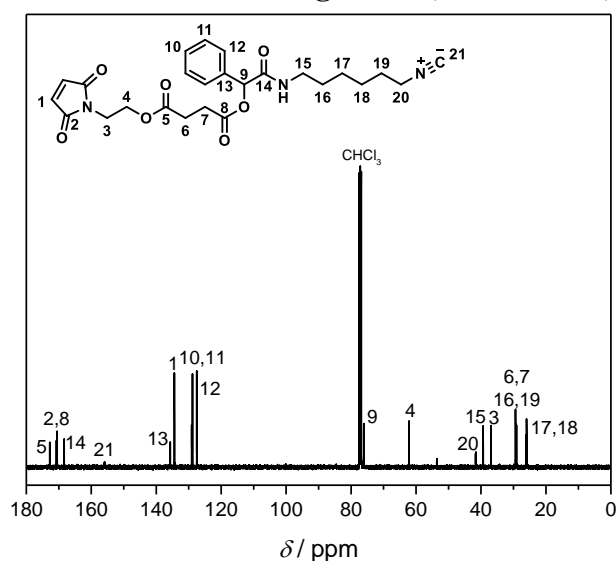


Figure S9. ¹³C NMR spectrum of the Passerini linker **1b** recorded in CDCl₃ at 101 MHz. For the resonance assignments refer to the depicted structure.

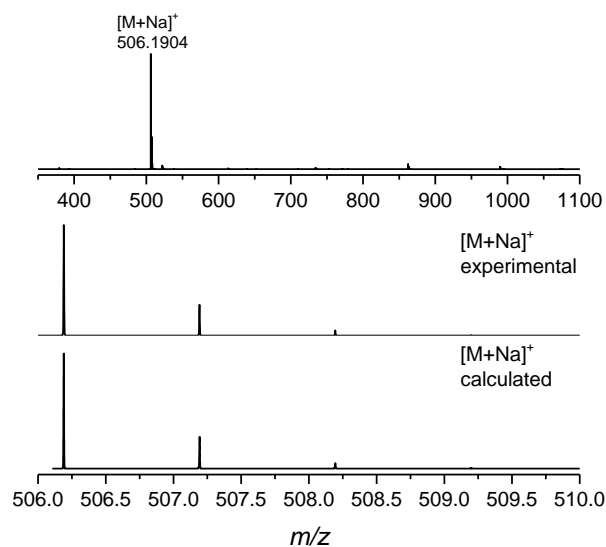


Figure S10. Full ESI-MS spectrum of the Passerini linker **1b** (top) recorded in THF/MeOH (3:2). ESI-MS spectra of the Passerini linker **1b** isotopic pattern (bottom). Recorded mass spectra shown are in excellent agreement with the calculated isotope pattern.

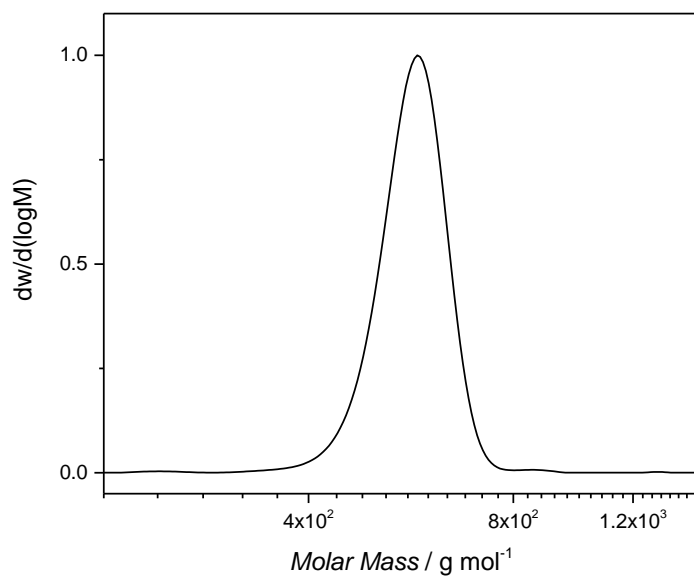
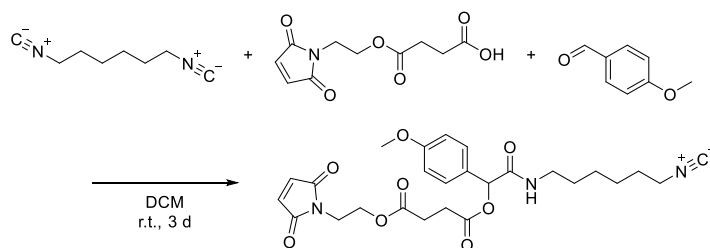


Figure S11. SEC trace of the Passerini linker **1b** recorded in THF at 35 °C. ($D = 1.01$, $M_n = 580 \text{ g mol}^{-1}$).

Synthesis of 2-(2,5-dioxo-2,5-dihydro-1H-pyrrol-1-yl) ethyl (2-((6-isocyanoethyl) amino)-2-oxo-1-phenylethyl) succinate **1c**



5. Experimental Section

In a 50 mL round-bottom flask 1,6-diisocyanohexane **4** (1179 mg, 8.66 mmol, 4.35 eq.) was stirred in 5 mL DCM, subsequently 4-methoxybenzaldehyde **3c** (1084 mg, 7.96 mmol, 4.00 eq.) was added. Finely powdered maleimide-acid **2** (480 mg, 1.99 mmol, 1.00 eq.) was added in small portions to the stirring isocyanide/aldehyde mixture. The resulting reaction mixture was stirred at ambient temperature for 3 d. The crude mixture was concentrated under reduced pressure. Purification was performed *via* flash column chromatography (Puriflash, 12 g, 30 mL min⁻¹) with CH and a EA gradient of 1.7 % per column volume. Isocratic phases of a constant EA content were applied at 17, 33, 50, 67 and 100 % (10 CV). The target compound was obtained as 713 mg of a yellow oil (63.8 %).

¹H NMR (400 MHz, CDCl₃): δ = 7.31 (d, *J* = 8.8 Hz, 2H, ArH), 6.86 (d, *J* = 8.8 Hz, 2H, ArH), 6.69 (s, 2H, CH=CH), 6.63 (t, *J* = 5.9 Hz, 1H, NH), 6.00 (s, 1H, Ar-CH), 4.23 (t, *J* = 5.3 Hz, 2H, CH₂-O), 3.84 – 3.71 (m, 5H, CH₂-N, CH₃-O), 3.37 – 3.32 (m, 2H, CH₂-N⁺), 3.31 – 3.18 (m, 2H, CH₂-NH), 2.77 – 2.56 (m, 4H, CH₂-COO), 1.73 – 1.58 (m, 2H, CH₂), 1.58 – 1.49 (m, 2H, CH₂), 1.49 – 1.37 (m, 2H, CH₂), 1.37 – 1.16 (m, 2H, CH₂) ppm. **¹³C NMR** (100 MHz, CDCl₃): δ = 172.43 (COO), 170.67 (COO), 170.31 (N-C=O), 168.44 (HN-C=O), 159.90 (C_{Ar}-O), 155.60 (t, N≡C⁻), 134.15 (CH=CH), 128.82 (C_{Ar}H), 127.65 (C_{Ar}), 113.94 (C_{Ar}H), 75.45 (O-CH-CO), 61.80 (CH₂-O), 55.19 (CH₃-O), 41.28 (t, CH₂-N⁺), 39.00 (CH₂-NH), 36.55 (CH₂), 29.03 (CH₂), 28.87 (CH₂), 28.77 (CH₂), 25.76 (CH₂), 25.65 (CH₂) ppm. **MS** (ESI) *m/z*: [M + Na]⁺ calcd. for C₂₆H₃₁N₃O₈, 536.2003; found, 536.2014. Details of the ¹H NMR chemical shift assignments can be found in **Figure 20** (Section 3.1.1).

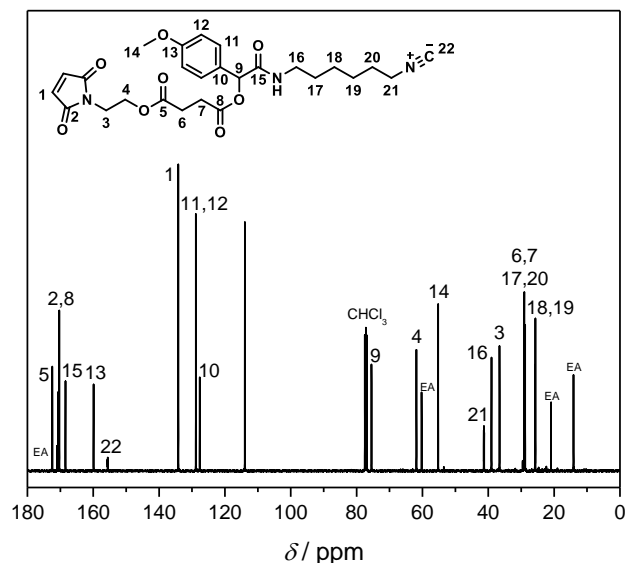


Figure S12. ¹³C NMR spectrum of the Passerini linker **1c** recorded in CDCl₃ at 101 MHz. For the resonance assignments refer to the depicted structure.

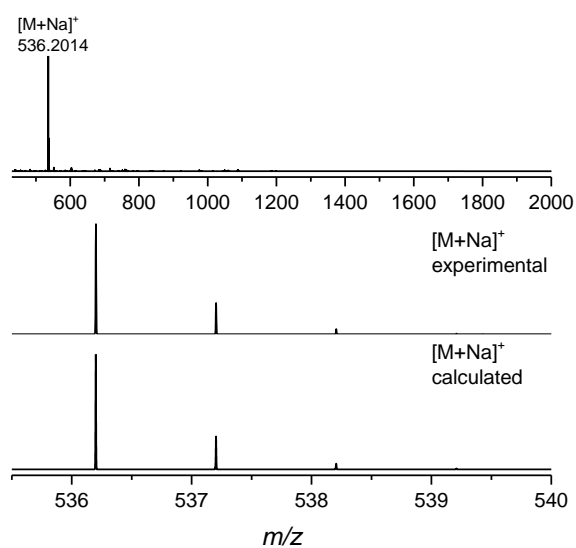


Figure S13. Full ESI-MS spectrum of the Passerini linker **1c** (top) recorded in THF/MeOH (3:2). ESI-MS spectra of the Passerini linker **1c** isotopic pattern (bottom). Recorded mass spectra shown are in excellent agreement with the calculated isotope pattern.

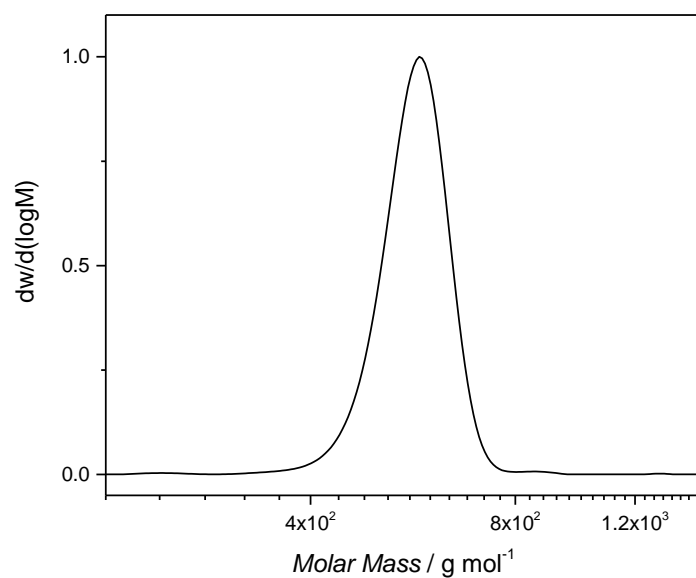
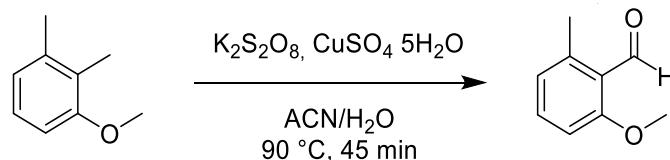


Figure S14. SEC trace of the Passerini linker **1c** recorded in THF at 35 °C. ($D = 1.01$, $M_n = 590\ g\ mol^{-1}$).

5.3.2. Synthesis of Photosensitive Compounds

Synthesis of 2-methoxy-6-methylbenzaldehyde **12a**^[256-257]



The synthesis was performed according to a literature procedure being slightly adapted. 2,3-Dimethyl anisole (7.03 g, 51.6 mmol, 1.00 eq.), copper sulfate pentahydrate (13.11 g, 52.5 mmol, 1.02 eq.) and potassium peroxodisulfate (41.85 g, 154.8 mmol, 3.00 eq.) were added to a mixture of acetonitrile/water (1:1, 500 mL). The vigorously stirred suspension was placed in a thermostatted oil bath kept at 90 °C until TLC showed no starting material remaining. After approx. 45 min the reaction mixture was cooled to ambient temperature and the undissolved copper salt was removed by filtration. DCM (150 mL) was added and the phases were separated. The aqueous phase was extracted two times with dichloromethane (100 mL) and the combined organic layers were dried over magnesium sulfate. The brown crude product was employed for the subsequent synthetic step without any further purification.

¹H NMR (400 MHz, CDCl₃): δ = 10.64 (s, 1H, CHO), 7.38 (t, J = 7.97 Hz, 1H, Ar H), 6.81 (t, J = 7.97 Hz, 2H, Ar), 3.89 (s, 3H, OCH₃), 2.57 (s, 3H, CH₃) ppm. **¹³C NMR** (101 MHz, CDCl₃): δ = 192.42, 163.29, 142.16, 134.55, 124.22, 123.48, 109.17, 77.16, 55.90, 21.60 ppm. **MS** (ESI) m/z : [M + H]⁺ calcd. for C₉H₁₀O₂, 151.0754; found 151.0754.

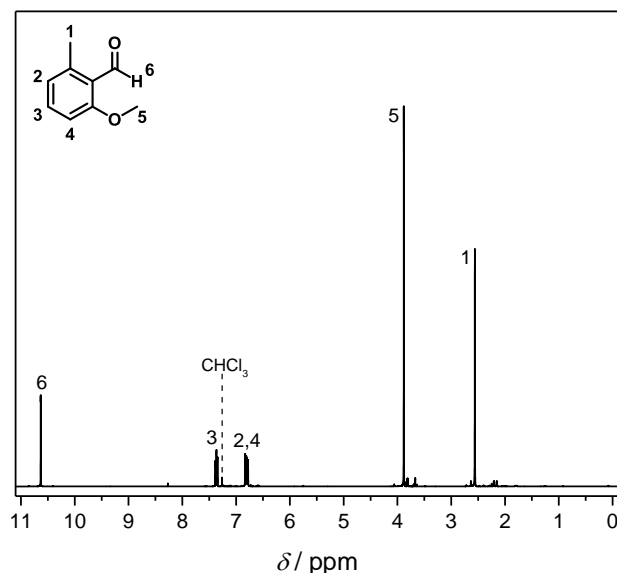


Figure S15. ¹H NMR spectrum of 2-methoxy-6-methylbenzaldehyde **12a** recorded in CDCl₃ at 400 MHz. For the resonance assignments refer to the depicted structure.

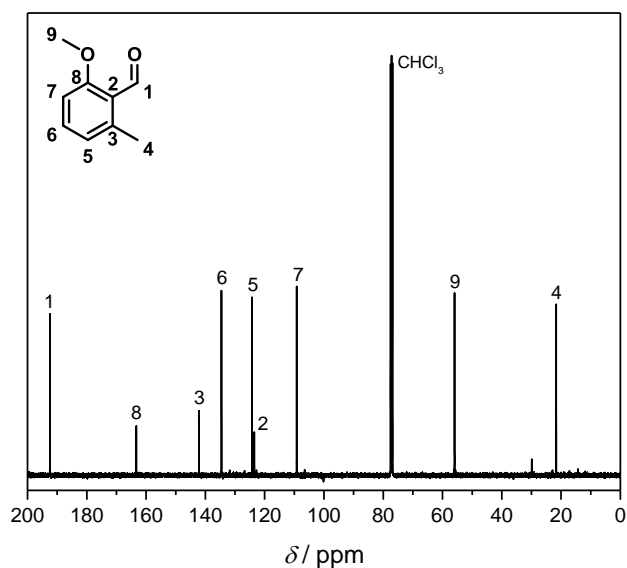


Figure S16. ^{13}C NMR spectrum of 2-methoxy-6-methylbenzaldehyde **12a** recorded in CDCl_3 at 101 MHz. For the resonance assignments refer to the depicted structure.

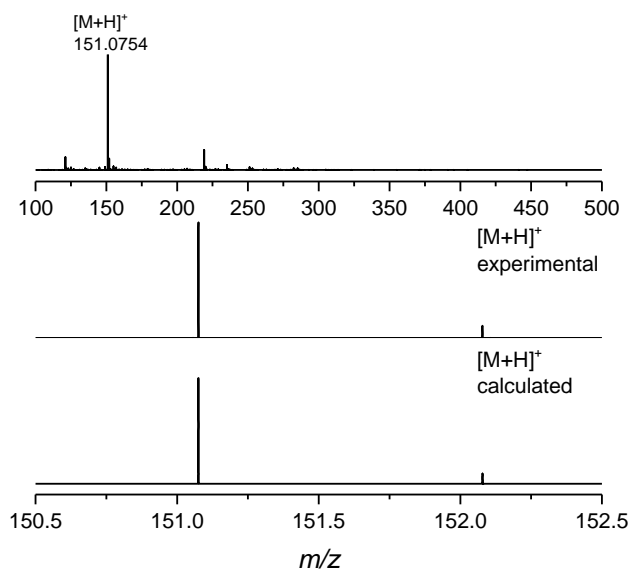
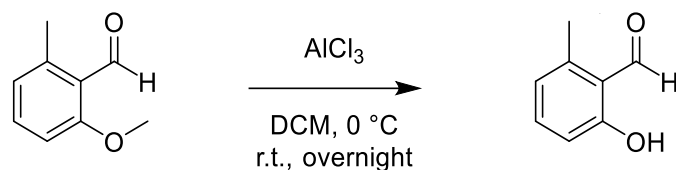


Figure S17. Mass spectrum of 2-methoxy-6-methylbenzaldehyde **12a** recorded in DCM. ESI-MS spectra of **12a** isotopic pattern (bottom). Recorded mass spectra shown are in excellent agreement with the calculated isotope pattern.

Synthesis of 2-hydroxy-6-methylbenzaldehyde 12b^[246]

2-Methoxy-6-methylbenzaldehyde **12a** (4.10 g, 27.3 mmol, 1.00 eq.) was dissolved in dry DCM (60 mL) and cooled to $0\text{ }^\circ\text{C}$. AlCl_3 (10.9 g, 81.9 mmol, 3.00 eq.) was added and the mixture was stirred at ambient temperature overnight. For quenching, the reaction mixture was poured dropwise into an ice-bath (80 mL) and the phases were separated. The aqueous layer was extracted three times with DCM (80 mL). The combined organic layers were dried over magnesium sulfate and the solvent was evaporated. The final purification was carried out by column chromatography (silica gel, solid deposit from Celite, CH/EA 2:1) yielding in 3.9 g (82 %) of a yellow solid.

$^1\text{H NMR}$ (400 MHz, CDCl_3): δ = 11.91 (s, 1H, OH), 10.32 (s, 1H, CHO), 7.37 (dd, J = 8.4, 7.4 Hz, 1H, Ar H), 6.81 (d, J = 8.2 Hz, 1H, Ar H), 6.71 (d, J = 7.5 Hz, 1H, Ar H), 2.60 (s, 3H, CH_3) ppm. **$^{13}\text{C NMR}$** (101 MHz, CDCl_3): δ = 195.33, 163.15, 142.15, 137.38, 118.52, 116.04, 77.16, 18.03 ppm. **MS** (ESI) m/z : $[\text{M} + \text{H}]^+$ calcd. for $\text{C}_8\text{H}_8\text{O}_2$, 137.0597; found 137.0597.

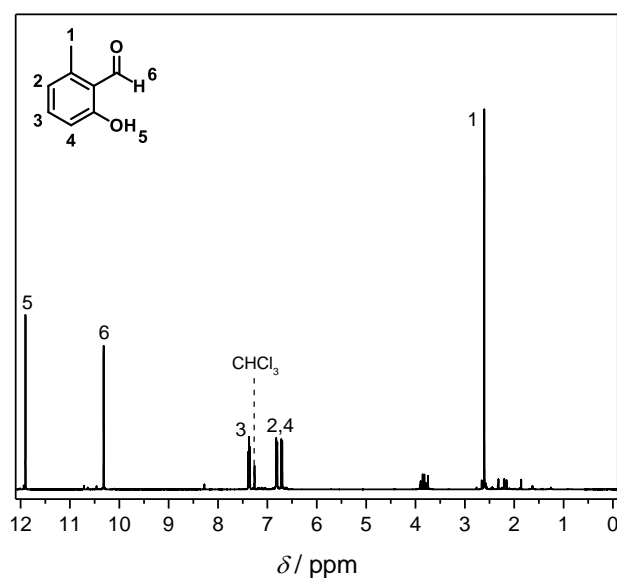


Figure S18. $^1\text{H NMR}$ spectrum of 2-hydroxy-6-methylbenzaldehyde **12b** recorded in CDCl_3 at 400 MHz. For the resonance assignments refer to the depicted structure.

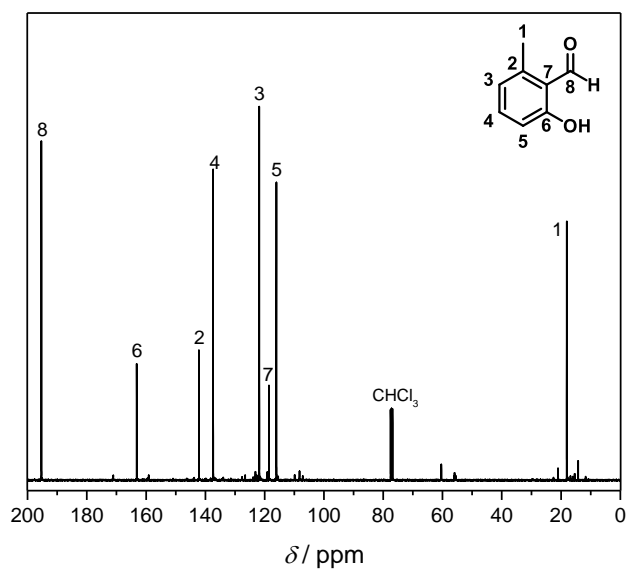


Figure S19. ^{13}C NMR spectrum of 2-hydroxy-6-methylbenzaldehyde **12b** recorded in CDCl_3 at 101 MHz. For the resonance assignments refer to the depicted structure.

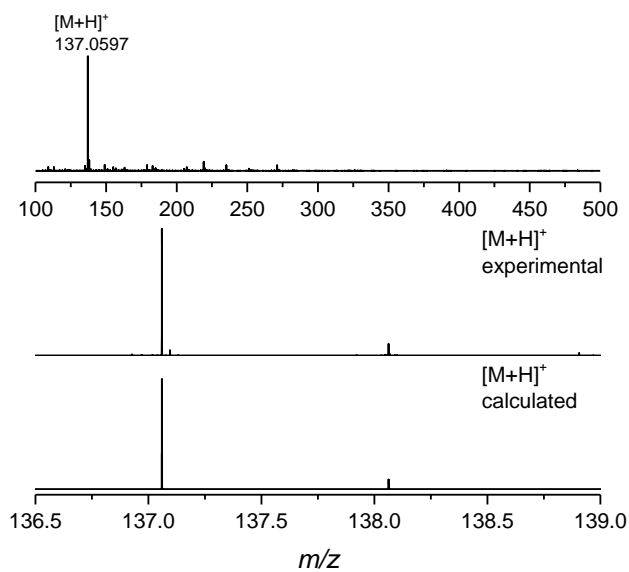
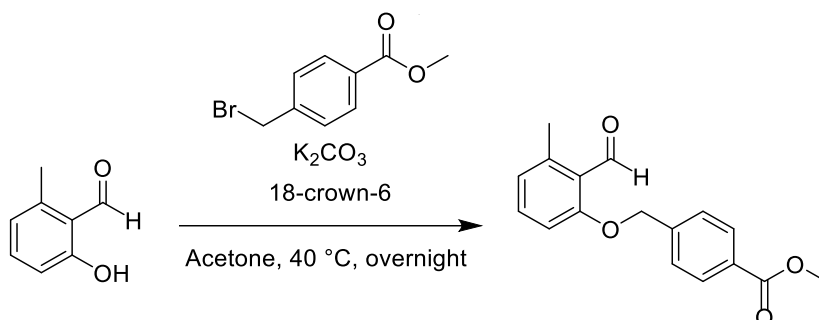


Figure S20. Mass spectrum of 2-hydroxy-6-methylbenzaldehyde **12b** recorded in DCM. ESI-MS spectra of **12b** isotopic pattern (bottom). Recorded mass spectra shown are in excellent agreement with the calculated isotope pattern.

Synthesis of methyl 4-((2-formyl-3-methylphenoxy)methyl)benzoate **12c**^[246]

In a round bottom flask 2-hydroxy-6-methylbenzaldehyde **12b** (2.00 g, 14.7 mmol, 1.00 eq.) and methyl 4-(bromomethyl) benzoate (3.70 g, 16.2 mmol, 1.10 eq.) were dissolved in acetone (100 mL). K_2CO_3 (3.05 g, 22.0 mmol, 1.50 eq.) and 18-crown-6 (50.0 mg, 0.20 mmol, 0.015 eq.) were added to the solution. The resulting dark brown suspension was stirred overnight at 40 °C. The undissolved K_2CO_3 was filtered off and the solvent was evaporated. The residue was dissolved in DCM/ H_2O (200 mL, 1:1), the phases were separated and the aqueous layer was extracted with DCM (2 x 40 mL). The combined organic layers were dried over $MgSO_4$ and the solvent was removed under reduced pressure. The product was purified by recrystallization from CH/EA (7:1) yielding 2.83 g (68 %) of a white solid.

1H NMR (400 MHz, $CDCl_3$): δ = 10.76 (s, 1H, CHO), 8.07 (d, J = 8.2 Hz, 2H, ArH), 7.50 (d, J = 8.2 Hz, 2H, ArH), 7.35 (t, J = 8.2 Hz, 1H, ArH), 6.85 (dd, J = 8.1, 2.9 Hz, 2H, ArH), 5.23 (s, 2 H, CH_2), 3.93 (s, 3H, CH_3), 2.59 (s, 3H, C_3) ppm. **^{13}C NMR** (101 MHz, $CDCl_3$): δ = 192.11, 166.81, 162.02, 142.41, 141.46, 134.53, 130.12, 130.09, 126.94, 124.81, 123.78, 110.43, 77.16, 70.04, 52.31, 21.60 ppm. **MS** (ESI) m/z : $[M + Na]^+$ calcd. for $C_{17}H_{16}O_4$, 307.0941; found 307.0942.

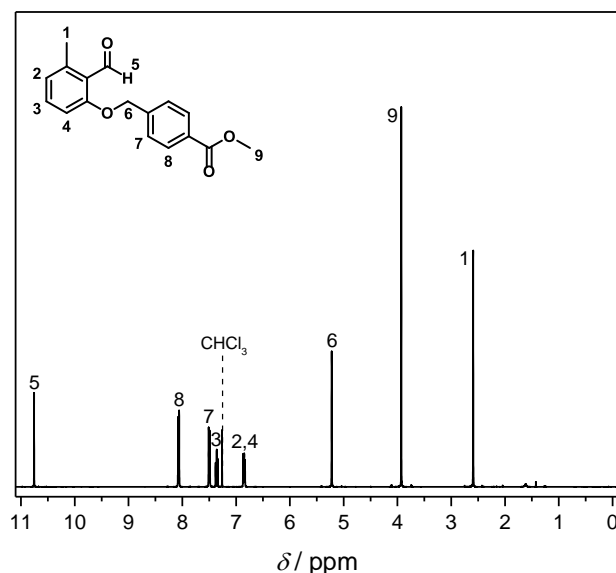


Figure S21. 1H NMR spectrum of methyl 4-((2-formyl-3-methylphenoxy)methyl)benzoate **12c** recorded in $CDCl_3$ at 400 MHz. For the resonance assignments refer to the depicted structure.

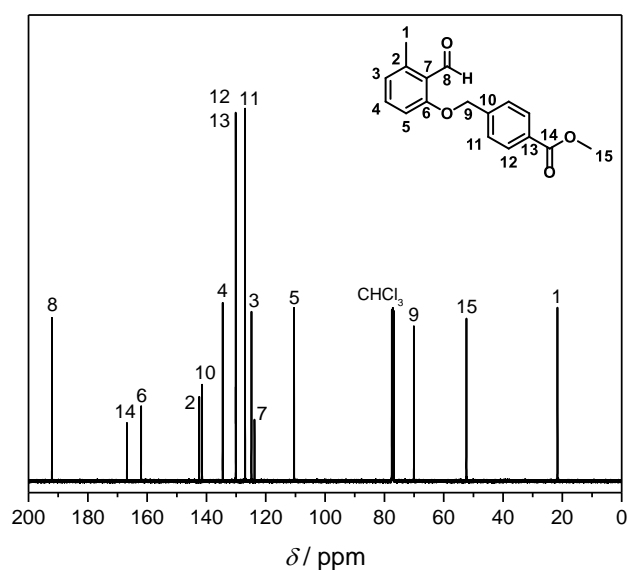


Figure S22. ^{13}C NMR spectrum of methyl 4-((2-formyl-3-methylphenoxy)methyl)benzoate **12c** recorded in CDCl_3 at 101 MHz. For the resonance assignments refer to the depicted structure.

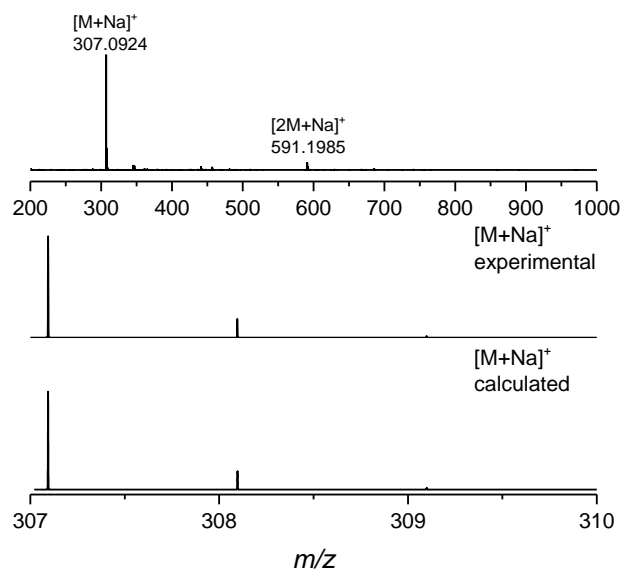


Figure S23. Mass spectrum of methyl 4-((2-formyl-3-methylphenoxy)methyl)benzoate **12c** recorded in THF/MeOH (3:2). ESI-MS spectra of **12c** isotopic pattern (bottom). Recorded mass spectra shown are in excellent agreement with the calculated isotope pattern.

5. Experimental Section

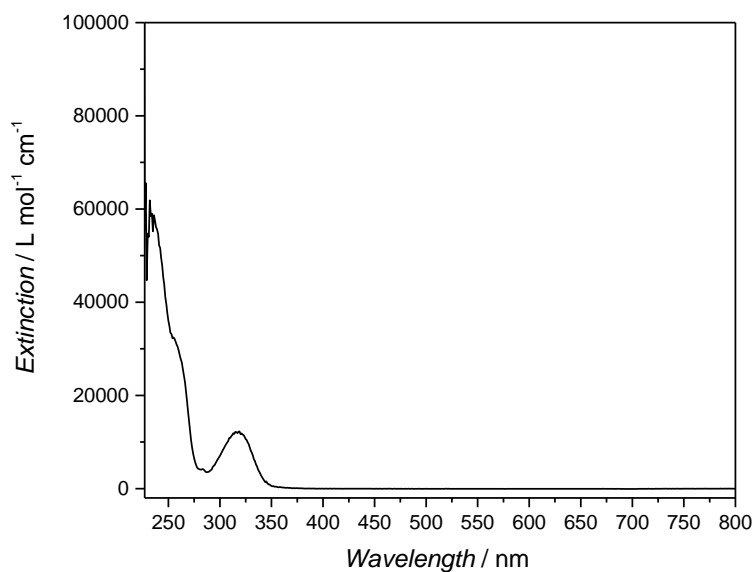


Figure S24. UV-Vis spectrum of methyl 4-((2-formyl-3-methylphenoxy)methyl)benzoate **12c** recorded in DCM ($5.02 \cdot 10^{-5}$ mol L⁻¹).

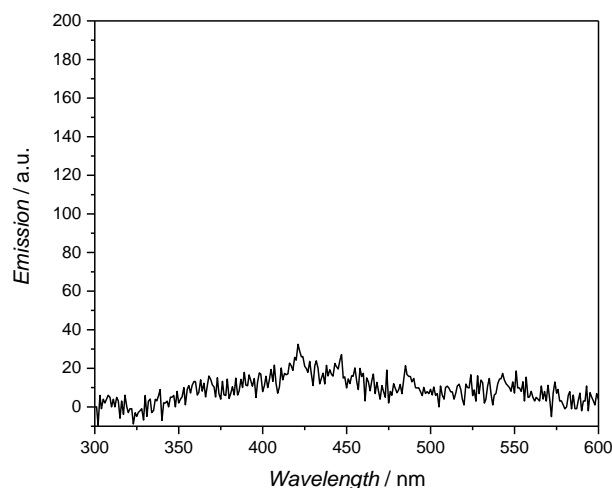
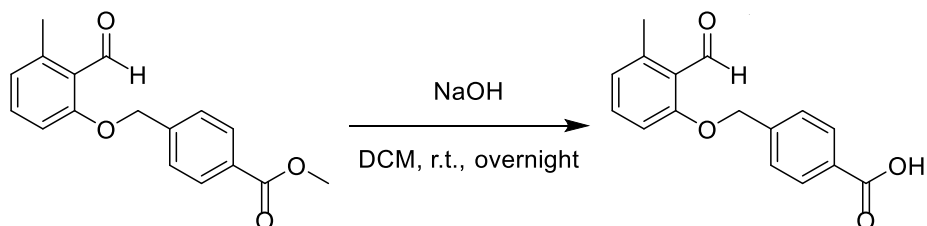


Figure S25. Fluorescence spectrum of methyl 4-((2-formyl-3-methylphenoxy)methyl)benzoate **12c** recorded in DCM ($5.02 \cdot 10^{-5}$ mol L⁻¹) at 210 nm (Excitation). No Fluorescence could be detected.

Synthesis of 4-((2-formyl-3-methylphenoxy)methyl)benzoic acid **12**^[246]



Methyl 4-((2-formyl-3-methylphenoxy)methyl)benzoate **12c** (6.3 g, 22.2 mmol, 1.00 eq.) was dissolved in DCM (315 mL) and NaOH (2.66 g, 66.5 mmol, 3.00 eq.) dissolved in

MeOH (35 mL) was added. The reaction mixture was stirred overnight at ambient temperature. The solvents were removed under reduced pressure and the residue was subsequently dissolved in DCM:water (1:1, 400 mL). The organic layer was extracted with water, all water layers were combined and acidified with aqueous HCl (3 %) to pH 3. The aqueous layer was subsequently extracted three times with DCM and the combined organic layers were dried over magnesium sulfate. The solvent was removed under reduced pressure to give the product as a white powder (75 %).

¹H NMR (600 MHz, acetone-*d*⁶): δ = 10.74 (s, 1H, CHO), 8.12 – 8.07 (m, 2H, Ar H), 7.71 – 7.65 (m, 2H, Ar H), 7.45 (dd, *J* = 8.4, 7.6 Hz, 1H, Ar H), 7.13 (d, *J* = 8.4 Hz, 1H, Ar H), 6.89 (d, *J* = 7.6 Hz, 1H, Ar H), 5.39 (s, 2H, CH₂), 2.90 (bs, 1H, COOH), 2.52 (s, 3H, CH₃) ppm. **¹³C NMR** (101 MHz, DMSO-*d*⁶): δ = 191.57, 167.04, 161.46, 141.56, 140.68, 134.79, 130.30, 129.54, 127.27, 124.18, 123.09, 111.37, 69.38, 39.52, 20.84 ppm. **MS** (ESI) *m/z*: [M - H]⁻ calcd. for C₁₆H₁₃O₄, 269.0819; found 269.0817. Details of the ¹H NMR chemical shift assignments can be found in **Figure 29** (Section 3.2.1).

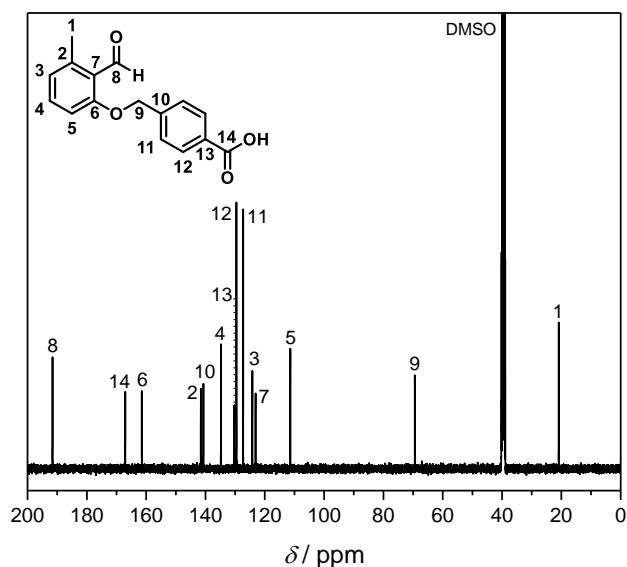


Figure S26. ¹³C NMR spectrum of 4-((2-formyl-3-methylphenoxy)methyl)benzoic acid **12** recorded in DMSO at 101 MHz. For the resonance assignments refer to the depicted structure.

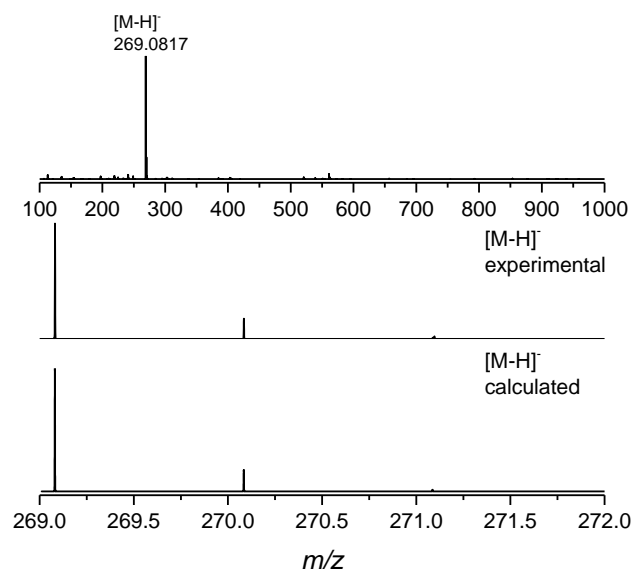
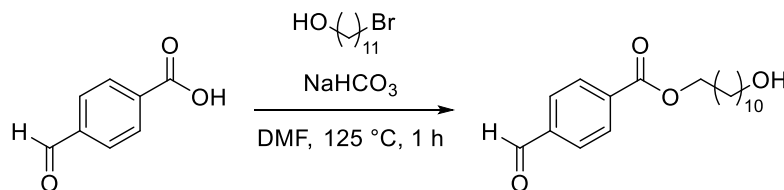


Figure S27. Mass spectrum of 4-((2-formyl-3-methylphenoxy)methyl)benzoic acid **12** recorded in THF/MeOH (3:2). ESI-MS spectra of **12** isotopic pattern (bottom). Recorded mass spectra shown are in excellent agreement with the calculated isotope pattern.

Synthesis of 11-hydroxyundecyl 4-formylbenzoate **11a**^[79]



The synthesis was performed according to a literature procedure and slightly adapted. Under argon, 4-formylbenzoic acid (414 mg, 2.76 mmol, 1.00 eq.) and 11-bromoundecan-1-ol (800 mg, 3.20 mmol, 1.20 eq.) were dissolved in 5 mL dry DMF and NaHCO₃ (463 mg, 5.51 mmol, 2.00 eq.) was added. The reaction mixture was stirred for 1 h at 125 °C. After cooling down to room temperature the reaction mixture was diluted with 100 mL ethyl acetate washed with 1M HCl (3x100 mL) and dried over MgSO₄. Ethyl acetate was removed under reduced pressure. The crude product was purified *via* column chromatography on silica gel using cyclohexane/ethyl acetate (1:1, R_f = 0.62) as the eluent. After drying under high vacuum 781 mg of the title compound were obtained as white solid (88 %).

¹H NMR (400 MHz, CDCl₃): δ = 10.11 (s, 1H), 8.23–8.18 (m, 2H), 7.98–7.93 (m, 2H), 4.38–4.33 (m, 2H), 3.66–3.63 (m, 2H), 1.84–1.80 (m, 2H), 1.59–1.54 (m, 2H), 1.40–1.25 (m, 14H) ppm. **¹³C NMR** (101 MHz, CDCl₃): δ = 191.7, 165.7, 139.1, 135.5, 130.2, 129.5, 65.8, 63.1, 32.8, 29.6, 29.5, 29.4, 29.2, 28.6, 26.0, 25.7 ppm. **MS** (ESI) *m/z*: [M + Na]⁺ calcd. for C₁₉H₂₈O₄, 343.1880; found 343.1879.

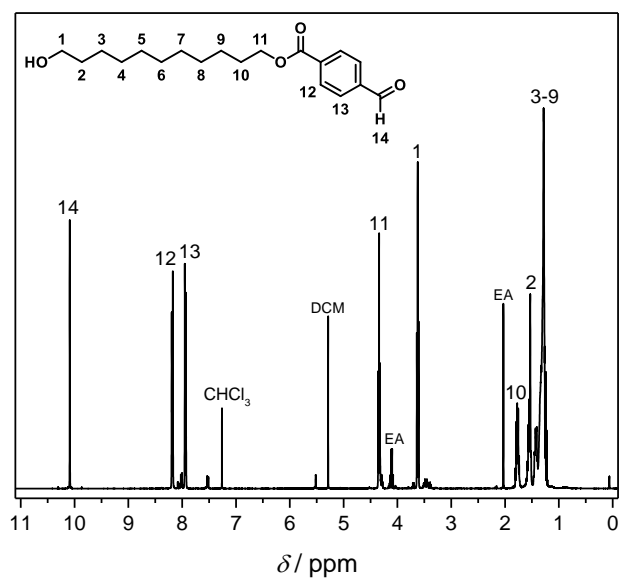


Figure S28. ¹H NMR spectrum of 11-hydroxyundecyl 4-formylbenzoate **11a** recorded in CDCl₃ at 400 MHz. For the resonance assignments refer to the depicted structure.

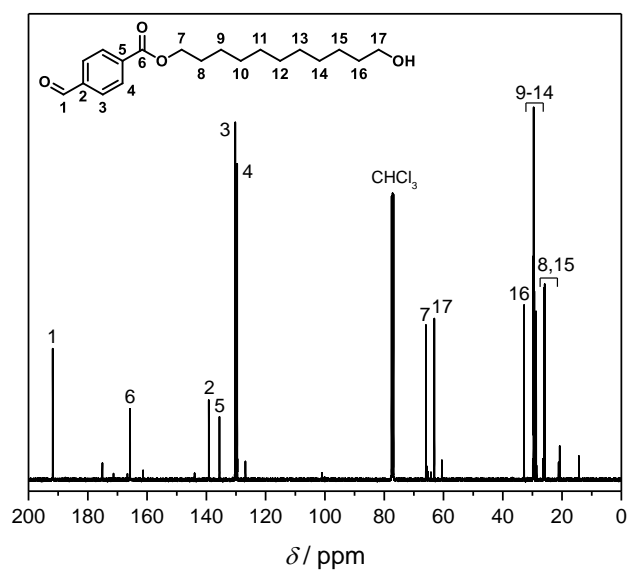


Figure S29. ¹³C NMR spectrum of 11-hydroxyundecyl 4-formylbenzoate **11a** recorded in CDCl₃ at 101 MHz. For the resonance assignments refer to the depicted structure.

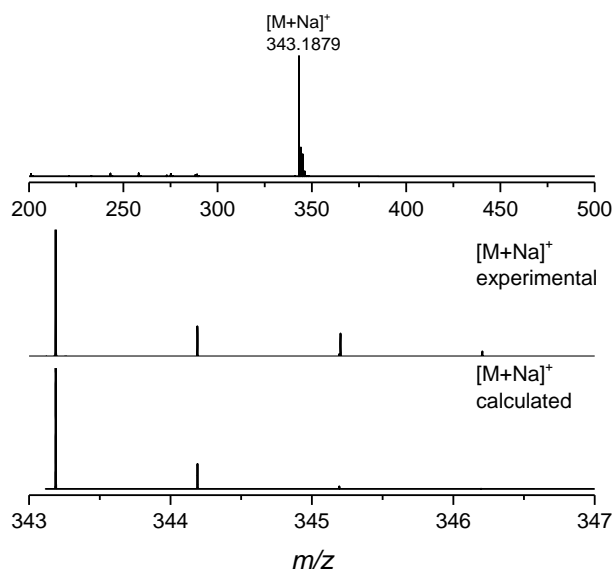
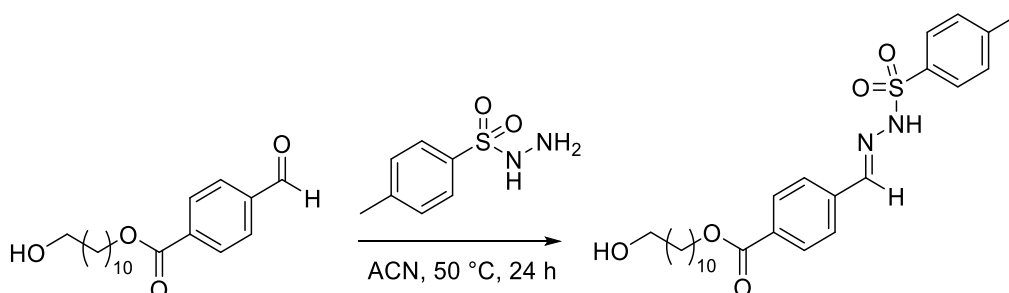


Figure S30. Mass spectrum of 11-hydroxyundecyl 4-formylbenzoate **11a** recorded in THF/MeOH (3:2). ESI-MS spectra of **11a** isotopic pattern (bottom). Recorded mass spectra shown are in excellent agreement with the calculated isotope pattern.

Synthesis of 11-hydroxyundecyl-4-((2-tosylhydrazineylidene)methyl)benzoate **11b**^[79]



The synthesis was adapted from a literature procedure. A mixture of 11-hydroxyundecyl 4-formylbenzoate **11a** (9.44 g, 29.5 mmol, 1.00 eq.) and 4-methylbenzenesulfonylhydrazide (6.03 g, 32.4 mmol, 1.20 eq.) in 275 mL acetonitrile was stirred at 50 °C overnight. The solvent was removed under reduced pressure. The intermediate was employed for the next step without any further purification.

¹H NMR (400 MHz, CDCl₃): δ = 8.84 (s, 1H), 7.98 (d, J = 8.1 Hz, 2H), 7.86 (d, J = 8.0 Hz, 2H), 7.81 (s, 1H), 7.61 (d, J = 8.2 Hz, 2H), 7.29 (d, J = 8.0 Hz, 2H), 4.29 (t, J = 6.6 Hz, 2H), 3.67 – 3.56 (m, 2H), 2.38 (s, 3H), 1.82 – 1.67 (m, 2H), 1.60 – 1.47 (m, 2H), 1.47 – 1.15 (m, 14H) ppm. **¹³C NMR** (101 MHz, CDCl₃): δ = 166.07, 146.00, 144.47, 137.18, 135.18, 131.87, 129.84, 129.76, 127.94, 127.12, 67.98, 65.42, 63.07, 32.77, 29.55, 29.46, 29.42, 29.21, 28.64, 26.00, 25.74, 21.62 ppm. **MS** (ESI) m/z : [M + Na]⁺ calcd. for C₂₆H₃₆N₂O₅S, 511.2237; found 511.2239.

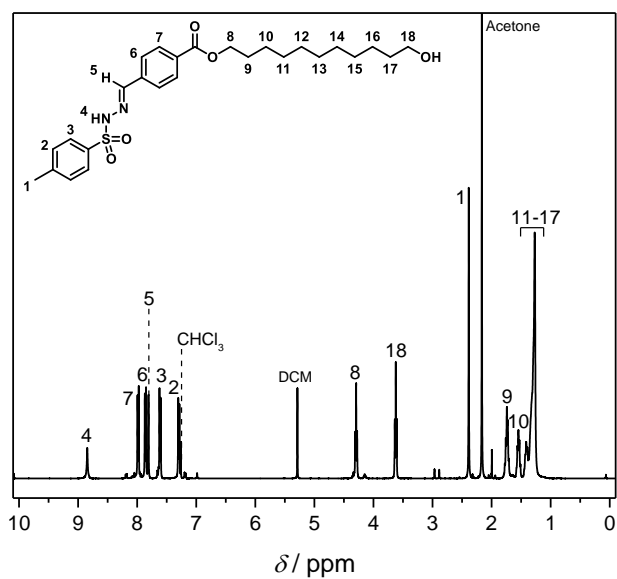


Figure S31. ¹H NMR spectrum of 11-hydroxyundecyl-4-((2-tosylhydrazineylidene)methyl)benzoate **11b** recorded in CDCl₃ at 400 MHz. For the resonance assignments refer to the depicted structure.

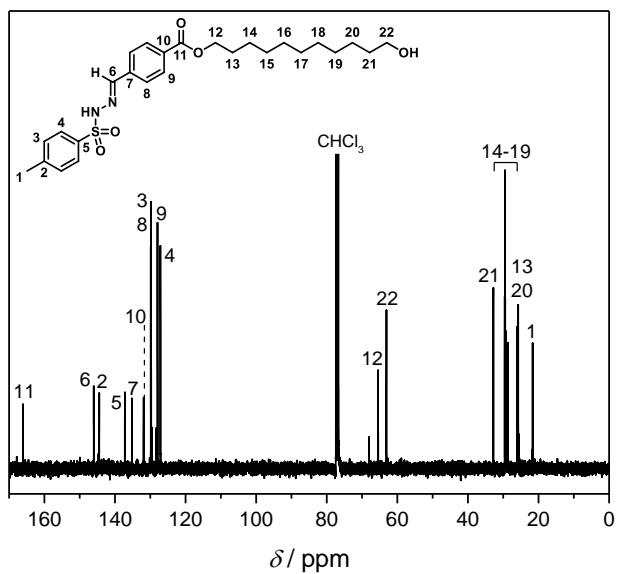


Figure S32. ¹³C NMR spectrum of 11-hydroxyundecyl-4-((2-tosylhydrazineylidene)methyl)benzoate **11b** recorded in CDCl₃ at 101 MHz. For the resonance assignments refer to the depicted structure.

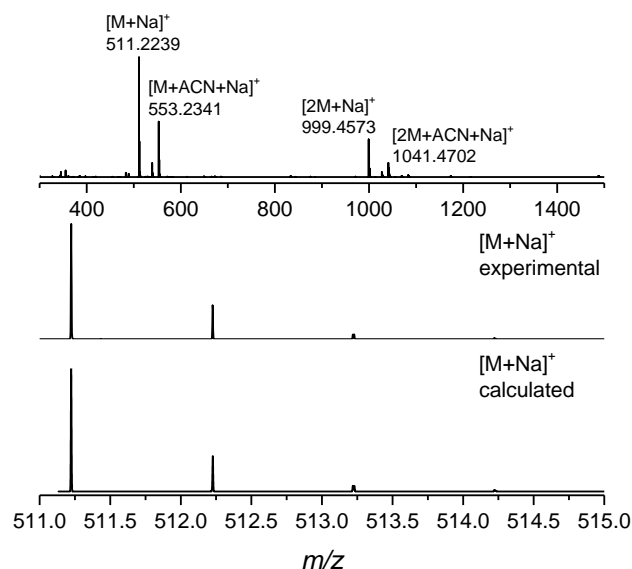
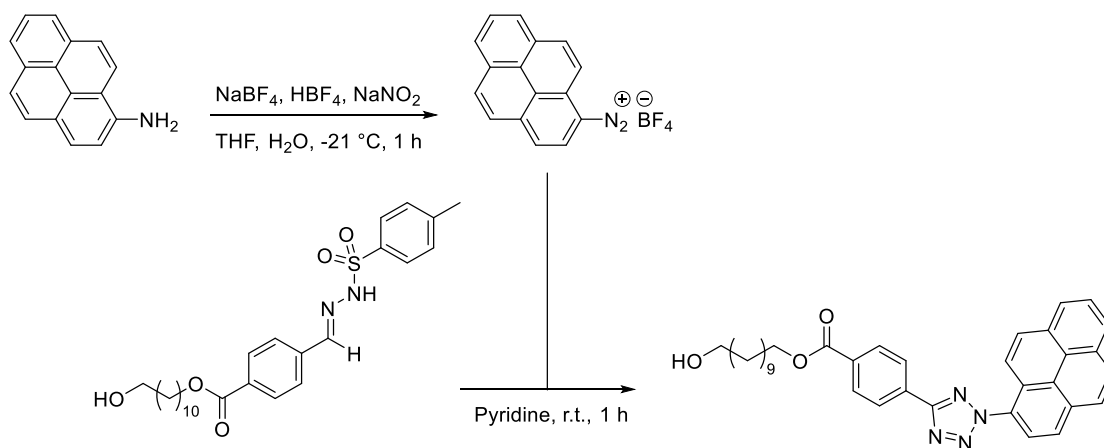


Figure S33. Mass spectrum of 11-hydroxyundecyl-4-((2-tosylhydrazineylidene)methyl)benzoate **11b** recorded in THF/MeOH (3:2). ESI-MS spectra of **11b** isotopic pattern (bottom). Recorded mass spectra shown are in excellent agreement with the calculated isotope pattern.

Synthesis of 11-hydroxyundecyl 4-(2-(pyren-1-yl)-2H-tetrazol-5-yl)benzoate (PAT)^[79]



The synthesis was adapted from a literature procedure. 11-Hydroxyundecyl-4-((2-tosylhydrazineylidene)methyl)benzoate **11b** (2.35 g, 4.8 mmol, 1.00 eq.) was dissolved in 80 mL pyridine (solvent A). In parallel 1-aminopyrene (840.0 mg, 3.86 mmol, 0.80 eq.) was dissolved in dry THF (90 mL), cooled to $-21\text{ }^\circ\text{C}$ and degassed for 30 min with nitrogen (solution B). A solution of $NaBF_4$ (3.41 g, 31.0 mmol, 6.45 eq.) in 32 mL HBF_4 (50 % solution in water) and 13 mL H_2O was degassed for 20 min and was added to solution B (1-aminopyrene) slowly. The reaction mixture (solution B) was stirred for 20 min at $-21\text{ }^\circ\text{C}$. $NaNO_2$ (307.0 mg, 4.5 mmol, 0.93 eq.) in 6 mL H_2O was degassed for 20 min and added dropwise to the 1-aminopyrene solution. An orange precipitate was formed after stirring solution B at $-21\text{ }^\circ\text{C}$ for additional 20 min and for 10 min at ambient temperature. The solid was collected and added to solution A. The reaction mixture (solution A) was stirred for 1 h at room temperature. Afterwards, the reaction mixture was poured into aqueous 1M hydrochloric

acid (fivefold volume of pyridine, 500 mL). The crude product was purified *via* recrystallization in EtOH (150 mL). After drying under high vacuum, 1.19 g of the title compound were obtained as a brown solid (55 %).

^1H NMR (400 MHz, CDCl_3): δ = 8.40–8.06 (m, 13H), 4.43–4.35 (m, 2H), 3.70–3.63 (m, 2H), 1.79–1.70 (m, 2H), 1.55–1.22 (m, 16H) ppm. **^{13}C NMR** (101 MHz, CDCl_3): δ = 166.25, 164.68, 132.91, 132.43, 131.32, 131.22, 130.68, 130.39, 130.21, 130.17, 129.49, 127.17, 127.09, 127.00, 126.82, 126.43, 125.24, 125.11, 124.91, 124.19, 122.83, 121.52, 65.64, 63.19, 32.94, 29.71, 29.63, 29.56, 29.40, 28.84, 26.18, 25.89 ppm. **MS** (ESI) m/z : $[\text{M} + \text{Na}]^+$ calcd. for $\text{C}_{35}\text{H}_{36}\text{N}_4\text{O}$, 583.2685; found 583.2685. Details of the ^1H NMR chemical shift assignments can be found in **Figure 28** (Section 3.2.1).

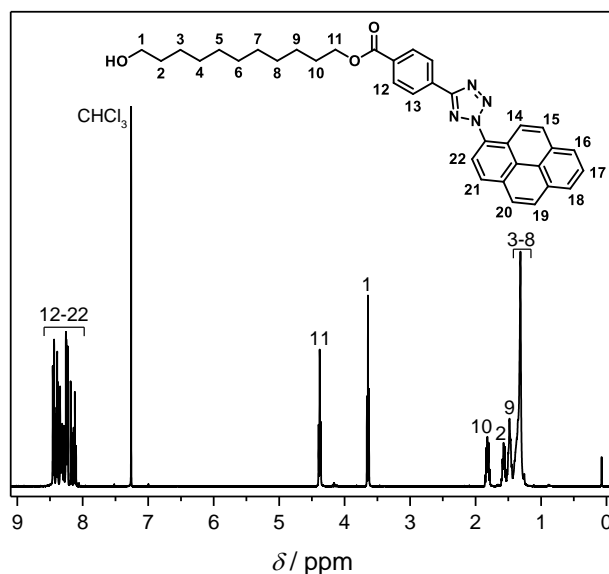


Figure S34. ^1H NMR spectrum of 11-hydroxyundecyl 4-(2-(pyren-1-yl)-2H-tetrazol-5-yl)benzoate **11** recorded in CDCl_3 at 400 MHz. For the resonance assignments refer to the depicted structure.

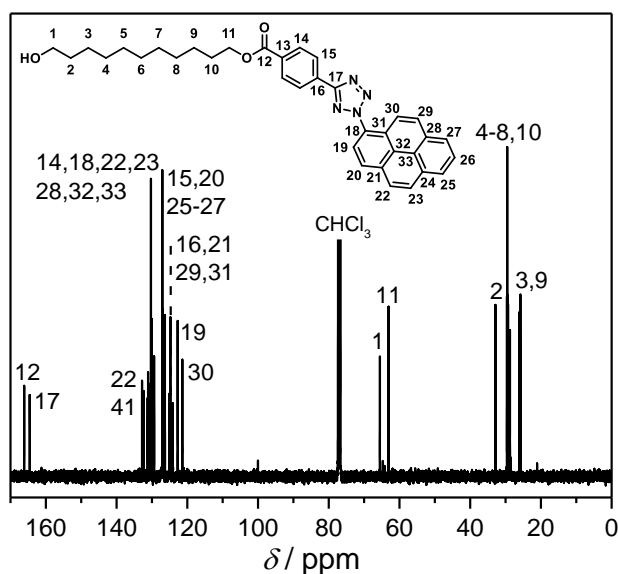


Figure S35. ^{13}C NMR spectrum of 11-hydroxyundecyl 4-(2-(pyren-1-yl)-2H-tetrazol-5-yl)benzoate **11** recorded in CDCl_3 at 101 MHz. For the resonance assignments refer to the depicted structure.

5. Experimental Section

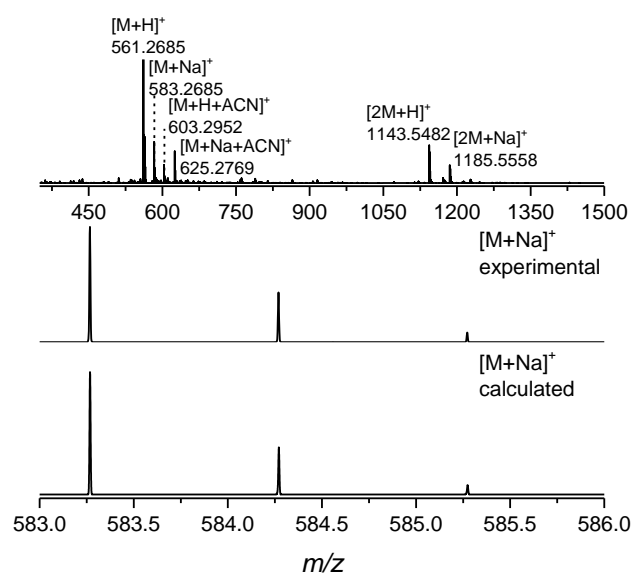


Figure S36. Mass spectrum of 11-hydroxyundecyl 4-(2-(pyren-1-yl)-2H-tetrazol-5-yl)benzoate **11** recorded in THF/MeOH (3:2). ESI-MS spectra of **11** isotopic pattern (bottom). Recorded mass spectra shown are in excellent agreement with the calculated isotope pattern.

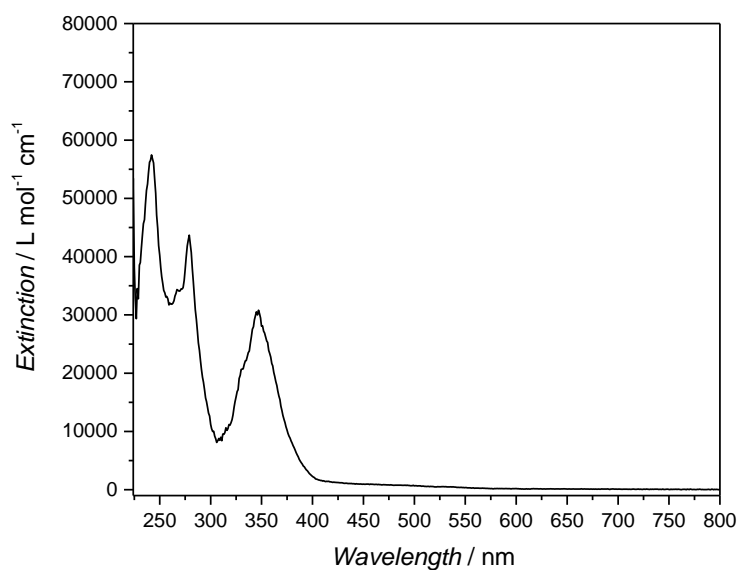


Figure S37. UV-Vis spectrum of 11-hydroxyundecyl 4-(2-(pyren-1-yl)-2H-tetrazol-5-yl)benzoate **11** recorded in DCM ($1.4 \cdot 10^{-5}$ mol L⁻¹).

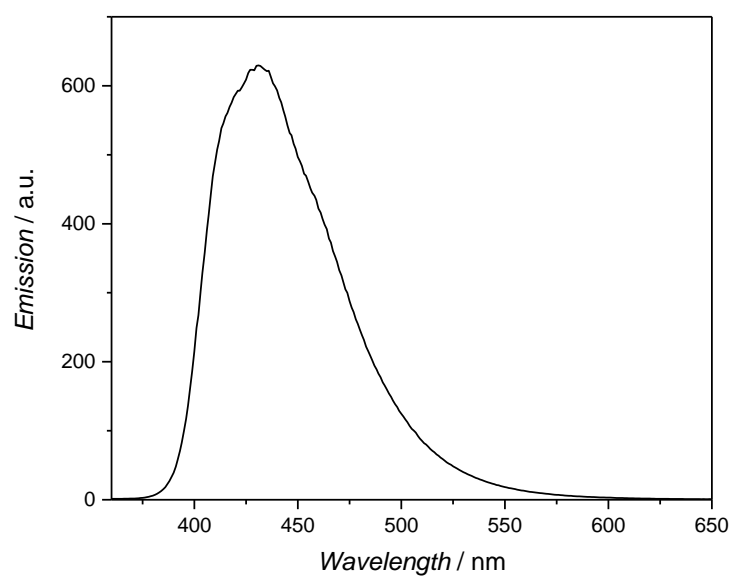
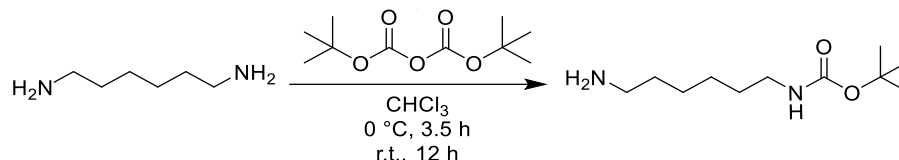


Figure S38. Fluorescence spectrum of 11-hydroxyundecyl 4-(2-(pyren-1-yl)-2H-tetrazol-5-yl)benzoate **11** recorded in DCM ($1.4 \cdot 10^{-5}$ mol L⁻¹) at 344 nm (Excitation).

5.3.3. Synthesis of Building Blocks and Core Units

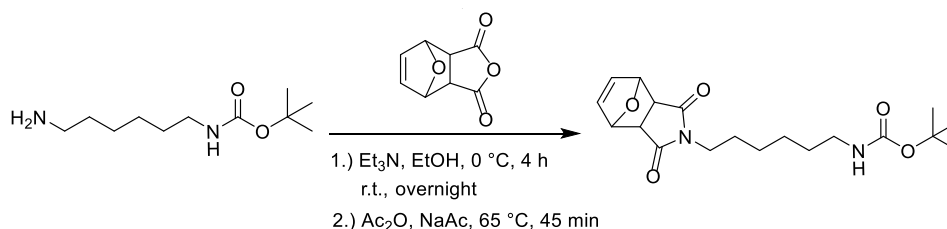
Synthesis of *tert*-Butyl (6-aminohexyl)carbamate



Boc₂O (45.9 g, 52.7 mmol, 1.00 eq.) dissolved in CHCl₃ (200 mL) was added dropwise to a solution of 1,6-hexanediamine (11.5 g, 395.1 mmol, 7.50 eq.) dissolved in CHCl₃ (400 mL) at 0 °C over the course of 3 h. Afterwards, the reaction mixture was stirred for 30 min at 0 °C and stirred overnight at ambient temperature. After removal of the solvent under reduced pressure, the residue was dissolved in 1.5 N Na₂CO₃ (700 mL) and extracted twice with DCM (60 mL). The combined organic layers were washed three times with brine (100 mL) and dried over MgSO₄. After removal of the solvent under reduced pressure, the crude product was purified by recrystallization of residual 1,6-hexanediamine from toluene (-20 °C). The target compound was obtained as a yellow oil from the filtrate after evaporation of the solvent (7.6 g, 33 %).

¹H NMR (400 MHz, CDCl₃): δ = 4.56 (s, 1H), 3.09 (dd, *J* = 12.4, 6.1 Hz, 2H), 2.66 (td, *J* = 7.0, 4.0 Hz, 2H), 1.48–1.36 (m, 12H), 1.35–1.25 (m, *J* = 3.6 Hz, 4H), 1.20 (s, 2H) ppm.
¹³C NMR (100 MHz, CDCl₃, δ): 156.1, 79.1, 42.3, 40.6, 33.9, 30.2, 28.5, 26.9, 26.7 ppm.

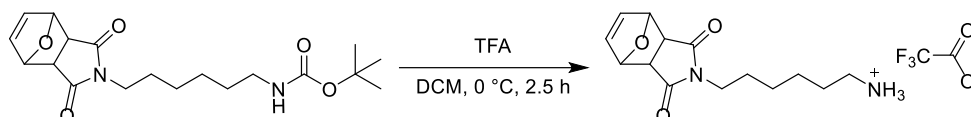
Synthesis of *tert*-butyl (6-(1,3-dioxo-1,3,3*a*,4,7,7*a*-hexahydro-2*H*-4,7-epoxyisobenzofuran-2-yl)hexyl)-carbamate



All operations were conducted under argon atmosphere. A solution of 3*a*,4,7,7*a*-tetrahydro-4,7-epoxyisobenzofuran-1,3-dione **2a** (3.66 g, 16.90 mmol, 1.20 eq.) and Et₃N (3.51 mL, 25.36 mmol, 1.80 eq.) in dry EtOH (150 mL) was added slowly to *tert*-Butyl (6-aminohexyl)carbamate (2.34 g, 14.09 mmol, 1.00 eq.) dissolved in dry 1,4-dioxane (40 mL) at 0 °C. Subsequently, the reaction mixture was stirred for 4 h at 0 °C and overnight at ambient temperature. The solvent was removed *in vacuo* and the residue was diluted with acetic anhydride (50 mL). NaAc (1.42 g, 17.3 mmol, 1.23 eq.) was added and the mixture was heated for 45 minutes to 65 °C. Afterwards, the reaction mixture was dried *in vacuo* to eliminate the excess of Ac₂O. The residue was then cooled to 0 °C and neutralized with saturated aqueous solution of NaHCO₃. The resulting solution was extracted 5 times with EA (80 mL) and the collected organic layers were washed twice with saturated NaHCO₃ (80 mL), to be finally dried over Na₂SO₄. After filtration and removal of the solvent, the product was purified by column chromatography (EA:CH:MeOH 47.5:47.5:5, solid deposition, R_f = 0.45) to provide a yellow solid (4.11 g, 53 %).

¹H NMR (400 MHz, CDCl₃): δ = 6.44 (s, 2H), 5.19 (s, 2H), 4.49 (s, 1H), 3.38 (t, *J* = 7.3 Hz, 2H), 3.01 (s, 2H), 2.77 (s, 2H), 1.53–1.44 (m, 4H), 1.37 (dd, *J* = 16.9, 3.5 Hz, 9H), 1.29–1.15 (m, 4H) ppm. **¹³C NMR** (100 MHz, CDCl₃): δ = 176.5, 156.2, 136.6, 80.9, 78.9, 47.4, 40.4, 38.8, 29.8, 28.4, 27.5, 27.4, 26.2 ppm.

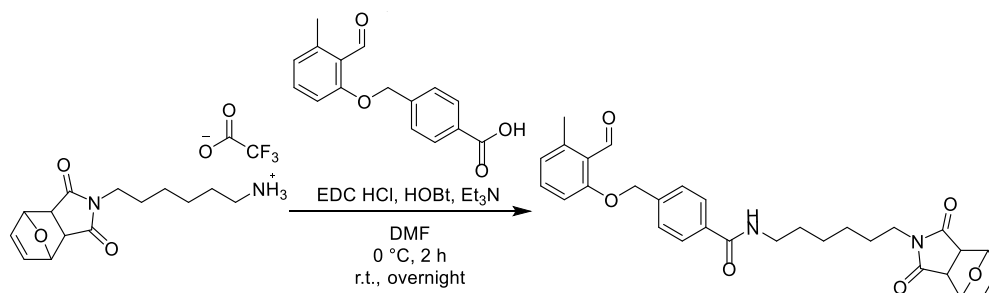
Synthesis of 6-(1,3-Dioxo-1,3,3*a*,4,7,7*a*-hexahydro-2*H*-4,7-epoxyisoindol-2-yl)hexan-1-aminium 2,2,2-trifluoroacetate



All operations were conducted under argon atmosphere. Bock protected maleimide (1.82 g, 5 mmol, 1.00 eq.) was dissolved in dry DCM (225 mL) and cooled to 0 °C. TFA (11.55 mL, 149.92 mmol, 32 eq.) was slowly added and the reaction mixture was stirred for 2.5 h until thin layer chromatography (TLC) showed the absence of starting material. The solvent and TFA were subsequently removed *in vacuo* at 20 °C by threefold dissolution of the residue in DCM and subsequent evaporation. The resulting residue was weighed in order to quantify the excess amount of residual TFA to determine the excess amount of Et₃N necessary for the next synthetic step (2.05 g, 100 %).

¹H NMR (500 MHz, CDCl₃): δ = 7.83 (s, 3H), 6.44 (s, 2H), 5.17 (s, 2H), 3.39 (t, *J* = 7.0 Hz, 2H), 2.84–2.78 (m, 4H), 1.62–1.52 (m, 4H), 1.34–1.11 (m, 4H) ppm. **¹³C NMR** (125 MHz, CDCl₃): δ = 176.6, 136.5, 80.9, 47.4, 39.6, 38.4, 27.1, 27.0, 25.5, 25.3 ppm.

Synthesis of *N*-(6-(1,3-Dioxo-1,3,3*a*,4,7,7*a*-hexahydro-2*H*-4,7-epoxyisoindol-2-yl)hexyl)-4-((2-formyl-3-methylphenoxy)methyl)benzamide **5a**



All operations were conducted under argon atmosphere. Maleimide (1.90 g, 5.01 mmol, 1.00 eq.), 4-((2-formyl-3-methylphenoxy)methyl)-benzoic acid **12** (1.49 g, 5.51 mmol, 1.10 eq.) and HOBt (1.02 g, 7.62 mmol, 1.50 eq.) were dissolved in DMF (60 mL) and cooled to 0 °C. Et₃N (1.60 mL, 11.53 mmol, 2.30 eq.) was added dropwise to the mixture. Subsequently EDC·HCl (1.11 g, 3.75 mmol, 1.15 eq.) was added and the reaction mixture was stirred for 2 h at 0 °C and overnight at ambient temperature. The mixture was diluted with EA (250 mL), washed twice with saturated NaHCO₃ (25 mL) and brine (50 mL). Afterwards, the organic layer was dried over MgSO₄ and the solvent was evaporated *in vacuo*. Purification was carried out by column chromatography (EA, *R_f* = 0.45, DCM:MeOH 98:2, *R_f* = 0.3) to provide 869.9 mg of the product as a white solid (65.2 %). The product is light sensitive and was stored protected from light.

¹H NMR (500 MHz, CDCl₃): δ = 10.66 (s, 1H), 7.74 (d, *J* = 8.2 Hz, 2H), 7.40 (d, *J* = 8.2 Hz, 2H), 7.29 (t, *J* = 8.0 Hz, 1H), 6.82–6.73 (m, 2H), 6.48–6.38 (m, 3H), 5.17 (s, 2H), 5.13 (s,

5. Experimental Section

2H), 3.41 (t, $J = 7.1$ Hz, 2H), 3.35 (dd, $J = 12.9, 6.8$ Hz, 2H), 2.76 (s, 2H), 2.51 (s, 3H), 1.52 (d, $J = 7.5$ Hz, 4H), 1.47–1.37 (m, 2H), 1.37–1.25 (m, 2H) ppm. ^{13}C NMR (125 MHz, CDCl_3): $\delta = 192.1, 176.4, 167.0, 162.0, 142.3, 139.6, 136.5, 134.7, 134.5, 127.4, 127.1, 124.6, 123.6, 110.4, 81.0, 70.0, 47.4, 39.6, 38.6, 29.3, 27.3, 26.0, 25.8, 21.5$ ppm. MS (ESI) m/z : $[\text{M} + \text{Na}]^+$ calcd. for $\text{C}_{30}\text{H}_{32}\text{N}_2\text{O}_6\text{Na}$, 539.2153; found, 539.2189. Details of the ^1H NMR chemical shift assignments can be found in **Figure 21** (Section 3.1.2).

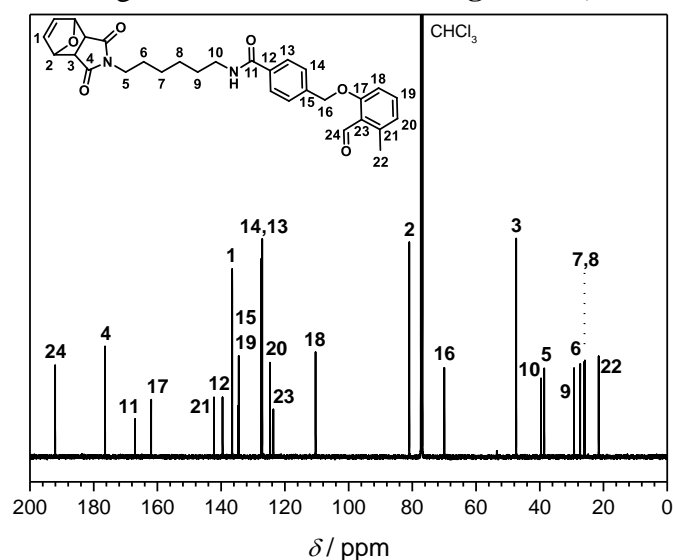


Figure S39. ^{13}C NMR spectrum of the photomonomer **5a** recorded in CDCl_3 at 101 MHz. For the resonance assignments refer to the depicted structure.

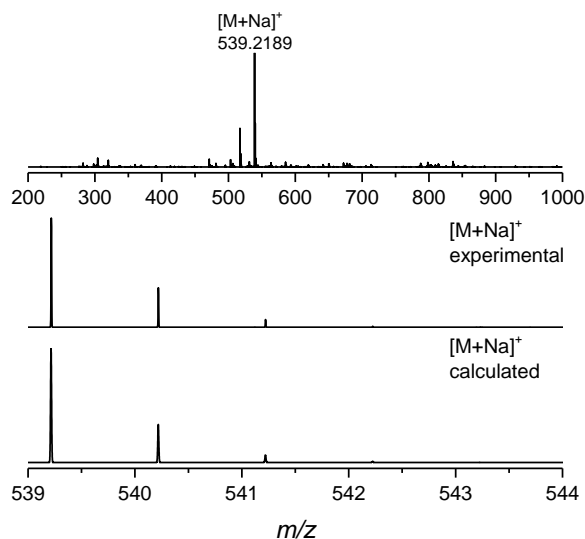


Figure S40. Full ESI-MS spectrum of the photomonomer **5a** (top) recorded in THF/MeOH (3:2). ESI-MS spectra of the photomonomer **5a** isotopic pattern (bottom). Recorded mass spectra shown are in excellent agreement with the calculated isotope pattern.

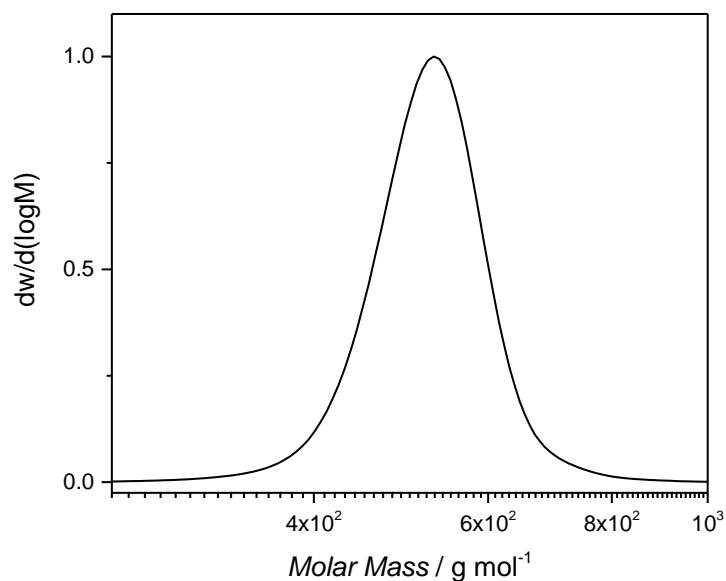


Figure S41. SEC trace of the photomonomer **5a** recorded in THF at 35 °C. ($\bar{D} = 1.01$, $M_n = 520 \text{ g mol}^{-1}$).

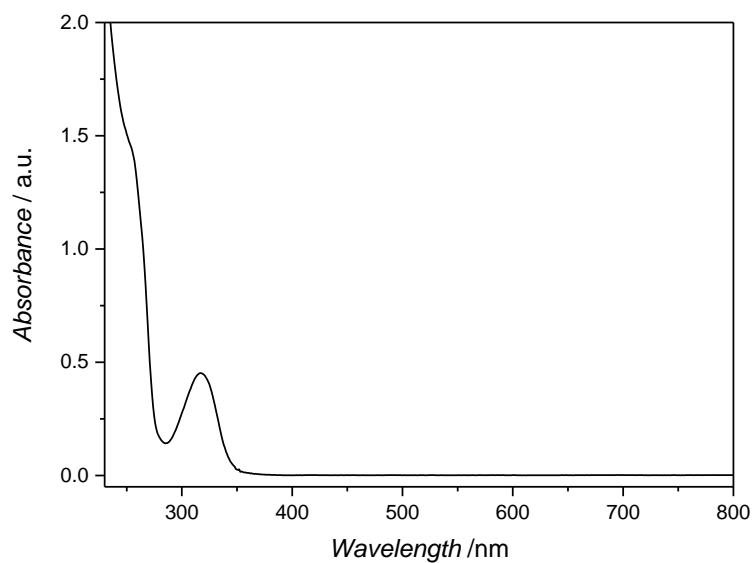
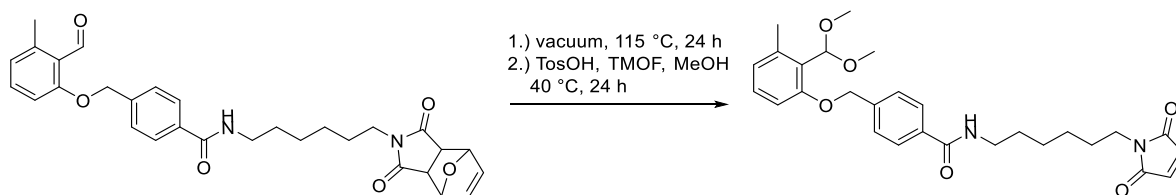


Figure S42. UV-Vis spectrum of the photomonomer **5a** in DCM (0.04 mg mL⁻¹).

Synthesis of 4-((2-(Dimethoxymethyl)-3-methylphenoxy)methyl)-N-(6-(2,5-dioxo-2,5-dihydro-1H-pyrrol-1-yl)hexyl)benzamide **5a***



5. Experimental Section

All operations were conducted under argon atmosphere and protected from light. **5a** (210.6 mg, 0.41 mmol, 1.00 eq.) was heated at 115 °C for 24 h under vacuum to quantitatively remove the furan protecting group. The intermediate was employed for further modification without any purification. pTsoH (6.2 mg, 32.6 μ mol, 0.08 eq.), TMOF (180 μ L, 1.63 mmol, 4.00 eq.) and anhydrous MeOH (4.5 mL) were added to the furan deprotected compound. The suspension was heated to 40 °C and stirred for 24 h. The crude reaction mixture was filtrated over silica (DCM, 5 % Et₃N) and the solvent was removed under reduced pressure to provide a pink oil.

¹H NMR (400 MHz, CDCl₃): δ = 7.80 (d, J = 8.3 Hz, 2H), 7.50–7.46 (m, 2H), 7.14–7.10 (m, 1H), 6.80 (d, J = 7.6 Hz, 1H), 6.73 (d, J = 8.3 Hz, 1H), 6.68 (s, 2H), 6.24–6.18 (m, 1H), 5.11 (s, 1H), 3.53 (t, J = 7.1 Hz, 2H), 3.44 (q, J = 7.1, 5.8 Hz, 2H), 3.41 (s, 6H), 3.33 (s, 3H), 1.66–1.56 (m, 4H), 1.46–1.37 (m, 2H), 1.37–1.23 (m, 2H) ppm.

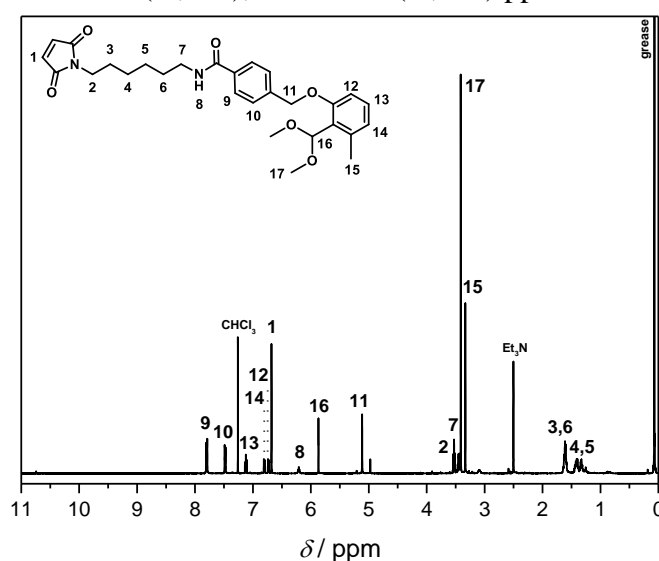
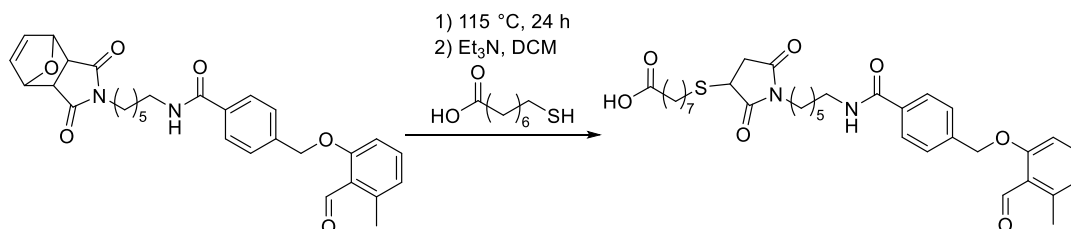


Figure S43. ¹H NMR spectrum of the photomonomer acetal **5a*** recorded in CDCl₃ at 400 MHz. For the resonance assignments refer to the depicted structure.

Synthesis of 8-((1-(6-(4-((2-formyl-3-methylphenoxy) methyl) benzamido) hexyl)-2,5-dioxopyrrolidin-3-yl) thio) octanoic acid **6a**



Photomonomer **5a** (250.0 mg, 0.48 mmol, 1.00 eq.) was heated to 115 °C for 24 h *in vacuo*. The intermediate was employed for further synthesis without any purification. Mercaptooctanoic acid (102 mg, 0.58 mmol, 1.20 eq.) and TEA (97.9 mg, 0.97 mmol, 2.00 eq.) were added and in DCM (15.0 mL). The reaction was allowed to stir overnight. The mixture was diluted with DCM (50 mL), washed with saturated NaHCO₃ solution (25 mL), water (25 mL) and dried over MgSO₄. The solvent was removed under reduced pressure to yield the target compound as a yellow oil (257 mg, 87.6 %).

^1H NMR (400 MHz, CDCl_3): δ = 10.73 (s, 1H, CHO), 7.81 (d, J = 8.3 Hz, 2H, ArH), 7.48 (d, J = 8.3 Hz, 2H, Ar H), 7.36 (dd, J = 8.4, 7.6 Hz, 1H, Ar H), 6.85 (dd, J = 8.4 Hz, 1H, Ar H), 6.40 (t, J = 5.8 Hz, 1H, NH), 5.20 (s, 2H, $\text{CH}_2\text{-O}$), 3.70 (dd, J = 9.0, 3.4 Hz, 1H, CH-S), 3.52 (t, J = 7.1 Hz, 2H, $\text{CH}_2\text{-N}$), 3.48–3.38 (m, 2H, $\text{CH}_2\text{-NH}$), 3.12 (dd, J = 18.7, 9.0 Hz, 1H, $\text{CH}_{\text{cis}}\text{-CO}$), 2.95–2.66 (m, 2H, $\text{CH}_2\text{-S}$), 2.58 (s, 3H, Ar CH_3), 2.50 (dd, J = 18.7, 3.5 Hz, 1H, $\text{CH}_{\text{trans}}\text{-CO}$), 2.33 (t, J = 7.4 Hz, 2H, $\text{CH}_2\text{-COOH}$), 1.71–1.55 (m, 8H, CH_2), 1.47–1.19 (m, 10H, CH_2) ppm. **^{13}C NMR** (101 MHz, CDCl_3): δ = 192.24 (CHO), 178.02 (COOH), 176.97 (N-C=O), 175.09 (N-C=O), 167.27 (HN-C=O), 162.07 ($\text{C}_{\text{Ar}}\text{-O}$), 142.35 ($\text{C}_{\text{Ar}}\text{-CH}_3$), 139.74 ($\text{C}_{\text{Ar}}\text{-C=O}$), 136.61 ($\text{C}_{\text{Ar}}\text{-CH}_2$), 134.59 ($\text{C}_{\text{Ar}}\text{-H}$), 127.49 ($\text{C}_{\text{Ar}}\text{-H}$), 127.20 ($\text{C}_{\text{Ar}}\text{-H}$), 124.72 ($\text{C}_{\text{Ar}}\text{-H}$), 123.68 ($\text{C}_{\text{Ar}}\text{-CHO}$), 110.46 ($\text{C}_{\text{Ar}}\text{-H}$), 70.03 (Ar- $\text{CH}_2\text{-O}$), 39.82 ($\text{CH}_2\text{-N}$), 39.12 (CH-S), 38.70 ($\text{CH}_2\text{-N}$), 36.19 ($\text{CH}_2\text{-CO}$), 34.13 ($\text{CH}_2\text{-COOH}$), 31.73 ($\text{CH}_2\text{-S}$), 29.41 (CH_2), 28.96 (CH_2), 28.94 (CH_2), 28.78 (CH_2), 28.56 (CH_2), 27.47 (CH_2), 26.17 (CH_2), 26.09 (CH_2), 24.78 (CH_2), 21.57 (Ar- CH_3) ppm. **MS** (ESI) m/z : $[\text{M} + \text{Na}]^+$ calcd. for $\text{C}_{34}\text{H}_{44}\text{N}_2\text{O}_7\text{S}$, 647.2761; found 647.2757. Details of the ^1H NMR chemical shift assignments can be found in **Figure 22** (Section 3.1.2).

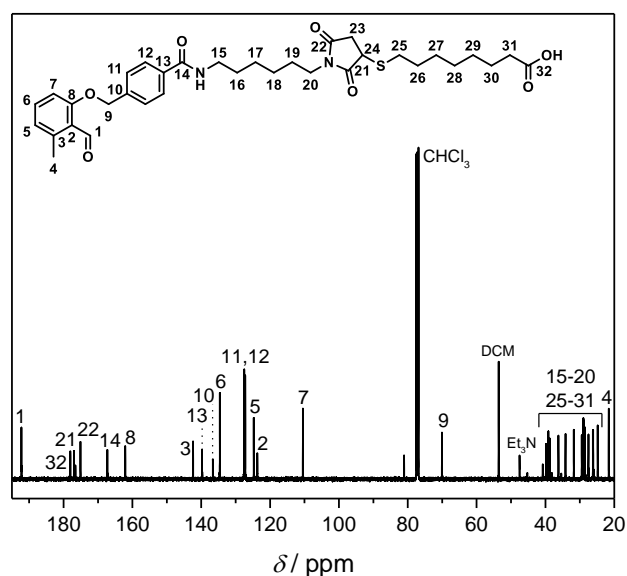


Figure S44. ^{13}C NMR spectrum of the modified photomonomer **6a** recorded in CDCl_3 at 101 MHz. For the resonance assignments refer to the depicted structure.

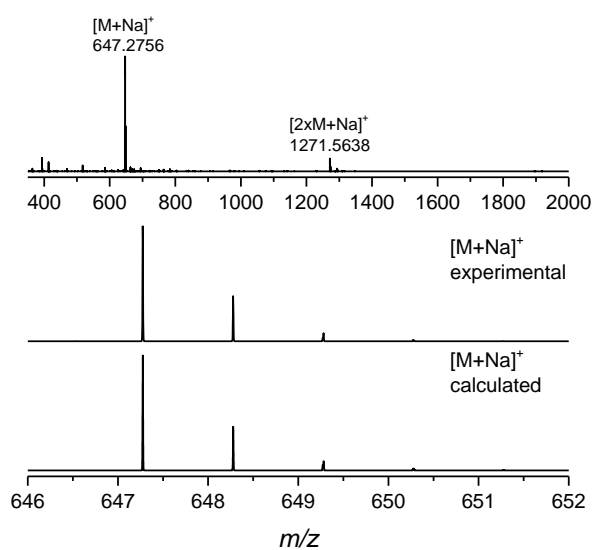


Figure S45. Full ESI-MS spectrum of the modified photomonomer **6a** (top) recorded in THF/MeOH (3:2). ESI-MS spectra of the modified photomonomer **6a** isotopic pattern (bottom). Recorded mass spectra shown are in excellent agreement with the calculated isotope pattern.

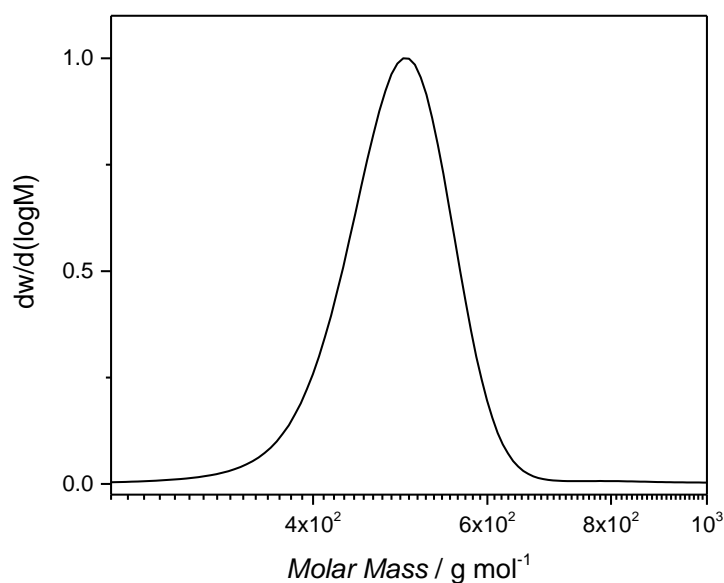
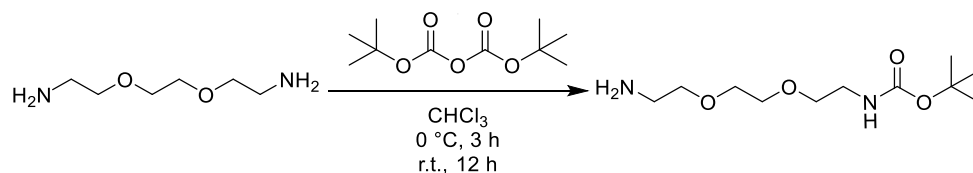


Figure S46. SEC trace of the modified photomonomer **6a** recorded in THF at 35 °C. ($\bar{D} = 1.01$, $M_n = 490 \text{ g mol}^{-1}$).

Synthesis of *tert*-Butyl (2-(2-(2-aminoethoxy)ethoxy)ethyl)carbamate

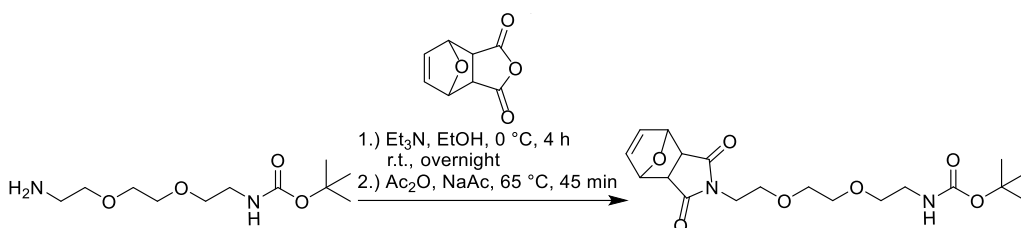


2-(2-(2-Aminoethoxy)ethoxy)ethylamine (27.3 g, 184.36 mmol, 7.50 eq.) dissolved in CHCl₃ (400 mL), cooled to 0 °C was added to a solution of Boc₂O (0.57 g, 24.6 mmol,

1.00 eq.) in CHCl_3 (200 mL) dropwise over the course of 3 h. Afterwards, the reaction mixture was stirred for 30 minutes at 0 °C and overnight at ambient temperature. After removal of the solvent under reduced pressure, the residue was dissolved in 3 M Na_2CO_3 (400 mL) and extracted twice with DCM (60 mL). The combined organic layers were washed three times with brine (100 mL) and dried over MgSO_4 . After removal of the solvent under reduced pressure, the target compound was obtained as a yellow oil (5.5 g, 90.0 %).

$^1\text{H NMR}$ (400 MHz, CDCl_3): δ = 5.17 (s, 1H), 3.66–3.56 (m, 4H), 3.52 (dd, J = 11.1, 5.9 Hz, 4H), 3.29 (s, 2H), 2.92–2.80 (m, 2H), 1.72 (s, 2H), 1.41 (s, 9H) ppm. $^{13}\text{C NMR}$ (101 MHz, CDCl_3): δ = 156.1, 79.3, 77.2, 73.4, 70.3, 41.8, 40.4, 28.5 ppm.

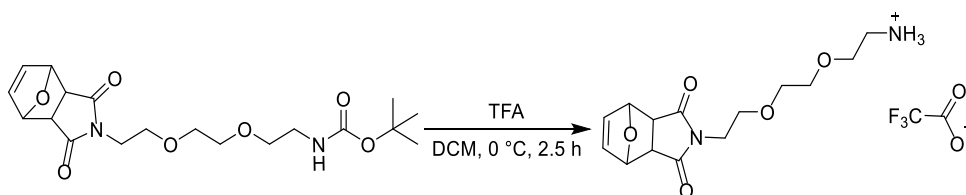
Synthesis of *tert*-Butyl (2-(2-(2-(1,3-dioxo-1,3,3a,4,7,7a-hexahydro-2H-4,7-epoxyisoindol-2-yl)ethoxy)ethoxy)ethyl)carbamate



All operations were conducted under argon atmosphere. 3a,4,7,7a-Tetrahydro-4,7-epoxyisobenzofuran-1,3-dione **2a** (2.34 g, 14.09 mmol, 1.00 eq.) dissolved in dry 1,4-dioxane (40 mL) was slowly added to a solution of *tert*-butyl (2-(2-(2-aminoethoxy)ethoxy)ethyl)carbamate (4.20 g, 16.90 mmol, 1.20 eq.) and Et_3N (3.52 mL, 25.36 mmol, 1.80 eq.) dissolved in dry EtOH (150 mL) at 0 °C. Subsequently, the mixture was stirred for 4 h at 0 °C and overnight at ambient temperature. The solvent was removed *in vacuo* and the residue was diluted with acetic anhydride (50 mL). NaAc (1.42 g, 17.32 mmol, 1.23 eq.) was added and the mixture was heated for 45 minutes to 65 °C. Afterwards, the excess of acetic anhydride was removed under reduced pressure. The residue was then cooled to 0 °C and neutralized with saturated NaHCO_3 . The mixture was extracted 5 times with EA (80 mL) and the combined organic layers were washed twice with saturated NaHCO_3 (80 mL), to be finally dried over Na_2SO_4 . After filtration and the removal of the solvent, the product was purified by column chromatography (EA/CH 10:1, solid deposition from Celite, R_f = 0.4) to provide the target compound as a yellow oil (4.46 g, 66.7 %).

$^1\text{H NMR}$ (400 MHz, CDCl_3): δ = 6.45 (s, 2H), 5.20 (s, 2H), 5.03 (s, 1H), 3.60 (dt, J = 11.2, 5.9 Hz, 4H), 3.51 (qd, J = 6.0, 2.8 Hz, 4H), 3.44 (t, J = 5.1 Hz, 2H), 3.23 (d, J = 3.4 Hz, 2H), 2.80 (s, 2H), 1.37 (s, 9H) ppm. $^{13}\text{C NMR}$ (101 MHz, CDCl_3): δ = 176.0, 156.0, 136.6, 80.9, 79.3, 70.3, 70.0, 69.8, 67.2, 47.6, 40.5, 38.2, 28.4 ppm.

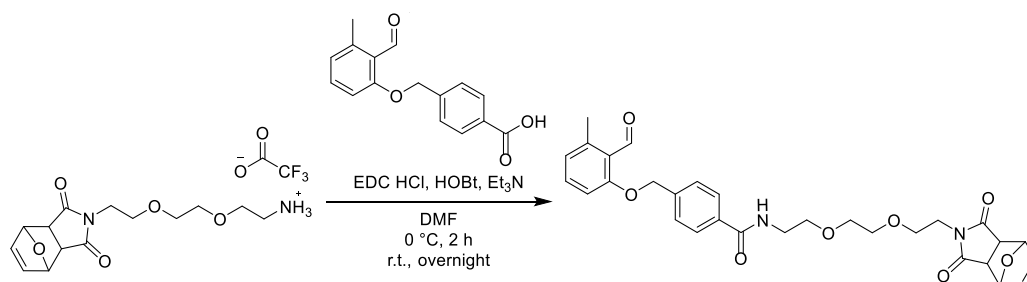
Synthesis of 2-(2-(2-(1,3-Dioxo-1,3,3,4,7,7-hexahydro-2H-4,7-epoxyisoindol-2-yl)ethoxy)ethoxy)-ethan aminium 2,2,2-trifluoroacetate



5. Experimental Section

All operations were conducted under argon atmosphere. Bock protected maleimide (1.98 g, 5.00 mmol, 1.00 eq.) was dissolved in dry DCM (230 mL) and cooled to 0 °C. TFA (14.6 mL, 160 mmol, 32 eq.) was slowly added and the reaction mixture was stirred for 2.5 h. The solvent and TFA were subsequently removed *in vacuo* at 20 °C by threefold dissolution of the residue in DCM and subsequent evaporation. The resulting residue was weighed in order to quantify the excess amount of residual TFA to determine the excess amount of Et₃N necessary for the next synthetic step. The product was directly employed for the next reaction without any further characterization.

Synthesis of *N*-(2-(2-(2-(1,3-Dioxo-1,3,3a,4,7,7a-hexahydro-2*H*-4,7-epoxyisoindol-2-yl)ethoxy)ethoxy)ethyl)-4-((2-formyl-3-methylphenoxy)methyl)benzamid 5b



All operations were conducted under argon atmosphere. 2-(2-(2-(1,3-Dioxo-1,3,3,4,7,7-hexahydro-2*H*-4,7-epoxyisoindol-2-yl)ethoxy)ethoxy)-ethan aminium 2,2,2-trifluoroacetate (2.06 g, 5.01 mmol, 1.00 eq.), 4-((2-formyl-3-methylphenoxy)methyl)-benzoic acid **12** (1.49 g, 5.51 mmol, 1.10 eq.) and HOBt (1.02 g, 7.62 mmol, 1.50 eq.) were dissolved in DMF (60 mL) and cooled to 0 °C. Subsequently, Et₃N (1.6 mL, 11.53 mmol, 2.30 eq.) and EDC·HCl (1.11 g, 3.75 mmol, 1.15 eq.) were added, the reaction mixture was stirred for 2 h at 0 °C and overnight at ambient temperature. Afterwards, the reaction mixture was diluted with EA (250 mL), washed twice with 1 N HCl (20 mL), twice with saturated NaHCO₃ (25 mL) and brine (50 mL). The organic layer was dried over MgSO₄ and the solvent was evaporated *in vacuo*. Purification was carried out by column chromatography (EA:Hex:MeOH 47.5:47.5:5, R_f = 0.36) to provide the product as a white solid (2.2 g, 80.3 %).

¹H NMR (400 MHz, CDCl₃): δ = 10.68 (s, 1H), 7.82 (d, *J* = 8.3 Hz, 2H), 7.44 (d, *J* = 8.3 Hz, 2H), 7.30 (t, *J* = 8.0 Hz, 1H), 6.96 (s, 1H), 6.81 (d, *J* = 8.4 Hz, 1H), 6.77 (d, *J* = 7.4 Hz, 1H), 6.38 (s, 2H), 5.20–5.06 (m, 4H), 3.67–3.44 (m, 12H), 2.73 (s, 2H), 2.52 (s, 3H) ppm. **¹³C NMR** (101 MHz, CDCl₃): δ = 192.1, 176.2, 167.0, 162.0, 142.3, 139.7, 136.5, 134.5, 134.4, 127.6, 127.1, 124.6, 123.7, 110.4, 80.9, 70.3, 70.0, 69.7, 69.7, 67.2, 47.5, 39.8, 38.2, 21.5 ppm. **MS** (ESI) *m/z*: [M + Na]⁺ calcd. for C₃₀H₃₂N₂O₈Na, 571.2050; found, 571.2089. Details of the ¹H NMR chemical shift assignments can be found in **Figure 21** (Section 3.1.2).

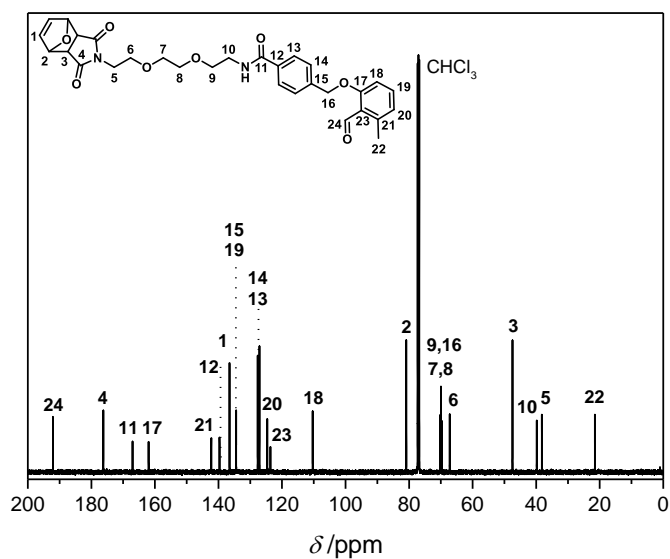


Figure S47. ^{13}C NMR spectrum of the photomonomer **5b** recorded in CDCl_3 at 101 MHz. For the resonance assignments refer to the depicted structure.

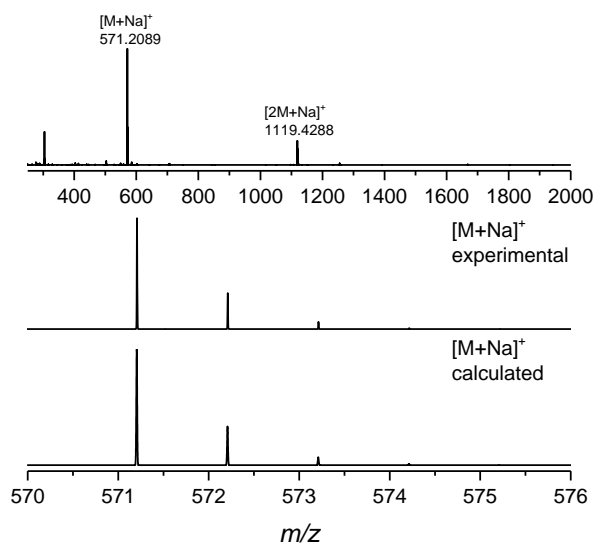


Figure S48. Full ESI-MS spectrum of the photomonomer **5b** (top) recorded in THF/MeOH (3:2). ESI-MS spectra of the photomonomer **5b** isotopic pattern (bottom). Recorded mass spectra shown are in excellent agreement with the calculated isotope pattern.

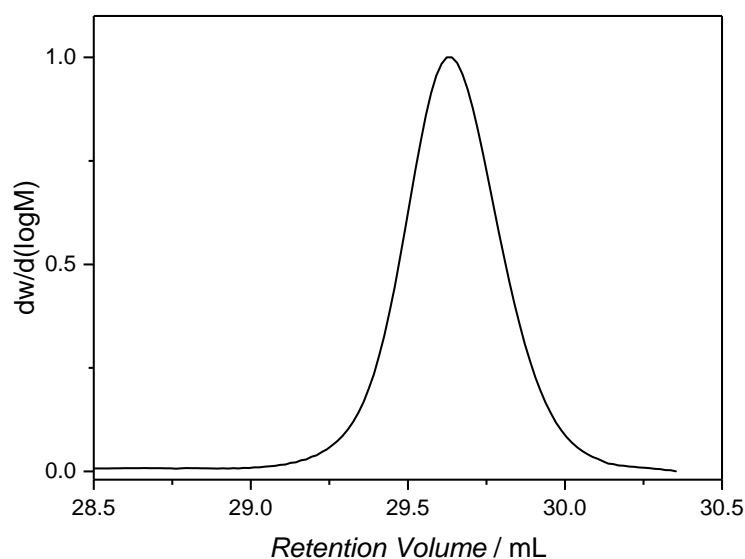


Figure S49. SEC trace of the photomonomer **5b** recorded in THF at 35 °C. ($\bar{M}_w = 1.01$, $V_p = 29.6$ mL).

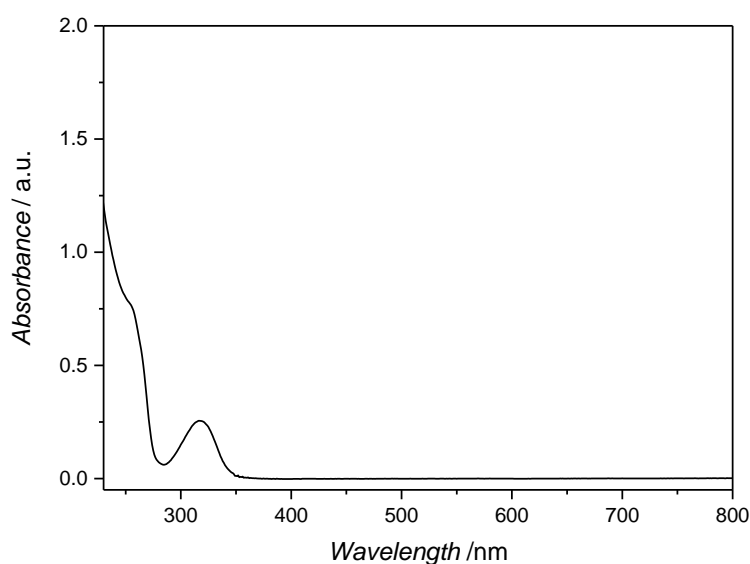
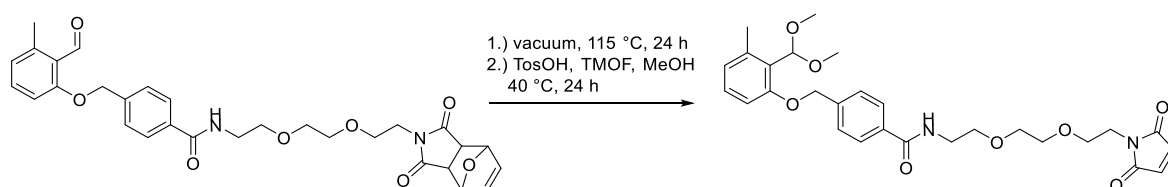


Figure S50. UV-Vis spectrum of the photomonomer **5b** in DCM (0.04 mg mL^{-1}).

Synthesis of 4-((2-(dimethoxymethyl)-3-methylphenoxy)methyl)-N-(2-(2-(2-(2,5-dioxo-2,5-dihydro-1H-pyrrol-1-yl)ethoxy)ethoxy)ethyl)benzamide **5b***



All operations were conducted under argon atmosphere and protected from light. **5b** (63.6 mg, 11.0 μmol , 1.00 eq.) was heated at 115 °C for 24 h under vacuum to quantitatively

remove the furan protecting group. The intermediate was employed for further modification without any purification. pTsOH (1.7 mg, 9.1 μmol , 0.08 eq.), TMOF (50 μL , 0.45 mmol, 4.00 eq.) and anhydrous MeOH (1.0 mL) were added to the furan deprotected compound. The suspension was heated to 40 $^{\circ}\text{C}$ and stirred for 24 h. The crude reaction mixture was filtrated over silica (DCM, 5 % Et_3N) and the solvent was removed under reduced pressure to provide a pink oil.

$^1\text{H NMR}$ (500 MHz, CDCl_3): δ = 7.84 (d, J = 8.2 Hz, 2H), 7.47 (d, J = 8.2 Hz, 2H), 7.10 (t, J = 7.9 Hz, 2H), 6.86 – 6.81 (m, 1H), 6.78 (d, J = 7.6 Hz, 1H), 6.72 (d, J = 8.1 Hz, 1H), 6.61 (s, 2H), 5.86 (s, 1H), 5.10 (s, 2H), 3.70 (t, J = 5.6 Hz, 2H), 3.67 – 3.56 (m, 10H), 3.39 (s, 6H), 2.48 (s, 3H) ppm.

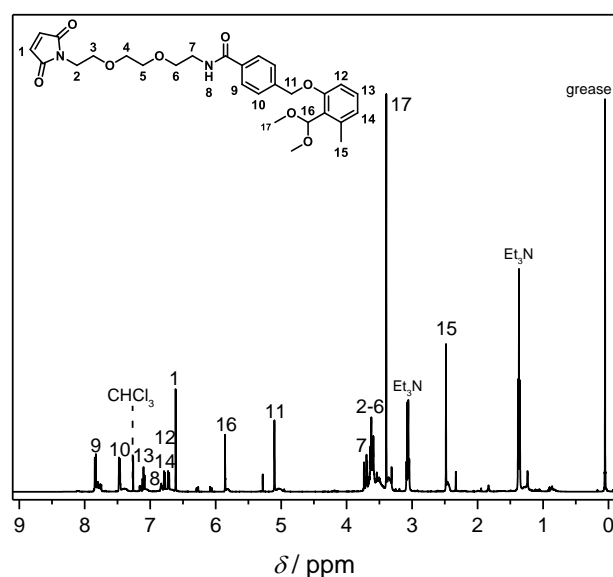
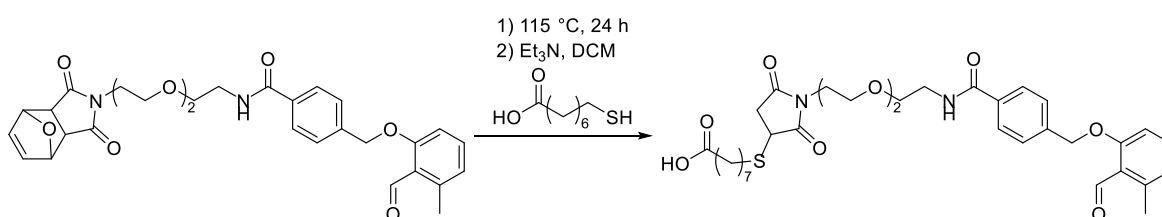


Figure S51. $^1\text{H NMR}$ spectrum of the photomonomer acetal **5b*** recorded in CDCl_3 at 500 MHz. For the resonance assignments refer to the depicted structure.

Synthesis of 8-((1-(2-(2-(2-(4-((2-formyl-3-methylphenoxy) methyl) benzamido) ethoxy) ethoxy) ethyl) -2,5-dioxopyrrolidin-3-yl) thio) octanoic acid **6b**



Photomonomer **5b** (430 mg, 0.83 mmol, 1.00 eq.) was heated to 115 $^{\circ}\text{C}$ for 24 h *in vacuo*. Without further purification, mercaptooctanoic acid (176 mg, 1.00 mmol, 1.20 eq.) and TEA (168 mg, 1.66 mmol, 2.00 eq.) were added and dissolved in DCM (20 mL). The reaction was allowed to stir overnight. The mixture was diluted with DCM (50 mL), washed with saturated NaHCO_3 solution (10 mL), water (10 mL) and dried over MgSO_4 . The solvent was removed under reduced pressure to yield the target compound as a brown oil (404 mg, 79.9 %).

5. Experimental Section

¹H NMR (400 MHz, CDCl₃): δ = 10.72 (s, 1H, CHO), 7.87 (d, ³J = 8.3 Hz, 2H, ArH), 7.49 (d, ³J = 8.2 Hz, 2H, ArH), 7.35 (dd, ³J = 8.4, 7.7 Hz, 1H, ArH), 7.03 (d, ³J = 5.7 Hz, 1H, NH), 6.86 (d, ³J = 8.4 Hz, 1H, ArH), 6.82 (d, ³J = 7.6 Hz, 1H, ArH), 5.20 (s, 2H, Ar-CH₂-O), 3.80 – 3.56 (m, 13H, CH₂-N, CH₂-O), 3.09 (dd, ³J = 18.7, 9.1 Hz, 1H, CH_{cis}-CO), 2.90 – 2.63 (m, 2H, CH₂-S), 2.57 (s, 3H, Ar-CH₃), 2.47 (dd, ³J = 18.6, 3.7 Hz, 1H, CH_{trans}-CO), 2.30 (t, ³J = 7.4 Hz, 2H, CH₂-COOH), 1.70 – 1.50 (m, 4H, CH₂), 1.44 – 1.17 (m, 6H, CH₂) ppm. **¹³C NMR** (100 MHz, CDCl₃): δ = 192.26 (CHO), 178.23 (COOH), 176.81 (N C O), 174.99 (N-C=O), 167.29 (HN-C=O), 162.10 (C_{Ar}-O), 142.36 (C_{Ar}-Me), 139.83 (C_{Ar}-CO), 134.57 (C_{Ar}-H), 134.35 (C_{Ar}-CH₂), 127.72 (C_{Ar}-H), 127.17 (C_{Ar}-H), 124.73 (C_{Ar}-H), 123.72 (C_{Ar}-CHO), 110.46 (C_{Ar}-H), 70.32 (CH₂-O), 70.05 (Ar-CH₂-O), 69.95 (CH₂-O), 69.90 (CH₂-O), 67.12 (CH₂-O), 39.93 (CH₂-NH), 39.26 (CH-S), 38.29 (CH₂-N), 36.26 (CH₂-CO), 33.99 (CH₂-COOH), 31.71 (CH₂-S), 28.89 (CH₂), 28.86 (CH₂), 28.72 (CH₂), 28.51 (CH₂), 24.68 (CH₂), 21.59 (Ar-CH₂) ppm. **MS** (ESI) *m/z*: [M + Na]⁺ calcd. for C₃₄H₄₄N₂O₉S, 679.2660; found 679.2657. Details of the ¹H NMR chemical shift assignments can be found in **Figure 22** (Section 3.1.2).

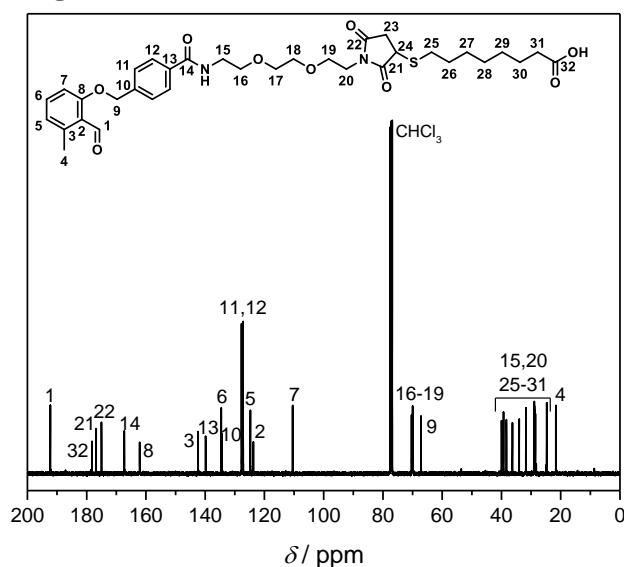


Figure S52. ¹³C NMR spectrum of the modified photomonomer **6b** recorded in CDCl₃ at 101 MHz. For the resonance assignments refer to the depicted structure.

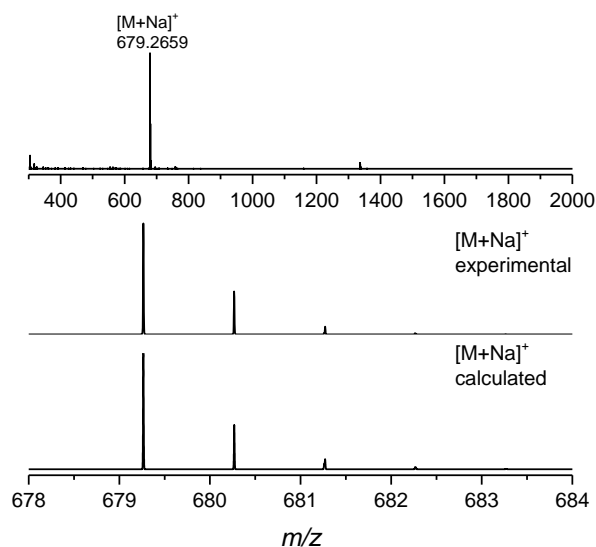
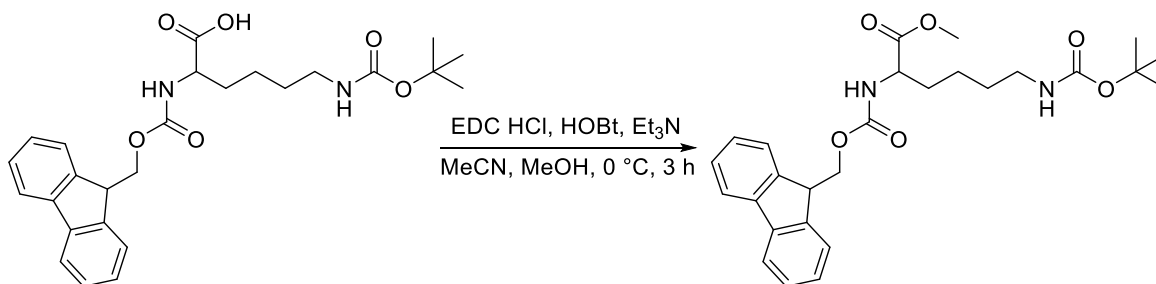


Figure S53. Full ESI-MS spectrum of the modified photomonomer **6b** (top) recorded in THF/MeOH (3:2). ESI-MS spectra of the modified photomonomer **6b** isotopic pattern (bottom). Recorded mass spectra shown are in excellent agreement with the calculated isotope pattern.

Synthesis of Methyl 2-(((9H-fluoren-9-yl)methoxy)carbonyl)amino)-6-((tert-butoxycarbonyl)-amino)hexanoate



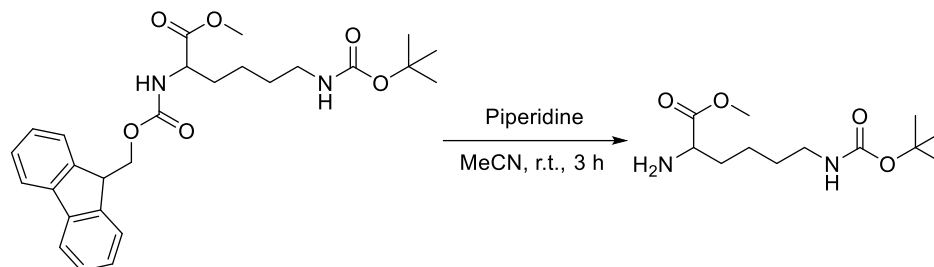
All operations were conducted under argon atmosphere. Lysine-Fmoc-NBoc (5.8 g, 12.4 mmol, 1.00 eq.) and HOBT (2.5 g, 18.5 mmol, 1.50 eq.) were dissolved in dry MeCN (60 mL) and cooled to 0 °C. Dry MeOH (50 mL) and Et₃N (2.6 mL, 20.5 mmol, 1.65 eq.) were added dropwise to the mixture. EDC·HCl (2.7 g, 14.1 mmol, 1.15 eq.) was dissolved in dry MeCN (40 mL) and dry MeOH (10 mL) and was subsequently added dropwise to the mixture. The reaction mixture was stirred for 3 h at 0 °C. Subsequently, the reaction mixture was allowed to warm to ambient temperature and was diluted with DCM (100 mL). The mixture was acidified with 0.25 N HCl (50 mL) and dispersed in saturated NaHCO₃ (50 mL) in order to precipitate a white solid. After filtration, the filtrate was washed once with saturated NaHCO₃ (50 mL) and the aqueous layer was extracted twice with DCM (50 mL). The combined organic layers were washed twice with brine (50 mL) and dried over MgSO₄. After filtration, the solvent was removed *in vacuo* to provide the product as a yellow oil. (Yield: 97.3 %, 5.81 g).

¹H NMR (500 MHz, CDCl₃): δ = 7.69 (d, J = 7.5 Hz, 2H), 7.53 (dd, J = 7.1, 3.6 Hz, 2H), 7.33 (t, J = 7.4 Hz, 2H), 7.24 (t, J = 6.9 Hz, 2H), 5.36 (d, J = 7.6 Hz, 1H), 4.51 (s, 1H), 4.39 – 4.24 (m, 3H), 4.15 (t, J = 7.0 Hz, 1H), 3.67 (s, 3H), 3.04 (d, J = 6.0 Hz, 2H), 1.78 (ddd, J = 15.5, 10.7, 5.5 Hz, 2H), 1.49 – 1.10 (m, 13H) ppm. ¹³C NMR (125 MHz, CDCl₃):

5. Experimental Section

$\delta = 173.1, 156.1, 156.0, 143.9, 141.3, 128.0, 127.1, 125.1, 120.0, 79.3, 67.0, 53.7, 52.5, 47.2, 40.1, 32.1, 29.6, 28.4, 22.4$ ppm.

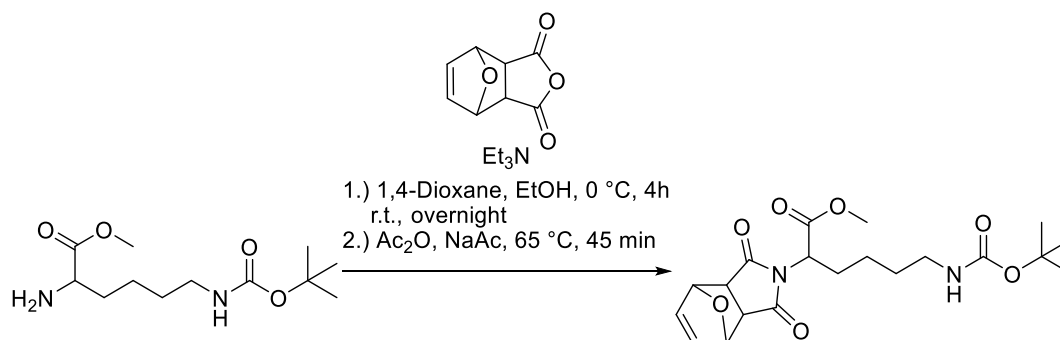
Synthesis of Methyl 2-amino-6-((tert-butoxycarbonyl)amino)hexanoate



All operations were conducted under argon atmosphere. Methyl 2-(((9H-fluoren-9-yl)methoxy)carbonyl)amino)-6-((tert-butoxycarbonyl)amino)hexanoate (5.81 g, 12.0 mmol, 1.00 eq.) was dissolved in dry MeCN (100 mL) under inert atmosphere. Piperidine (10 mL, 8.62 g, 101 mmol, 8.40 eq.) was added dropwise to the solution and the mixture was stirred for 3 h at ambient temperature. After removal of the solvent under reduced pressure, the crude product was purified by flash chromatography after solid deposition from DCM employing different eluents to remove side-products (Hex:EA 4:1, EA, DCM). The target compound was collected employing a gradient of DCM:MeOH from 98:2 to 95:5 (stained *via* KMnO_4). After evaporation of the solvent, the product was obtained as a yellow oil and was employed for the next reaction step without any further purification. (Yield: 84.0 %, 2.63 g).

$^1\text{H NMR}$ (500 MHz, CDCl_3): $\delta = 4.63$ (s, 1H), 3.71 (s, 3H), 3.45 (dd, $J = 7.4, 5.5$ Hz, 1H), 3.17 – 3.03 (m, 2H), 1.82 – 1.45 (m, 6H) ppm. $^{13}\text{C NMR}$ (125 MHz, CDCl_3): $\delta = 176.3, 156.0, 79.0, 54.3, 52.0, 40.3, 34.3, 29.8, 28.4, 22.8$ ppm.

Synthesis of Methyl 6-((tert-butoxycarbonyl)amino)-2-(1,3-dioxo-3a,4,7,7a-tetrahydro-1H-4,7-epoxyisoindol-2(3H)-yl)hexanoate

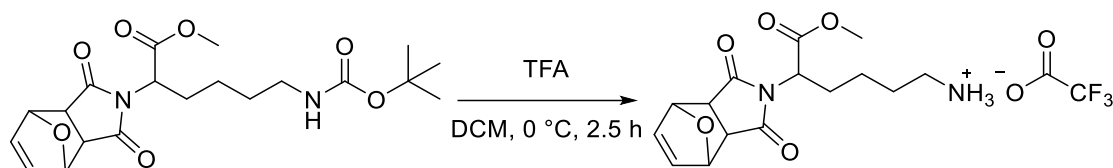


All operations were conducted under argon atmosphere. 3a,4,7,7a-Tetrahydro-4,7-epoxyisoindol-1,3-dione **2a** (2.01 g, 12.12 mmol, 1.20 eq.) was dissolved in a mixture of dry EtOH and 1,4-dioxane (4:1, 150 mL) (solution A) and methyl 2-amino-6-((tert-butoxycarbonyl)amino)hexanoate (2.63 g, 10.10 mmol, 1.00 eq.) in 30 mL of the same solvent mixture separately (solution B). The solutions were cooled to 0 °C and solution B was subsequently transferred dropwise to solution A. Et_3N (1.34 mL, 18.2 mmol, 1.80 eq.) was added dropwise and the reaction mixture was stirred for 4 h at 0 °C and overnight at ambient temperature. The target compound was obtained after purification *via* column chromatography (EA:Hex 50:50, solid deposition from DCM). Once the yellow fractions were separated, the

eluent mixture was changed to EA:Hex (60:40, $R_f = 0.5$, stained *via* KMnO_4). (Yield: 41.0 %, 1.7 g).

$^1\text{H NMR}$ (500 MHz, CDCl_3): $\delta = 6.46$ (s, 2H), 5.23 (d, $J = 3.7$ Hz, 2H), 4.64–4.50 (m, 2H), 3.65 (s, 3H), 2.98 (s, 1H), 2.84 (dd, $J = 24.2, 6.5$ Hz, 2H), 2.13 – 1.94 (m, 2H), 1.50 – 1.25 (m, 11H), 1.24 – 1.06 (m, 2H) ppm. $^{13}\text{C NMR}$ (125 MHz, CDCl_3): $\delta = 175.7, 175.4, 155.9, 136.5, 81.1, 79.0, 52.7, 52.5, 47.6, 47.1, 40.0, 29.0, 28.4, 27.3, 22.8$ ppm.

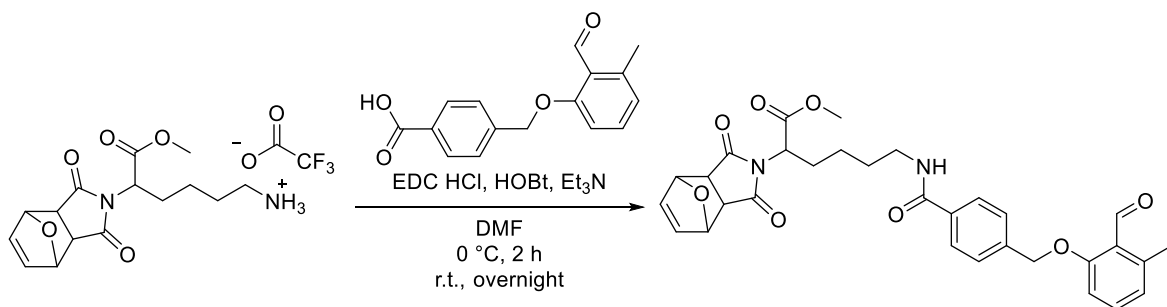
Synthesis of 5-(1,3-Dioxo-3a,4,7,7a-tetrahydro-1H-4,7-epoxyisoindol-2(3H)-yl)-6-methoxy-6-oxohexan-1-aminium 2,2,2-trifluoroacetate



All operations were conducted under argon atmosphere. Methyl 6-((tert-butoxycarbonyl)amino)-2-(1,3-dioxo-3a,4,7,7a-tetrahydro-1H-4,7-epoxyisoindol-2(3H)-yl)hexanoate (1.7 g, 4.16 mmol, 1.00 eq.) was dissolved in dry DCM (150 mL) and cooled to 0 °C. TFA (10.2 mL, 133.12 mmol, 32 eq.) dissolved in dry DCM (50 mL) was added dropwise (total concentration of TFA in the reaction mixture was 5 %) and the reaction mixture was stirred for 3 h at 0 °C. The solvent and TFA were subsequently removed *in vacuo* at ambient temperature by threefold dissolution of the residue in DCM (100 mL) and subsequent evaporation. The amount of TFA residue was determined gravimetrically. (Yield: 100 %, 1.76 g).

$^1\text{H NMR}$ (500 MHz, CDCl_3): $\delta = 7.16$ (s, 2H), 6.46 (s, 2H), 5.20 (s, 2H), 4.56 (t, $J = 7.6$ Hz, 1H), 3.65 (s, 3H), 3.11 – 2.76 (m, 4H), 2.90 (s, 2H), 2.13 – 1.88 (m, 2H), 1.59 (s, 2H), 1.31 – 1.12 (m, 3H) ppm. $^{13}\text{C NMR}$ (125 MHz, CDCl_3): $\delta = 176.3, 169.2, 136.5, 81.2, 53.0, 52.2, 47.6, 47.1, 40.1, 26.9, 26.2, 22.0$ ppm.

Synthesis of Methyl 2-(1,3-dioxo-3a,4,7,7a-tetrahydro-1H-4,7-epoxyisoindol-2(3H)-yl)-6-(4-((2-formyl-3-methylphenoxy)methyl)benzamido)hexanoate 19a



All operations were conducted under argon atmosphere. 5-(1,3-Dioxo-3a,4,7,7a-tetrahydro-1H-4,7-epoxyisoindol-2(3H)-yl)-6-methoxy-6-oxohexan-1-aminium 2,2,2-trifluoroacetate (1.76 g, 4.16 mmol, 1.00 eq.) was dissolved in dry DMF (30 mL), cooled to 0 °C and Et_3N (0.97 g, 9.56 mmol, 2.30 eq.) was added. 4-((2-formyl-3-methylphenoxy)methyl)-benzoic acid **12** (1.24 g, 4.58 mmol, 1.10 eq.) and HOBT (846 mg, 6.24 mmol, 1.50 eq.) were dissolved in dry DMF (30 mL), cooled to 0 °C and were added to the reaction mixture afterwards. Subsequently, EDC·HCl (916 mg, 4.78 mmol, 1.15 eq.) dissolved in dry DMF (20 mL), cooled to 0 °C was added dropwise and the reaction mixture was stirred for 2 h at

5. Experimental Section

0 °C and overnight at ambient temperature. The reaction mixture was diluted with DCM (250 mL), washed twice with saturated NaHCO₃ (50 mL) and brine (100 mL). The organic layer was dried over MgSO₄ and the solvent was evaporated *in vacuo*. The target compound was obtained as a yellow oil after purification by column chromatography (DCM:MeOH 98:2, R_f = 0.14). (Yield: 62 %, 1.45 g).

¹H NMR (500 MHz, CDCl₃): δ = 9.41 (s, 1H), 7.72 (d, J = 8.3 Hz, 2H), 7.37 (d, J = 8.2 Hz, 2H), 7.29 (t, J = 8.0 Hz, 1H), 6.85 – 6.73 (m, 2H), 6.41 (s, 2H), 6.34 – 6.22 (m, 1H), 5.12 (s, 4H), 4.60 (dd, J = 10.4, 5.3 Hz, 1H), 3.65 (s, 3H), 3.35 (dd, J = 12.3, 6.4 Hz, 2H), 2.81 (dd, J = 29.6, 6.5 Hz, 2H), 2.51 (s, 3H), 2.21 – 2.00 (m, 2H), 1.71 – 1.36 (m, 2H), 1.33 – 1.09 (m, 2H) ppm. **¹³C NMR** (125 MHz, CDCl₃): δ = 192.0, 175.7*, 175.4*, 169.0, 167.0, 161.9, 142.3, 139.5, 136.5, 134.6, 134.5, 127.5, 127.0, 124.7, 123.7, 110.4, 81.1, 70.0, 52.7, 52.5, 47.6*, 47.1*, 39.6, 28.5, 27.4, 23.0, 21.5 ppm. **UV-VIS**: λ_{max} 318 nm. **ESI-MS** (*m/z*): [M-Na]⁺ calcd. for C₃₁H₃₂N₂O₈Na, 583.2051; found, 583.2075. The signal marked with a * are split (refer to comment in the method description). Details of the ¹H NMR chemical shift assignments can be found in **Figure 41** (Section 3.3.1).

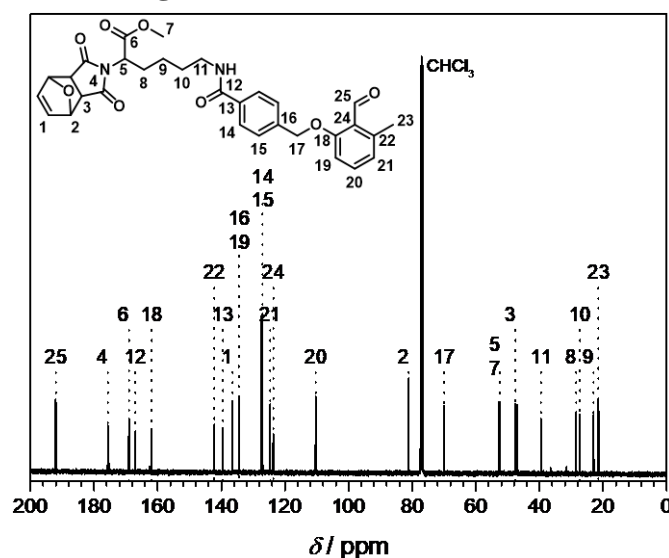


Figure S54. ¹³C NMR spectrum of the photomonomer **19a** recorded in CDCl₃ at 125 MHz. For the resonance assignments refer to the depicted structure.

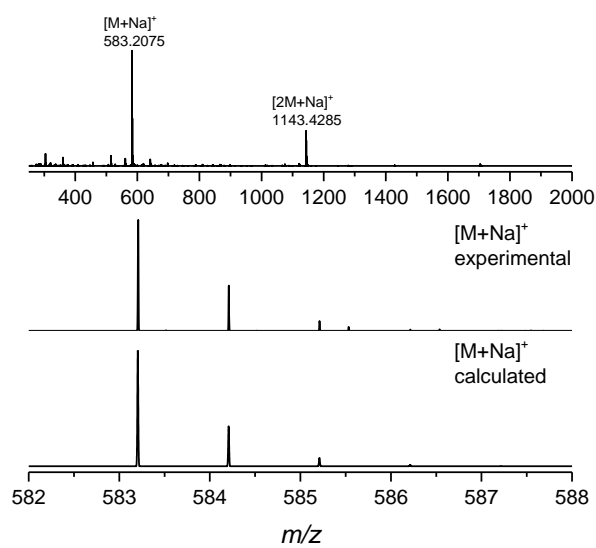


Figure S55. Full ESI-MS spectrum of the photomonomer **19a** (top) recorded in THF/MeOH (3:2). ESI-MS spectra of the photomonomer **19a** isotopic pattern (bottom). Recorded mass spectra shown are in excellent agreement with the calculated isotope pattern.

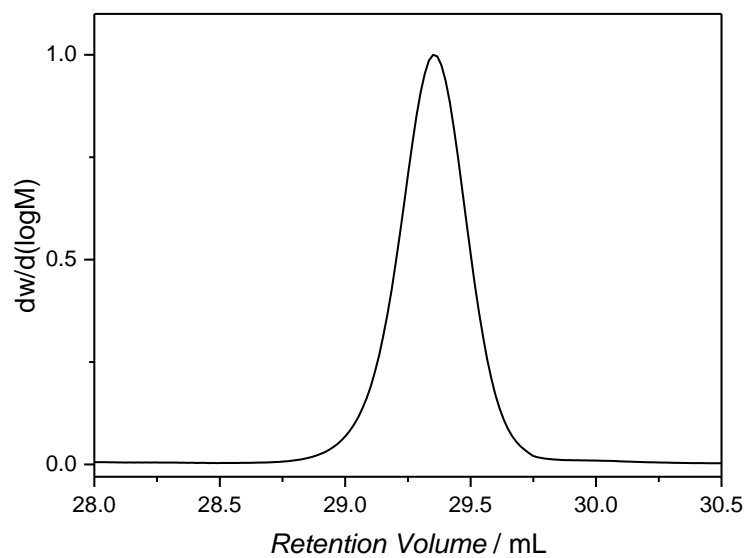


Figure S56. SEC trace of the photomonomer **19a** recorded in THF at 35 °C. ($D = 1.01$, $V_p = 29.4$ mL).

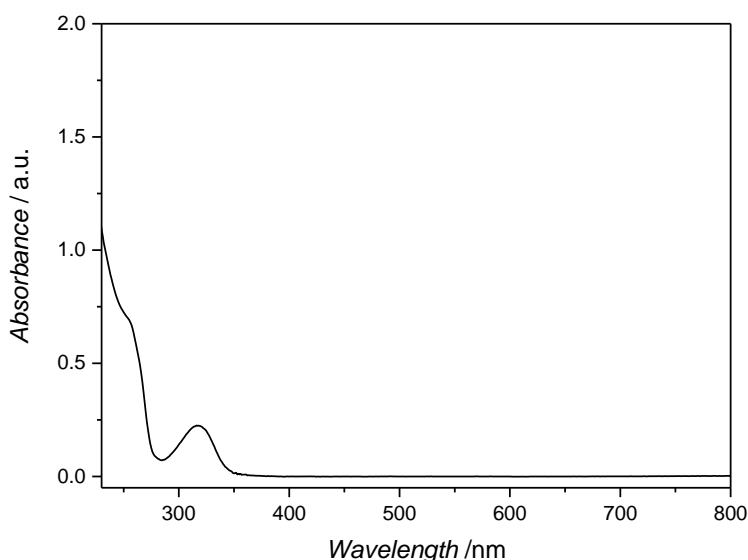
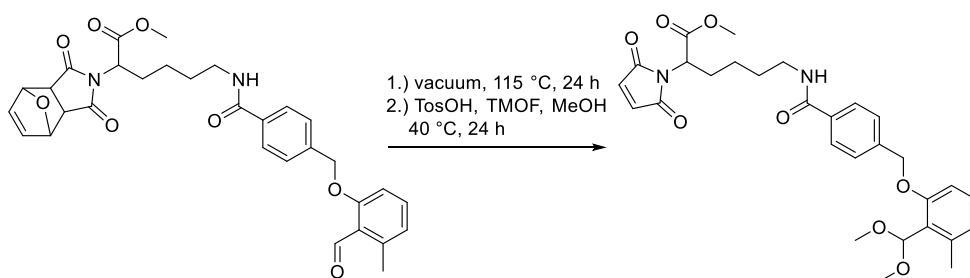


Figure S57. UV-Vis spectrum of the photomonomer **19a** in DCM (0.04 mg mL^{-1}).

Synthesis of Methyl 6-(4-((2-(dimethoxymethyl)-3-methylphenoxy)methyl)benzamido)-2-(2,5-dioxo-2,5-dihydro-1H-pyrrol-1-yl)hexanoate **19a***



All operations were conducted under argon atmosphere and protected from light. **19a** (52.4 mg, 95.5 μmol , 1.00 eq.) was heated to 115 $^{\circ}\text{C}$ for 24 h under vacuum to quantitatively remove the furan protecting group. The intermediate was employed for further modification without any purification. pTsOH (1.5 mg, 7.6 μmol , 0.08 eq.), TMOF (42 μL , 0.62 mmol, 4.00 eq.) and anhydrous MeOH (1.0 mL) were added to the furan deprotected compound. The suspension was heated to 40 $^{\circ}\text{C}$ and stirred for 24 h. The crude reaction mixture was filtrated over silica (DCM, 5 % Et_3N) and the solvent was removed under reduced pressure to provide a pink oil.

$^1\text{H NMR}$ (500 MHz, CDCl_3): δ = 7.87 – 7.69 (m, 3H), 7.49 (d, J = 8.1 Hz, 2H), 7.20 – 7.11 (m, 1H), 6.82 (d, J = 7.6 Hz, 1H), 6.75 (d, J = 8.3 Hz, 1H), 6.71 (s, 2H), 6.33 – 6.28 (m, 1H), 5.88 (s, 1H), 4.99 (s, 1H), 4.71 – 4.64 (m, 2H), 3.74 (d, J = 3.4 Hz, 1H), 3.43 (s, 3H), 3.34 (s, 6H), 2.52 (s, 3H), 2.23 – 2.05 (m, 2H), 1.78 – 1.56 (m, 2H), 1.40 – 1.29 (m, 2H) ppm.

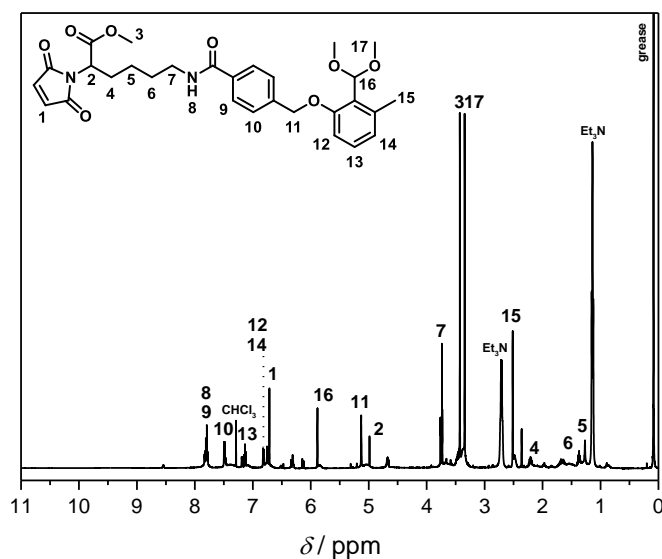
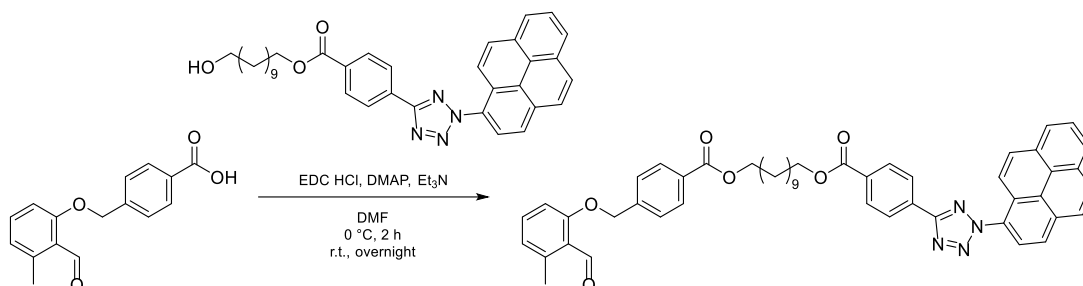


Figure S58. ^1H NMR spectrum of the photomonomer acetal **19a*** recorded in CDCl_3 at 500 MHz. For the resonance assignments refer to the depicted structure.

Synthesis of 11-((4-((2-formyl-3-methylphenoxy)methyl)benzoyl)oxy)undecyl 4-(2-pyren-1-yl)-2H-tetrazol-5-yl)benzoate **13**



All operations were conducted under nitrogen atmosphere. PAT **11** (0.95 g, 1.69 mmol, 1.00 eq.), 4-((2-formyl-3-methylphenoxy)methyl)benzoic acid **12** (0.55 g, 2.03 mmol, 1.20 eq.) and DMAP (104.0 mg, 0.85 mmol, 0.50 eq.) were dissolved in anhydrous DMF (30 mL) and cooled to 0 °C. Subsequently, EDC·HCl (0.65 g, 3.39 mmol, 2.00 eq.) and Et_3N (0.47 mL, 343.0 mg, 3.39 mmol, 2.00 eq.) were added and the reaction mixture was stirred for 30 min at 0 °C and for 72 h at 35 °C. The reaction mixture was diluted with EA (80 mL) and washed with 1 N HCl (70 mL), NaHCO_3 (70 mL) and brine (70 mL). The organic layer was dried over MgSO_4 and the solvent was evaporated in *vacuo*. The crude product was purified *via* flash chromatography using an aluminum oxide flash column (Puriflash alumina, N 32/63 μm , F0040) employing a gradient of CH/DCM (20 mL min^{-1}) as eluent. UV-Vis detection was turned off for the purification. Isocratic phases of a constant EA content have been applied at 10 (6 CV), 25 (7 CV), 35 (7 CV), 50 (5 CV) and 100 % (2 CV). The product was eluted in the range between 7 and 22 CV yielding 825 mg of a brown solid (60 %). The product is light sensitive and was stored protected from light.

^1H NMR (400 MHz, CDCl_3): δ = 10.63 (s, 1H), 8.38 – 7.89 (m, 15H), 7.35 (d, J = 8.2 Hz, 2H), 7.21 (t, J = 8.0 Hz, 1H), 6.70 (d, J = 8.0 Hz, 2H), 5.05 (s, 2H), 4.25 (dt, J = 22.2, 6.7 Hz, 4H), 2.47 (s, 3H), 1.80 – 1.59 (m, 4H), 1.54 – 1.03 (m, 16H) ppm. ^{13}C NMR (101 MHz, CDCl_3): δ = 192.13, 166.41, 166.26, 164.72, 162.04, 142.43, 141.32, 134.51, 132.97, 132.46,

5. Experimental Section

131.35, 131.28, 130.74, 130.50, 130.41, 130.26, 130.24, 130.10, 129.54, 127.20, 127.15, 127.05, 126.93, 126.86, 126.48, 125.31, 125.18, 124.96, 124.81, 124.26, 123.81, 122.89, 121.57, 110.43, 70.07, 65.64, 65.39, 29.64, 29.42, 28.87, 26.20, 21.63 ppm. **MS** (ESI) m/z : $[M + Na]^+$ calcd. for $C_{51}H_{48}N_4O_6$, 835.3466; found 835.3469. Details of the 1H NMR chemical shift assignments can be found in **Figure 30** (Section 3.2.1).

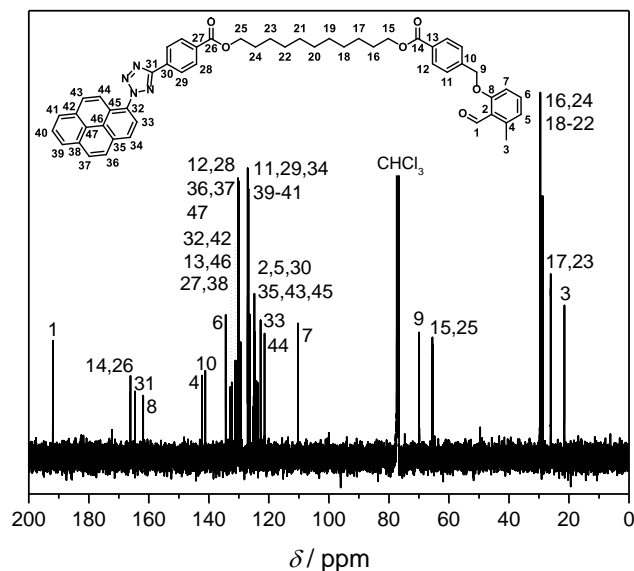


Figure S59. ^{13}C NMR spectrum of the monomer **13** recorded in $CDCl_3$ at 101 MHz. For the resonance assignments refer to the depicted structure.

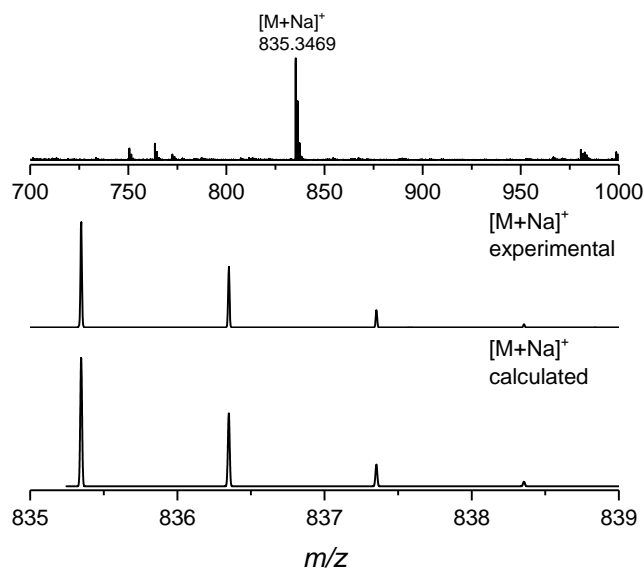


Figure S60. Mass spectrum of the monomer **13** recorded in THF/MeOH (3:2). ESI-MS spectra of the monomer **13** isotopic pattern (bottom). Recorded mass spectra shown are in excellent agreement with the calculated isotope pattern.

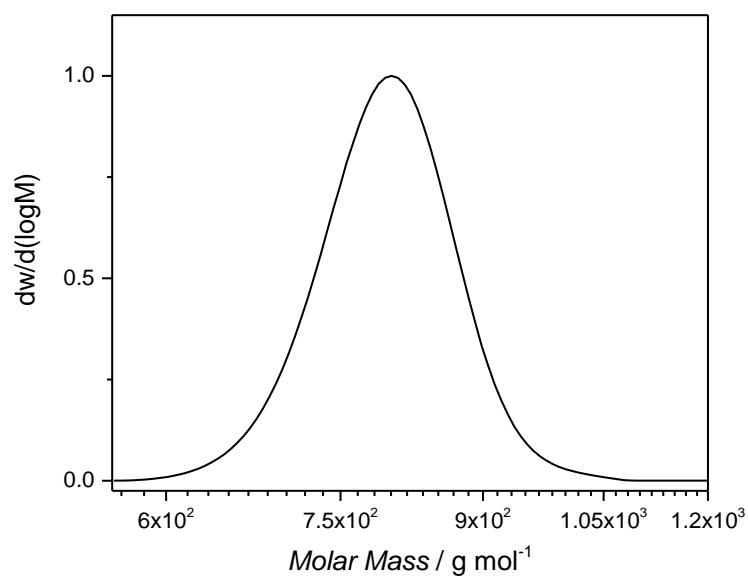


Figure S61. SEC trace of the monomer **13** recorded in THF at 35 °C. ($\bar{D} = 1.01$, $M_n = 870$ g mol⁻¹).

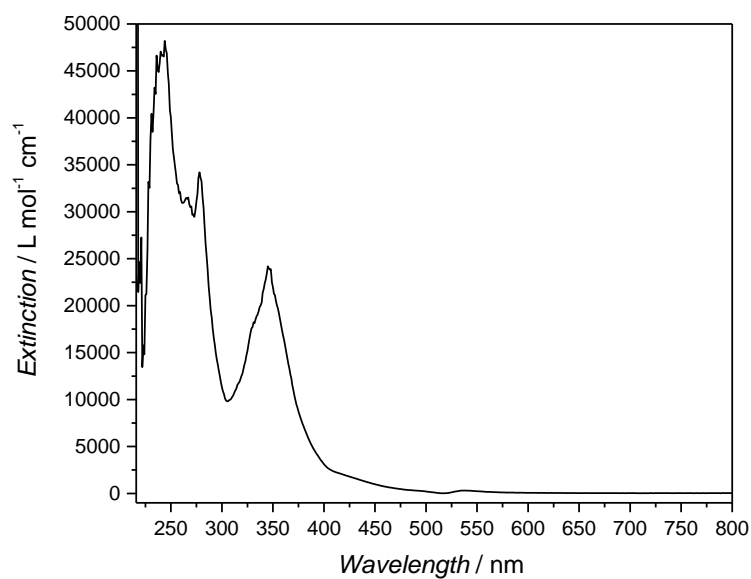


Figure S62. UV-Vis spectrum of the monomer **13** recorded in DCM ($7.38 \cdot 10^{-5}$ mol L⁻¹).

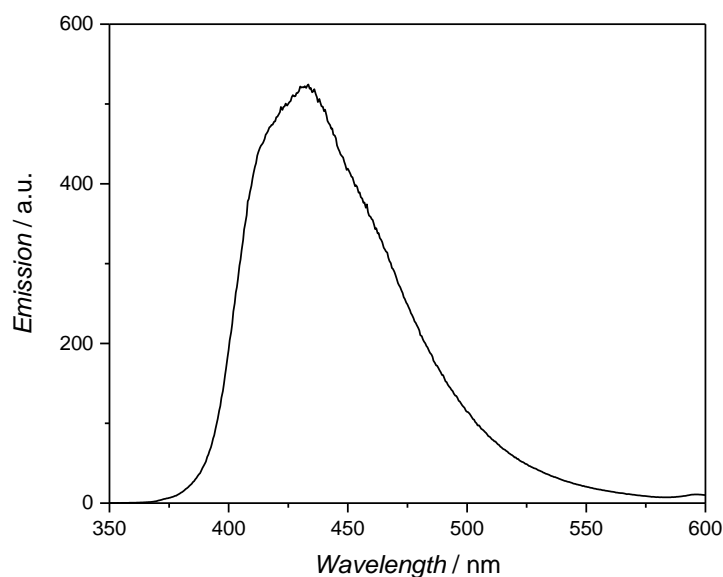
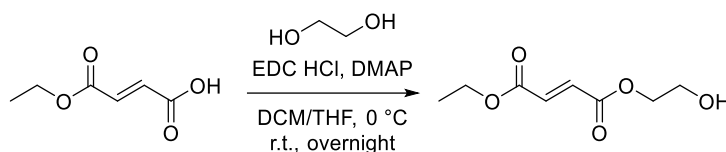


Figure S63. Fluorescence spectrum of the monomer **13** recorded in DCM ($7.38 \cdot 10^{-5}$ mol L⁻¹) at 300 nm (Excitation).

Synthesis of ethyl (2-hydroxyethyl) fumarate **14a**^[261]



In a round bottom flask monoethyl fumarate (2.00 g, 13.88 mmol, 1.00 eq.), ethylene glycol (8.61 g 138.77 mmol, 10.00 eq.) and 4-(*N,N*-dimethylamino) pyridine (DMAP) (339 mg 2.78 mmol, 0.20 eq.) were dissolved in a mixture of dry DCM and dry THF (3:1, 27 mL 9 mL). The solution was cooled to 0°C and EDC·HCl (3.19 g, 16.65 mmol, 1.20 eq.) was added. The solution was allowed to reach ambient temperature and left to stir overnight. After the reaction, the solvent was evaporated under reduced pressure. Subsequently, the crude product was dissolved in EA and washed with 5 % hydrochloric acid, saturated NaHCO₃ solution and brine. The combined organic phase was dried over MgSO₄ and the solvent was removed under reduced pressure. The crude product was purified by column chromatography (silica gel, CH/EA, 1/1) to obtain 2.01 g of a colorless oil (77 %).

¹H NMR (400 MHz, CDCl₃): δ = 6.87 (s, 2H), 4.35 – 4.30 (m, 2H), 4.25 (q, J = 7.1 Hz, 2H), 3.90 – 3.84 (m, 2H), 2.12 (s, 1H), 1.30 (t, J = 7.1 Hz, 3H) ppm. **¹³C NMR** (101 MHz, CDCl₃): δ = 165.3 (HC=CH), 165.0 (HC=CH), 134.5 (C=O), 133.1 (C=O), 67.0 (HOCH₂-CH₂-C=O), 61.6 (CH₃-CH₂-C=O), 61.1 (HOCH₂-CH₂-C=O), 14.2 (CH₃-CH₂-C=O) ppm. **MS** (ESI) m/z : [M + Na]⁺ calcd. for C₈H₁₂O₅, 211.0577; found 211.0578.

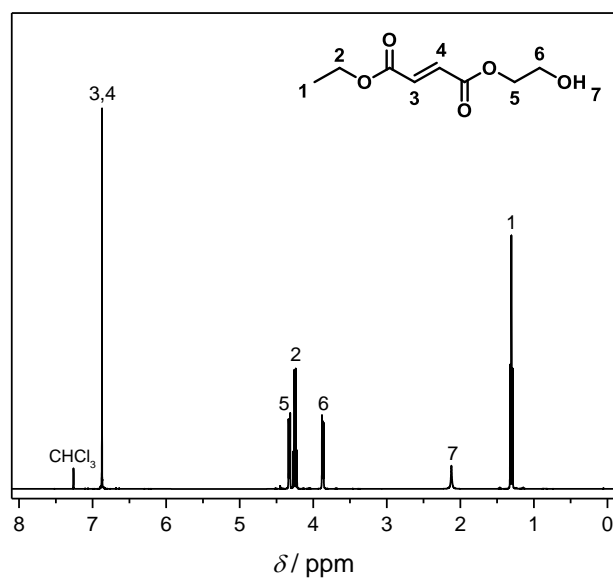


Figure S64. ¹H NMR spectrum of ethyl (2-hydroxyethyl) fumarate **14a** recorded in CDCl₃ at 400 MHz. For the resonance assignments refer to the depicted structure.

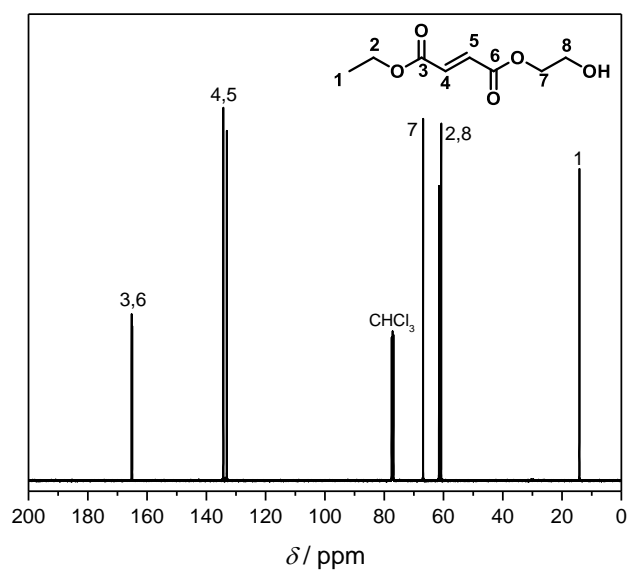


Figure S65. ¹³C NMR spectrum of ethyl (2-hydroxyethyl) fumarate **14a** recorded in CDCl₃ at 101 MHz. For the resonance assignments refer to the depicted structure.

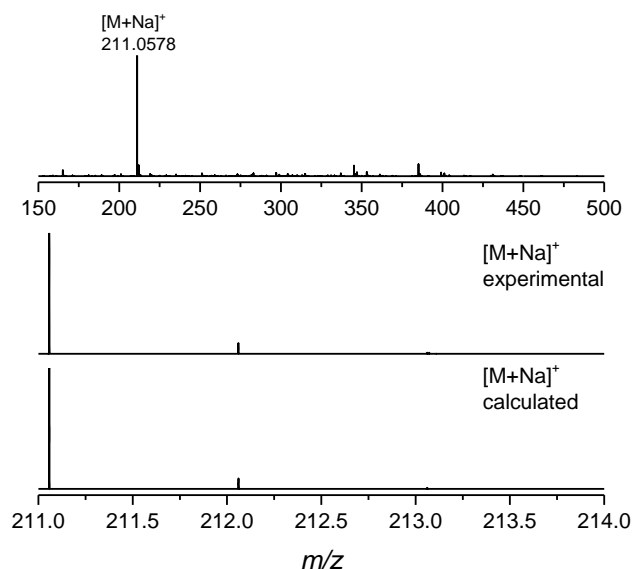
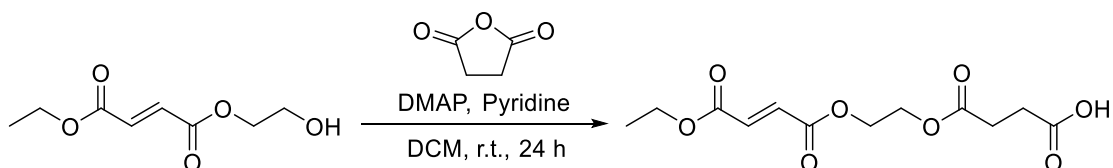


Figure S66. Mass spectrum of ethyl (2-hydroxyethyl) fumarate **14a** recorded in THF/MeOH (3:2).

Synthesis of 4-(2-((4-ethoxy-4-oxobut-2-enoyl)oxy)ethoxy)-4-oxobutanoic acid **14**



A mixture of ethyl (2-hydroxyethyl) fumarate **14a** (1.42 g, 7.56 mmol, 1.00 eq.), succinic anhydride (3.03 g, 30.02 mmol, 4.00 eq.), and DMAP (0.92 g, 7.56 mmol, 1.00 eq.) was placed in a 250 mL Schleck flask and dissolved in anhydrous DCM (75 mL). Pyridine (3.06 mL, 2.99 g, 37.80 mmol, 5.00 eq.) was added and the reaction was stirred for 24 h at ambient temperature. The reaction mixture was poured into an ice/water mixture and warmed to ambient temperature. The organic layer was separated and the aqueous layer was extracted with DCM (2x100 mL). The combined organic layers were washed with 5 % HCl, sat. NaHCO₃, brine, dried over MgSO₄, filtered and concentrated in *vacuo* to yield 2.07 g of the title compound as a white solid (95 %).

¹H NMR (400 MHz, CDCl₃): δ = 6.85 (d, *J* = 1.6 Hz, 2H), 4.42 – 4.33 (m, 4H), 4.25 (q, *J* = 7.1 Hz, 2H), 2.71 – 2.62 (m, 4H), 1.31 (t, *J* = 7.1 Hz, 3H) ppm. **¹³C NMR** (101 MHz, CDCl₃) δ: δ = 177.65, 172.02, 165.01, 164.83, 134.48, 132.93, 77.48, 77.16, 76.84, 63.01, 62.31, 61.59, 28.87, 28.81, 14.19 ppm. **MS** (ESI) *m/z*: [M + Na]⁺ calcd. for C₁₂H₁₆O₈, 311.0737; found 311.0736. Details of the ¹H NMR and ¹³C NMR chemical shift assignments can be found in **Figure 31** (Section 3.2.1).

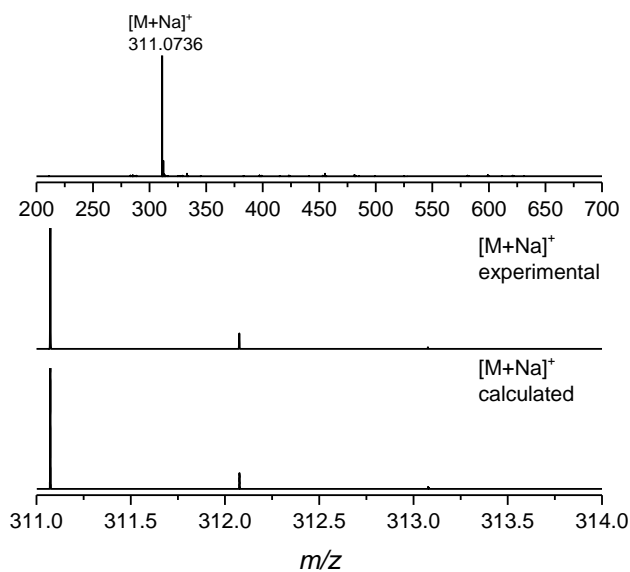


Figure S67. Mass spectrum of the monomer **14** recorded in THF/MeOH (3:2). ESI-MS spectra of the monomer **14** isotopic pattern (bottom). Recorded mass spectra shown are in excellent agreement with the calculated isotope pattern.

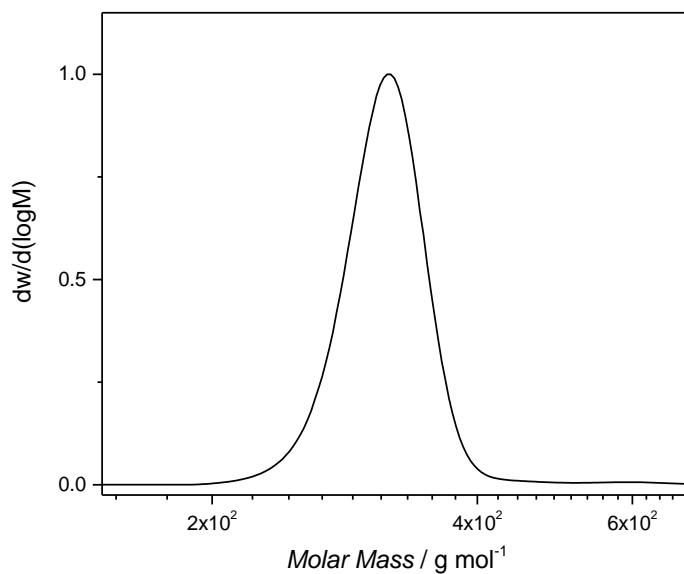


Figure S68. SEC trace of monomer **14** recorded in THF at 35 °C. ($\bar{M}_w/\bar{M}_n = 1.01$, $M_n = 310$ g mol⁻¹).

was removed under reduced pressure and the residue was dissolved in saturated NaHCO_3 solution (40 mL). After acidifying the mixture to $\text{pH} = 1$ using HCl , the aqueous phase was extracted with CHCl_3 (3x60 mL). The organic layers were combined, washed with brine (80 mL) and dried over MgSO_4 . The crude product was purified by flash chromatography using cyclohexane and a gradient of ethyl acetate yielding 1.52 g of a pale yellow oil (75 %).

^1H NMR (400 MHz, CDCl_3): $\delta = 4.31 - 4.22$ (m, 4H), $3.73 - 3.60$ (m, 12H), $2.72 - 2.58$ (m, 8H) ppm. ^{13}C NMR (101 MHz, CDCl_3): $\delta = 177.00, 172.27, 77.16, 70.65, 70.54, 69.08, 63.93, 29.20, 29.11$ ppm. MS (ESI) m/z : $[\text{M} + \text{Na}]^+$ calcd for $\text{C}_{16}\text{H}_{26}\text{O}_{11}$, 417.1367; found 417.1364. Details of the ^1H NMR and ^{13}C NMR chemical shift assignments can be found in **Figure 32** (Section 3.2.1).

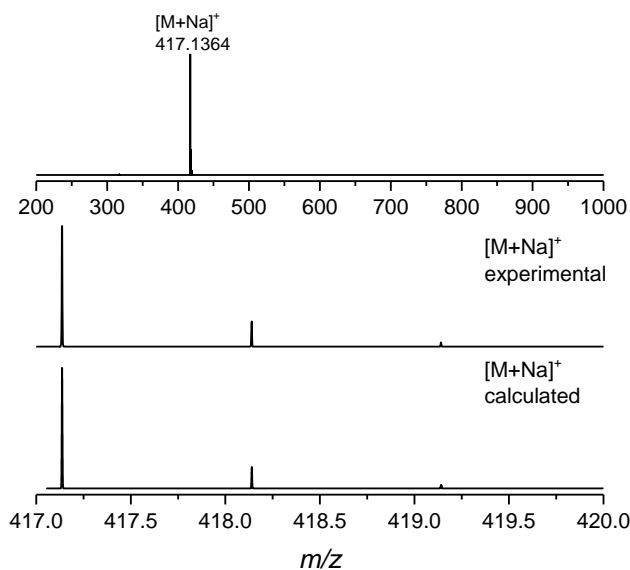


Figure S71. Mass spectrum of the core unit **15** recorded in THF/MeOH (3:2). ESI-MS spectra of the core unit **15** isotopic pattern (bottom). Recorded mass spectra shown are in excellent agreement with the calculated isotope pattern.

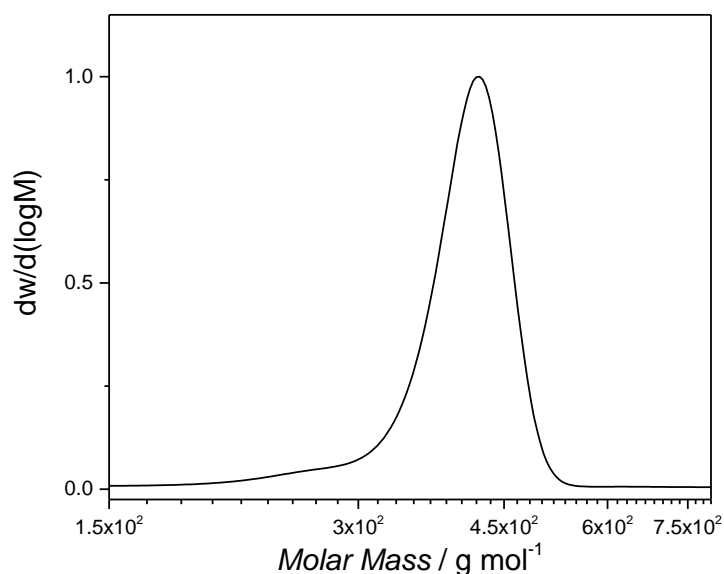


Figure S72. SEC trace of the core unit **15** recorded in THF at 35°C . ($\bar{M}_n = 400$ g mol^{-1}).

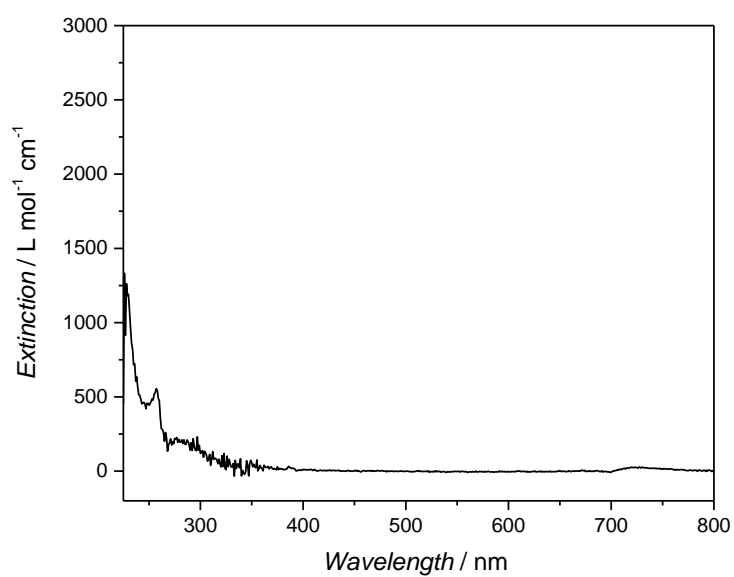


Figure S73. UV-Vis spectrum of the core unit **15** recorded in DCM ($1.27 \cdot 10^{-4}$ mol L⁻¹).

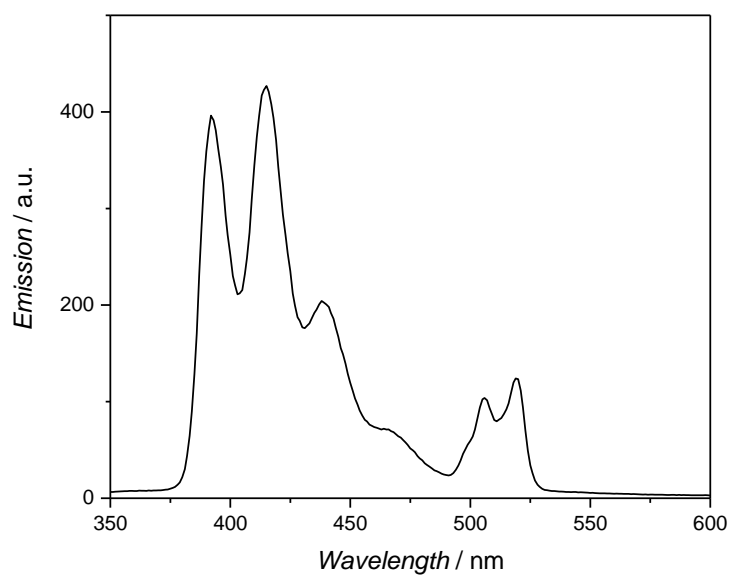
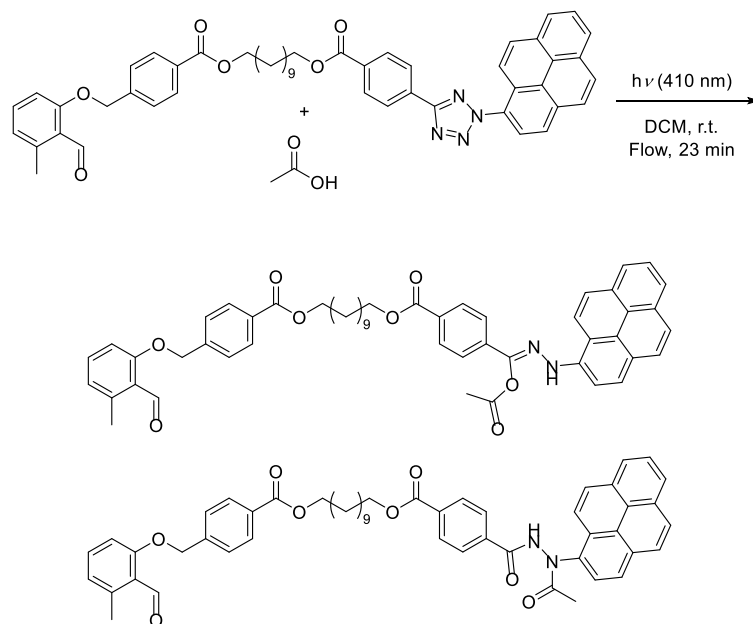


Figure S74. Fluorescence spectrum of the core unit **15** recorded in DCM ($1.27 \cdot 10^{-4}$ mol L⁻¹) at 255 nm (Excitation).

5.3.4. Photoreactions

5.3.4.1. Photoreactions of the Test Systems

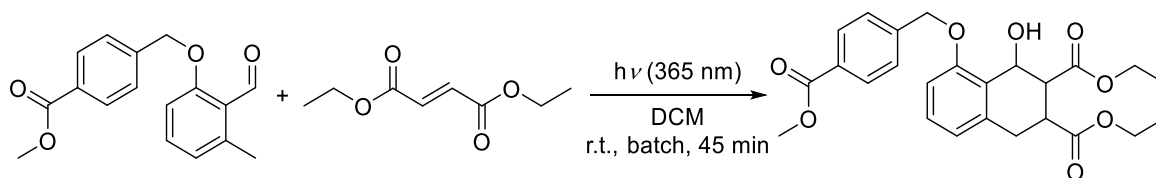
NICAL Test Reaction of the Photomonomer **13** and Acetic Acid



Photomonomer **13** (10.0 mg, 12.3 μmol , 1.00 eq.) was dissolved with acetic acid (5 μL , 4.8 mg, 8.0 μmol , 6.50 eq.) in 80 mL DCM and the reaction mixture was irradiated in a custom build flow reactor (7 mL reactor volume) using LEDs (3 x 410 nm, 0.3 mL min^{-1} , residence time 23 min, peristaltic pump) as light source after purging the reactor with anhydrous DCM under nitrogen atmosphere. Afterwards, the solvent was removed under reduced pressure and the crude product was analyzed without any purification.

Details of the ^1H NMR chemical shift assignments can be found in **Figure 34** (Section 3.2.2).

DA Test Reaction of *o*-MBA **12c** and Diethyl Fumarate **17**



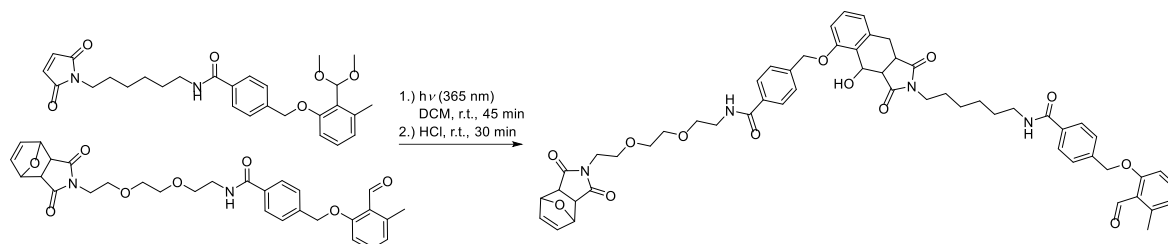
Methyl 4-((2-formyl-3-methylphenoxy)methyl)benzoate **12c** (22.4 mg, 0.078 mmol, 1.00 eq.) and diethyl fumarate **17** (27.1 mg, 0.16 mmol, 2.00 eq.) were dissolved in anhydrous DCM (20 mL) under nitrogen atmosphere. Afterwards, the reaction mixture was transferred into degassed head space vials and the solution was purged for 5 min with nitrogen. The reaction mixture was irradiated at room temperature in a custom build photoreactor using PL-L mercury lamps (3 x 365 nm). DCM was removed under reduced pressure and the crude product was analyzed without any purification.

Details of the ^1H NMR chemical shift assignments can be found in **Figure 35** (Section 3.2.2).

5.3.5. Synthesis of Sequence-Defined Macromolecules

5.3.5.1. Combination Approach for the Synthesis of Sequence-Defined Macromolecules Based on P-3CR and *o*-MBAs

Synthesis of Photodimer 7



All operations were conducted under argon atmosphere. Photomonomer **5b** (237 mg, 433 μmol , 1.05 eq.) was added to the furan deprotected and acetal protected monomer **5a*** (204 mg, 412 μmol , 1.00 eq.) and was dissolved in anhydrous DCM (150 mL, 5.0 mmol L^{-1}). The monomer solution was subsequently filled into sealed and previously degassed head space vials (10 mL) and purged for 5 minutes with argon, to be finally exposed to UV-light (PL-L, 365 nm) for 45 minutes (batch conditions). After irradiation, the single fractions were gathered and the solvent was removed under reduced pressure. The purification was performed *via* reverse phase flash chromatography (SNAP C18 12 g, 12 mL min^{-1}) with Milli-Q water and a THF gradient of 1.0 % per CV. Isocratic phases of a constant THF content have been applied at 20, 25, 30, 35 % (5 CV respectively), and 40 % (35 CV). The product was eluted as the THF content reached 40 % in the mobile phase. After acidic workup with 0.5 M HCl for 30 min the aldehyde functionality was regenerated (301 mg, 68.3 %).

$^1\text{H NMR}$ (400 MHz, CDCl_3): δ = 10.72 (s, 1H), 7.71–7.65 (m, 4H), 7.36 (dd, J = 8.2, 1.9 Hz, 3H), 7.29 (d, J = 8.1 Hz, 2H), 7.16 (t, J = 7.9 Hz, 1H), 6.90–6.70 (m, 4H), 6.47 (d, J = 1.0 Hz, 2H), 5.89 (d, J = 3.3 Hz, 1H), 5.53 (ddd, J = 15.3, 5.1, 1.8 Hz, 1H), 5.22 (d, J = 1.0 Hz, 2H), 5.14 (s, 2H), 5.05–4.88 (m, 2H), 4.06–3.13 (m, 20H), 2.81 (s, 2H), 2.57 (s, 3H), 2.16–1.18 (m, 10H) ppm. **MS** (ESI) m/z : $[\text{M} + \text{Na}]^+$ calcd. for $\text{C}_{56}\text{H}_{60}\text{N}_4\text{O}_{13}\text{Na}$, 1019.4049; found, 1019.4074. Details of the $^1\text{H NMR}$ chemical shift assignments can be found in **Figure 23** (Section 3.1.2).

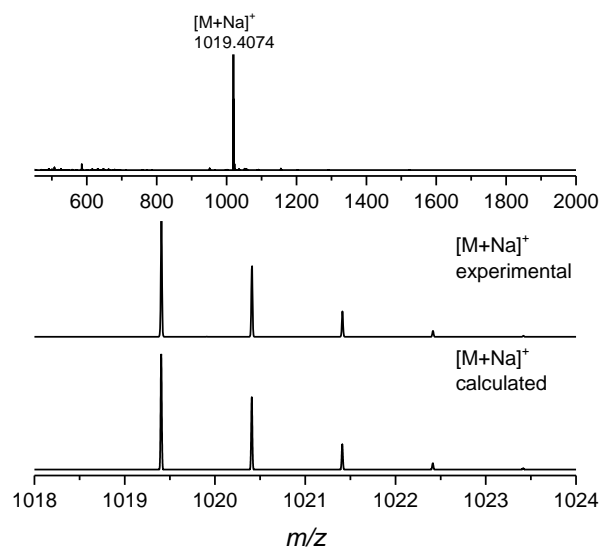


Figure S75. Full ESI-MS spectrum of the photodimer **7** (top) recorded in THF/MeOH (3:2). ESI-MS spectra of the photodimer **7** isotopic pattern (bottom). Recorded mass spectra shown are in excellent agreement with the calculated isotope pattern.

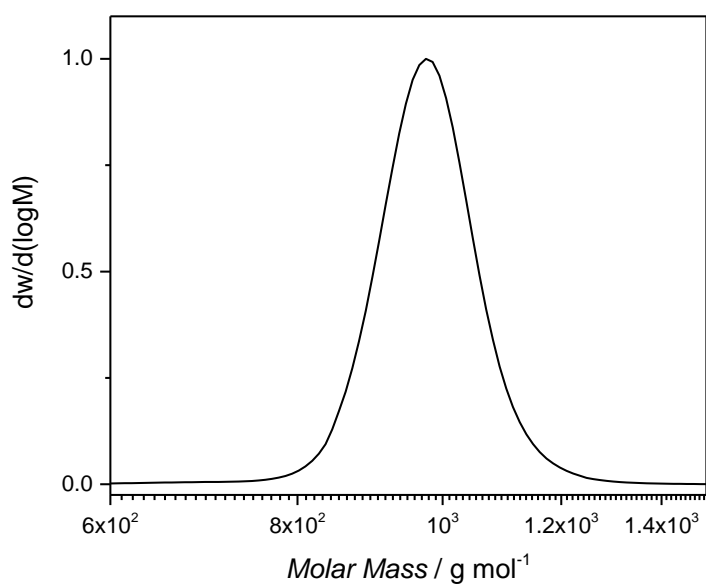
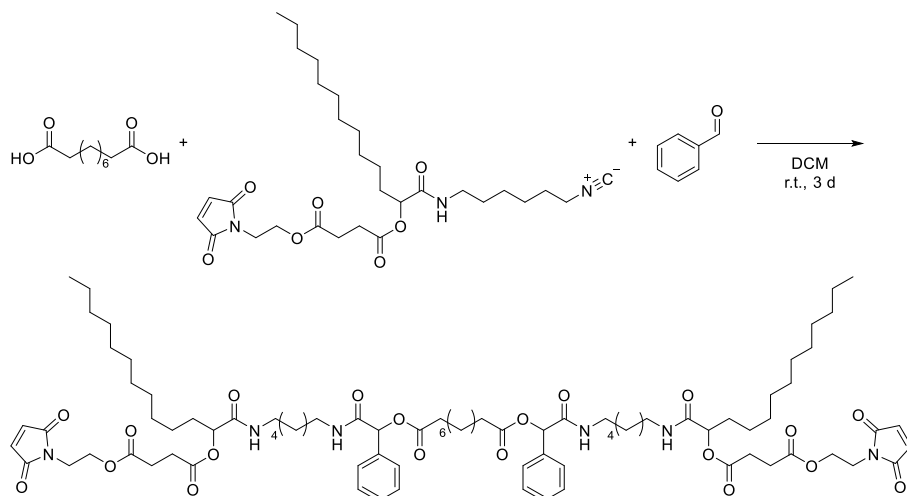


Figure S76. SEC trace of the photodimer **7** recorded in THF at 35 °C. ($D = 1.01$, $M_n = 980\ g\ mol^{-1}$).

Synthesis of the Symmetric Tetra-Substituted Oligomer **9**



Sebacic acid **8** (74.6 mg, 0.37 mmol, 1.00 eq.) was suspended in DCM (0.7 mL, 0.5 M). Subsequently, benzaldehyde **3b** (0.13 mL, 141 mg, 1.33 mmol, 3.60 eq.) and the lauric aldehyde-linker **1a** (621 mg, 1.11 mmol, 3.00 eq.) were added and the reaction mixture was stirred at room temperature for 3 d. The solvent was removed under reduced pressure. Purification was performed *via* flash column chromatography (Puriflash, 12 g, 30 mL min⁻¹) with CH and a EA gradient of 1.7 % per column volume (CV). Isocratic phases of a constant EA content were applied at 17, 33, 50, 67 and 100 % (10 CV respectively). The target compound was obtained as a white solid (381 mg, 67.2 %).

¹H NMR (400 MHz, CDCl₃): δ = 7.43–7.26 (m, 10H, Ar H), 6.67 (s, 4H, CH-CH), 6.58 (t, *J* = 3.1 Hz, 2H, NH), 6.48 (s, 2H, NH), 6.00 (s, 2H, Ar-CH-O), 5.09 (dd, *J* = 7.8, 4.1 Hz, 2H, CH-O), 4.19 (t, *J* = 5.3 Hz, 4 H, CH₂-O), 3.73 (q, *J* = 4.8 Hz, 4H, CH₂-N), 3.28–3.07 (m, 8H, CH₂-NH), 2.70–2.51 (m, 8H, CH₂-COO), 2.38 (q, *J* = 7.2 Hz, 4H, CH₂-COO), 1.90–1.69 (m, 4H, CH₂), 1.58 (t, *J* = 7.2 Hz, 4H, CH₂), 1.43 (q, *J* = 6.7 Hz, 8H, CH₂), 1.33–1.14 (m, 52H, CH₂), 0.83 (t, *J* = 6.6 Hz, 6H, CH₃) ppm. MS (ESI) *m/z*: [M + Na]⁺ calcd. for C₈₄H₁₂₄N₆O₂₀, 1559.8763; found 1559.8799.

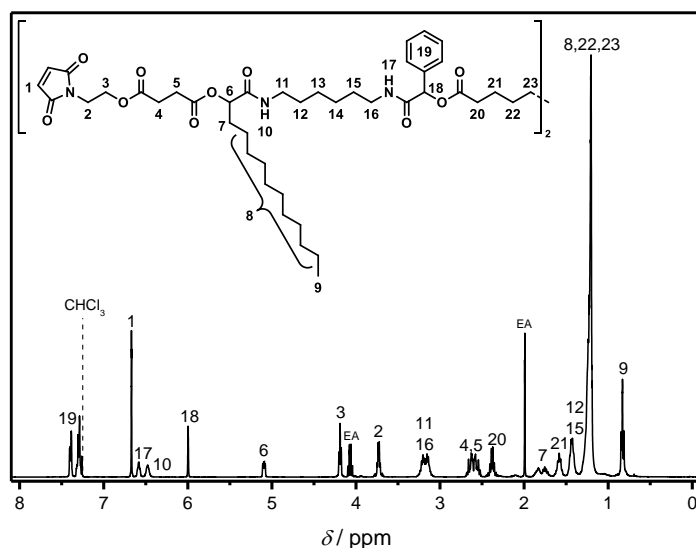


Figure S77. ¹H-NMR spectrum of the obtained tetramer **9** recorded in CDCl₃ at 400 MHz. For the signal assignments refer to the depicted structure.

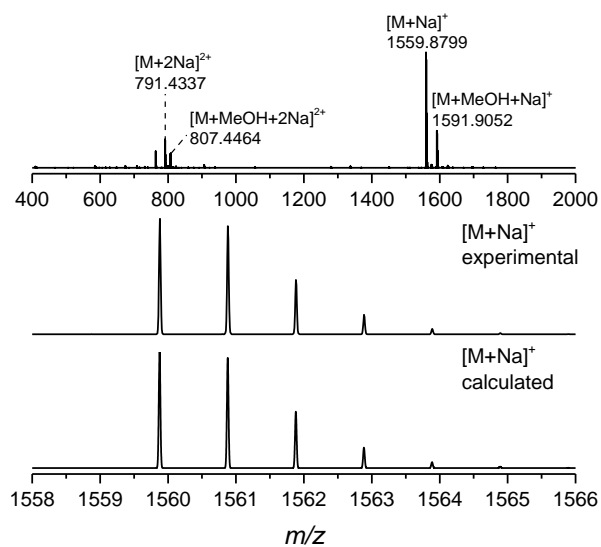


Figure S78. Full ESI-MS spectrum of the tetramer **9** (top) recorded in THF/MeOH (3:2). ESI-MS spectra of the tetramer **9** isotopic pattern (bottom). Recorded mass spectra shown are in excellent agreement with the calculated isotope pattern.

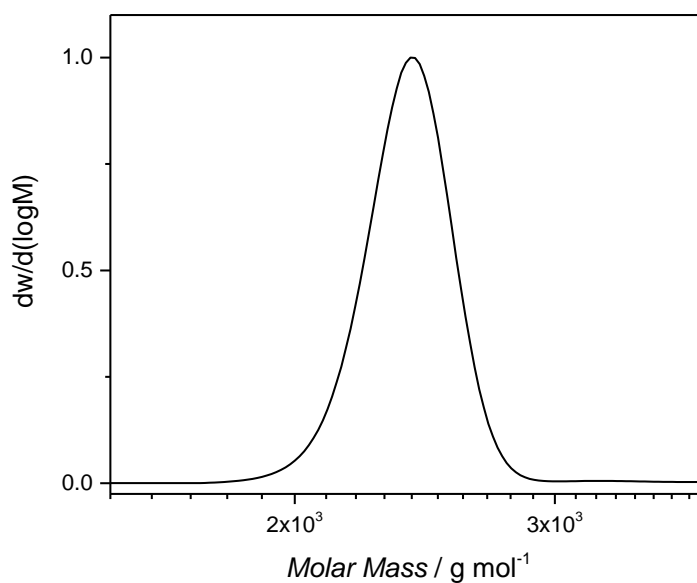
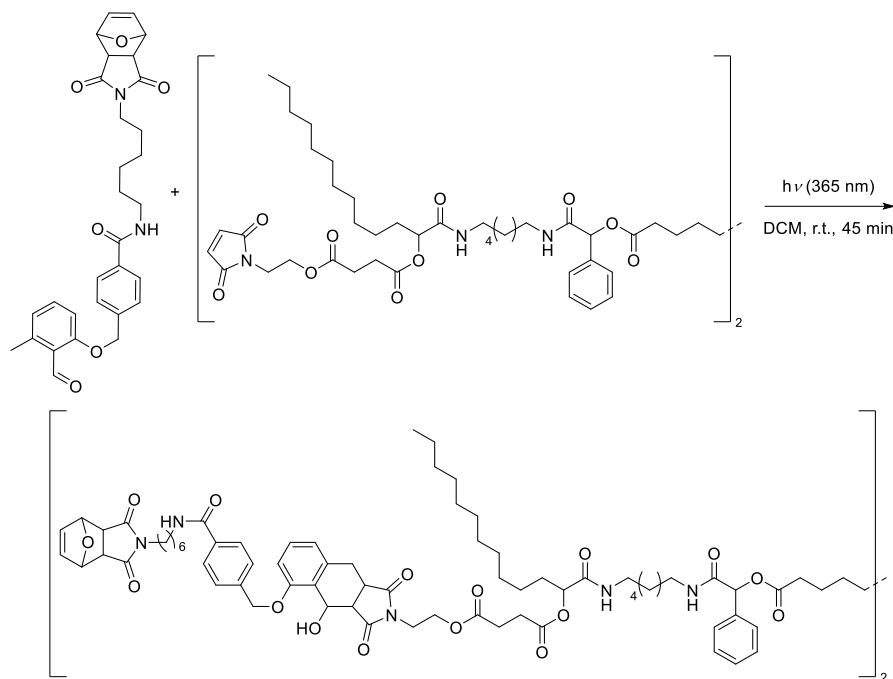


Figure S79. SEC trace of the tetramer **9** recorded in THF at 35 °C. ($D = 1.01$, $M_n = 2400\ g\ mol^{-1}$).

Synthesis of the Symmetric Photo-Passerini Hexamer 10a



Under nitrogen atmosphere, the tetra-substituted macromolecule **9** (135.1 mg, 0.09 mmol, 1.00 eq.) and photomonomer **5a** (136 mg, 0.26 mmol, 3.00 eq.) were dissolved in dry DCM (30 mL). The reaction mixture was transferred into a sealed and degassed head space vial and purged with nitrogen for 5 min. Subsequently, the mixture was irradiated with UV-light (365 nm) for 45 min. The solvent was removed under reduced pressure. Purification was performed *via* reversed phase flash column chromatography (Puriflash C18-HP, 12 g, 30 mL min⁻¹) with water and a THF gradient of 1 % per column volume (CV). Isocratic phases of a constant EA content were applied at 5, 15, 25, 35, 45, 55, 65 and 100 % (5 CV respectively). 25.0 mg of the target compound were obtained as a yellow solid (11.1 %).

MS (ESI) *m/z*: [M + Na]⁺ calcd. for C₁₄₂H₁₈₄N₁₀O₃₂, 2593.3317; found 2593.3369. Details of the ¹H NMR chemical shift assignments can be found in **Figure S80** and the mass spectrometric assignments in **Figure 25** (Section 3.1.3).

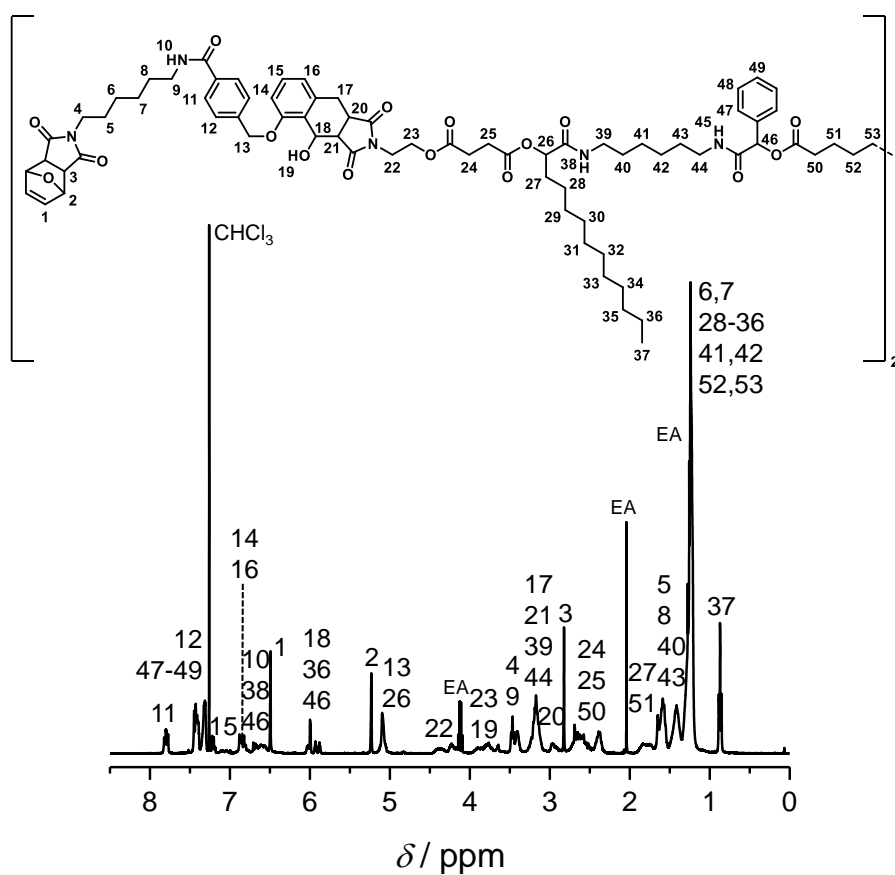


Figure S80. $^1\text{H-NMR}$ spectrum of the obtained hexamer **10a** recorded in CDCl_3 at 400 MHz. For the signal assignments refer to the depicted structure.

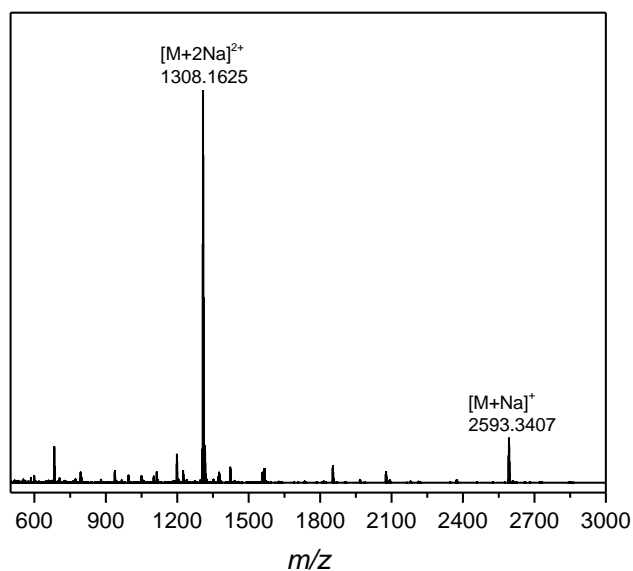


Figure S81. Full ESI-MS spectrum of the hexamer **10a** recorded in THF/MeOH (3:2).

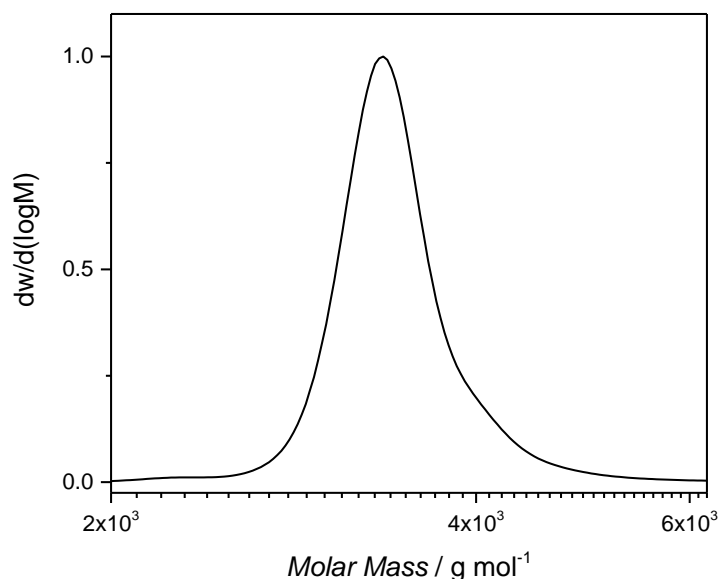
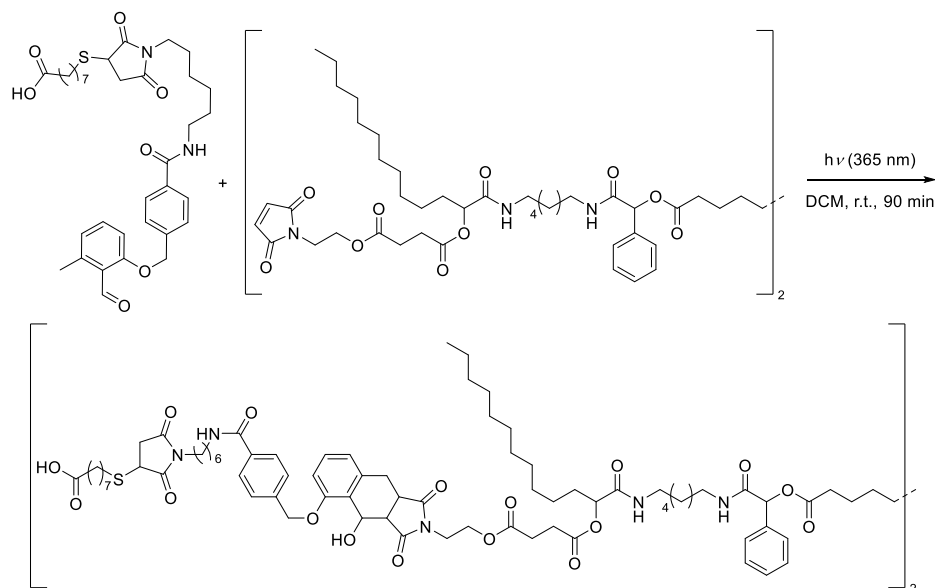


Figure S82. SEC trace of the hexamer **10a** recorded in THF at 35 °C. ($\bar{D} = 1.01$, $M_n = 3500 \text{ g mol}^{-1}$).

Synthesis of the Symmetric Photo-Passerini Hexamer **10b**



Under argon atmosphere, the tetra-substituted macromolecule **9** (300 mg, 0.20 mmol, 1.00 eq.) and modified photomonomer **6a** (320 mg, 0.49 mmol, 2.50 eq.) were dissolved in dry DCM (140 mL). The reaction mixture was transferred into a sealed and degassed head space vials (10 mL) and purged with nitrogen for 5 min. Subsequently, the mixture was irradiated with UV-light (365 nm) for 45 min. The solvent was removed under reduced pressure. The crude mixture was purified by reversed phase flash column chromatography (Puriflash, 12 g, 30 mL min⁻¹) with CH and a EA gradient of 1.7 % per column volume (CV). Isocratic phases of a constant EA content were applied at 17, 33, 50, 67 and 100 % (10 CV). The target compound was obtained as a white solid (199 mg, 32 %).

MS (ESI) m/z : $[M + 2Na]^{2+}$ calcd. for $C_{142}H_{184}N_{10}O_{36}$, 1448.2111; found 1448.2110. Details of the NMR chemical shift assignments can be found in **Figure S83** and the mass spectrometric assignments in **Figure 25** (Section 3.1.3).

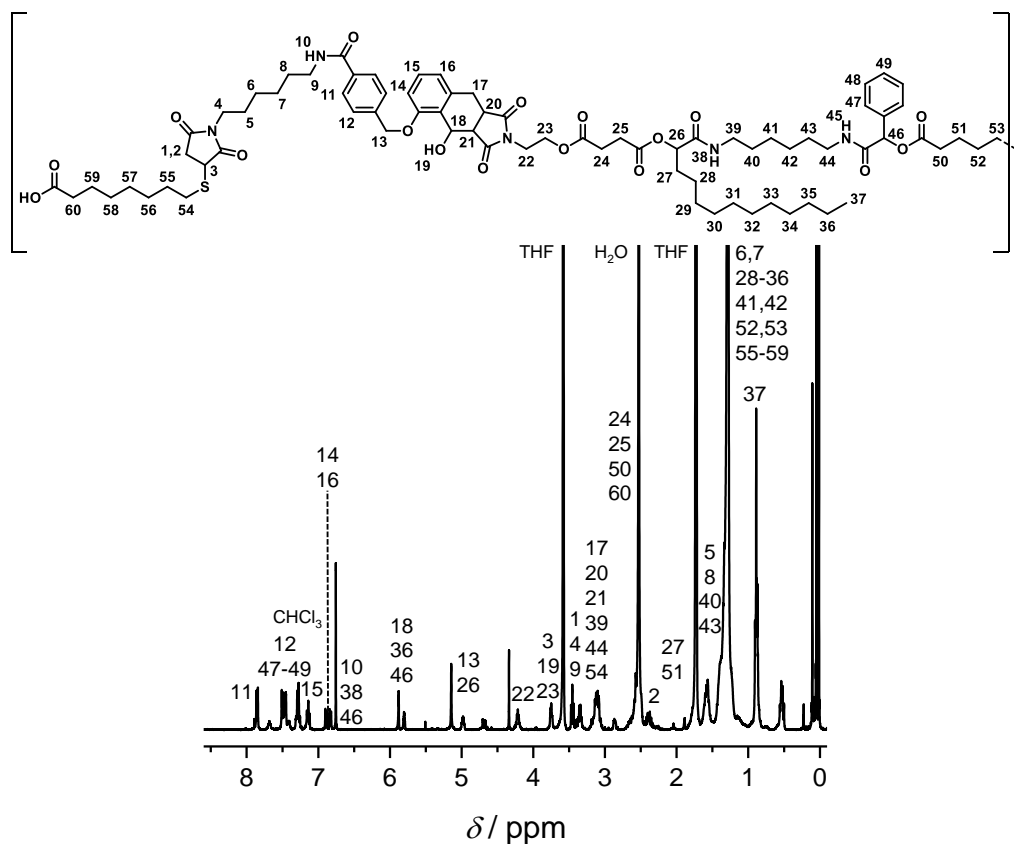


Figure S83. $^1\text{H-NMR}$ spectrum of the obtained hexamer **10b** recorded in CDCl_3 at 400 MHz. For the signal assignments refer to the depicted structure.

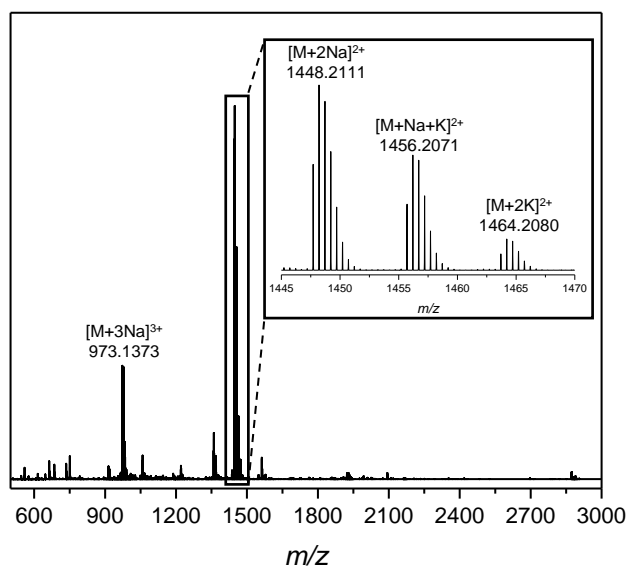


Figure S84. Full ESI-MS spectrum of the hexamer **10b** recorded in THF/MeOH (3:2). The hexamer **10b** was detected in its oxidized state as sulfone.

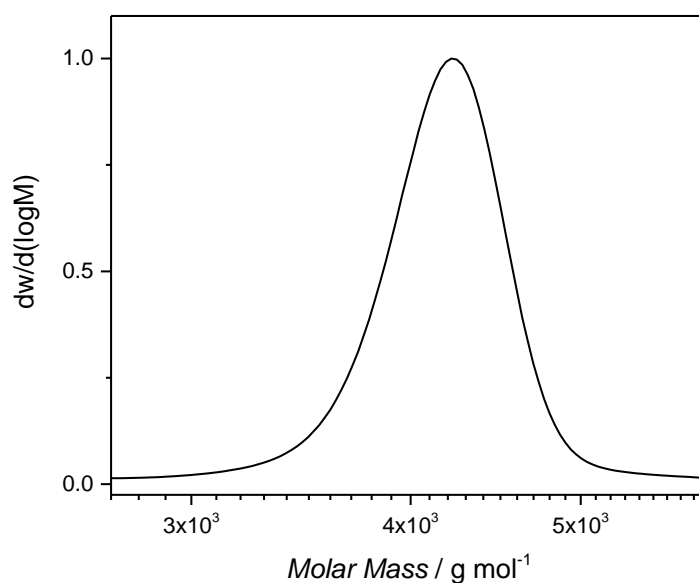
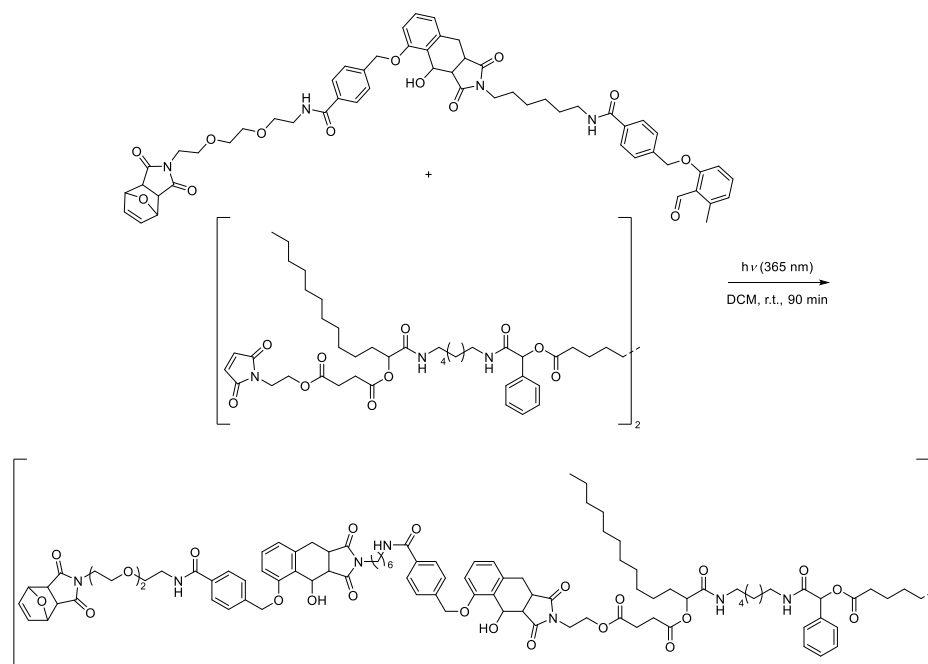


Figure S85. SEC trace of the hexamer **10b** recorded in THF at 35 °C. ($\bar{D} = 1.01$, $M_n = 4000 \text{ g mol}^{-1}$).

Synthesis of the Symmetric Photo-Passerini Octamer **10c**



Under argon atmosphere, the tetra-substituted macromolecule **9** (173 mg, 0.11 mmol, 1.00 eq.) and photodimer **7** (280 mg, 0.28 mmol, 2.50 eq.) were dissolved in dry DCM (75 mL). The reaction mixture was transferred into a sealed and degassed head space vials (10 mL) and purged with argon for 5 min. Subsequently, the mixture was irradiated with UV-light (365 nm) for 90 minutes. The solvent was removed under reduced pressure. The crude mixture was purified by reversed phase flash column chromatography (Puriflash, 12 g, 30 mL min^{-1}) with CH and a EA gradient of 1.7 % per column volume (CV). Isocratic phases of a constant EA content were applied at 17, 33, 50, 67 and 100 % (10 CV). The target compound was obtained as a white solid (364 mg, 80.4 %).

MS (ESI) m/z : $[M + 2Na]^{2+}$ calcd. for $C_{142}H_{184}N_{10}O_{32}$, 1788.8516, found 1788.8500. Details of the 1H NMR chemical shift assignments and the mass spectrometric assignments can be found in **Figure 24**, **Figure 25**, and **Figure 26** (Section 3.1.3).

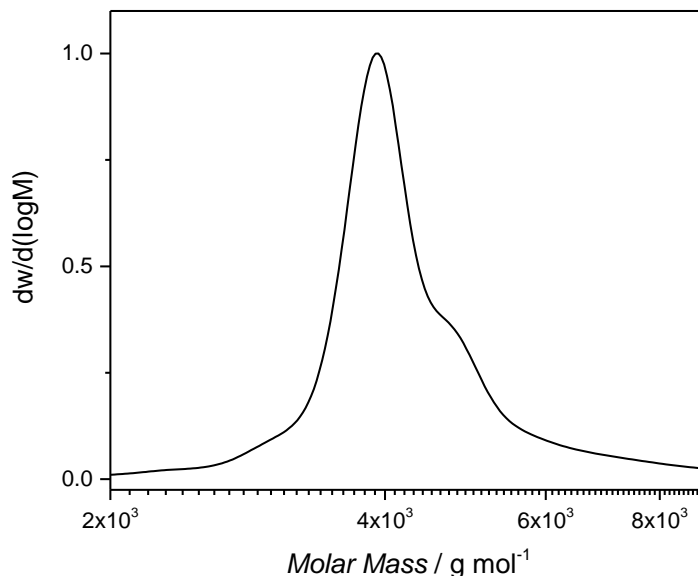
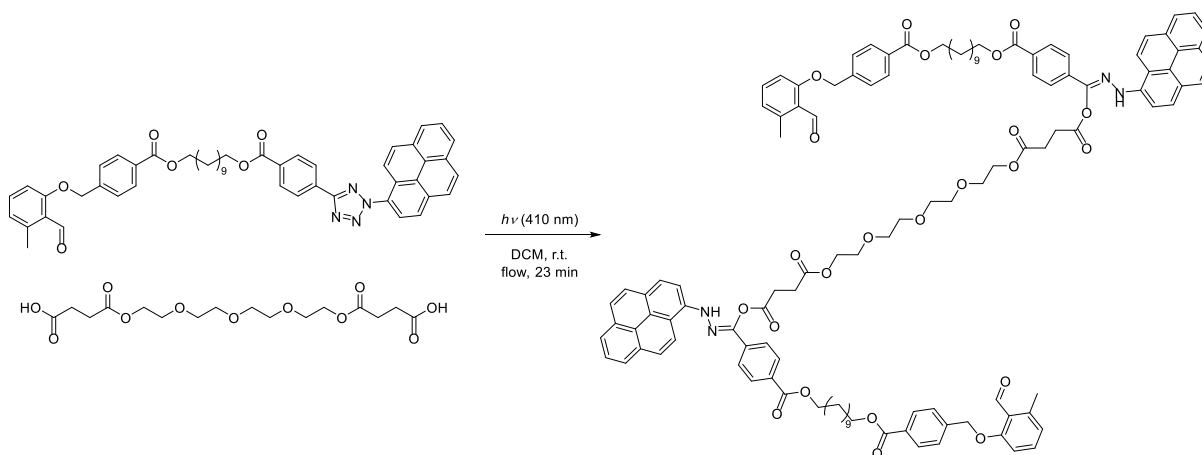


Figure S86. SEC trace of the octamer **10c** recorded in THF at 35 °C. ($D = 1.03$, $M_n = 4100$ g mol $^{-1}$).

5.3.5.2. Protection Group Free Synthesis of Sequence-Defined Macromolecules Based on Tetrazoles and *o*-MBAs

Synthesis of Dimer 18a



Monomer **13** (112.8 mg, 0.139 mmol, 2.30 eq.) was dissolved with the core unit **15** (23.8 mg, 0.061 mmol, 1.00 eq.) in anhydrous DCM (100 mL) under nitrogen atmosphere. The reaction mixture was irradiated at room temperature in a custom build flow reactor (7 mL reactor volume) using LEDs (3 x 410 nm, 0.3 mL min $^{-1}$, residence time 23 min, peristaltic pump) as light source after purging the reactor with anhydrous DCM under nitrogen atmosphere. Afterwards, the solvent was removed under reduced pressure and the crude product was purified using a flash system. Normal phase silica (Puriflash F0040, 30 μ m) was used employing

5. Experimental Section

a gradient of CH/EA (20 mL min^{-1}) as eluent. The fractions were collected according to UV-Vis detection. Isocratic phases of a constant EA content have been applied at 25 (2 CV), 50 (2 CV), 75 (1 CV), 90 (2 CV), 95 (1 CV) and 100 % (6 CV) with a runtime of 29 CV in total. The product was eluted in the range between 15 and 18 CV yielding 106 mg of a yellow resin (89 %). The product is light sensitive and was stored protected from light.

In addition, dimer **18a** formation was successfully performed in a Vapourtec flow system employing similar reaction conditions conducted by Christian Fengler.^[255]

Details of the ^1H NMR chemical shift assignments can be found in **Figure S87**. MS (ESI) m/z : $[\text{M} + \text{Na}]^+$ calcd. for $\text{C}_{118}\text{H}_{122}\text{N}_4\text{O}_{23}$, 1985.8392; found 1985.8406.

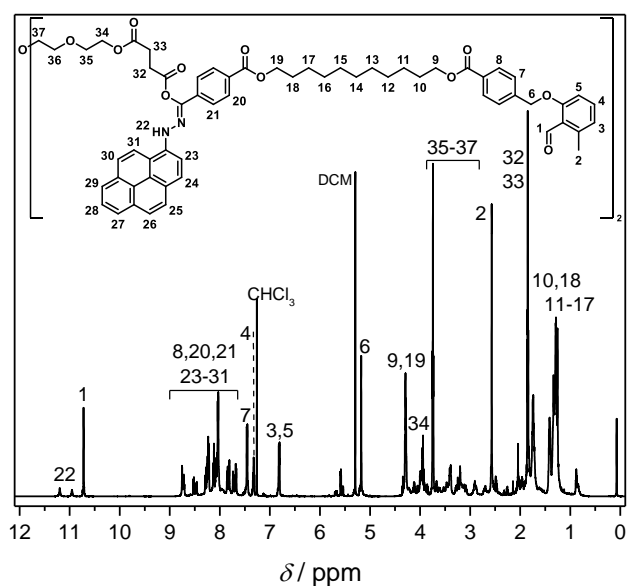


Figure S87. ^1H NMR spectrum of the dimer **18a** recorded in CDCl_3 at 400 MHz. For the resonance assignments refer to the depicted structure.

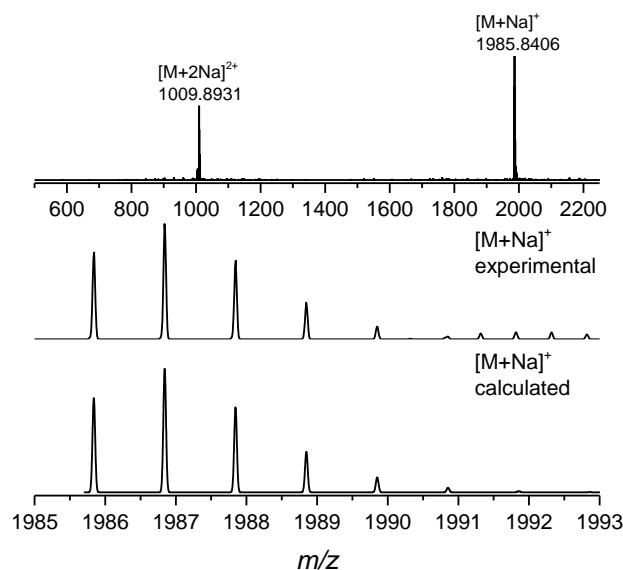


Figure S88. Mass spectrum of the dimer **18a** recorded in THF/MeOH (3:2). ESI-MS spectra of the dimer **18a** isotopic pattern (bottom). Recorded mass spectra shown are in excellent agreement with the calculated isotope pattern.

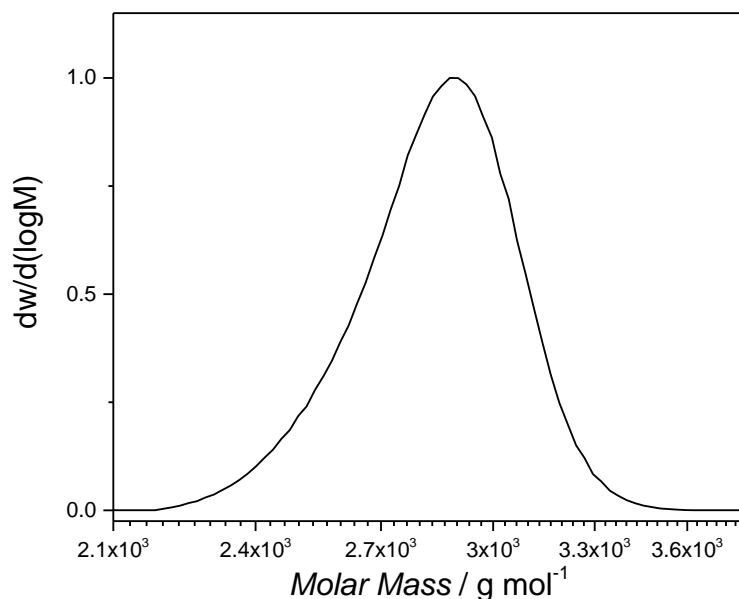
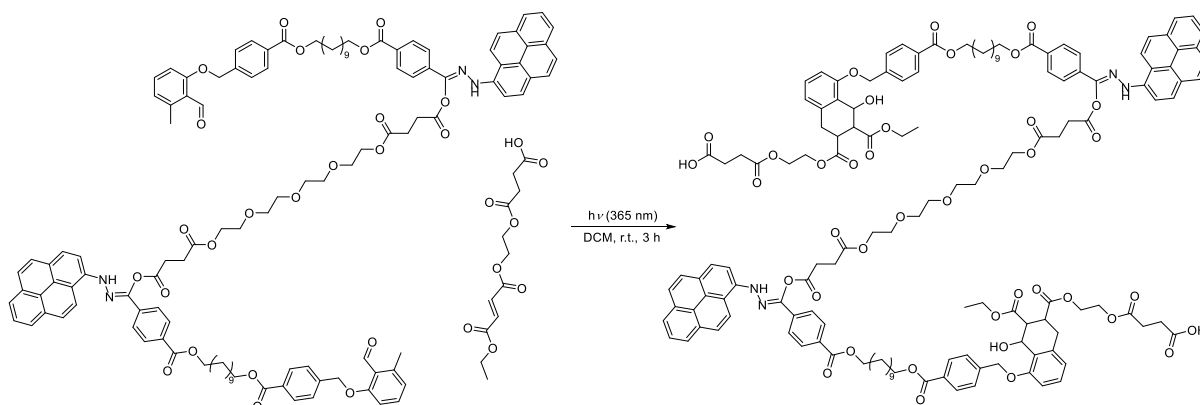


Figure S89. SEC trace of the dimer **18a** recorded in THF at 35 °C. ($\bar{D} = 1.01$, $M_n = 2800 \text{ g mol}^{-1}$).

Synthesis of Tetramer **18b**



The dimer **18a** (85.1 mg, 0.043 mmol, 1.00 eq.) was dissolved with monomer **14** (50.0 mg, 173.3 μmol , 4.00 eq.) in anhydrous DCM (50 mL) under nitrogen atmosphere and transferred into degassed head space vials equipped with a stirring bar. After purging the reaction mixture for 5 min with nitrogen, the reaction mixture was irradiated at room temperature in a custom build photoreactor using PL-L mercury lamps (3 x 365 nm). Afterwards, the crude mixture was diluted with DCM (100 mL total volume) and washed with diluted NaHCO_3 solution (3 x 100 mL) to extract excess monomer **14**. The DCM layer was further extracted with saturated NaHCO_3 solution (3 x 100 mL). Tetramer **18b** was obtained by acidification of the combined saturated NaHCO_3 phases and extraction with DCM (3 x 150 mL) yielding 94 mg of the target compound as a yellow resin (85 %).

In addition, tetramer **18b** formation was successfully performed in a Vapourtec flow system employing similar reaction scale with a flow rate of 0.50 mL min^{-1} and a residence time of 20 min conducted by Christian Fengler.^[255]

Details of the ^1H NMR chemical shift assignments can be found in **Figure S90**. MS (ESI) m/z : $[\text{M} + \text{Na}]^+$ calcd. for $\text{C}_{142}\text{H}_{154}\text{N}_4\text{O}_{39}$, 2562.0082; found 2562.0100.

5. Experimental Section

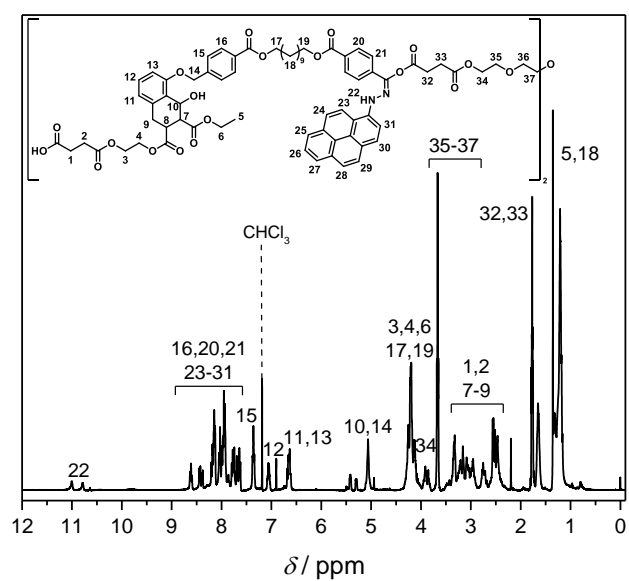


Figure S90. ^1H NMR spectrum of the tetramer **18b** recorded in CDCl_3 at 400 MHz. For the resonance assignments refer to the depicted structure.

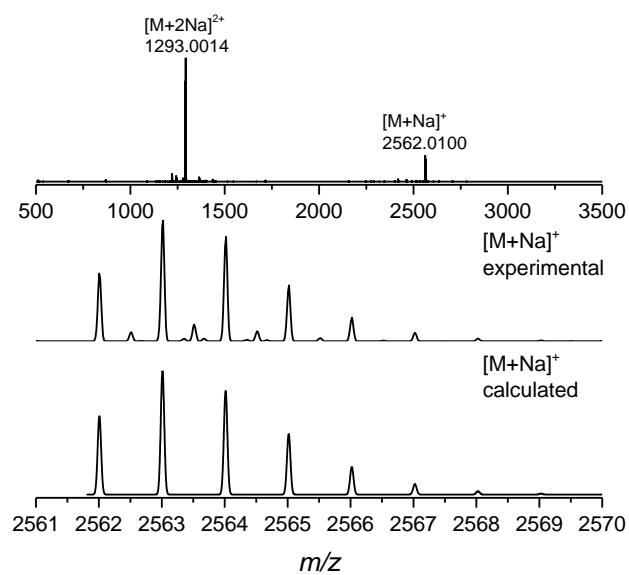


Figure S91. Mass spectrum of the tetramer **18b** recorded in THF/MeOH (3:2). ESI-MS spectra of the tetramer **18b** isotopic pattern (bottom). Recorded mass spectra shown are in excellent agreement with the calculated isotope pattern.

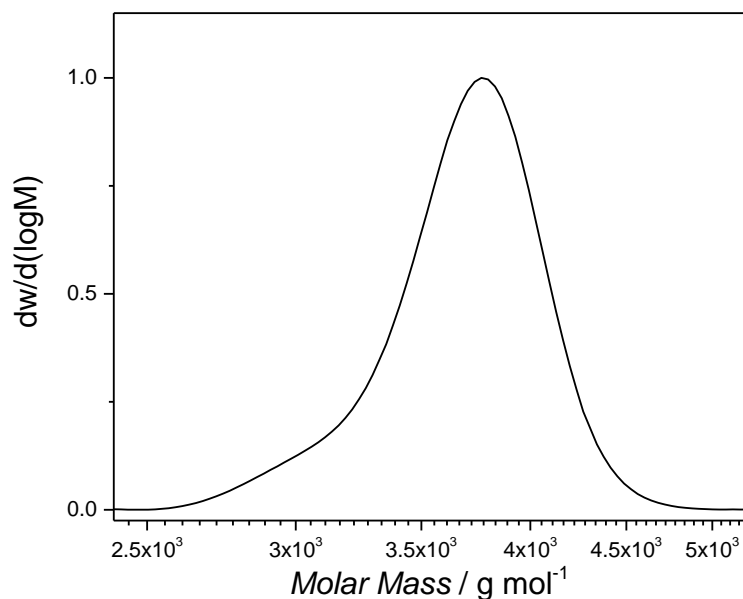
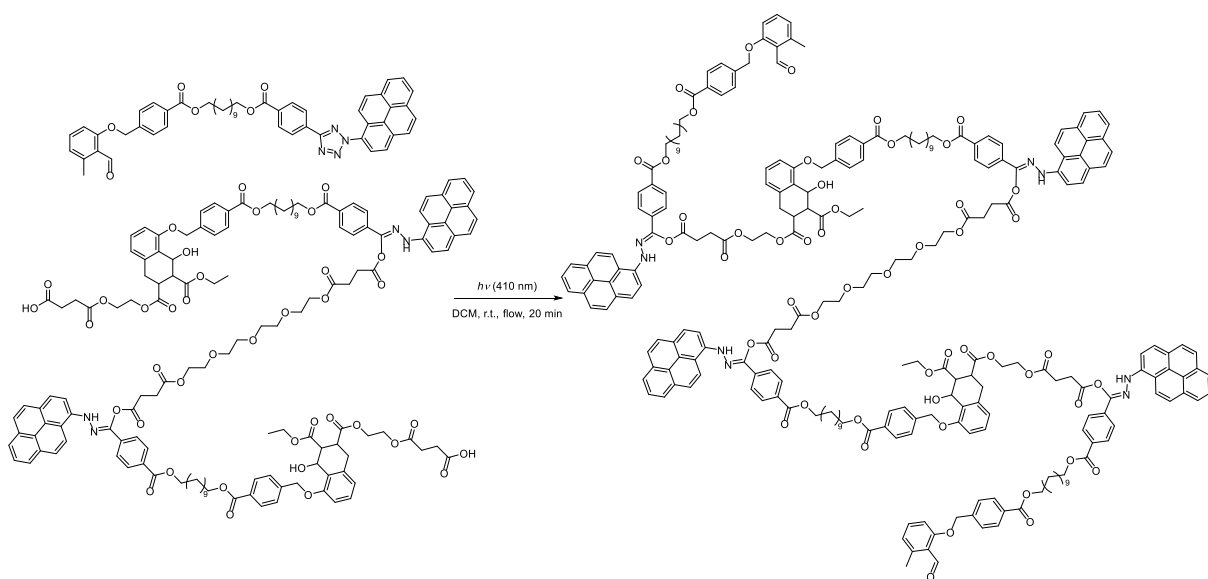


Figure S92. SEC trace of the tetramer **18b** recorded in THF at 35 °C. ($\bar{D} = 1.01$, $M_n = 3600 \text{ g mol}^{-1}$).

Synthesis of Hexamer **18c**



Monomer **13** (56.0 mg, 0.689 mmol, 2.50 eq.) was dissolved with tetramer **18b** (70.0 mg, 0.076 mmol, 1.00 eq.) in anhydrous DCM (60 mL) under nitrogen atmosphere. The reaction mixture was irradiated at room temperature in a custom build flow reactor (7 mL reactor volume) using LEDs (3 x 410 nm, 0.3 mL min^{-1} , residence time 23 min, peristaltic pump) as light source after purging the reactor with anhydrous DCM under nitrogen atmosphere. Afterwards, the solvent was removed under reduced pressure and the crude product was purified using a flash system. Normal phase silica (Puriflash F0040, $30 \mu\text{m}$) was used employing a gradient of CH/EA (20 mL min^{-1}) as eluent. The fractions were collected according to UV-Vis detection. The ratio of EA was increased to 80 % within the first 8 CV. Isocratic phases of a constant EA content have been applied at 90 (2 CV), 95 (1 CV), 98 (1 CV) and 100 % (2 CV) with a runtime of 29 CV in total. The product was eluted in the range between 12

5. Experimental Section

and 16 CV yielding 90.0 mg of a yellow resin (79 %). The product is light sensitive and was stored protected from light.

Details of the ^1H NMR chemical shift assignments can be found in **Figure S93**. MS (ESI) m/z : $[\text{M} + \text{Na}]^+$ calcd. for $\text{C}_{244}\text{H}_{250}\text{N}_8\text{O}_{51}$, 4132.7173; found 4132.7563.

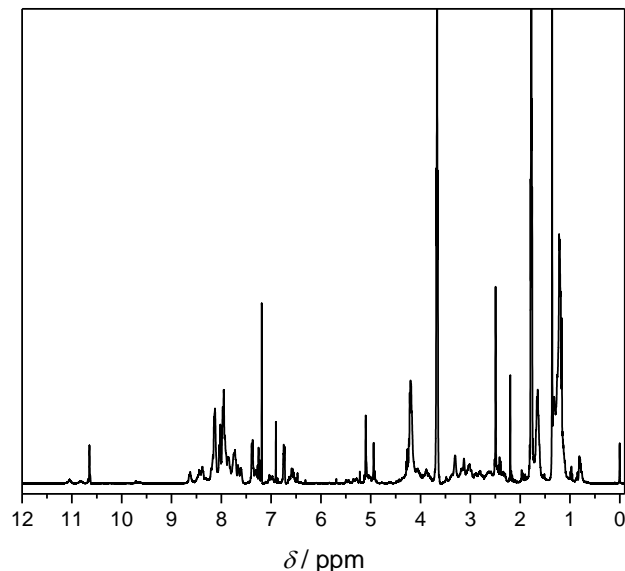


Figure S93. ^1H NMR spectrum of the hexamer **18c** recorded in CDCl_3 at 400 MHz. For the resonance assignments refer to **Figure S87** and **Figure S90**.

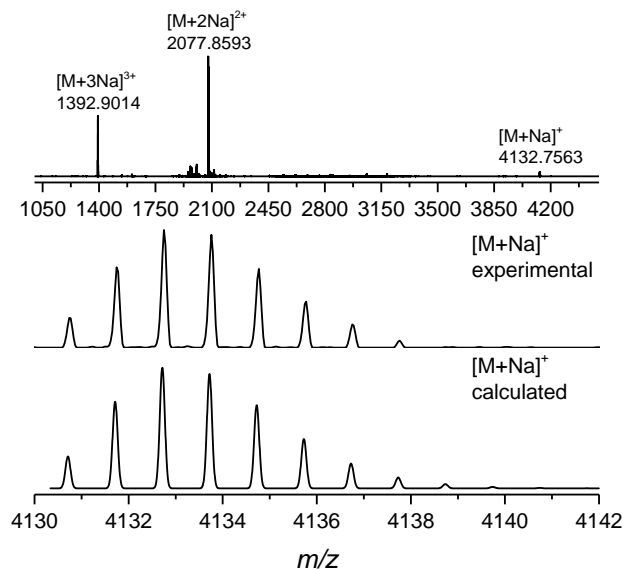


Figure S94. Mass spectrum of the hexamer **18c** recorded in THF/MeOH (3:2). ESI-MS spectra of the hexamer **18c** isotopic pattern (bottom). Recorded mass spectra shown are in excellent agreement with the calculated isotope pattern.

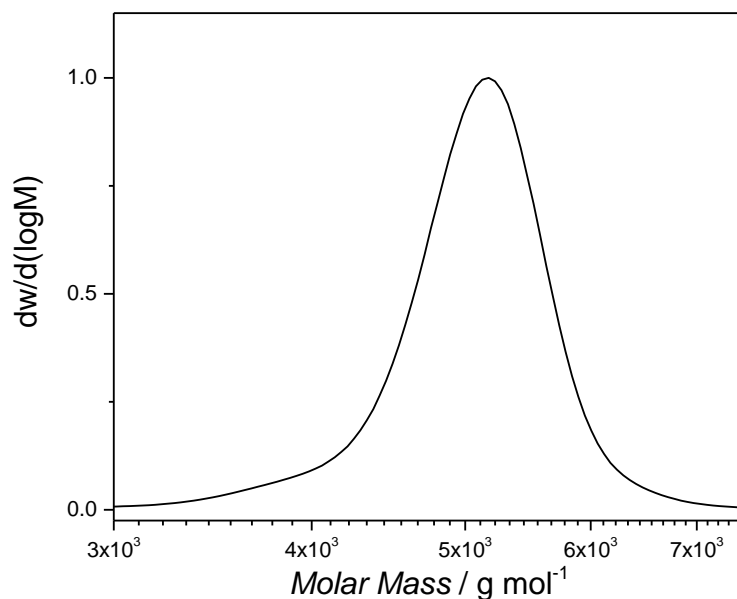
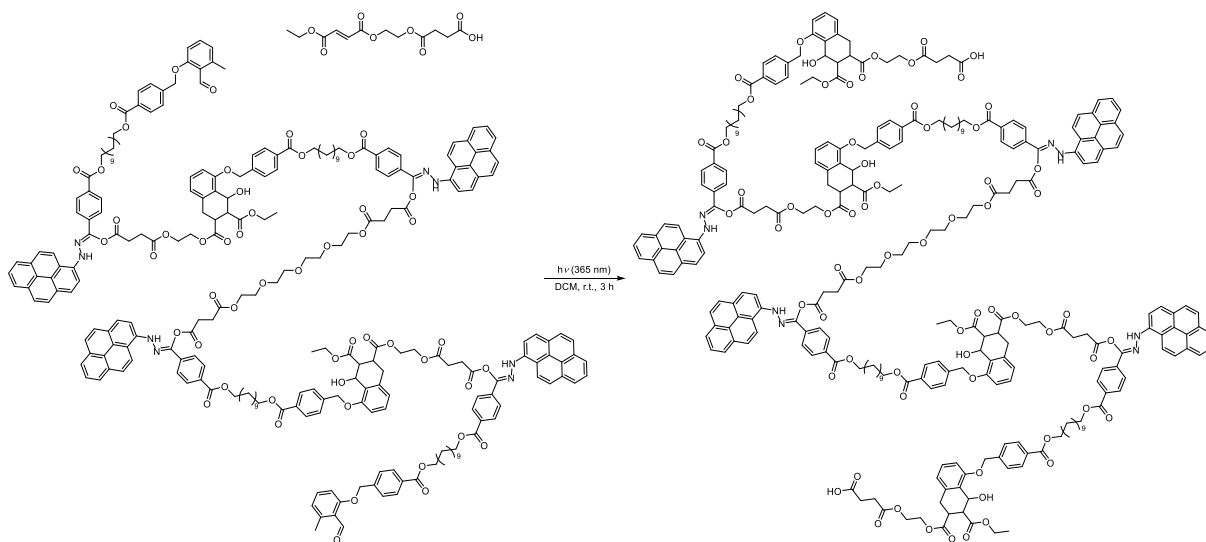


Figure S95. SEC trace of the hexamer **18c** recorded in THF at 35 °C. ($D = 1.01$, $M_n = 5200$ g mol⁻¹).

Synthesis of Octamer **18d**



The hexamer **18c** (42.3 mg, 0.01 mmol, 1.00 eq.) was dissolved with monomer **14** (11.9 mg, 0.041 mmol, 4.00 eq.) in anhydrous DCM (40 mL) under nitrogen atmosphere and transferred into degassed head space vials equipped with a stirring bar. After purging the reaction mixture for 5 min with nitrogen, the reaction mixture was irradiated at room temperature in a custom build photoreactor using PL-L mercury lamps (3 x 365 nm). Afterwards, the crude mixture was diluted with DCM (100 mL total volume) and washed with saturated NaHCO₃ solution (3 x 100 mL) to extract excess monomer **14**. The DCM layer was dried over MgSO₄, the solvent was removed under reduced pressure and the crude product was purified using a flash system. Normal phase silica (Puriflash F0024, 30 μm) was used employing a gradient of DCM/MeOH (15 mL min⁻¹) as eluent. The fractions were collected according to UV-Vis detection. The ratio of MeOH was increased to 7 % within the first 18 CV. Isocratic phases of a constant MeOH content have been applied at 0 (3 CV) and 100 % (5 CV) with a runtime

5. Experimental Section

of 42 CV in total. The product was eluted in the range between 16 and 20 CV yielding 32.0 mg of a yellow resin (65 %).

Details of the ^1H NMR chemical shift assignments can be found in **Figure S96**. MS (ESI) m/z : $[\text{M} + 2\text{Na}]^{2+}$ calcd for $\text{C}_{268}\text{H}_{282}\text{N}_8\text{O}_{67}$, 2365.9378; found 2365.9392.

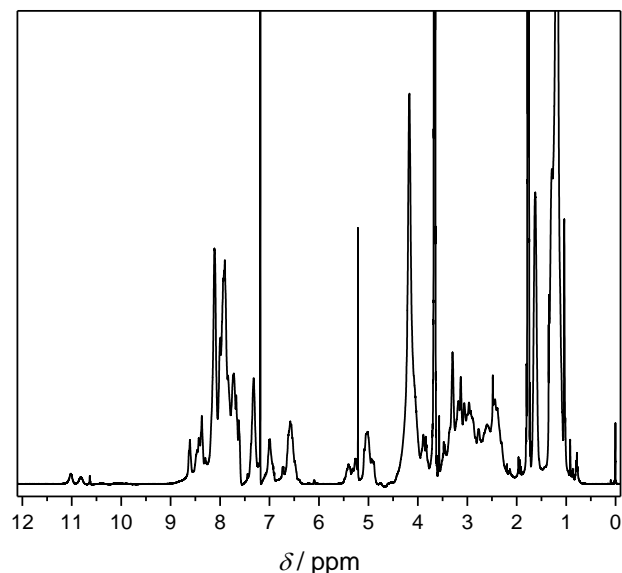


Figure S96. ^1H NMR spectrum of the octamer **18d** recorded in CDCl_3 at 400 MHz. For the resonance assignments refer to **Figure S87** and **Figure S90**.

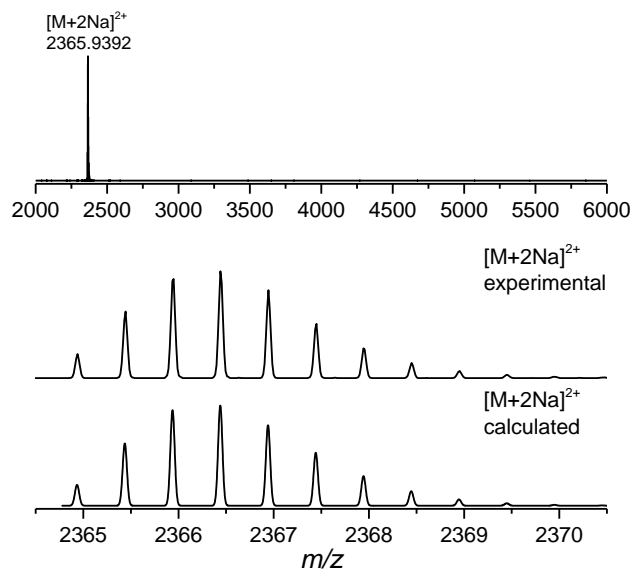


Figure S97. Mass spectrum of the octamer **18d** recorded in THF/MeOH (3:2). ESI-MS spectra of the octamer **18d** isotopic pattern (bottom). Recorded mass spectra shown are in excellent agreement with the calculated isotope pattern.

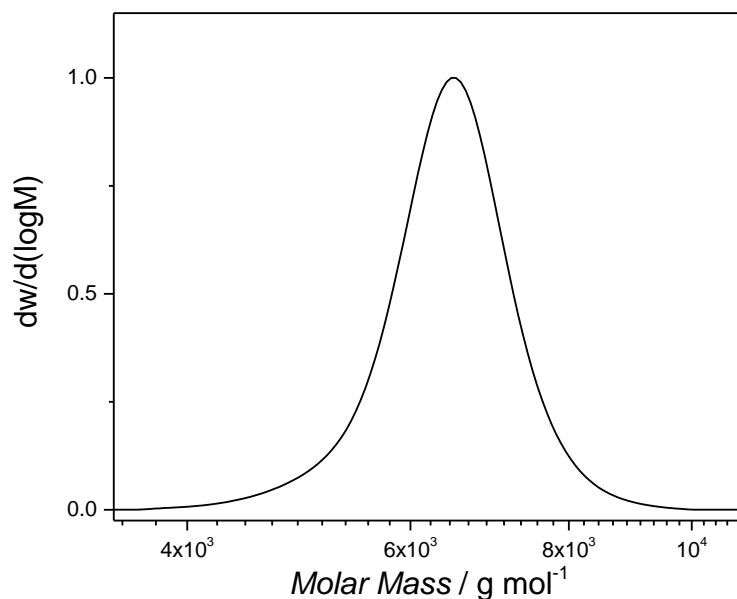
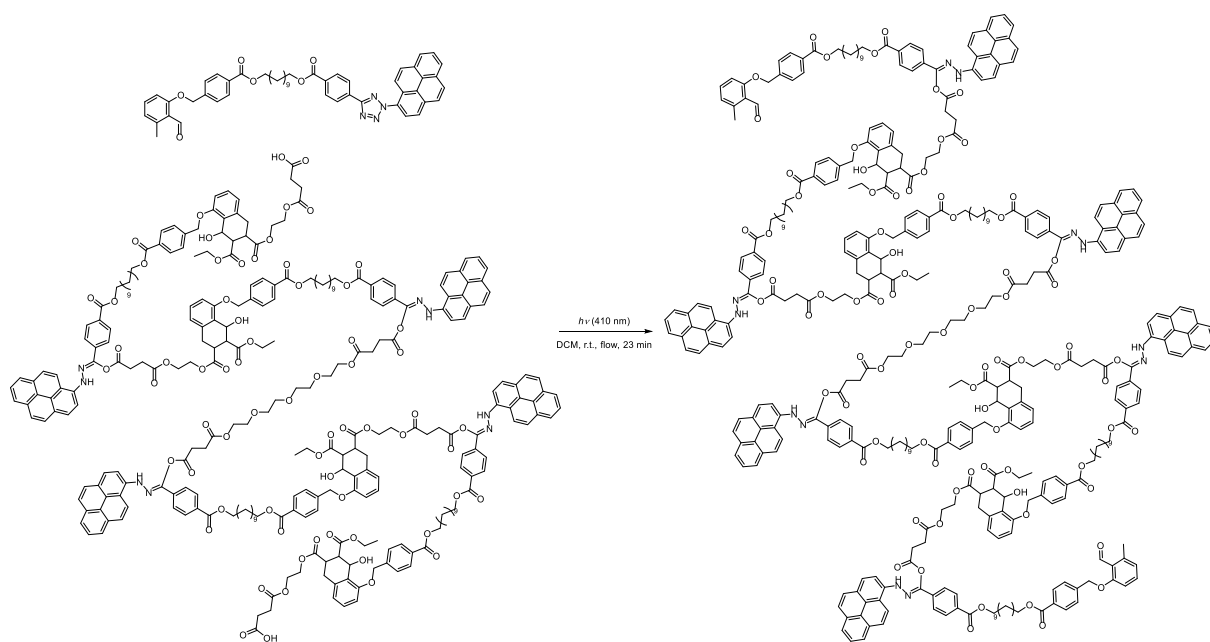


Figure S98. SEC trace of the octamer **18d** recorded in THF at 35 °C. ($\bar{D} = 1.01$, $M_n = 6300 \text{ g mol}^{-1}$).

Synthesis of Decamer **18e**



Monomer **13** (3.2 mg, 3.9 μmol , 3.00 eq.) was dissolved with octamer **18d** (6.1 mg, 1.3 μmol , 1.00 eq.) in anhydrous DCM (40 mL) under nitrogen atmosphere. The reaction mixture was irradiated at room temperature in a custom build flow reactor (7 mL reactor volume) using LEDs (3 x 410 nm, 0.3 mL min^{-1} , residence time 23 min, peristaltic pump) as light source after purging the reactor with anhydrous DCM under nitrogen atmosphere. Afterwards, the solvent was removed under reduced pressure and the crude product was purified using a flash system. Normal phase silica (Puriflash F0012, 30 μm) was used employing a gradient of CH/EA (10 mL min^{-1}) as eluent. The fractions were collected according to UV-Vis detection. The ratio of EA was increased to 80 % within the first 14 CV. Isocratic phases of a constant EA content have been applied at 90 (3.5 CV), 95 (2 CV), 98 (2 CV) and 100 %

5. Experimental Section

(3.5 CV) with a runtime of 50 CV in total. The product was eluted in the range between 17 and 20 CV yielding 6.1 mg of a yellow resin (75 %). The product is light sensitive and was stored protected from light.

Details of the ^1H NMR chemical shift assignments and the mass spectrometric assignments can be found in **Figure 37** and **Figure 38** (Section 3.2.2). **MS** (ESI) m/z : $[\text{M} + 2\text{Na}]^{2+}$ calcd. for $\text{C}_{370}\text{H}_{378}\text{N}_{12}\text{O}_{79}$, 3151.2924; found 3151.3119.

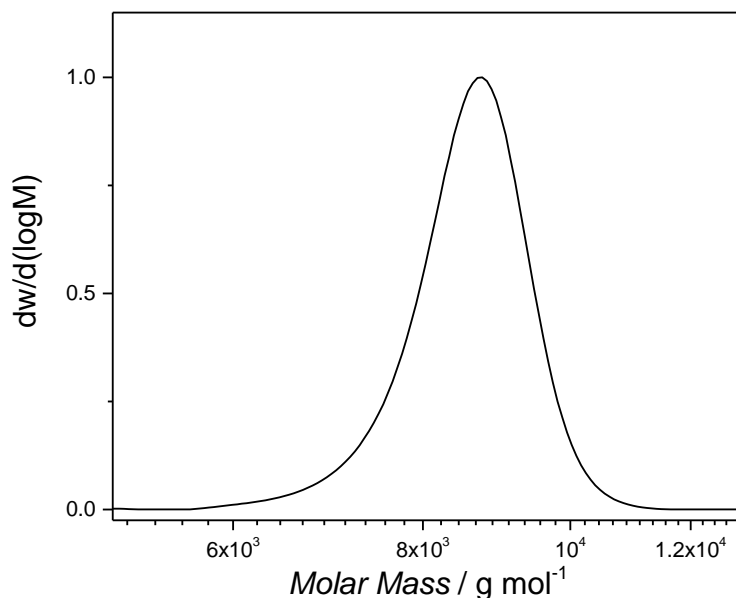
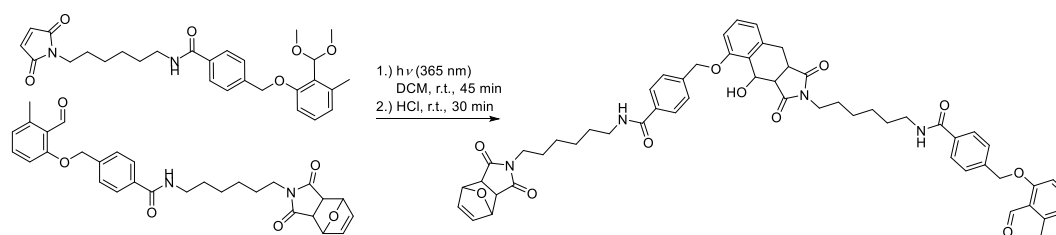


Figure S99. SEC trace of the decamer **18e** recorded in THF at 35 °C. ($D = 1.01$, $M_n = 8500 \text{ g mol}^{-1}$).

5.3.5.3. Synthesis of Sequence-Defined Macromolecules Based on *o*-MBAs and Maleimides

Synthesis of Photodimer 20a



All operations were conducted under argon atmosphere. To a solution of the furan deprotected and acetal protected monomer **5a*** (47.1 mg, 95.3 μmol , 1.00 eq.) dissolved in anhydrous DCM (15 mL), photomonomer **5a** (51.7 mg, 0.1 mmol, 1.05 eq.) dissolved in anhydrous DCM (25 mL) was added (5.0 mmol L^{-1}). The reaction mixture was subsequently filled into sealed and previously degassed head space vials (5 mL) and purged for 5 minutes with argon, to be finally exposed to UV-light (PL-L, 365 nm) for 45 minutes (batch conditions). After irradiation, the single fractions were gathered and the solvent was removed under reduced pressure. The purification was performed via reverse phase flash chromatography (SNAP C18 12 g, 12 mL min^{-1}) with MQ water and a THF gradient of 1.0 % per CV. Isocratic phases of a constant THF content have been applied at 20, 25, 30, 35 % (5 CV

respectively), and 40 % (35 CV). The product was eluted as the THF content reached 40 % in the mobile phase. An acidic workup was not performed since the aldehyde functionality was regenerated after the purification. (Yield: 58.2 %, 53.6 mg).

^1H NMR (500 MHz, CDCl_3): δ = 10.71 (s, 1H), 7.77 (dd, J = 21.2, 8.1 Hz, 4H), 7.45 (t, J = 7.0 Hz, 4H), 7.38 (t, J = 8.0 Hz, 1H), 7.22 (t, J = 7.9 Hz, 1H), 6.94 – 6.77 (m, 4H), 6.68 – 6.59 (m, 2H), 6.51 (s, 2H), 5.97 (d, J = 4.0 Hz, 1H), 5.60 (dd, J = 6.0, 1.8 Hz, 1H), 5.24 (s, 2H), 5.19 (s, 2H), 5.11 (s, 2H), 3.67 – 3.56 (m, 4H), 3.45 – 3.32 (m, 4H), 3.16 (d, J = 27.1 Hz, 3H), 2.98 (dd, J = 9.1, 4.0 Hz, 1H), 2.85 (s, 2H), 2.59 (s, 3H), 2.19 – 1.60 (m, 16H) ppm. **^{13}C NMR** (125 MHz, CDCl_3): δ = 192.2, 180.4, 177.7, 176.5, 167.2, 162.0, 154.8, 142.3, 140.0, 138.48, 139.6, 136.5, 134.6, 134.5, 129.6, 127.4, 127.3, 127.2, 127.1, 127.1, 126.5, 124.6, 123.6, 121.5, 111.1, 110.4, 80.9, 70.0, 69.9, 67.7, 61.4, 50.8, 47.4, 46.7, 39.7, 39.4, 38.7, 38.4, 29.2, 29.2, 27.4, 27.3, 26.1, 25.9, 25.7, 25.7, 25.3, 21.5 ppm. **MS** (ESI) m/z : $[\text{M} + \text{Na}]^+$ calcd. for $\text{C}_{56}\text{H}_{60}\text{N}_4\text{O}_{11}$, 987.4151; found 987.4163. Details of the ^1H NMR chemical shift assignments can be found in **Figure 42** (Section 3.3.2).

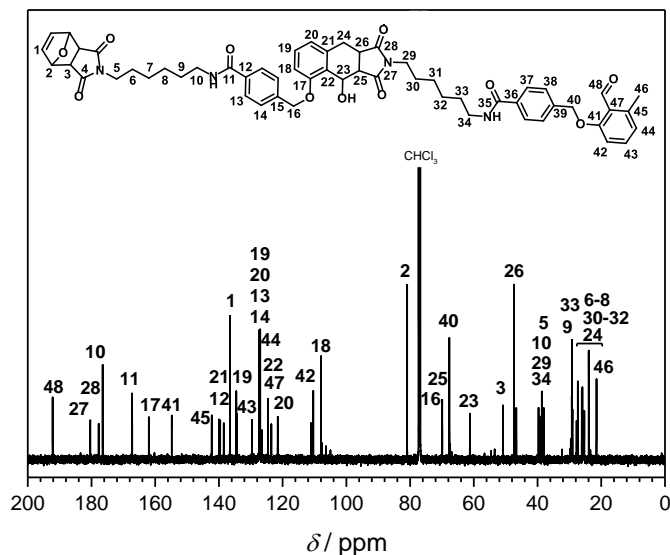


Figure S100. ^{13}C NMR spectrum of the dimer **20a** recorded in CDCl_3 at 125 MHz. For the resonance assignments refer to the depicted structure.

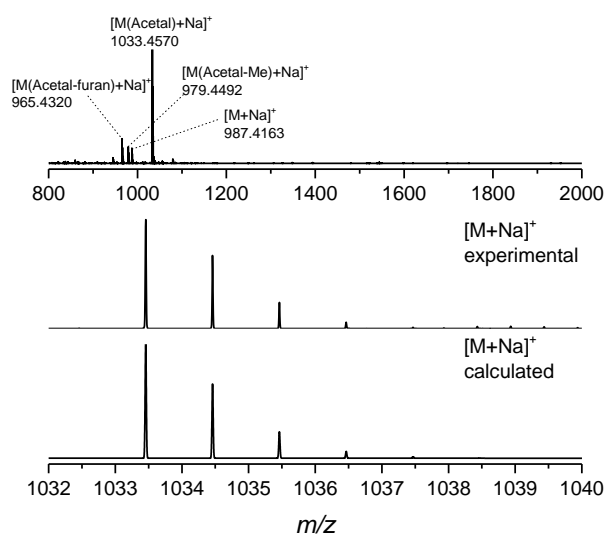


Figure S101. Full ESI-MS spectrum of the dimer **20a** (top) recorded in THF/MeOH (3:2). ESI-MS spectra of the dimer **20a** isotopic pattern (bottom). Recorded mass spectra shown are in excellent agreement with the calculated isotope pattern.

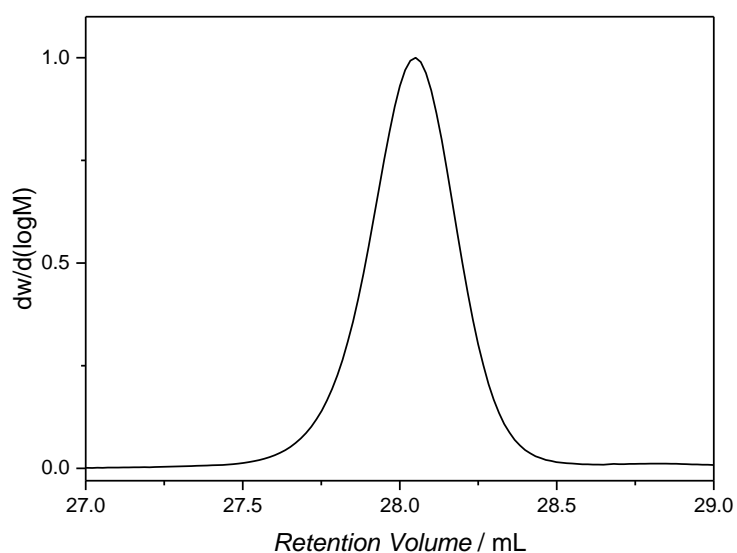
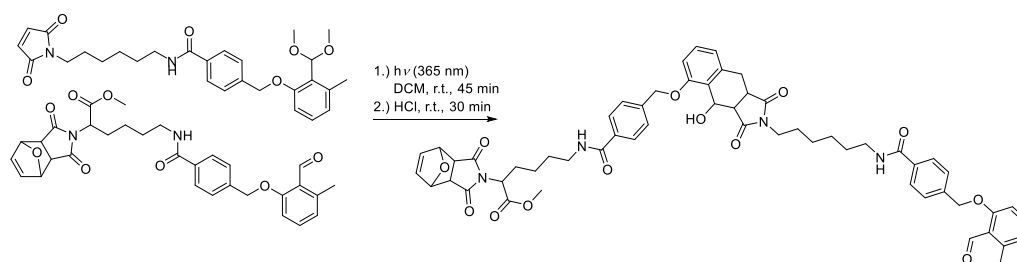


Figure S102. SEC trace of the dimer **20a** recorded in THF at 35 °C. ($D = 1.01$, $V_p = 28.1$ mL).

Synthesis of Photodimer **20b**



All operations were conducted under argon atmosphere. The synthesis of **20b** was performed under batch conditions similarly to **7** with the furan deprotected and acetal protected monomer **5a**^{*} (210.6 mg, 0.41 mmol, 1.00 eq.) and monomer **19a** (240.0 mg, 0.43 mmol, 1.05 eq.) dissolved in anhydrous DCM (170 mL). The purification was performed *via* reverse phase flash chromatography (SNAP C18 column 12 g, 12 mL min⁻¹) with MQ water and a THF gradient of 1.0 % per CV. Isocratic phases of a constant THF content have been applied at 20 % (5 CV), 25 % (10 CV), 30 % (18 CV), 35 % (6 CV) and 40 % (35 CV). The product was eluted as the THF content reached 40 % in the mobile phase. The fractions were gathered, the solvent was removed under reduced pressure and the residue was precipitated in Hex at ambient temperature. An acidic workup was not performed since the aldehyde functionality was regenerated after the purification. (Yield: 45 %, 52 mg).

¹H NMR (500 MHz, CDCl₃): δ = 10.73 (s, 1H), 7.79 (d, J = 7.9 Hz, 2H), 7.73 (d, J = 7.9 Hz, 2H), 7.48 – 7.41 (m, 4H), 7.38 (t, J = 8.0 Hz, 1H), 7.24 (t, J = 7.9 Hz, 1H), 6.94 – 6.81 (m, 4H), 6.56 – 6.44 (m, 4H), 5.98 (d, J = 4.1 Hz, 1H), 5.24 – 5.17 (m, 4H), 5.13 (s, 2H), 4.72 – 4.64 (m, 1H), 3.74 (s, 3H), 3.68 – 3.57 (m, 2H), 3.49 – 3.34 (m, 4H), 3.31 – 3.10 (m, 3H), 3.04 – 2.83 (m, 3H), 2.59 (s, 3H), 2.23 – 2.05 (m, 1H), 1.74 – 1.50 (m, 6H), 1.50 – 1.22 (m, 6H) ppm. **¹³C NMR** (125 MHz, CDCl₃): δ 192.2, 180.3, 177.6, 175.8, 167.2, 139.7, 138.5, 136.5, 134.5, 129.7, 127.4, 127.2, 127.1, 126.5, 124.6, 121.6, 111.1, 110.4, 81.1, 69.9, 61.3, 52.8, 52.5, 47.6, 47.1, 46.7, 39.6, 39.3, 38.4, 38.1, 29.0, 28.5, 27.8, 27.4, 27.3, 25.7, 25.3, 23.0, 21.5 ppm. **MS** (ESI) *m/z*: [M + Na]⁺ calcd. for C₅₇H₆₀N₄O₁₃, 1031.4049; found 1031.4067. Details of the ¹H NMR chemical shift assignments can be found in **Figure 42** (Section 3.3.2).

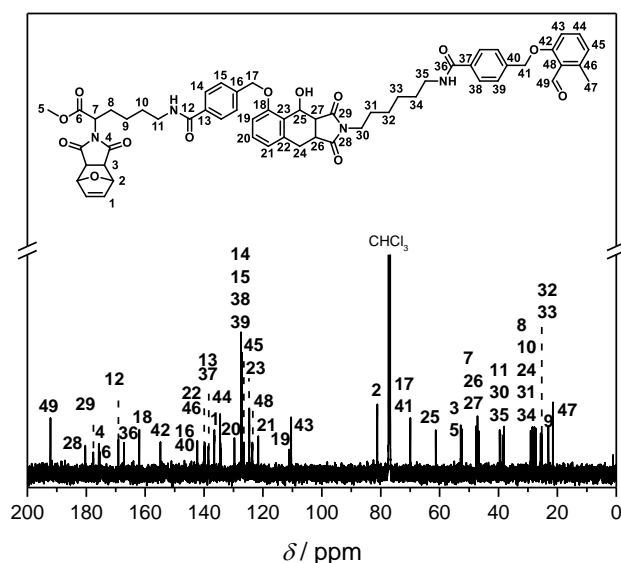


Figure S103. ¹³C NMR spectrum of the dimer **20b** recorded in CDCl₃ at 125 MHz. For the resonance assignments refer to the depicted structure.

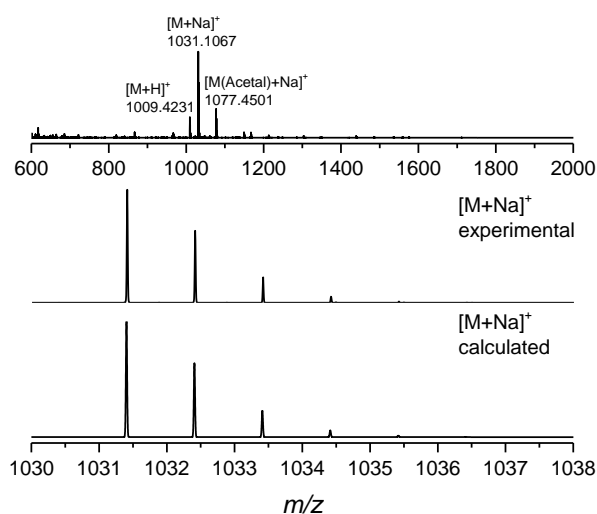


Figure S104. Full ESI-MS spectrum of the dimer **20b** (top) recorded in THF/MeOH (3:2). ESI-MS spectra of the dimer **20b** isotopic pattern (bottom). Recorded mass spectra shown are in excellent agreement with the calculated isotope pattern.

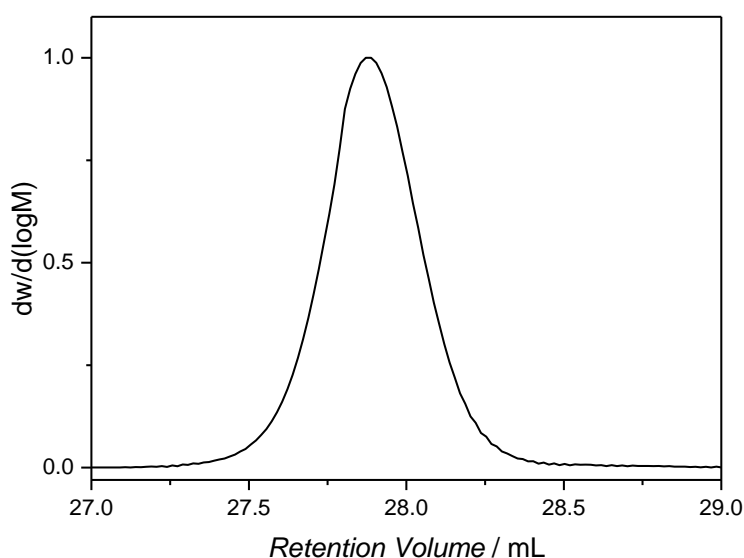
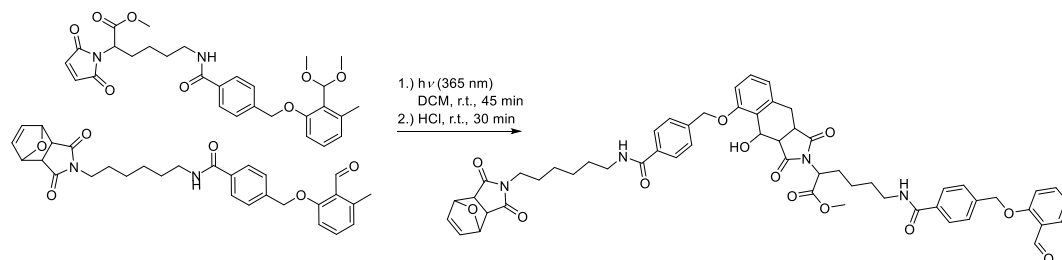


Figure S105. SEC trace of the dimer **20b** recorded in THF at 35 °C. ($\bar{M}_w = 1.01$, $V_p = 27.9$ mL).

Synthesis of Photodimer **20c**



All operations were conducted under argon atmosphere. The synthesis of **20c** was performed similarly to the photodimer **7** with the furan deprotected and acetal protected monomer **19a*** (63.6 mg, 0.11 mmol, 1.00 eq.) and monomer **5a** (61.5 mg, 0.12 mmol, 1.05 eq.) dissolved

in anhydrous DCM (40 mL). After irradiation and the removal of the solvent, **20c** was diluted with DCM (30 mL) and treated with aqueous 0.5 N HCl (30 mL) for 2 h. Subsequently, the layers were separated and the aqueous layer was extracted twice with DCM (20 mL). The purification was performed *via* reverse phase flash chromatography (SNAP C18 12 g, 12 mL min⁻¹) with MQ water and a THF gradient of 1.0 % per column volume. Isocratic phases of a constant THF content have been applied at 20 and 25 % (9 CV respectively), 30 % (23 CV), 35 % (5 CV) and 40 % (35 CV). The product was eluted as the THF content reached 40 % in the mobile phase. The fractions were gathered, the solvent was removed under reduced pressure and the residue was precipitated in Hex at ambient temperature. (Yield: 45 %, 52 mg).

¹H NMR (500 MHz, CDCl₃): δ = 10.70 (d, *J* = 5.6 Hz, 1H), 7.87 – 7.63 (m, 4H), 7.59 – 7.42 (m, 3H), 7.42 – 7.34 (m, 2H), 7.34 – 7.26 (m, 2H), 7.26 – 7.14 (m, 1H), 6.95 – 6.77 (m, 4H), 6.52 (s, 3H), 6.06 – 5.89 (m, 1H), 5.25 (s, 2H), 5.21 – 5.04 (m, 4H), 4.89 – 4.72 (m, 1H), 3.82 – 3.72 (m, 3H), 3.55 – 2.94 (m, 8H), 2.85 (s, 2H), 2.60 (s, 3H), 2.43 – 1.79 (m, 4H), 1.72 – 1.50 (m, 6H), 1.42 – 1.20 (m, 6H) ppm. **¹³C NMR** (125 MHz, CDCl₃): δ = 192.1, 179.6, 176.9, 176.5, 169.7, 169.4, 167.2, 162.0, 154.7, 142.3, 138.2, 136.6, 134.5, 127.4, 127.4, 127.1, 127.0, 126.6, 124.7, 123.6, 121.6, 111.4, 110.5, 81.0, 70.2, 70.0, 61.4, 61.2, 52.8, 52.5, 47.4, 47.2, 46.3, 40.0, 39.8, 39.7, 38.7, 38.1, 37.6, 29.5, 29.2, 28.8, 27.8, 27.4, 27.4, 26.1, 25.9, 22.9, 21.5 ppm. **MS** (ESI) *m/z*: [M + Na]⁺ calcd. for C₅₇H₆₀N₄O₁₃, 1031.4049; found 1031.4116. Details of the ¹H NMR chemical shift assignments can be found in **Figure 42** (Section 3.3.2).

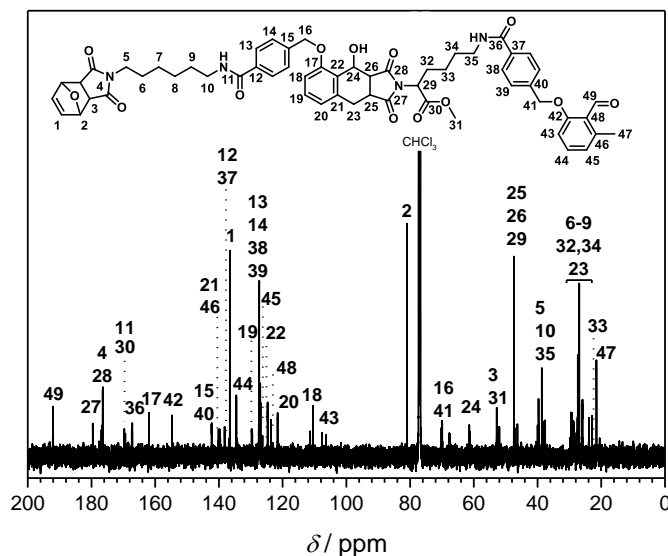


Figure S106. ¹³C NMR spectrum of the dimer **20c** recorded in CDCl₃ at 125 MHz. For the resonance assignments refer to the depicted structure.

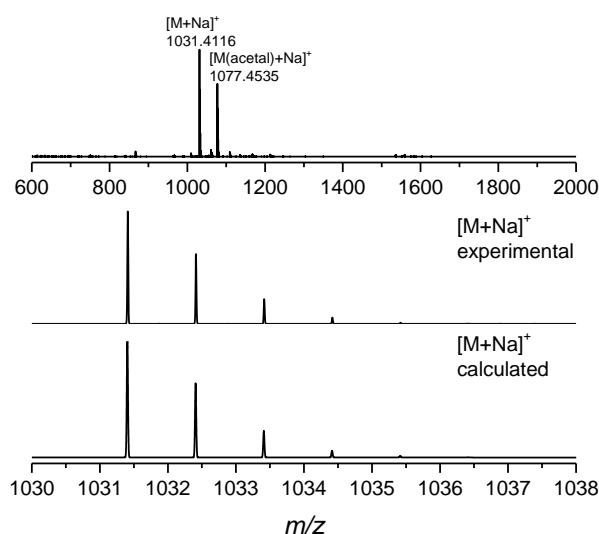


Figure S107. Full ESI-MS spectrum of the dimer **20c** (top) recorded in THF/MeOH (3:2). ESI-MS spectra of the dimer **20c** isotopic pattern (bottom). Recorded mass spectra shown are in excellent agreement with the calculated isotope pattern.

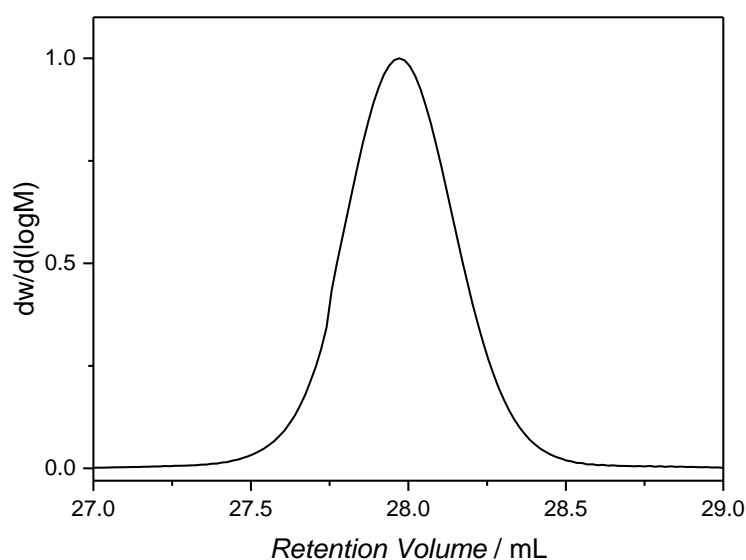
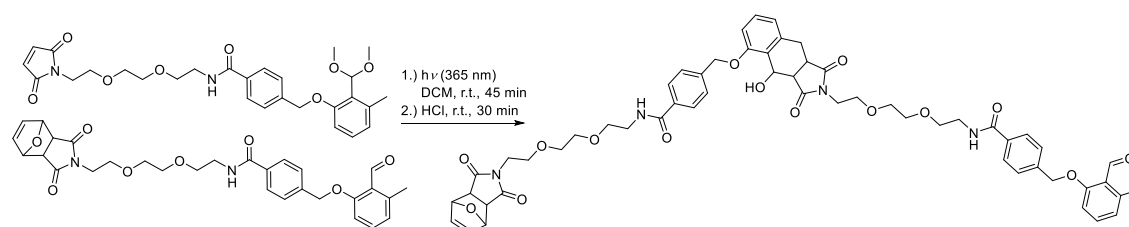


Figure S108. SEC trace of the dimer **20c** recorded in THF at 35 °C. ($D = 1.01$, $V_p = 28.0$ mL).

Synthesis of Photodimer **20d**



All operations were conducted under argon atmosphere. The synthesis of **20d** was performed under batch conditions similarly to **7** with the furan deprotected and acetal protected mono-

mer **5b*** (52.4 mg, 95.5 μmol , 1.00 eq.) and monomer **5b** (55.0 mg, 0.1 mmol, 1.05 eq.) dissolved in anhydrous DCM (40 mL). After irradiation, the single fractions were gathered and the solvent removed under reduced pressure. The residue was diluted with DCM (30 mL) and treated with aqueous 0.5 N HCl (30 mL) for 2 h. Subsequently, the layers were separated and the aqueous layer was extracted twice with DCM (20 mL). The purification was performed *via* reverse phase flash chromatography (SNAP C18 12 g column 12 mL min⁻¹) with MQ water and a THF gradient of 1.0 % per CV. Isocratic phases of a constant THF content have been applied at 20 % and 25 % (5 CV) and 30 % (20 CV). The product was eluted as the THF content reached 30 % in the mobile phase. The fractions were gathered, the solvent was removed under reduced pressure and the residue was precipitated in Hex at ambient temperature. (Yield: 45 %, 44.3 mg).

¹H NMR (500 MHz, CDCl₃): δ = 10.76 (s, 1H), 7.82 (d, J = 8.2 Hz, 2H), 7.64 (d, J = 8.1 Hz, 2H), 7.43 (d, J = 7.9 Hz, 2H), 7.39 (t, J = 8.0 Hz, 1H), 7.36 – 7.31 (m, 2H), 7.28 (d, J = 8.8 Hz, 2H), 7.15 (t, J = 7.9 Hz, 1H), 6.91 – 6.84 (m, 3H), 6.71 (d, J = 8.3 Hz, 1H), 6.47 (s, 2H), 5.95 (d, J = 3.3 Hz, 1H), 5.20 (d, J = 4.0 Hz, 2H), 5.16 (s, 2H), 5.09 – 4.93 (m, 2H), 4.11 – 3.91 (m, 2H), 3.82 – 3.73 (m, 2H), 3.73 – 3.57 (m, 18H), 3.56 – 3.47 (m, 2H), 3.47 – 3.40 (m, 1H), 3.39 – 3.27 (m, 2H), 3.27 – 3.18 (m, 2H), 3.06 – 2.98 (m, 1H), 2.82 (s, 2H), 2.61 (s, 3H) ppm. **¹³C NMR** (125 MHz, CDCl₃): δ = 192.3, 180.4, 177.9, 176.4, 167.6, 166.9, 162.1, 154.8, 142.3, 139.8, 139.4, 138.4, 136.6, 134.8, 134.6, 133.9, 129.8, 127.7, 127.6, 126.8, 125.4, 124.7, 123.7, 121.3, 110.5, 110.4, 81.0, 71.0, 70.3, 70.1, 70.00, 69.9, 69.5, 67.9, 67.3, 61.5, 48.0, 47.6, 39.9, 39.4, 38.3, 38.0, 37.6, 27.3, 21.2 ppm. **MS** (ESI) *m/z*: [M + Na]⁺ calcd. for C₅₆H₆₀N₄O₁₅, 1051.3947; found 1051.3957.

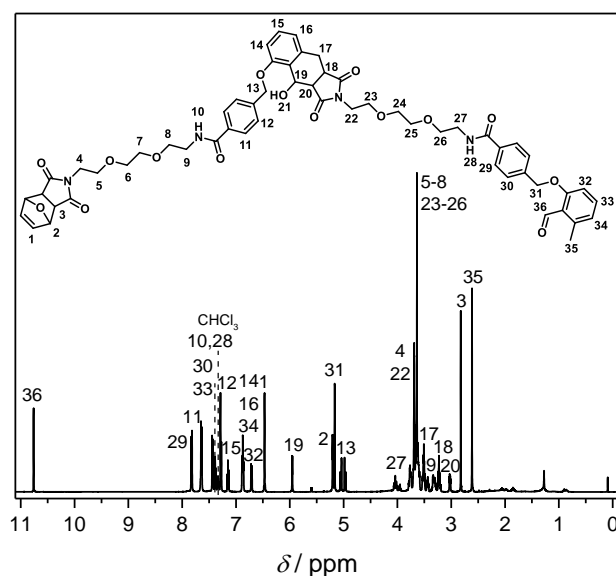


Figure S109. ¹H NMR spectrum of the dimer **20d** recorded in CDCl₃ at 400 MHz. For the resonance assignments refer to the depicted structure.

5. Experimental Section

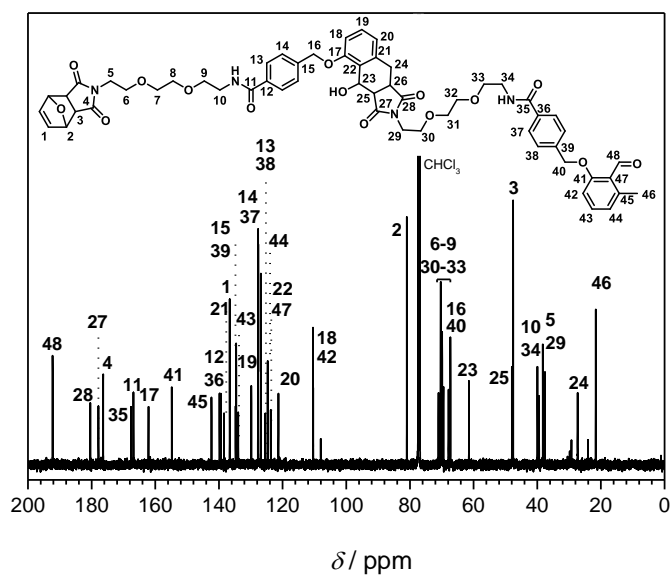


Figure S110. ^{13}C NMR spectrum of the dimer **20d** recorded in CDCl_3 at 125 MHz. For the resonance assignments refer to the depicted structure.

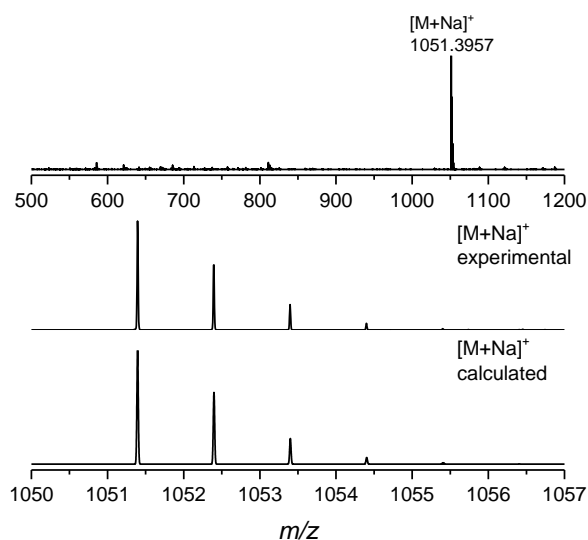


Figure S111. Full ESI-MS spectrum of the dimer **20d** (top) recorded in THF/MeOH (3:2). ESI-MS spectra of the dimer **20d** isotopic pattern (bottom). Recorded mass spectra shown are in excellent agreement with the calculated isotope pattern.

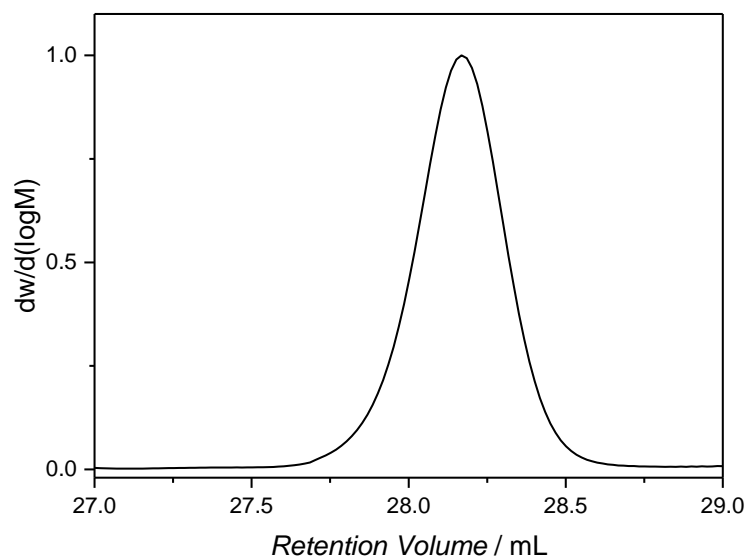
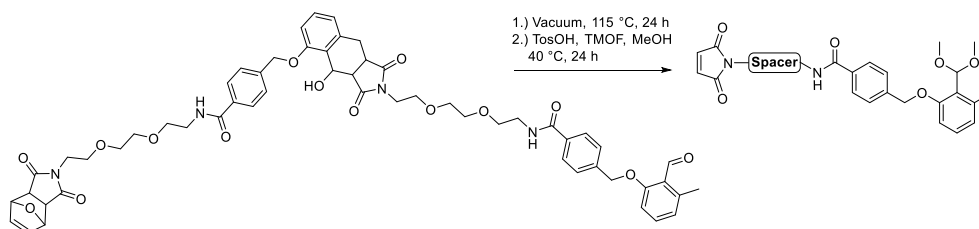


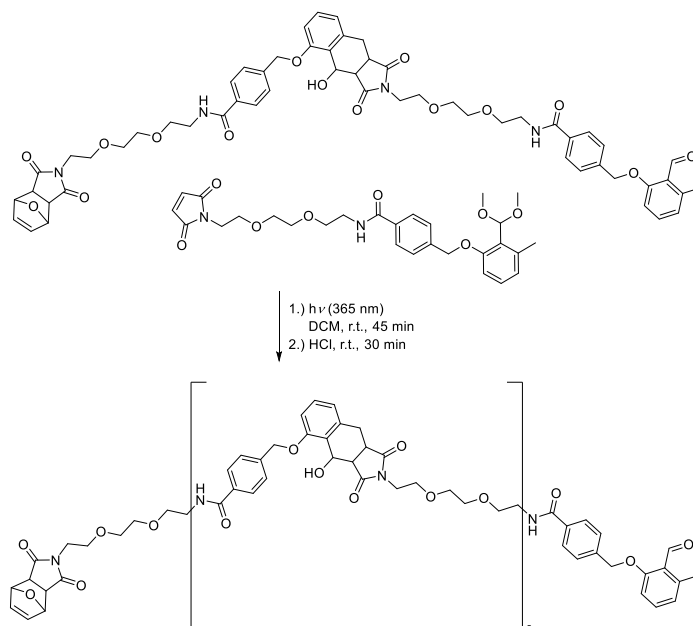
Figure S112. SEC trace of the dimer **20d** recorded in THF at 35 °C. ($\bar{D} = 1.01$, $V_p = 28.2$ mL).

Synthesis of the Dimer Acetal **20d***



All operations were conducted under argon atmosphere and protected from light. The synthesis of **20d*** was performed similarly to **5a***. Dimer **20d** (25.6 mg, 16.6 μmol , 1.00 eq.) was heated at 115 °C for 8 h under vacuum and was kept under vacuum at ambient temperature overnight for two cycles to quantitatively remove the furan protecting group. The product was employed without any further purification. Furan deprotected dimer **20d** (24.0 mg, 23.3 μmol , 1.00 eq.), pTsOH (0.4 mg, 1.9 μmol , 0.08 eq.) and TMOF (10 μL , 93.3 μmol , 4.00 eq.) were suspended in anhydrous MeOH (1.0 mL). The reaction suspension was heated to 40 °C and the reaction mixture was stirred for 24 h. Afterwards, the crude reaction mixture was filtrated over silica (anhydrous DCM/MeOH 4:1, 1.0 % Et₃N) and the solvent was removed under reduced pressure to provide the target compound as an orange oil. **20d*** was immediately employed for the synthesis of **21b**.

Synthesis of the Trimer 21a



All operations were conducted under argon atmosphere. The reaction was conducted under batch conditions similarly to the synthesis of dimer **20d**. The furan deprotected and acetal protected monomer **5b*** (36.0 mg, 65.6 μmol , 1.50 eq.) and dimer **20d** (45.0 mg, 43.7 μmol , 1.00 eq.) were mixed and dissolved in anhydrous DCM (25 mL). The purification was carried out *via* reverse phase flash chromatography (SNAP C18 12 g column 12 mL min^{-1}) with water and a THF gradient of 1.0 % per CV. Isocratic phases of a constant THF content have been applied at 20 and 25 % (9 CV respectively), 30 % (15 CV), 35 % (24 CV) and 40 % (12 CV). The product was eluted as the THF content reached 40 % in the mobile phase. The fractions were gathered, the solvent was removed under reduced pressure and the residue was precipitated in CH at ambient temperature. An acidic workup was not performed since the aldehyde functionality was regenerated after the purification. (Yield: 61 %, 28 mg).

^1H NMR (500 MHz, CDCl_3): δ = 10.76 (s, 1H), 8.00 – 7.77 (m, 2H), 7.78 – 7.70 (m, 2H), 7.70 – 7.59 (m, 2H), 7.59 – 7.52 (m, 2H), 7.51 – 7.33 (m, 3H), 7.33 – 7.21 (m, 3H), 7.21 – 7.10 (m, 2H), 6.98 – 6.82 (m, 4H), 6.81 – 6.63 (m, 2H), 6.47 (s, 2H), 5.96 (s, 2H), 5.27 – 5.12 (m, 4H), 5.12 – 4.86 (m, 4H), 4.10 – 3.93 (m, 2H), 3.84 – 3.59 (m, 30H), 3.58 – 3.46 (m, 4H), 3.47 – 3.28 (m, 2H), 3.29 – 3.18 (m, 4H), 3.03 (s, 2H), 2.82 (s, 2H), 2.62 (s, 3H) ppm. **^{13}C NMR** (125 MHz, CDCl_3): δ 192.3, 180.4, 176.4, 166.8, 162.2, 154.9, 142.4, 140.0, 139.4, 138.4, 136.7, 134.6, 129.9, 127.7, 127.6, 127.6, 127.4, 126.9, 124.7, 123.7, 110.5, 110.5, 81.0, 70.4, 70.1, 69.9, 69.6, 69.5, 67.9, 67.3, 61.6, 61.4, 48.0, 47.9, 47.6, 40.0, 39.6, 38.3, 38.0, 37.6, 27.3, 27.0, 21.6 ppm. **MS** (ESI) m/z : $[\text{M} + \text{Na}]^+$ calcd. for $\text{C}_{82}\text{H}_{88}\text{NaN}_6\text{O}_{22}$, 1531.5844; found 1531.5918.

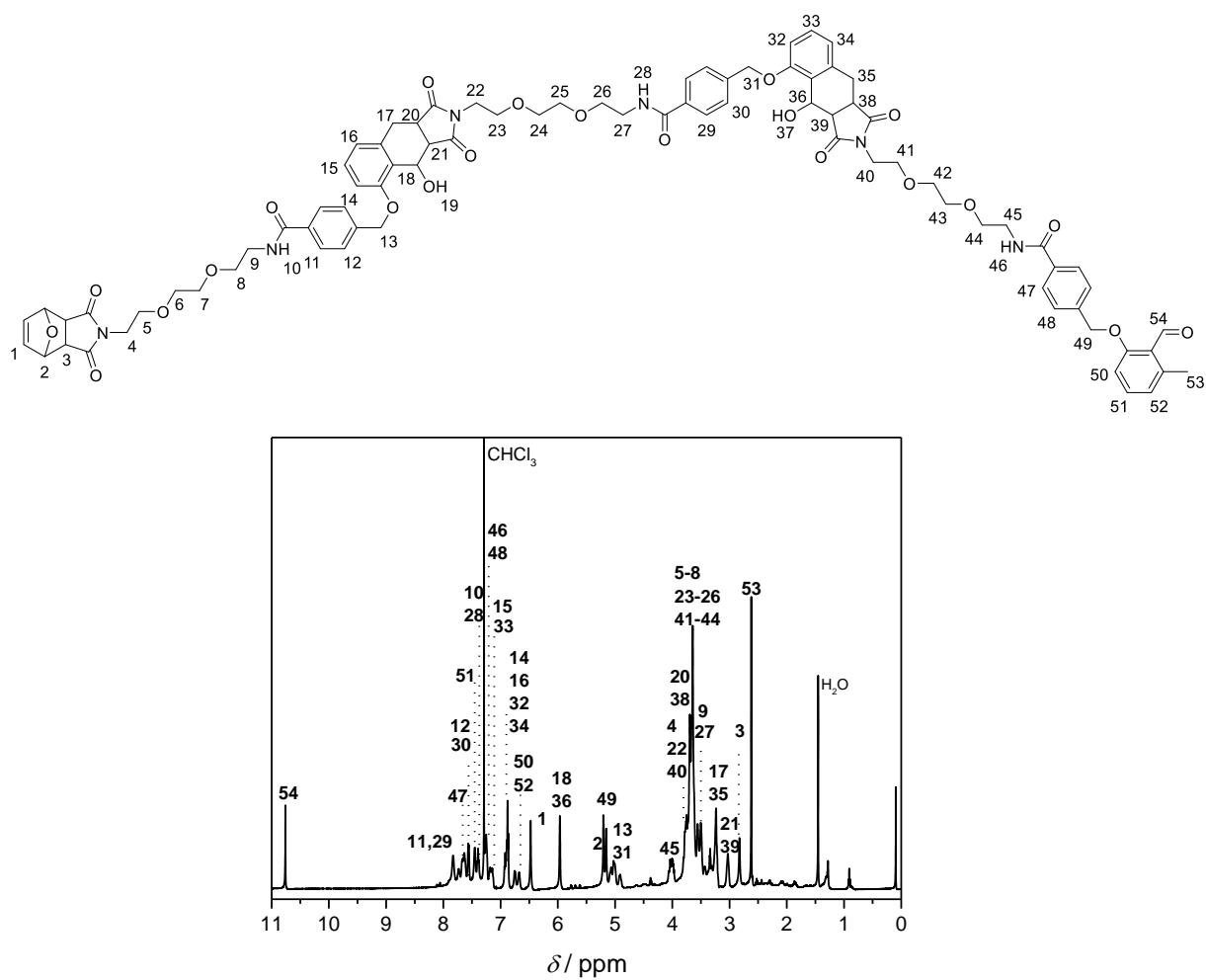


Figure S113. ^1H NMR spectrum of the trimer **21a** recorded in CDCl_3 at 400 MHz. For the resonance assignments refer to the depicted structure.

5. Experimental Section

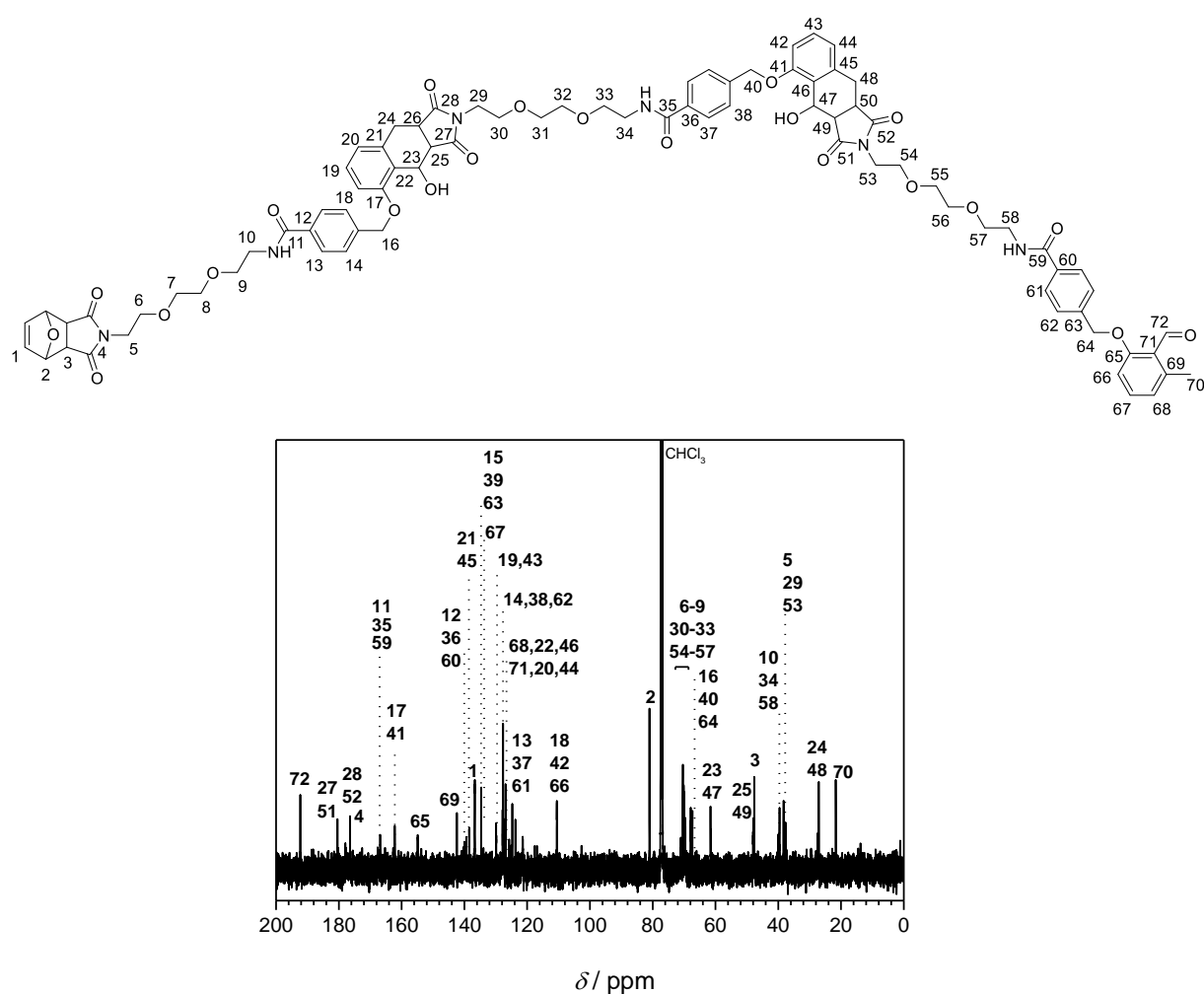


Figure S114. ^{13}C NMR spectrum of the trimer **21a** recorded in CDCl_3 at 125 MHz. For the resonance assignments refer to the depicted structure.

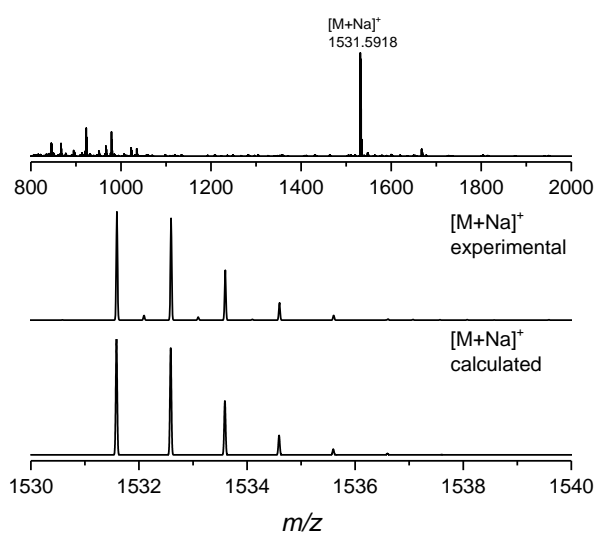


Figure S115. Full ESI-MS spectrum of the trimer **21a** (top) recorded in THF/MeOH (3:2). ESI-MS spectra of the trimer **21a** isotopic pattern (bottom). Recorded mass spectra shown are in excellent agreement with the calculated isotopic pattern.

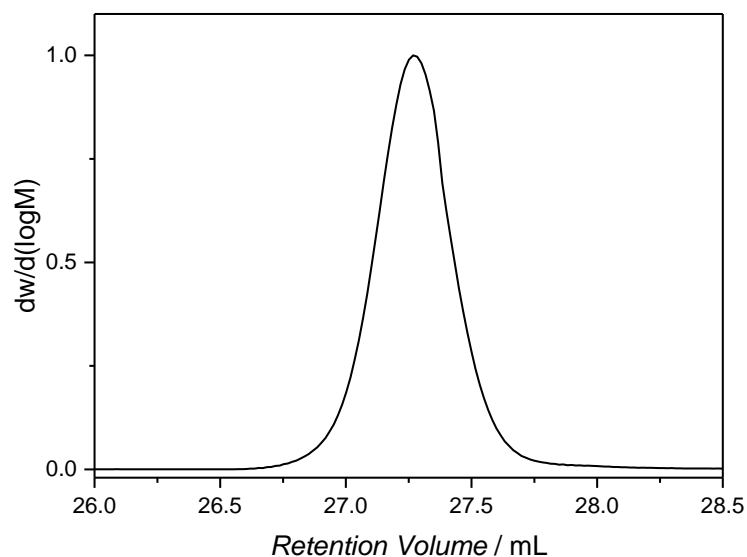
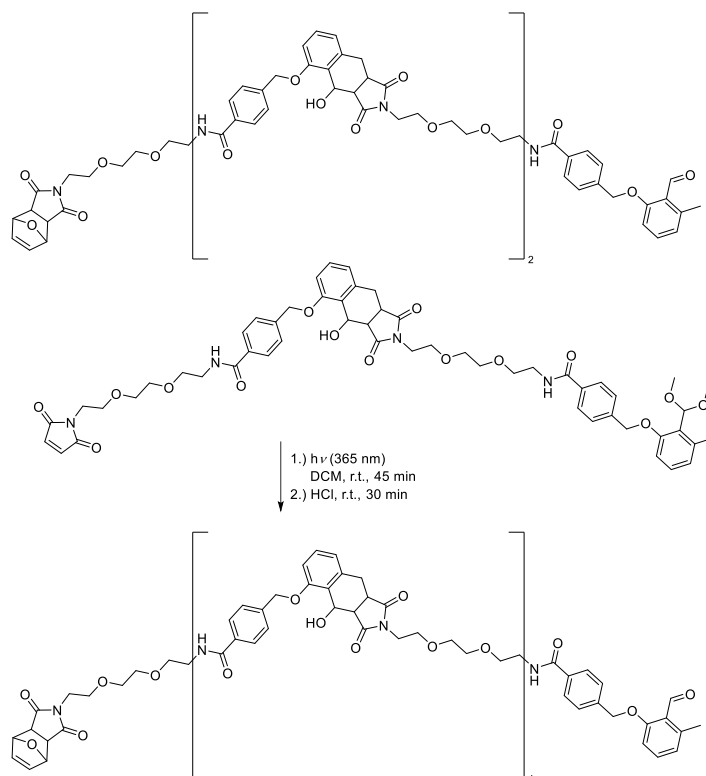


Figure S116. SEC trace of the trimer **21a** recorded in THF at 35 °C. ($D = 1.01$, $V_p = 27.3$ mL).

Synthesis of the α,ω -Functionalized Pentamer **21b**



The reaction was conducted under batch conditions similarly to the synthesis of dimer **20d**. Under inert atmosphere, furan deprotected and acetal protected dimer **20d*** (24.0 mg, 23.3 μmol , 1.50 eq.) and trimer **21a** (23.5 mg, 15.5 μmol , 1.00 eq.) were mixed and dissolved in anhydrous DCM (10 mL). Purification was carried out *via* reverse phase flash chromatography (SNAP C18 12 g column 12 mL min^{-1}) with MQ water and a THF gradient of 1.0 % per CV. Isocratic phases of a constant THF content have been applied at 25 % (9 CV), 30 % (15 CV), 35 % (21 CV) and 40 % (18 CV). The product was eluted as the THF

5. Experimental Section

content reached 40 % in the mobile phase. The fractions were gathered, the solvent was removed under reduced pressure and the residue was precipitated in Hex at ambient temperature. An acidic workup was not performed since the aldehyde functionality was regenerated after the purification. (Yield: 20 %, 7 mg).

MS (MALDI) m/z : $[M + H]^+$ calcd. for $C_{134}H_{144}N_{10}O_{36}$, 2469.98; found 2469.45.

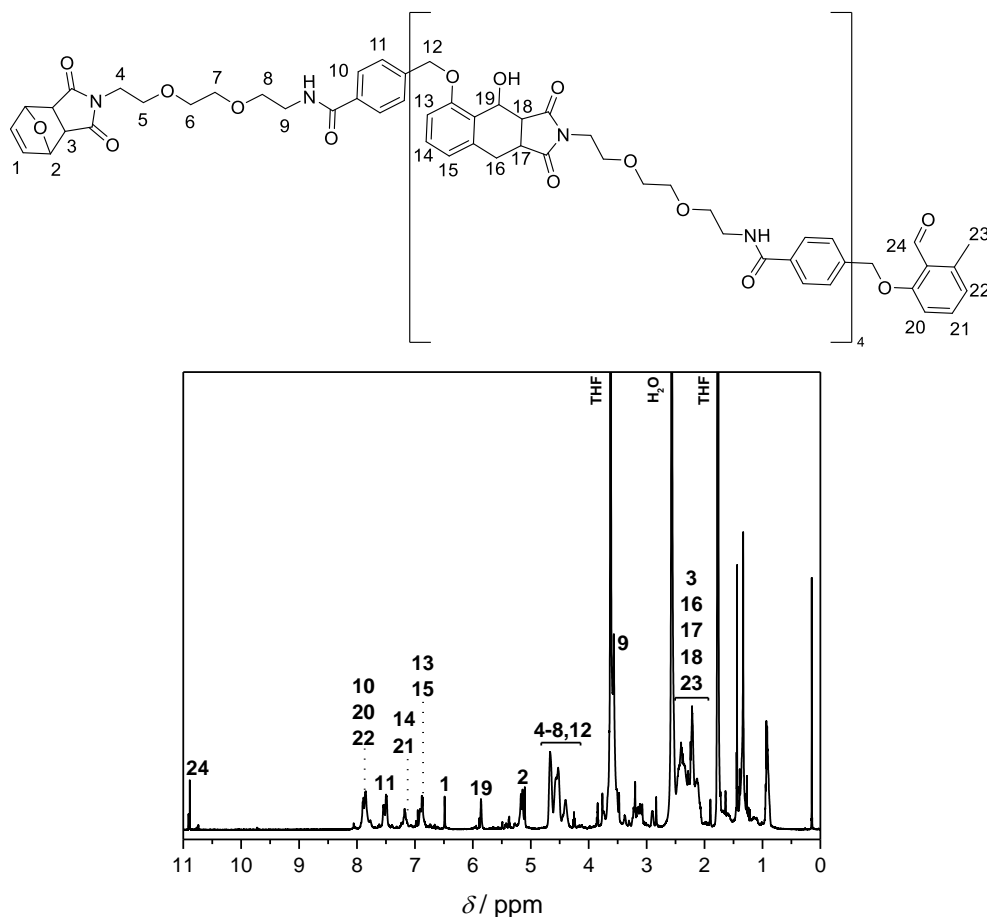


Figure S117. 1H NMR spectrum of the pentamer **21b** recorded in $CDCl_3$ at 400 MHz. For the resonance assignments refer to the depicted structure.

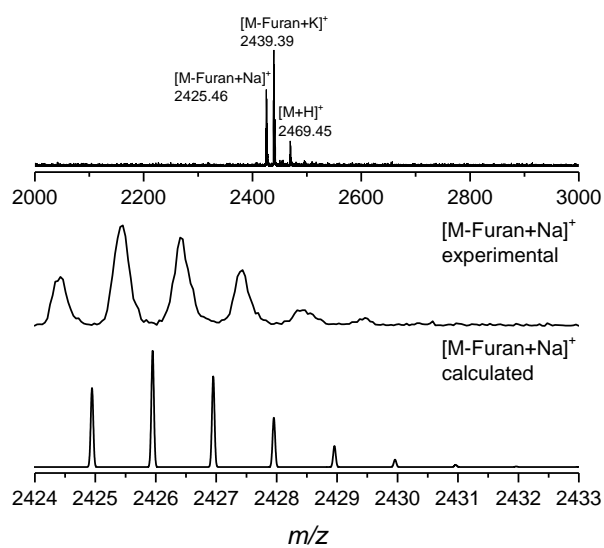


Figure S118. Full MALDI-ToF spectrum of the pentamer **21b** (top). MALDI-ToF spectra of the pentamer **21b** isotopic pattern (bottom). Recorded mass spectra shown are in excellent agreement with the calculated isotope pattern.

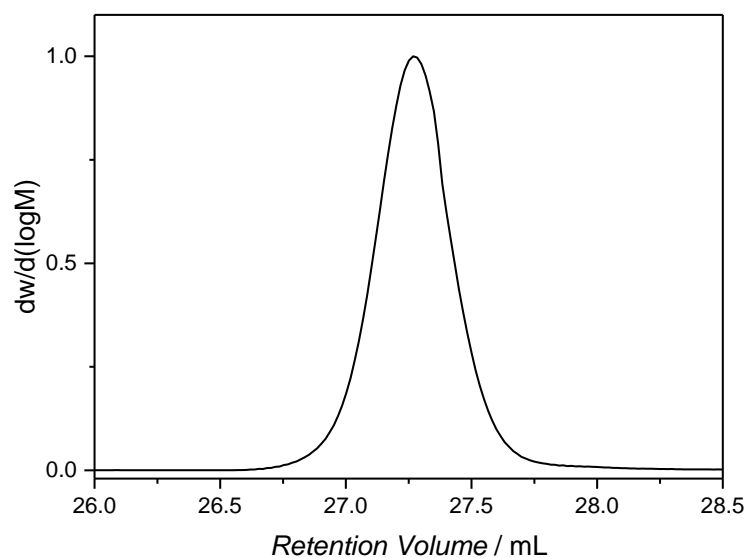


Figure S119. SEC trace of the pentamer **21b** recorded in THF at 35 °C. ($D = 1.01$, $V_p = 26.3$ mL).

List of Abbreviations

A	Absorbance
AFIR	Artificial force induced reaction
ATRP	Atom transfer radical polymerization
B-3CR	Biginelli three-component reaction
Boc	<i>tert</i> -Butyloxycarbonyl
CH	Cyclohexane
CID	Collision-induced dissociation
CRP	Controlled radical polymerization
CT	Charge-Transfer
CuAAC	Copper-catalyzed azide-alkyne cycloaddition
<i>D</i>	Dispersity
DA	Diels–Alder
Da	Dalton
DCC	<i>N,N'</i> -Dicyclohexylcarbodiimide
DCM	Dichloromethane
DFT	Density functional theory
DMAc	Dimethylacetamide
DMAP	4-Dimethylaminopyridine
DMBD	2,3-Dimethyl butadiene
DMF	Dimethylformamide
DMSO	Dimethyl sulfoxide
DNA	Deoxyribonucleic acid
EA	Ethyl acetate
EDC·HCl	1-Ethyl-3-(3-dimethylaminopropyl)carbodiimide
EDG	Electron donating groups
ESI-MS	Electrospray ionization – mass spectrometry
<i>et al.</i>	<i>et alii</i>
EWG	Electron withdrawing groups
FAS	Phenacyl sulfide
FMO	Frontier molecular orbital
Fmoc	Fluoromethoxycarbonyl
FT-IR	Fourier transformed infrared spectroscopy
h	Hour
H-3CR	Hantzsch three-component reaction
H-4CR	Hantzsch four-component reaction
HBTU	2-(1H-Benzotriazol-1-yl)-1,1,3,3-tetramethyluronium hexafluorophosphate
HDA	Hetero Diels–Alder
HOBt	Hydroxybenzotriazole
HOMO	Highest occupied molecular orbital

HPLC	High-performance liquid chromatography
i.e.	id est
IC	Internal conversion
IEG	Iterative exponential growth
IMCR	Isocyanide-based multicomponent reaction
ISC	Intersystem crossing
IUPAC	International union of pure and applied chemistry
λ	Wavelength
LbL	Layer-by-Layer
LEDs	Light-emitting diode
LUMO	Lowest unoccupied molecular orbital
m/z	Mass-to-charge ratio
M-3CR	Mannich three-component reaction
MALDI	Matrix-assisted laser desorption/ionization
MCR	Multicomponent reactions
Me ₆ TREN	tris[2-(Dimethylamino)ethyl]amine
Hz	Hertz
min	Minute
MO	Molecular orbitals
MUMI	Multiple unit monomer insertions
nBuA	n-Butyl acrylate
NICAL	Nitrile imine carboxylic acid ligation
NITEC	Nitrile imine mediated tetrazole-ene cycloaddition
NMP	Nitroxide-mediated radical polymerization
NMR	Nuclear magnetic resonance spectroscopy
<i>o</i> -MBA	<i>o</i> -Methylbenzaldehyde
P-3CR	Passerini three-component reaction
PAT	Pyrene functional aryl tetrazole
PBS	Phosphate buffered saline
PEG	Poly(ethylene glycol)
PFA	Perfluoroalkoxy alkane
ppm	Parts per million
PS	Polystyrene
<i>p</i> -TsOH	<i>para</i> -Toluenesulfonic acid
PyBOP	Benzotriazol-1-yl-oxytripyrrolidino phosphonium hexafluorophosphate
QR	Quick Response
RAFT	Radical addition fragmentation chain transfer
rDA	retro-Diels–Alder
RDRP	Reversible-deactivation radical polymerization
RNA	Ribonucleic acid
S-3CR	Strecker three-component reaction

List of Abbreviations

SEC	Size exclusion chromatography
S_n	Singlet state
SPPS	Solid-phase peptide synthesis
SUMI	Single unit monomer insertions
T_n	Triplet state
τ	Life time
TBDMS	Tert-Butyldimethylsilylgruppe
TFA	Trifluoroacetic acid
THF	Tetrahydrofuran
TMOF	Trimethyl orthoformate
ToF	Time of flight
TS	Transition state
U-4CR	Ugi four-component reaction
UV	Ultraviolet
UV-Vis	Ultraviolet-visible spectroscopy
W-H	Woodward-Hoffmann
Φ	Quantum yield

List of Figures and Schemes

Figure 1. Graphical abstract for the photochemical synthesis of sequence-defined macromolecules.	2
Figure 2. Exemplary illustration for a suprafacial and an antarafacial reaction progression for <i>p</i> -orbitals and <i>p</i> -orbitals in conjugated π -systems. ^[84-85]	8
Figure 3. General mechanism of the concerted [4+2] cycloaddition and FMO interactions in DA reactions for unperturbed, normal, and inverse electron demand systems. Reproduced with permission from Springer. ^[82-83]	9
Figure 4. Illustration of Beer-Lambert's law for the determination of the Absorbance <i>A</i> of a light absorbing moiety, where <i>I</i> ₀ is the incident intensity of the light source, <i>I</i> the transmitted intensity, ϵ the wavelength depending extinction coefficient, <i>c</i> the concentration of the absorbing molecule, and <i>d</i> the length of the absorption path. ^[106]	11
Figure 5. Schematic Jablonski diagram showing radiative and non-radiative photochemical transitions. The electronic energy levels are portrayed in a simplified way to illustrate internal conversion (IC) and intersystem crossing (ISC) as well as the principle of fluorescence and phosphorescence. ^[107]	12
Figure 6. The Franck-Condon principle with vertical depicted electronic transitions between electronic states with the highest overlap of the vibrational wave function. ^[108]	13
Figure 7. Visualization of the absorption wavelengths in relation of the main electronic transitions in organic molecules occurring upon irradiation of light. ^[111]	15
Figure 8. Comparison of FMOs of formaldehyde and thioformaldehyde as calculated by Vedejs <i>et al.</i> ^[132] ..	19
Figure 9. Tetrazoles with different substituents at their <i>N</i> -position and respective excitation wavelengths. ^[79, 150-151]	27
Figure 10. Overview of resins employed as solid support in solid-phase synthesis. From left to right: chloromethyl resin (Merrifield resin), 2-chlorotrityl chloride resin, Rink amide resin, Sieber amide resin. ^[191]	38
Figure 11. General structures of peptides (amino acid backbone) and peptoids (<i>N</i> -glycine backbone). ^[191,200]	40
Figure 12. Exemplary structure of a synthetic oligonucleotide applying the phosphoramidite strategy with the DNA-bases adenine, cytosine, thymine, and guanine. ^[210-211]	42
Figure 13. (a) Phosphoramidite based monomer units for the synthesis of sequence-encoded macromolecules. (b) Iterative approach using a solid support starting after the TTT sequence introduction with i) DMT deprotection, ii) coupling step, iii) oxidation, iv) capping, and v) cleavage. Reprinted with permission from A. A. Ouahabi <i>et al.</i> , <i>ACS Macro Lett.</i> 2015 , <i>4</i> , 1077-1080. Copyright 2015 American Chemical Society. ^[56]	44
Figure 14. (a) Basic structure of the sequence-defined macromolecule synthesized by an automated phosphoramidite chemistry approach. Two bytes are linked with an alkoxyamine containing a NO-C bond for tandem MS fragmentation. The single bytes contain a mass tag for identification after CID fragmentation. (b) Structure of the monomer units employed for binary coding of information into the macromolecule. (c) Structure of the respective mass tags. (d) Schematic representation of the read-out of a 4 bytes containing macromolecule by tandem MS under CID conditions. In the first step, the macromolecule undergoes fragmentation at the NO-C bonds (depicted in yellow inside the grey spacers) resulting in the single byte fragments. Based on the mass tag the single byte fragments are sorted out by mass. In the next step, the single bytes are analyzed to identify their sequence order. The figure was reprinted from a publication of Al Ouahabi <i>et al.</i> licensed under a Creative Commons Attribution license. ^[229]	46
Figure 15. Schematic illustration for encoding and decoding of a QR code using a Chemcoder and Chemreader. The QR code is first translated into a bit string and transferred into a pentadecimal numeral system (base-20) and divided into smaller fragments of the identical length containing an index system (purple). After readout of the sequences by tandem MS and analysis by the Chemreader,	

the original sequence is reconverted by the Chemreader resulting in the QR code. The figure was reprinted from a publication of Martens <i>et al.</i> licensed under a Creative Commons Attribution license. ^[42]	48
Figure 16. Sequence readout using tandem MS (MALDI-MS/MS) of a pentamer with different side chain functionalities. Fragmentation pattern and recurrence of the encoded oligomer is highlighted from right to left in blue and from left to right in purple. The figure was reprinted from a publication of Martens <i>et al.</i> licensed under a Creative Commons Attribution license. ^[42]	50
Figure 17. Graphical abstract for the combination of the P-3CR and photoinduced <i>o</i> -MBA conjugation. The aquarelle was prepared by Fabian Blößer.....	64
Figure 18. ¹ H NMR spectra of the maleimide-acid 2 and its precursors 2a-c recorded in CDCl ₃ at 400 MHz. For the signal assignments refer to the depicted structures.	67
Figure 19. ¹ H NMR (top) and ¹³ C NMR (bottom) spectrum of 1,6-diisocyanohexane 4 recorded in CDCl ₃ at 400 and 101 MHz, respectively. For the signal assignments refer to the depicted structure.	68
Figure 20. ¹ H NMR spectra of the Passerini linker units 1a-c (top to bottom) recorded in CDCl ₃ at 400 MHz. For the signal assignments refer to the depicted structures.	70
Figure 21. ¹ H NMR spectra of the photomonomer units 5a-b (top to bottom) recorded in CDCl ₃ at 400 MHz. For the signal assignments refer to the depicted structures.	73
Figure 22. ¹ H NMR spectra of the photomonomer acids 6a-b (top to bottom) recorded in CDCl ₃ at 400 MHz. For the signal assignments refer to the depicted structures.	74
Figure 23. ¹ H NMR spectrum of the photodimer 7 recorded in CDCl ₃ at 400 MHz. For the signal assignments refer to the depicted structure.....	75
Figure 24. (a-c) SEC traces of the synthesized sequence-defined macromolecules 10a-c alternately consisting of Passerini and photoblocks. Additionally, the core unit sebacic acid 8 , the building blocks 1a , 5a , and 6a as well as the tetramer 9 are depicted. All SEC traces were recorded on a THF based SEC system. (d) Full MS spectrum of 10c in the mass range of <i>m/z</i> 500 to 2500 recorded in positive ion mode.	79
Figure 25. Recorded (top) and calculated (bottom) ESI-MS spectra of the oligomers isotopic pattern 10a (a), 10b (b), and 10c (c).	81
Figure 26. ¹ H NMR spectrum of the sequence-defined octamer 10c recorded in CDCl ₃ at 400 MHz. For the signal assignments refer to the depicted structure.	82
Figure 27. Graphical abstract for the synthesis of sequence-defined macromolecules <i>via</i> the combination of two photoinduced conjugation methods, i.e. NICAL ligation and DA cycloaddition based on fumarates and <i>o</i> -MBAs.	84
Figure 28. ¹ H NMR spectrum of the PAT 11 recorded in CDCl ₃ at 400 MHz. For the signal assignments refer to the depicted structure.	88
Figure 29. ¹ H NMR spectrum of the <i>o</i> -MBA 12 recorded in acetone at 600 MHz. For the signal assignments refer to the depicted structure.	89
Figure 30. ¹ H NMR spectrum of the photomonomer 13 recorded in CDCl ₃ at 400 MHz. For the signal assignments refer to the depicted structure.....	91
Figure 31. ¹ H NMR (top) and ¹³ C NMR (bottom) spectrum of the monomer 14 recorded in CDCl ₃ at 400 MHz and 101 MHz, respectively. For the signal assignments refer to the depicted structure.	93
Figure 32. ¹ H NMR (top) and ¹³ C NMR (bottom) spectrum of the symmetrical core unit 15 recorded in CDCl ₃ at 400 MHz and 101 MHz, respectively. For the signal assignments refer to the depicted structure.	95
Figure 33. Peristaltic pump with a viton (0.8 mm ID) tubing for transporting the reaction mixture into the flow reactor (top). Perfluoroalkoxy alkane (PFA) polymer tubing wrapped around an aluminum carousel (reactor volume 7.5 mL) standing on an aluminum plate with LED holders and LEDs (410-420 nm) as radiation source (bottom left). Flow reactor in operation mode (bottom right).	96
Figure 34. ¹ H NMR spectrum of the reaction mixture described in Scheme 45 after irradiation in a flow reactor, recorded in CDCl ₃ at 400 MHz. For the signal assignments refer to the depicted structure.	98

Figure 35. ^1H NMR spectrum of the reaction mixture described in Scheme 46 after irradiation in a batch reactor, recorded in CDCl_3 at 400 MHz. For the signal assignments refer to the depicted structure. ...	100
Figure 36. SEC traces of the synthesized sequence-defined macromolecules 18a-e alternately chain end functionalized with benzaldehydes or carboxylic acids. Additionally, the core unit 15 , the photomonomer 13 , and monomer 14 are depicted. All SEC traces were recorded on a THF based SEC system.	103
Figure 37. (a) Full MS spectrum of 18e in the mass range of m/z 1500 to 5000 recorded in positive ion mode. (b) Recorded (top) and calculated (bottom) ESI-MS spectrum of the oligomer's 18e isotopic pattern.	105
Figure 38. ^1H NMR spectrum of the sequence-defined decamer 18e recorded in CDCl_3 at 400 MHz. For the signal assignments refer to the depicted structure. The CHCl_3 resonance is marked with a star (*). ..	106
Figure 39. Graphical abstract for the synthesis of sequence-defined macromolecules <i>via</i> photoinduced DA cycloaddition based on maleimides and <i>o</i> -MBAs. The abstract was prepared by Florian Feist.	108
Figure 40. Photomonomers including an <i>o</i> -MBA and a furan protected maleimide employed for the synthesis of functional linear sequence-defined macromolecules. The monomers 5a and 5b were equipped with a hexane and a PEG based spacer unit, whereas the photomonomers 19a-d were prepared based on a lysine spacer unit functionalized with a methyl ester, hexanol, adamantly, and a fluorobenzyl moiety.	109
Figure 41. ^1H NMR spectrum of the photomonomer 19a recorded in CDCl_3 at 400 MHz. For the signal assignments refer to the depicted structure.	111
Figure 42. ^1H NMR spectrum of the dimers 20a-c (top to bottom) recorded in CDCl_3 at 400 MHz. For the signal assignments refer to the depicted structures.	113
Figure 43. SEC traces of the synthesized non-symmetric α,ω -functionalized sequence-defined pentamer 21b (26.3 mL) and its precursors the dimer 20d (28.2 mL) and the trimer 21a (27.3 mL). In addition, the SEC trace of the photomonomer 5b (29.6 mL) is depicted. All SEC traces were recorded on a SEC system with THF as eluent.	115
Figure 44. MALDI-ToF spectra of the α,ω -functionalized pentamer 21b (depicted in the m/z range of 2000 to 4000) as well as of the dimer 20d and the trimer 21a (visible in the m/z range of 800 to 4000). The increase of m/z 480 corresponds to the addition of one equivalent of the photomonomer 5b , whereas the increase of m/z 961 corresponds to the addition of one equivalent of the dimer 20d . Dimer 20d : m/z 983.69 ([20d -furan+Na] $^+$, m/z_{calc} . 983.37, $\Delta m/z$ 0.32). Trimer 21a : m/z 1463.85 ([21a -furan+Na] $^+$, m/z_{calc} . 1463.56, $\Delta m/z$ 0.28). Pentamer 21b : m/z 2424.95 ([21b -furan+Na] $^+$, m/z_{calc} . 2424.47, $\Delta m/z$ 0.48).	116
Figure 45. SEC traces of the successively synthesized sequence-defined decamers 23a-c varying in their monomer sequence order. Additionally, the core unit, the photomonomers 5a and 19a , the α,ω -functionalized dimers 20a-c , and the symmetrical hexamers 22a-d are represented. All SEC traces were recorded on a THF based SEC system.	119
Figure 46. Overlaid MALDI-ToF mass spectra of the symmetric sequence-defined decamers 23a-d and its precursors the hexamers 22a-d as well as α,ω -functionalized dimers 20a-c . The MALDI-ToF spectra are depicted in different m/z -ranges, 800–4000 for the dimers as well as hexamers and 3500–5500 for the decamers. The m/z -intervals between the hexamers and decamers are characteristic for the addition of two dimer blocks (m/z 1797 for 20a , m/z 1883 for 20b , and m/z 1886 for 20c) at the chain termini.	120
Figure 47. Tandem mass spectrometry <i>via</i> MALDI-ToF-ToF with the symmetrical hexamers 22b (a) and 22d (b).	122
Scheme 1. DA reaction of a diene and a dienophile occurs <i>via</i> a six-membered transition state in order to form a cyclohexene derivative. Reproduced with permission of Springer. ^[82-83]	7
Scheme 2. Diastereomers (endo/exo adducts) obtained from the DA reaction between furan and maleimide. Thermal treatment leads to a rDA reaction and release of the starting materials.	10

Scheme 3. The Norrish type I reaction of aldehydes and ketones with an α -cleavage after light induced excitation results in highly reactive alkyl and acyl radicals leading to a mixture of multiple reaction pathways. The Norrish type II reaction of aldehydes and ketones with an intramolecular [1,5]-H shift of excited carbonyl functionalities resulting in various reaction products. ^[112-114]	16
Scheme 4. Mechanism for the light induced formation of thioaldehydes generated from FAS groups. ^[58]	18
Scheme 5. Mechanism and lifetimes of intermediates (for R = Ph) for the photoinduced enolization of <i>o</i> -alkylbenzophenones. Upon light absorption and the formation of excited singlet states, ISC occurs and leads to two isomeric <i>o</i> -quinodimethanes after hydrogen abstraction. The Z-isomer undergoes a 1,5-sigmatropic rearrangement to the starting material (singlet ground state), whereas the E-isomer is suitable as reactant for DA cycloadditions. ^[135]	21
Scheme 6. Photoinduced transformation of an <i>o</i> -MBA into an <i>o</i> -quinodimethane intermediate (Norrish type II reaction) with stabilizing hydrogen bonding and subsequent DA trapping by a maleimide as dienophile resulting in a tetrahydro benzoisoindole dione. Please note that the Z isomer, which is depicted in this scheme, possesses the same structural motif as the E isomer in Scheme 5 . The categorization into E or Z isomers is derived from the Cahn-Ingold-Prelog priority rules and therefore no connection between reactivity and lifetimes can be drawn from the categorization into E or Z. ^[135]	22
Scheme 7. Light induced decomposition of 2,5-disubstituted tetrazoles leading to the formation of nitrile imines, which can undergo subsequent reactions. ^[140-142]	23
Scheme 8. Reaction overview of the intermediate 1,3-nitrile imine dipole generated by dissociation upon irradiation of tetrazoles. The adducts with imidazoles, carboxylic acids (NICAL), thiols, water, acetonitrile, double bonds, which are usually substituted with EWGs (NITEC), and self-dimerization, leading to a mixture of dimers, are depicted in clockwise order. ^[143-149]	24
Scheme 9. Overview of photoreactions carried out with a tetrazole and a mixture of a functionalized enes as well as nucleophiles in competition reactions in acetonitrile and PBS at 302 nm. It is demonstrated that the nitrile imine generated upon UV-irradiation favorably forms NICAL products or adducts obtained after a nucleophilic attack rather than a NITEC adduct with less activated enes. ^[147]	26
Scheme 10. Classification of MCRs into three basic types with A and B as starting materials, C and D as intermediates and P as final product. MCRs of type I are a combination of reversible equilibrium reactions. In type II MCRs the reaction step towards the final product is irreversible. Type III MCRs consist of a sequence of non-reversible individual reaction steps. ^[152]	28
Scheme 11. Chronologically ordered important MCRs according to the reported synthetic routes from Strecker (1850), Hantzsch (1882 and 1890), Biginelli (1891), and Mannich (1912). ^[155-160]	29
Scheme 12. Mesomeric resonance structures of isocyanides are depicted including a carbene like and a zwitterionic configuration. ^[153]	30
Scheme 13. Overview of synthetic methods for the formation of isocyanides developed by Lieke (1859), Hofmann (1867), and Ugi (1958, 1960) in chronological order. ^[163-167]	31
Scheme 14. Overview of the IMCRs reported by Passerini (1921) and Ugi (1959). ^[168-170]	32
Scheme 15. Mechanism of the U-4CR as introduced by Ugi in 1961 and proposed by Fleurat-Lessard. After imine formation, a proton transfer proceeds from the carboxylic acid to the imine followed by an α -addition of the isocyanide. The α -acylaminoamide is formed after Mumm rearrangement. ^[152, 171]	33
Scheme 16. Mechanism of the P-3CR proposed by Baker and Ugi. In the first step, a six-membered transition state is formed followed by the α -addition of an isocyanide species leading to the α -acyloxyamide after Mumm rearrangement. ^[175-176]	34
Scheme 17. P-3CR mechanism based on the DFT calculations of Morokuma and co-workers. Aldehyde activation by hydrogen bonding and subsequent nucleophilic addition of an isocyanide equivalent leading to a nitrilium species. The Passerini adduct is obtained after the addition of a carboxylic acid moiety and Mumm rearrangement. ^[178]	35
Scheme 18. Schematic overview of SPPS with the Merrifield resin. First an amino acid is coupled to the linker by S_N2 followed by a deprotection step. Chain extension is performed by coupling under Steglich conditions. The final peptide is obtained after cleavage from the solid support and deprotection	

of the <i>N</i> -terminus. ^[10,191]	39
Scheme 19. Sub-monomer method developed by Zuckermann. Acylation in a S_N2 reaction and subsequent S_N2 reaction addition of amines to the resin results in the targeted oligopeptoid after cleavage from the solid support. ^[191,200]	41
Scheme 20. Iterative two-step approach for the synthesis of sequence-defined oligomers based on thiolactones on a solid support. Side chain functionalization is introduced by aminolysis using amine components. ^[27]	47
Scheme 21. Strategy of an IEG approach for the synthesis of sequence-defined macromolecules as reported by Johnson and co-workers. The cycle is depicted starting from the chiral key monomer equipped with an epoxide and a protected alkyne group. Ring opening with sodium azide enables subsequent functionalization with acetic acid or benzyl bromide. The combination of a deprotected and a functionalized building block generates monodisperse macromolecules <i>via</i> exponential chain growth by CuAAC. ^[23-24]	51
Scheme 22. Preparation of two sets of sequence-defined oligoacrylate RAFT agents by insertion of four single monomer units. Published by The Royal Society of Chemistry, licensed under a Creative Commons Attribution license. ^[19]	53
Scheme 23. A library of monodisperse sequence-defined macromolecules prepared by photoinduced ATRP <i>via</i> SUMI reactions. Published by The Royal Society of Chemistry, licensed under a Creative Commons Attribution license. ^[20]	54
Scheme 24. Synthesis of sequence-defined macromolecules using an iterative two-step strategy combining P-3CR and the thiol-ene addition reaction. Adapted from a report of Solleder <i>et al.</i> with permission from Wiley. ^[55]	55
Scheme 25. Two-step iterative P-3CR approach by employing protection chemistry. An isocyanide monomer that carries a benzyl protected acid functionality reacts with an aldehyde and stearic acid in a P-3CR. After deprotection of the acid functionality by hydrogenation with a palladium based catalyst, chain extension <i>via</i> P-3CR can be performed. ^[180]	56
Scheme 26. Synthesis of sequence-defined macromolecules as potential data storage materials. In the first step a Biginelli reaction is performed with an urea (green), an aromatic aldehyde (blue), and an acetoacetate (red) yielding a Biginelli acid. Subsequently, a P-3CR is performed employing the Biginelli acid, an aldehyde (orange), and a diisocyanide (purple) to form an isocyanide monomer (monomer-NC). An iterative two-step approach with convergent P-3CR and hydrogenolytic benzyl deprotection affords the target sequence-defined macromolecule. ^[41]	58
Scheme 27. Schematic overview of the synthesis of sequence-defined oligomers reported by Barner-Kowollik and co-workers. The MBA bearing monomer unit is coupled to the core unit <i>via</i> an irradiation step. Subsequently, the second monomer unit is added under irradiation to form a tetramer. Thermal treatment releases the furan protecting groups and yields the maleimide group on either chain end enabling further chain extension. ^[60]	59
Scheme 28. Two-step iterative approach based on <i>o</i> -MBAs as photocaged dienes. Symmetrical monodisperse macromolecules are obtained starting from a bifunctional core unit exploiting acetals as protection group for the <i>o</i> -MBAs. Reprinted with the permission from the authors. ^[61]	60
Scheme 29. Schematic illustration of the consecutive chain extension switching between P-3CR and photochemistry. Starting from a bifunctional core unit, symmetrical sequence-defined macromolecules consisting of Passerini- and photoblocks are obtained. ^[247]	65
Scheme 30. Retrosynthetic analysis of the Passerini linker 1 . The linker can be prepared from a maleimide carrying carboxylic acid 2 , an aldehyde 3 , and an isocyanide 4	65
Scheme 31. Preparation of the maleimide-acid 2 as building unit for the synthesis of the Passerini linker 1 . Protection of maleic anhydride with furan, maleimide formation with ethanolamine, ring-opening of succinic anhydride and subsequent deprotection of the furan-protected maleimide intermediate 2c yielded the maleimide acid 2	66
Scheme 32. Synthesis of 1,6-diisocyanohexane 4 starting from 1,6-diaminohexane. The diamine was	

converted into the corresponding formamide 4a by refluxing in ethyl formate. Dehydration in basic medium employing phosphorous oxychloride yielded the desired diisocyanohexane 4	68
Scheme 33. Synthesis of the Passerini linkers 1a-c via a P-3CR using 1,6-diisocyanohexane 4 , the maleimide-acid 2 , and a commercially available aldehyde 3a-c	69
Scheme 34. Synthesis of the photomonomers 5a-b . First the spacer units were equipped with a tert-butyloxycarbonyl protecting group on one side followed by the maleimide formation. The Boc protecting group was removed under acidic conditions prior to the amidification of the <i>o</i> -MBA moiety.	72
Scheme 35. Synthesis of the photomonomer acids 6a-b . The furan protecting group was first removed by thermal treatment under vacuum. Thiol-Michael addition using mercaptooctanoic acid yielded the target compounds.	73
Scheme 36. Synthesis of photodimer 7 . In a first step photomonomer 5a was deprotected on the maleimide side and a dimethyl acetal protecting group was introduced to prevent the benzaldehyde from reacting. The photodimer 7 was obtained under irradiation of UV-light at 365 nm using the monomers 5a* and 5b	74
Scheme 37. Synthesis of the symmetrical tetramer 9 in a Passerini reaction starting from the symmetrical core unit sebacic acid 8 and the Passerini linker 1a . Benzaldehyde 3b was employed for the introduction of side chain substituents.	76
Scheme 38. Sequential and modular strategies for the synthesis of sequence-defined oligomers alternatingly consisting of Passerini and photoblocks. The tetramer 9 was extended with the photomonomer 5a , a modified photomonomer 6a , and a photodimer 7 to afford the functional oligomers equipped with furan capped maleimides (10a and 10c) or a terminal carboxylic acid group at both chain ends (10b).	78
Scheme 39. Synthesis of sequence-defined macromolecules by chain extension of a symmetrical core unit circumventing protection group strategies. The sequential light induced chain extension is carried out by switching between NICAL ligation and DA cycloaddition. Reprinted with permission from a publication of W. Konrad <i>et al.</i> ^[253]	85
Scheme 40. Synthesis of PAT 11 starting from 4-formylbenzoic acid and aminopyrene. First, formylbenzoate 11a is formed with bromo undecanol under basic conditions. The tosylhydrazone 11b is obtained from the hydrazide formation by employing tosylhydrazide. In the last step, PAT 11 is synthesized from tosylhydrazone 11b and pyrene diazonium tetrafluoroborate 11c in pyridine.	86
Scheme 41. Synthesis of the <i>o</i> -MBA 12 starting from dimethyl anisole by oxidation. Afterwards, 12b was obtained by methyl ether cleavage followed by ether formation under Williamson conditions leading to 12c . The target compound 12 was formed by saponification in the final step.	89
Scheme 42. Formation of the photomonomer 13 by esterification of PAT 11 and <i>o</i> -MBA 12 under Steglich conditions using EDC·HCl and DMAP.	90
Scheme 43. Synthesis of monomer 14 starting from mono-ethyl fumarate by esterification with an excess of glycol under Steglich conditions and subsequent nucleophilic ring-opening of succinic anhydride.	92
Scheme 44. Synthesis of the symmetric bifunctional carboxylic acid 15 by a nucleophilic ring-opening reaction starting from tetraethylene glycol.	94
Scheme 45. NICAL test reaction conducted under flow conditions with the photomonomer 13 and acetic acid at residence times of 10, 15, and 23 min. Adduct 16a is obtained via reaction of the nitrile imine and the acid derivative, whereas rearrangement of the photoadduct leads to the hydrazide 16b	97
Scheme 46. DA cycloaddition of the <i>o</i> -MBA 12c and an excess of diethyl fumarate 17 as test system conducted under conventional batch conditions employing nitrogen-flushed headspace vials and a PL-L lamp ($\lambda_{\max} = 365$ nm) as irradiation source.	99
Scheme 47. Sequential approach for the photochemical synthesis of sequence-defined macromolecules avoiding protection chemistry by wavelength selective switching between NICAL ligation and DA cycloaddition. Starting from the core unit 15 , a symmetrical decamer 18e was synthesized using the monomers 13 and 14 iteratively by bidirectional chain extension. The NICAL chain extension yielded macromolecules with benzaldehydes as end-groups (18a , 18c , and 18e), while DA cycloaddition	

afforded terminal carboxylic acids (18b and 18d).....	101
Scheme 48. The photomonomer 19a was prepared starting from a α,ω -Fmoc-Boc protected lysine spacer unit. Selective deprotection and introduction of the side chain functional group, i.e. furan protected maleimide and benzaldehyde, lead to the targeted compound 19a	110
Scheme 49. Selective end-group transformation of the monomers 5a and 19a by thermal treatment for unlocking of the maleimide and following acetalization resulted in the modified monomers 5a* and 19a* . The photoreaction between the modified and non-modified monomers yielded the dimers 20a-c	112
Scheme 50. (A) Maleimide deprotection by thermal treating and acetal formation starting from the photomonomer 5b yielding the modified monomer 5b* . (B) Formation of the dimer 20d employing the photomonomer 5b and the modified monomer 5b* . (C) Formation of the trimer 21a by combining dimer 20d and the modified monomer 5b* . (D) Maleimide deprotection by thermal treating and acetal formation starting from the dimer 20d yielding the modified dimer 20d* . (E) Synthesis of the pentamer 21b employing the dimer 20d yielding the modified dimer 20d*	114
Scheme 51. Modular strategy for the synthesis of sequence-defined decamers 23a-d . The hexamers 22a-d were prepared by Nicolas Zydziak. The decamers 23a-d varying in their chemical composition were obtained by chain extension employing, the in the black frame highlighted, α,ω -functionalized dimers 20a-c synthesized by the author.....	118

Acknowledgments

An dieser Stelle möchte ich mich bei allen Personen bedanken, die mich während meiner Promotion begleitet und unterstützt haben.

An erster Stelle möchte ich meinem Doktorvater Prof. Christopher Barner-Kowollik für die Aufnahme in die macroarc Gruppe herzlich danken. Ich möchte mich für die Art und Weise deiner Betreuung bedanken, die sich durch dein Vertrauen in meine eigenen Fähigkeiten auszeichnet und du mir dadurch ermöglicht hast selbständig Forschungsprojekte zu gestalten und durchzuführen. Dein Enthusiasmus hat mich schon während deinen Vorlesungen beeindruckt womit du mich in die Polymerchemie gelockt hast. Deine Hingabe für die Forschung und deine Gruppe sind einzigartig. Ich möchte dir außerdem danken, dass du meinen Forschungsaufenthalt an der Queensland University of Technology (QUT) in Brisbane (Australien) ermöglicht hast.

Ich danke der Deutschen Forschungsgesellschaft (DFG) für die Finanzierung meiner Doktorarbeit im Rahmen des Sonderforschungsbereichs (SFB) 1176. Besonderer Dank gilt auch den Verantwortlichen Prof. Michael Meier, Prof. Manfred Wilhelm, Dr. Dominik Voll und Cornelia Weber für die Betreuung und Organisation des SFB 1176 sowie des Graduiertenkollegs. Gleichzeitig danke ich dem A3 Team des SFB, allen voran Fabian Blößer und Katharina Wetzl für die Kooperation und die schöne Zeit zusammen.

Außerdem gebührt ein großer Dank an Dr. Maria Schneider, Dr. Anja Goldmann, Dr. Eva Blasco, Evelyn Stühling, Vincent Schüler, Katharina Elies und Birgit Huber, für ihre Arbeit rund um die Arbeitsgruppe, die ohne eure Organisation nicht laufen würde. Zusätzlich möchte ich allen Doktoranden danken die den „Laden“ am Laufen gehalten haben.

Ein besonderer Dank geht auch an Tanja Rieder, Fabian Blößer, Christian Fengler, Sarrah Putwa und Swetha Sarangarajan die ihre Masterarbeit, Vertiefearbeit oder Praktikum unter meiner Betreuung durchgeführt haben. Vielen Dank, dass ihr mich während meiner Promotion begleitet habt.

Danke an die Korrekturleser Janin Offenloch, Katharina Wetzels, Michael Kaupp, Divya Varadharajan, Rhiannon Batchelor und Thomas Gegenhuber für eure Verbesserungsvorschläge.

Insbesondere gilt großer Dank meinen Kollegen und Kolleginnen der macroarc Gruppe in Deutschland und Australien ohne die eine gute Doktorarbeit nicht möglich wäre. Vielen Dank für die wissenschaftlichen Diskussionen, die Kaffeepausen, die gemeinsamen sommerlichen Grillabende nach Feierabend und natürlich Doktorfeiern. Meinen Laborkollegen bei all meinen Stationen aus 322, Soft Matter Lab, M4 und dem Altbau sowie meinen Bürokollegen danke ich für die tolle Atmosphäre, wodurch Spaß bei der Arbeit immer garantiert war. Zusätzlich möchte ich den vielen wechselnden Kollegen im Masseteam danken, die zusammen mit mir die oftmals zickige Orbitrap am Laufen gehalten haben.

Meinen Freunden, die ich am KIT gewonnen habe, sei es im Laufe meines Studiums oder in der macroarc Gruppe, möchte ich für die großartige Zeit bedanken die wir zusammen verbringen durften und den Spaß den wir im Laufe unseres Studiums und darüber hinaus hatten. Die ersten haben Karlsruhe schon verlassen und ich hoffe, dass wir den Kontakt halten können, so wie wir es auch schon über Kontinente hinweg geschafft haben. Besonders hervorheben möchte ich den Stammtisch, insbesondere die großen vier Lenz, Wolfi, Dennis und David. Meinen beiden langjährigen Freunden Martin und Benjamin möchte ich für die gemeinsame Zeit und eure Unterstützung danken. Wenn es mal nicht so lief konnte ich bei euch immer Kraft tanken und meinen Stress vergessen. Vielen Dank Dasha für deine Unterstützung, ich bin froh dich an meiner Seite zu haben.

Abschließend gebührt die größte Dankbarkeit meiner Mutter Elena und meiner Großmutter Martha. Der Weg war lange und anstrengend den wir zusammen gegangen sind und ich bin sehr dankbar euch zu haben. Vielen Dank für eure Unterstützung und Liebe die ich von euch mein Leben lang erhalten habe. Vielen Dank für die finanzielle Unterstützung meines Studiums. Alles was ihr mir gegeben habt kann ich euch nicht zurückzahlen und bin einfach nur froh auf euch zählen zu können. Man sollte nie vergessen wo man herkommt!

Bibliography

- [1] N. Badi, J.-F. Lutz, *Chem. Soc. Rev.* **2009**, *38*, 3383-3390.
- [2] F. Alsubaie, A. Anastasaki, P. Wilson, D. M. Haddleton, *Polym. Chem.* **2015**, *6*, 406-417.
- [3] A. Anastasaki, V. Nikolaou, N. W. McCaul, A. Simula, J. Godfrey, C. Waldron, P. Wilson, K. Kempe, D. M. Haddleton, *Macromolecules* **2015**, *48*, 1404-1411.
- [4] G. R. Jones, Z. Li, A. Anastasaki, D. J. Lloyd, P. Wilson, Q. Zhang, D. M. Haddleton, *Macromolecules* **2016**, *49*, 483-489.
- [5] W. Zhang, W. Xue, W. Ming, Y. Weng, G. Chen, D. M. Haddleton, *Macromol. Rapid Commun.* **2017**, *38*, 1700511.
- [6] G. Gody, T. Maschmeyer, P. B. Zetterlund, S. Perrier, *Nat. Commun.* **2013**, *4*, 2505.
- [7] L. Martin, G. Gody, S. Perrier, *Polym. Chem.* **2015**, *6*, 4875-4886.
- [8] J. Zhang, R. Deubler, M. Hartlieb, L. Martin, J. Tanaka, E. Patyukova, P. D. Topham, F. H. Schacher, S. Perrier, *Macromolecules* **2017**, *50*, 7380-7387.
- [9] J.-F. Lutz, *Polym. Chem.* **2010**, *1*, 55-62.
- [10] R. B. Merrifield, *J. Am. Chem. Soc.* **1963**, *85*, 2149-2154.
- [11] R. B. Merrifield, *Angew. Chem. Int. Ed.* **1985**, *24*, 799-810.
- [12] R. P. Cheng, S. H. Gellman, W. F. DeGrado, *Chem. Rev.* **2001**, *101*, 3219-3232.
- [13] E. Uhlmann, A. Peyman, G. Breipohl, D. W. Will, *Angew. Chem. Int. Ed.* **1998**, *37*, 2796-2823.
- [14] R. J. Simon, R. S. Kania, R. N. Zuckermann, V. D. Huebner, D. A. Jewell, S. Banville, S. Ng, L. Wang, S. Rosenberg, C. K. Marlowe, *Proc. Natl. Acad. Sci. U.S.A.* **1992**, *89*, 9367-9371.
- [15] H. Herzner, T. Reipen, M. Schultz, H. Kunz, *Chem. Rev.* **2000**, *100*, 4495-4538.
- [16] S. L. Beaucage, R. P. Iyer, *Tetrahedron* **1992**, *48*, 2223-2311.
- [17] J. K. Young, J. C. Nelson, J. S. Moore, *J. Am. Chem. Soc.* **1994**, *116*, 10841-10842.
- [18] Y. Hibi, M. Ouchi, M. Sawamoto, *Nat. Commun.* **2016**, *7*, 11064.
- [19] J. Vandenbergh, G. Reekmans, P. Adriaensens, T. Junkers, *Chem. Commun.* **2013**, *49*, 10358-10360.
- [20] J. Vandenbergh, G. Reekmans, P. Adriaensens, T. Junkers, *Chem. Sci.* **2015**, *6*, 5753-5761.
- [21] J. Xu, C. Fu, S. Shanmugam, C. J. Hawker, G. Moad, C. Boyer, *Angew. Chem. Int. Ed.* **2017**, *56*, 8376-8383.
- [22] C. Fu, Z. Huang, C. J. Hawker, G. Moad, J. Xu, C. Boyer, *Polym. Chem.* **2017**, *8*, 4637-4643.
- [23] J. C. Barnes, D. J. C. Ehrlich, A. X. Gao, F. A. Leibfarth, Y. Jiang, E. Zhou, T. F. Jamison, J. A. Johnson, *Nat. Chem.* **2015**, *7*, 810-815.
- [24] F. A. Leibfarth, J. A. Johnson, T. F. Jamison, *Proc. Natl. Acad. Sci. U.S.A.* **2015**, *112*, 10617-10622.
- [25] Y. Jiang, M. R. Golder, H. V. T. Nguyen, Y. Wang, M. Zhong, J. C. Barnes, D. J. C. Ehrlich, J. A. Johnson, *J. Am. Chem. Soc.* **2016**, *138*, 9369-9372.
- [26] S. Martens, J. Van den Begin, A. Madder, F. E. Du Prez, P. Espeel, *J. Am. Chem. Soc.* **2016**, *138*, 14182-14185.
- [27] P. Espeel, L. L. G. Carrette, K. Bury, S. Capenberghs, J. C. Martins, F. E. Du Prez, A. Madder, *Angew. Chem. Int. Ed.* **2013**, *52*, 13261-13264.
- [28] N. F. König, A. Al Ouahabi, S. Poyer, L. Charles, J.-F. Lutz, *Angew. Chem. Int. Ed.* **2017**, *56*, 7297-7301.
- [29] N. Zydziak, W. Konrad, F. Feist, S. Afonin, S. Weidner, C. Barner-Kowollik, *Nat. Commun.* **2016**, *7*, 13672.
- [30] A. Burel, C. Carapito, J.-F. Lutz, L. Charles, *Macromolecules* **2017**, *50*, 8290-8296.
- [31] D. Estupiñán, T. Gegenhuber, J. P. Blinco, C. Barner-Kowollik, L. Barner, *ACS Macro Lett.* **2017**, *6*, 229-234.
- [32] P. Mueller, M. M. Zieger, B. Richter, A. S. Quick, J. Fischer, J. B. Mueller, L. Zhou, G. U.

- Nienhaus, M. Bastmeyer, C. Barner-Kowollik, M. Wegener, *ACS Nano* **2017**, *11*, 6396-6403.
- [33] J.-F. Lutz, J.-M. Lehn, E. W. Meijer, K. Matyjaszewski, *Nat. Rev. Mater.* **2016**, 16024.
- [34] J.-F. Lutz, *Nat. Chem.* **2010**, *2*, 84-85.
- [35] Y. Hibi, M. Ouchi, M. Sawamoto, *Angew. Chem. Int. Ed.* **2011**, *50*, 7434-7437.
- [36] J.-F. Lutz, M. Ouchi, D. R. Liu, M. Sawamoto, *Science* **2013**, *341*, 1238149.
- [37] D. Chan-Seng, M. Zamfir, J.-F. Lutz, *Angew. Chem. Int. Ed.* **2012**, *51*, 12254-12257.
- [38] J.-F. Lutz, *Macromolecules* **2015**, *48*, 4759-4767.
- [39] L. Charles, C. Laure, J.-F. Lutz, R. K. Roy, *Macromolecules* **2015**, *48*, 4319-4328.
- [40] S. Urnauer, S. Morys, A. Krhac Levacic, A. M. Müller, C. Schug, K. A. Schmohl, N. Schwenk, C. Zach, J. Carlsen, P. Bartenstein, E. Wagner, C. Spitzweg, *Molecular Therapy* **2016**, *24*, 1395-1404.
- [41] A. C. Boukis, M. A. R. Meier, *Eur. Polym. J.* **2018**, *104*, 32-38.
- [42] S. Martens, A. Landuyt, P. Espeel, B. Devreese, P. Dawyndt, F. Du Prez, *Nat. Commun.* **2018**, *9*, 4451.
- [43] S. Poyer, T. Fouquet, H. Sato, J.-F. Lutz, L. Charles, *Macromol. Chem. Phys.* **2018**, *219*, 1800173.
- [44] A. B. Chang, G. M. Miyake, R. H. Grubbs, in *Sequence-Controlled Polymers: Synthesis, Self-Assembly, and Properties, Vol. 1170*, American Chemical Society, **2014**, pp. 161-188.
- [45] T. T. Trinh, L. Oswald, D. Chan-Seng, J.-F. Lutz, *Macromol. Rapid Commun.* **2014**, *35*, 141-145.
- [46] A. Al Ouahabi, L. Charles, J.-F. Lutz, *J. Am. Chem. Soc.* **2015**, *137*, 5629-5635.
- [47] C. Laure, D. Karamessini, O. Milenkovic, L. Charles, J. F. Lutz, *Angew. Chem. Int. Ed.* **2016**, *55*, 10722-10725.
- [48] L. Charles, C. Laure, J.-F. Lutz, R. K. Roy, *Rapid Commun. Mass Spectrom.* **2016**, *30*, 22-28.
- [49] L. Charles, G. Cavallo, V. Monnier, L. Oswald, R. Szweda, J.-F. Lutz, *J. Am. Soc. Mass. Spectrom.* **2017**, *28*, 1149-1159.
- [50] Y. Erlich, D. Zielinski, *Science* **2017**, *355*, 950-954.
- [51] A. C. Boukis, K. Reiter, M. Frölich, D. Hofheinz, M. A. R. Meier, *Nat. Commun.* **2018**, *9*, 1439.
- [52] R. R. Batchelor, E. Blasco, K. N. R. Wuest, H. Lu, M. Wegener, C. Barner-Kowollik, M. H. Stenzel, *Chem. Commun.* **2018**, *54*, 2436-2439.
- [53] B. Zhao, Z. Gao, Y. Zheng, C. Gao, *J. Am. Chem. Soc.* **2019**.
- [54] H. C. Kolb, M. G. Finn, K. B. Sharpless, *Angew. Chem. Int. Ed.* **2001**, *40*, 2004-2021.
- [55] S. C. Solleder, M. A. R. Meier, *Angew. Chem. Int. Ed.* **2014**, *53*, 711-714.
- [56] A. A. Ouahabi, M. Kotera, L. Charles, J.-F. Lutz, *ACS Macro Lett.* **2015**, *4*, 1077-1080.
- [57] N. C. Yang, C. Rivas, *J. Am. Chem. Soc.* **1961**, *83*, 2213-2213.
- [58] M. C. Caserio, W. Lauer, T. Novinson, *J. Am. Chem. Soc.* **1970**, *92*, 6082-6084.
- [59] F. Feist, J. P. Menzel, T. Weil, J. P. Blinco, C. Barner-Kowollik, *J. Am. Chem. Soc.* **2018**, *140*, 11848-11854.
- [60] N. Zydziak, F. Feist, B. Huber, J. O. Mueller, C. Barner-Kowollik, *Chem. Commun.* **2015**, *51*, 1799-1802.
- [61] M. Van De Walle, K. De Bruycker, T. Junkers, J. P. Blinco, C. Barner-Kowollik, *ChemPhotoChem* **2019**, *3*, 225-228.
- [62] Z.-P. Yu, N. Liu, L. Yang, Z.-Q. Jiang, Z.-Q. Wu, *Macromolecules* **2017**, *50*, 3204-3214.
- [63] R. B. Woodward, T. J. Katz, *Tetrahedron* **1959**, *5*, 70-89.
- [64] W. Albrecht, *Liebigs Ann. Chem.* **1906**, *348*, 31-49.
- [65] O. Diels, J. H. Blom, W. Koll, *Liebigs Ann. Chem.* **1925**, *443*, 242-262.
- [66] O. Diels, K. Alder, *Liebigs Ann. Chem.* **1928**, *460*, 98-122.
- [67] O. Diels, K. Alder, *Liebigs Ann. Chem.* **1929**, *470*, 62-103.
- [68] O. Diels, K. Alder, *Ber. dtsch. Chem. Ges.* **1929**, *62*, 2081-2087.
- [69] O. Diels, K. Alder, *Ber. dtsch. Chem. Ges.* **1929**, *62*, 2087-2090.

- [70] O. Diels, K. Alder, *Ber. dtsh. Chem. Ges.* **1929**, *62*, 554-562.
- [71] O. Diels, K. Alder, *Ber. dtsh. Chem. Ges.* **1929**, *62*, 2337-2372.
- [72] O. Diels, K. Alder, *Liebigs Ann. Chem.* **1930**, *478*, 137-154.
- [73] O. Diels, K. Alder, *Liebigs Ann. Chem.* **1931**, *486*, 191-202.
- [74] O. Diels, K. Alder, E. Petersen, *Liebigs Ann. Chem.* **1931**, *486*, 202-210.
- [75] O. Diels, K. Alder, *Liebigs Ann. Chem.* **1931**, *486*, 211-225.
- [76] K. C. Nicolaou, S. A. Snyder, T. Montagnon, G. Vassilikogiannakis, *Angew. Chem. Int. Ed.* **2002**, *41*, 1668-1698.
- [77] M. Glassner, K. K. Oehlenschlaeger, T. Gruending, C. Barner-Kowollik, *Macromolecules* **2011**, *44*, 4681-4689.
- [78] T. Pauloehrl, A. Welle, K. K. Oehlenschlaeger, C. Barner-Kowollik, *Chem. Sci.* **2013**, *4*, 3503-3507.
- [79] P. Lederhose, K. N. R. Wust, C. Barner-Kowollik, J. P. Blinco, *Chem. Commun.* **2016**, *52*, 5928-5931.
- [80] K. Hildebrandt, M. Kaupp, E. Molle, J. P. Menzel, J. P. Blinco, C. Barner-Kowollik, *Chem. Commun.* **2016**, *52*, 9426-9429.
- [81] B. T. Tuten, J. P. Menzel, K. Pahnke, J. P. Blinco, C. Barner-Kowollik, *Chem. Commun.* **2017**, *53*, 4501-4504.
- [82] F. A. Carey, R. J. Sundberg, *Advanced Organic Chemistry: Part A: Structure and Mechanisms*, Springer US, Boston MA, **2007**.
- [83] F. A. Carey, R. J. Sundberg, *Advanced Organic Chemistry: Part B: Reactions and Synthesis*, Fifth Edition, Springer US, Boston MA, **2007**.
- [84] P. Geerlings, P. W. Ayers, A. Toro-Labbé, P. K. Chattaraj, F. De Proft, *Acc. Chem. Res.* **2012**, *45*, 683-695.
- [85] P. Y. Bruice, *Organische Chemie*, 5. engl. Aufl., Pearson Studium, München, **2007**.
- [86] K. Fukui, T. Yonezawa, H. Shingu, *The Journal of Chemical Physics* **1952**, *20*, 722-725.
- [87] E. Goldstein, B. Beno, K. N. Houk, *J. Am. Chem. Soc.* **1996**, *118*, 6036-6043.
- [88] W. C. Herndon, C. R. Grayson, J. M. Manion, *J. Org. Chem.* **1967**, *32*, 526-529.
- [89] V. Froidevaux, M. Borne, E. Laborbe, R. Auvergne, A. Gandini, B. Boutevin, *RSC Adv.* **2015**, *5*, 37742-37754.
- [90] P. Lederhose, D. Abt, A. Welle, R. Mueller, C. Barner-Kowollik, J. P. Blinco, *Chem. Eur. J.* **2018**, *24*, 576-580.
- [91] A. F. Hirschbiel, W. Konrad, D. Schulze-Sünninghausen, S. Wiedmann, B. Luy, B. V. K. J. Schmidt, C. Barner-Kowollik, *ACS Macro Lett.* **2015**, *4*, 1062-1066.
- [92] A. Kerbs, P. Mueller, M. Kaupp, I. Ahmed, A. S. Quick, D. Abt, M. Wegener, C. M. Niemeyer, C. Barner-Kowollik, L. Fruk, *Chem. Eur. J.* **2017**, *23*, 4990-4994.
- [93] H. Trommsdorff, *Ann. Pharm.* **1834**, *11*, 190-207.
- [94] G. Ciamician, P. Silber, *Ber. dtsh. Chem. Ges.* **1901**, *34*, 1530-1543.
- [95] G. Ciamician, P. Silber, *Ber. dtsh. Chem. Ges.* **1901**, *34*, 2040-2046.
- [96] G. Ciamician, P. Silber, *Ber. dtsh. Chem. Ges.* **1906**, *39*, 4343-4344.
- [97] G. Ciamician, P. Silber, *Ber. dtsh. Chem. Ges.* **1907**, *40*, 2415-2424.
- [98] G. Ciamician, P. Silber, *Ber. dtsh. Chem. Ges.* **1908**, *41*, 1928-1935.
- [99] M. Planck, *Ann. Phys.* **1901**, *309*, 553-563.
- [100] M. Planck, *Ann. Phys.* **1901**, *309*, 564-566.
- [101] A. Einstein, *Ann. Phys.* **1905**, *322*, 132-148.
- [102] C. Heiler, S. Bastian, P. Lederhose, J. P. Blinco, E. Blasco, C. Barner-Kowollik, *Chem. Commun.* **2018**, *54*, 3476-3479.
- [103] A. Albin, *Photochem. Photobiol. Sci.* **2016**, *15*, 319-324.
- [104] A. J. Allmand, *Trans. Faraday Soc.* **1926**, *21*, 438-452.

- [105] J. Olmsted, *J. Phys. Chem.* **1979**, *83*, 2581-2584.
- [106] P. W. Atkins, J. De Paula, *Physikalische Chemie*, 5. Aufl., Wiley-VCH, Weinheim, **2013**.
- [107] A. Jabłoński, *Zeitschrift für Physik* **1935**, *94*, 38-46.
- [108] E. U. Condon, *Am. J. Phys* **1947**, *15*, 365-374.
- [109] R. S. Becker, G. Favaro, *J. Photochem. Photobiol., C* **2011**, *12*, 167-176.
- [110] V. Balzani, P. Ceroni, A. Juris, *Photochemistry and photophysics : concepts, research, applications*, Wiley-VCH, Weinheim, **2014**.
- [111] H. G. O. Becker, *Einführung in die Photochemie*, 3. bearb. Aufl., Dt. Verl. d. Wiss., Berlin, **1991**.
- [112] R. G. W. Norrish, F. W. Kirkbride, *J. Chem. Soc.* **1932**, 1518-1530.
- [113] R. G. W. Norrish, C. H. Bamford, *Nature* **1937**, *140*, 195.
- [114] R. G. W. Norrish, C. H. Bamford, *Nature* **1936**, *138*, 1016.
- [115] L. Salem, *Science* **1976**, *191*, 822-830.
- [116] L. Kürti, B. Czako, *Strategic applications of named reactions in organic synthesis : 250 named reactions; background and detailed mechanisms*, Elsevier Academic Press, Amsterdam, **2005**.
- [117] R. S. Davidson, D. Goodwin, P. F. de Violet, *Tetrahedron Lett.* **1981**, *22*, 2485-2486.
- [118] P. J. Wagner, *Acc. Chem. Res.* **1971**, *4*, 168-177.
- [119] M. Glassner, K. K. Oehlenschlaeger, A. Welle, M. Bruns, C. Barner-Kowollik, *Chem. Commun.* **2013**, *49*, 633-635.
- [120] T. K. Claus, S. Telitel, A. Welle, M. Bastmeyer, A. P. Vogt, G. Delaittre, C. Barner-Kowollik, *Chem. Commun.* **2017**, *53*, 1599-1602.
- [121] S. Telitel, E. Blasco, L. D. Bangert, F. H. Schacher, A. S. Goldmann, C. Barner-Kowollik, *Polym. Chem.* **2017**, *8*, 4038-4042.
- [122] H. Frisch, J. P. Menzel, F. R. Bloesser, D. E. Marschner, K. Mundsinger, C. Barner-Kowollik, *J. Am. Chem. Soc.* **2018**, *140*, 9551-9557.
- [123] D. E. Marschner, H. Frisch, J. T. Offenloch, B. T. Tuten, C. R. Becer, A. Walther, A. S. Goldmann, P. Tzvetkova, C. Barner-Kowollik, *Macromolecules* **2018**, *51*, 3802-3807.
- [124] J. O. Mueller, F. G. Schmidt, J. P. Blinco, C. Barner-Kowollik, *Angew. Chem. Int. Ed.* **2015**, *54*, 10284-10288.
- [125] T. Krappitz, F. Feist, I. Lamparth, N. Moszner, H. John, J. P. Blinco, T. R. Dargaville, C. Barner-Kowollik, *Mater. Horiz.* **2019**, *6*, 81-89.
- [126] L. M. Campos, K. L. Killops, R. Sakai, J. M. J. Paulusse, D. Damiron, E. Drockenmuller, B. W. Messmore, C. J. Hawker, *Macromolecules* **2008**, *41*, 7063-7070.
- [127] D. Konetski, T. Gong, C. N. Bowman, *Langmuir* **2016**, *32*, 8195-8201.
- [128] G. W. Kirby, *Phosphorus, Sulfur, and Silicon and the Related Elements* **1993**, *74*, 17-29.
- [129] B. A. Jones, J. S. Bradshaw, *Chem. Rev.* **1984**, *84*, 17-30.
- [130] W. M. McGregor, D. C. Sherrington, *Chem. Soc. Rev.* **1993**, *22*, 199-204.
- [131] E. Vedejs, T. H. Eberlein, D. J. Mazur, C. K. McClure, D. A. Perry, R. Ruggeri, E. Schwartz, J. S. Stults, D. L. Varie, *J. Org. Chem.* **1986**, *51*, 1556-1562.
- [132] E. Vedejs, D. A. Perry, K. N. Houk, N. G. Rondan, *J. Am. Chem. Soc.* **1983**, *105*, 6999-7001.
- [133] E. Vedejs, T. H. Eberlein, R. G. Wilde, *J. Org. Chem.* **1988**, *53*, 2220-2226.
- [134] T. K. Claus, J. Zhang, L. Martin, M. Hartlieb, H. Mutlu, S. Perrier, G. Delaittre, C. Barner-Kowollik, *Macromol. Rapid Commun.* **2017**, *38*, 1700264.
- [135] G. Porter, M. F. Tchir, *J. Chem. Soc. A* **1971**, 3772-3777.
- [136] P. G. Sammes, *Tetrahedron* **1976**, *32*, 405-422.
- [137] K. Hildebrandt, T. Pauloehrl, J. P. Blinco, K. Linkert, H. G. Börner, C. Barner-Kowollik, *Angew. Chem. Int. Ed.* **2015**, *54*, 2838-2843.
- [138] T. Gruending, K. K. Oehlenschlaeger, E. Frick, M. Glassner, C. Schmid, C. Barner-Kowollik, *Macromol. Rapid Commun.* **2011**, *32*, 807-812.
- [139] R. Huisgen, M. Seidel, J. Sauer, J. McFarland, G. Wallbillich, *J. Org. Chem.* **1959**, *24*, 892-893.

- [140] J. S. Clovis, A. Eckell, R. Huisgen, R. Sustmann, *Chem. Ber.* **1967**, *100*, 60-70.
- [141] R. Sustmann, R. Huisgen, H. Huber, *Chem. Ber.* **1967**, *100*, 1802-1813.
- [142] V. Lohse, P. Leihkauf, C. Csongar, G. Tomaschewski, *J. Prakt. Chem.* **1988**, *330*, 406-414.
- [143] W. Song, Y. Wang, J. Qu, M. M. Madden, Q. Lin, *Angew. Chem. Int. Ed.* **2008**, *47*, 2832-2835.
- [144] W. Feng, L. Li, C. Yang, A. Welle, O. Trapp, P. A. Levkin, *Angew. Chem. Int. Ed.* **2015**, *54*, 8732-8735.
- [145] Y. Zhang, W. Liu, Z. K. Zhao, *Molecules* **2014**, *19*, 306-315.
- [146] S.-L. Zheng, Y. Wang, Z. Yu, Q. Lin, P. Coppens, *J. Am. Chem. Soc.* **2009**, *131*, 18036-18037.
- [147] Z. Li, L. Qian, L. Li, J. C. Bernhammer, H. V. Huynh, J.-S. Lee, S. Q. Yao, *Angew. Chem. Int. Ed.* **2016**, *55*, 2002-2006.
- [148] C. Heiler, J. T. Offenloch, E. Blasco, C. Barner-Kowollik, *ACS Macro Lett.* **2017**, *6*, 56-61.
- [149] J. O. Mueller, D. Voll, F. G. Schmidt, G. Delaittre, C. Barner-Kowollik, *Chem. Commun.* **2014**, *50*, 15681-15684.
- [150] Y. Wang, C. I. Rivera Vera, Q. Lin, *Org. Lett.* **2007**, *9*, 4155-4158.
- [151] S. Arndt, H.-A. Wagenknecht, *Angew. Chem. Int. Ed.* **2014**, *53*, 14580-14582.
- [152] A. Dömling, I. Ugi, *Angew. Chem. Int. Ed.* **2000**, *39*, 3168-3210.
- [153] A. Dömling, *Chem. Rev.* **2006**, *106*, 17-89.
- [154] S. C. Solleder, K. S. Wetzel, M. A. R. Meier, *Polym. Chem.* **2015**, *6*, 3201-3204.
- [155] A. Strecker, *Liebigs Ann. Chem.* **1850**, *75*, 27-45.
- [156] A. Hantzsch, *Liebigs Ann. Chem.* **1882**, *215*, 1-82.
- [157] A. Hantzsch, *Ber. dtsh. Chem. Ges.* **1890**, *23*, 1474-1476.
- [158] P. Biginelli, *Ber. dtsh. Chem. Ges.* **1891**, *24*, 1317-1319.
- [159] C. Mannich, W. Krösche, *Arch. Pharm.* **1912**, *250*, 647-667.
- [160] R. Robinson, *J. Chem. Soc., Trans.* **1917**, *111*, 762-768.
- [161] N. Chatani, M. Oshita, M. Tobisu, Y. Ishii, S. Murai, *J. Am. Chem. Soc.* **2003**, *125*, 7812-7813.
- [162] R. Ramozzi, N. Chéron, B. Braïda, P. C. Hiberty, P. Fleurat-Lessard, *New J. Chem.* **2012**, *36*, 1137-1140.
- [163] W. Lieke, *Liebigs Ann. Chem.* **1859**, *112*, 316-321.
- [164] A. Gautier, *Liebigs Ann. Chem.* **1868**, *146*, 119-124.
- [165] A. W. Hofmann, *Liebigs Ann. Chem.* **1867**, *144*, 114-120.
- [166] I. Ugi, R. Meyr, *Angew. Chem.* **1958**, *70*, 702-703.
- [167] I. Ugi, R. Meyr, *Chem. Ber.* **1960**, *93*, 239-248.
- [168] I. Ugi, R. Meyr, U. Fetzer, C. Steinbrückner, *Angew. Chem.* **1959**, *71*, 386.
- [169] I. Ugi, C. Steinbrückner, *Angew. Chem.* **1960**, *72*, 267-268.
- [170] M. Passerini, L. Simone, *Gazz. Chim. Ital* **1921**, *51*, 126-129.
- [171] N. Chéron, R. Ramozzi, L. E. Kaïm, L. Grimaud, P. Fleurat-Lessard, *J. Org. Chem.* **2012**, *77*, 1361-1366.
- [172] G. A. Medeiros, W. A. da Silva, G. A. Bataglion, D. A. C. Ferreira, H. C. B. de Oliveira, M. N. Eberlin, B. A. D. Neto, *Chem. Commun.* **2014**, *50*, 338-340.
- [173] C. Iacobucci, S. Reale, J.-F. Gal, F. De Angelis, *Eur. J. Org. Chem.* **2014**, *2014*, 7087-7090.
- [174] J. Zhu, H. Bienaymé, *Multicomponent reactions*, 1st ed., Wiley-VCH, Weinheim, **2005**.
- [175] R. H. Baker, D. Stanonis, *J. Am. Chem. Soc.* **1951**, *73*, 699-702.
- [176] I. Ugi, R. Meyr, *Chem. Ber.* **1961**, *94*, 2229-2233.
- [177] S. Maeda, S. Komagawa, M. Uchiyama, K. Morokuma, *Angew. Chem. Int. Ed.* **2011**, *50*, 644-649.
- [178] R. Ramozzi, K. Morokuma, *J. Org. Chem.* **2015**, *80*, 5652-5657.
- [179] L. El Kaïm, L. Grimaud, *Eur. J. Org. Chem.* **2014**, *2014*, 7749-7762.

- [180] S. C. Solleder, D. Zengel, K. S. Wetzel, M. A. R. Meier, *Angew. Chem. Int. Ed.* **2016**, *55*, 1204-1207.
- [181] H. Staudinger, *Ber. dtsh. Chem. Ges.* **1926**, *59*, 3019-3043.
- [182] A. D. Jenkins, P. Kratochvíl, R. F. T. Stepto, U. W. Suter, *Pure Appl. Chem.* **1996**, *68*, 2287-2311.
- [183] M. Szwarc, *Nature* **1956**, *178*, 1168-1169.
- [184] M. Kato, M. Kamigaito, M. Sawamoto, T. Higashimura, *Macromolecules* **1995**, *28*, 1721-1723.
- [185] J.-S. Wang, K. Matyjaszewski, *J. Am. Chem. Soc.* **1995**, *117*, 5614-5615.
- [186] G. Moad, E. Rizzardo, *Macromolecules* **1995**, *28*, 8722-8728.
- [187] J. Chiefari, Y. K. Chong, F. Ercole, J. Krstina, J. Jeffery, T. P. T. Le, R. T. A. Mayadunne, G. F. Meijs, C. L. Moad, G. Moad, E. Rizzardo, S. H. Thang, *Macromolecules* **1998**, *31*, 5559-5562.
- [188] J.-F. Lutz, *ACS Macro Lett.* **2014**, *3*, 1020-1023.
- [189] S. J. Rowan, C. Barner-Kowollik, B. Klumperman, P. Gaspard, R. B. Grubbs, M. A. Hillmyer, L. R. Hutchings, M. K. Mahanthappa, D. Moatsou, R. K. O'Reilly, M. Ouchi, M. Sawamoto, T. P. Lodge, *ACS Macro Lett.* **2016**, *5*, 1-3.
- [190] J.-F. Lutz, M. Ouchi, M. Sawamoto, T. Y. Meyer, *Sequence-Controlled Polymers: Synthesis, Self-Assembly, and Properties, Vol. 1170*, American Chemical Society, Washington DC, **2014**.
- [191] R. N. Zuckermann, *Biopolymers* **2011**, *96*, 545-555.
- [192] B. Marglin, R. B. Merrifield, *J. Am. Chem. Soc.* **1966**, *88*, 5051-5052.
- [193] B. Gutte, R. B. Merrifield, *J. Biol. Chem.* **1971**, *246*, 1922-1941.
- [194] R. B. Merrifield, J. M. Stewart, *Nature* **1965**, *207*, 522-523.
- [195] P. E. Dawson, S. B. H. Kent, *Annu. Rev. Biochem.* **2000**, *69*, 923-960.
- [196] E. Saxon, C. R. Bertozzi, *Science* **2000**, *287*, 2007-2010.
- [197] B. L. Nilsson, L. L. Kiessling, R. T. Raines, *Org. Lett.* **2000**, *2*, 1939-1941.
- [198] M. Baca, T. W. Muir, M. Schnoelzer, S. B. H. Kent, *J. Am. Chem. Soc.* **1995**, *117*, 1881-1887.
- [199] G. G. Kochendoerfer, S.-Y. Chen, F. Mao, S. Cressman, S. Traviglia, H. Shao, C. L. Hunter, D. W. Low, E. N. Cagle, M. Carnevali, V. Gueriguian, P. J. Keogh, H. Porter, S. M. Stratton, M. C. Wiedeke, J. Wilken, J. Tang, J. J. Levy, L. P. Miranda, M. M. Crnogorac, S. Kalbag, P. Botti, J. Schindler-Horvat, L. Savatski, J. W. Adamson, A. Kung, S. B. H. Kent, J. A. Bradburne, *Science* **2003**, *299*, 884-887.
- [200] R. N. Zuckermann, J. M. Kerr, S. B. H. Kent, W. H. Moos, *J. Am. Chem. Soc.* **1992**, *114*, 10646-10647.
- [201] D. Zhang, S. H. Lahasky, L. Guo, C.-U. Lee, M. Lavan, *Macromolecules* **2012**, *45*, 5833-5841.
- [202] C. W. Wu, T. J. Sanborn, R. N. Zuckermann, A. E. Barron, *J. Am. Chem. Soc.* **2001**, *123*, 2958-2963.
- [203] S. M. Miller, R. J. Simon, S. Ng, R. N. Zuckermann, J. M. Kerr, W. H. Moos, *Bioorg. Med. Chem. Lett.* **1994**, *4*, 2657-2662.
- [204] P. A. Wender, D. J. Mitchell, K. Pattabiraman, E. T. Pelkey, L. Steinman, J. B. Rothbard, *Proc. Natl. Acad. Sci. U.S.A.* **2000**, *97*, 13003-13008.
- [205] C. W. Wu, T. J. Sanborn, K. Huang, R. N. Zuckermann, A. E. Barron, *J. Am. Chem. Soc.* **2001**, *123*, 6778-6784.
- [206] C. W. Wu, K. Kirshenbaum, T. J. Sanborn, J. A. Patch, K. Huang, K. A. Dill, R. N. Zuckermann, A. E. Barron, *J. Am. Chem. Soc.* **2003**, *125*, 13525-13530.
- [207] A. M. Rosales, R. A. Segalman, R. N. Zuckermann, *Soft Matter* **2013**, *9*, 8400-8414.
- [208] P. Armand, K. Kirshenbaum, R. A. Goldsmith, S. Farr-Jones, A. E. Barron, K. T. Truong, K. A. Dill, D. F. Mierke, F. E. Cohen, R. N. Zuckermann, E. K. Bradley, *Proc. Natl. Acad. Sci. U.S.A.* **1998**, *95*, 4309-4314.
- [209] K. T. Nam, S. A. Shelby, P. H. Choi, A. B. Marciel, R. Chen, L. Tan, T. K. Chu, R. A. Mesch, B.-C. Lee, M. D. Connolly, C. Kisielowski, R. N. Zuckermann, *Nat. Mater.* **2010**, *9*, 454.
- [210] V. T. Ravikumar, T. K. Wyrzykiewicz, D. L. Cole, *Tetrahedron* **1994**, *50*, 9255-9266.

- [211] W. S. Marshall, R. J. Kaiser, *Curr. Opin. Chem. Biol.* **2004**, *8*, 222-229.
- [212] M. Caruthers, *Science* **1985**, *230*, 281-285.
- [213] C. McCollum, A. Andrus, *Tetrahedron Lett.* **1991**, *32*, 4069-4072.
- [214] J. Katzhendler, S. Cohen, E. Rahamim, M. Weisz, I. Ringel, J. Deutsch, *Tetrahedron* **1989**, *45*, 2777-2792.
- [215] G. M. Church, Y. Gao, S. Kosuri, *Science* **2012**, *337*, 1628-1628.
- [216] V. Zhirnov, R. M. Zadegan, G. S. Sandhu, G. M. Church, W. L. Hughes, *Nat. Mater.* **2016**, *15*, 366.
- [217] N. Goldman, P. Bertone, S. Chen, C. Dessimoz, E. M. LeProust, B. Sipos, E. Birney, *Nature* **2013**, *494*, 77-80.
- [218] R. N. Grass, R. Heckel, M. Puddu, D. Paunescu, W. J. Stark, *Angew. Chem. Int. Ed.* **2015**, *54*, 2552-2555.
- [219] J. Bornholt, R. Lopez, D. M. Carmean, L. Ceze, G. Seelig, K. Strauss, *SIGOPS Oper. Syst. Rev.* **2016**, *50*, 637-649.
- [220] M. Blawat, K. Gaedke, I. Hütter, X.-M. Chen, B. Turczyk, S. Inverso, B. W. Pruitt, G. M. Church, *Procedia Computer Science* **2016**, *80*, 1011-1022.
- [221] H. Colquhoun, J.-F. Lutz, *Nat. Chem.* **2014**, *6*, 455-456.
- [222] G. Cavallo, A. Al Ouahabi, L. Oswald, L. Charles, J.-F. Lutz, *J. Am. Chem. Soc.* **2016**, *138*, 9417-9420.
- [223] L. Oswald, A. Al Ouahabi, L. Charles, J.-F. Lutz, *Chem. Eur. J.* **2016**, *22*, 3462-3469.
- [224] J.-A. Amalian, A. Al Ouahabi, G. Cavallo, N. F. König, S. Poyer, J.-F. Lutz, L. Charles, *J. Mass Spectrom.* **2017**, *52*, 788-798.
- [225] N. F. König, S. Telitel, S. Poyer, L. Charles, J.-F. Lutz, *Macromol. Rapid Commun.* **2017**, *38*, 1700651.
- [226] R. K. Roy, A. Meszynska, C. Laure, L. Charles, C. Verchin, J.-F. Lutz, *Nat. Commun.* **2015**, *6*, 7237.
- [227] J.-A. Amalian, T. T. Trinh, J.-F. Lutz, L. Charles, *Anal. Chem.* **2016**, *88*, 3715-3722.
- [228] J.-A. Amalian, S. Poyer, B. E. Petit, S. Telitel, V. Monnier, D. Karamessini, D. Gignes, J.-F. Lutz, L. Charles, *Int. J. Mass spectrom.* **2017**, *421*, 271-278.
- [229] A. Al Ouahabi, J.-A. Amalian, L. Charles, J.-F. Lutz, *Nat. Commun.* **2017**, *8*, 967.
- [230] R. K. Roy, C. Laure, D. Fischer-Krauser, L. Charles, J.-F. Lutz, *Chem. Commun.* **2015**, *51*, 15677-15680.
- [231] R. Szwedda, M. Tschopp, O. Felix, G. Decher, J.-F. Lutz, *Angew. Chem. Int. Ed.* **2018**, *57*, 15817-15821.
- [232] D. Karamessini, S. Poyer, L. Charles, J.-F. Lutz, *Macromol. Rapid Commun.* **2017**, *38*, 1700426.
- [233] Ufuk S. Gunay, Benoît E. Petit, D. Karamessini, A. Al Ouahabi, J.-A. Amalian, C. Chendo, M. Bouquey, D. Gignes, L. Charles, J.-F. Lutz, *Chem* **2016**, *1*, 114-126.
- [234] D. Karamessini, T. Simon-Yarza, S. Poyer, E. Konishcheva, L. Charles, D. Letourneur, J.-F. Lutz, *Angew. Chem. Int. Ed.* **2018**, *57*, 10574-10578.
- [235] J. O. Holloway, C. Mertens, F. E. Du Prez, N. Badi, *Macromol. Rapid Commun.* **2019**, *40*, 1800685.
- [236] J. O. Holloway, S. Aksakal, F. E. Du Prez, C. R. Becer, *Macromol. Rapid Commun.* **2017**, *38*, 1700500.
- [237] S. Celasun, F. E. Du Prez, H. G. Börner, *Macromol. Rapid Commun.* **2017**, *38*, 1700688.
- [238] S. Celasun, D. Remmler, T. Schwaar, M. G. Weller, F. Du Prez, H. G. Börner, *Angew. Chem. Int. Ed.* **2019**, *58*, 1960-1964.
- [239] S. C. Solleder, S. Martens, P. Espeel, F. Du Prez, M. A. R. Meier, *Chem. Eur. J.* **2017**, *23*, 13906-13909.
- [240] R. Huisgen, *Angew. Chem. Int. Ed.* **1963**, *2*, 565-598.
- [241] J. J. Haven, J. A. De Neve, T. Junkers, *ACS Macro Lett.* **2017**, *6*, 743-747.

-
- [242] O. Kreye, T. Tóth, M. A. R. Meier, *J. Am. Chem. Soc.* **2011**, *133*, 1790-1792.
- [243] A. Sehlinger, P.-K. Dannecker, O. Kreye, M. A. R. Meier, *Macromolecules* **2014**, *47*, 2774-2783.
- [244] A. Lv, X.-X. Deng, L. Li, Z.-L. Li, Y.-Z. Wang, F.-S. Du, Z.-C. Li, *Polym. Chem.* **2013**, *4*, 3659-3662.
- [245] K. S. Wetzel, M. A. R. Meier, *Polym. Chem.* **2019**, *10*, 2716-2722.
- [246] T. Pauloehrl, G. Delaittre, V. Winkler, A. Welle, M. Bruns, H. G. Börner, A. M. Greiner, M. Bastmeyer, C. Barner-Kowollik, *Angew. Chem. Int. Ed.* **2012**, *51*, 1071-1074.
- [247] W. Konrad, F. R. Bloesser, K. S. Wetzel, A. C. Boukis, M. A. R. Meier, C. Barner-Kowollik, *Chem. Eur. J.* **2018**, *24*, 3413-3419.
- [248] F. R. Bloesser, *Synthesis of Sequence-Defined Linear Macromolecules by Photo-Enol Conjugation and the Passerini Reaction*, Master Thesis, Karlsruhe, **2017**.
- [249] S. Mukherjee, W. L. A. Brooks, Y. Dai, B. S. Sumerlin, *Polym. Chem.* **2016**, *7*, 1971-1978.
- [250] B. Gacal, H. Durmaz, M. A. Tasdelen, G. Hizal, U. Tunca, Y. Yagci, A. L. Demirel, *Macromolecules* **2006**, *39*, 5330-5336.
- [251] R. W. Stephany, M. J. A. de Bie, W. Drenth, *Organic Magnetic Resonance* **1974**, *6*, 45-47.
- [252] I. Ugi, *Angew. Chem. Int. Ed.* **1962**, *1*, 8-21.
- [253] W. Konrad, C. Fengler, S. Putwa, C. Barner-Kowollik, *Angew. Chem. Int. Ed.* **2019**, *58*, 7133-7137.
- [254] W. Konrad, C. Fengler, S. Putwa, C. Barner-Kowollik, *Angew. Chem.* **2019**, *131*, 7207-7211.
- [255] C. Fengler, *Protection Group Free Synthesis of Sequence-Defined Oligomers via λ Orthogonal Photochemistry*, Vertiefearbeit, Karlsruhe, **2018**.
- [256] F. M. Hauser, S. R. Ellenberger, *Synthesis* **1987**, *1987*, 723-724.
- [257] A. Senthilmurugan, I. S. Aidhen, *Eur. J. Org. Chem.* **2010**, *2010*, 555-564.
- [258] C. Grewer, H.-D. Brauer, *J. Phys. Chem.* **1994**, *98*, 4230-4235.
- [259] H. E. Gottlieb, V. Kotlyar, A. Nudelman, *J. Org. Chem.* **1997**, *62*, 7512-7515.
- [260] G. R. Fulmer, A. J. M. Miller, N. H. Sherden, H. E. Gottlieb, A. Nudelman, B. M. Stoltz, J. E. Bercaw, K. I. Goldberg, *Organometallics* **2010**, *29*, 2176-2179.
- [261] T. Gegenhuber, A. M. Schenzel, A. S. Goldmann, P. B. Zetterlund, C. Barner-Kowollik, *Chem. Commun.* **2017**, *53*, 10648-10651.
- [262] B. Tuten, L. De Keer, S. Wiedbrauk, P. Van Steenberge, D. D'hooge, C. Barner-Kowollik, *Angew. Chem. Int. Ed.* **2019**, *58*, 5672-5676.